

FRONT TRACKING FINITE ELEMENT METHODS FOR TWO-PHASE NAVIER–STOKES FLOW

A THESIS PRESENTED FOR THE DEGREE OF
DOCTOR OF PHILOSOPHY OF IMPERIAL COLLEGE LONDON
AND THE
DIPLOMA OF IMPERIAL COLLEGE
BY
MARCO AGNESE

DEPARTMENT OF MATHEMATICS
IMPERIAL COLLEGE
180 QUEEN'S GATE, LONDON SW7 2BZ

SEPTEMBER 2017

I certify that this thesis, and the research to which it refers, are the product of my own work, and that any ideas or quotations from the work of other people, published or otherwise, are fully acknowledged in accordance with the standard referencing practices of the discipline.

Signed: Marcos Agnese

COPYRIGHT

The copyright of this thesis rests with the author and is made available under a Creative Commons Attribution Non-Commercial No Derivatives licence. Researchers are free to copy, distribute or transmit the thesis on the condition that they attribute it, that they do not use it for commercial purposes and that they do not alter, transform or build upon it. For any reuse or redistribution, researchers must make clear to others the licence terms of this work.

Front tracking finite element methods for two-phase Navier–Stokes flow

ABSTRACT

Fluid flow problems with a moving interface are found in many applications in physics and engineering. In these type of problems, apart from the unknown flow in the bulk domain, also the position of the free surface needs to be determined.

The goal of this thesis is to investigate front tracking finite element methods applied to two-phase incompressible Navier–Stokes flows. The front tracking approach consists on seeking a parametrization of the unknown interface over a reference manifold. A novel variational formulation for the interface evolution is used. This formulation preserves, in general, the interface mesh quality over time. Moreover, being a fitted approach, the interface mesh is made up of faces of elements belonging to the bulk mesh.

Several fully discrete finite element approximations are derived and, wherever possible, stability and existence results are proved. In order to demonstrate the accuracy and robustness of the proposed algorithms, extensive numerical experiments are carried out, both in 2d and in 3d. A variety of finite element spaces are used. Smoothing and remeshing routines are applied to the bulk mesh to avoid heavily distorted simplices.

A Silvia.

ACKNOWLEDGMENTS

My greatest thanks are for my supervisor, Robert, for his continuous help and support, and for the precious discussions which enriched my knowledge and passion for research. Without him none of this would have been possible.

I would also like to thank Imperial College for giving me this incredible opportunity and the Math department for being a second home during these past four years. A special thank you goes to the DUNE community and in particular the DUNE-FEM team from which I learned a lot. I would like to thank Andrea for all the help he gave me. A huge thank you is for my office mates in 757 with whom I spent many happy hours. Thank you guys for the board games lessons.

I want to thank all my London friends who were patient enough to put up with me during this long journey. As usual, my family has been the greatest source of support and love and I can never thank them enough for everything they do for me.

A final thank you to Silvia, who, without any hesitation, moved to London with me. Her continuous love and trust have been indispensable to go through this adventure.

LIST OF FIGURES

1.1	Two-phase flow	3
2.1	Mean curvature flow shrinking sphere	32
2.2	Mean curvature flow shrinking sphere radius	32
2.3	Surface diffusion equidistribution property	34
2.4	Surface diffusion equidistribution velocity	34
2.5	Surface diffusion cage	35
2.6	Surface diffusion cage section	35
2.7	Surface diffusion cage surface energy	36
3.1	Fitted and unfitted meshes	45
4.1	Stokes 2d stationary bubble initial mesh	68
4.2	Stokes 2d stationary bubble pressure	70
4.3	Stokes 2d expanding bubble initial meshes	71
4.4	Stokes expanding bubble pressure uniform mesh	74
4.5	Stokes expanding bubble pressure adaptive mesh	78
4.6	Stokes equidistribution property	79
4.7	Stokes equidistribution velocity	80
4.8	Stokes equidistribution property adaptive mesh	81
4.9	Stokes equidistribution velocity adaptive mesh	82
4.10	Stokes ellipse pressure	83
4.11	Stokes ellipse inner area and interface energy	84
4.12	Stokes ellipse pressure no remeshing	85

4.13	Stokes ellipse inner area and interface energy no remeshing . . .	86
4.14	Stokes 2d shear flow pressure	86
4.15	Stokes 2d shear flow velocity	87
4.16	Stokes 2d shear flow inner area	87
4.17	Conformal polyhedral sphere triangulation	89
4.18	Stokes 3d shear flow interface	91
4.19	Stokes 3d shear flow velocity	92
4.20	Stokes 3d shear flow inner volume	92
5.1	Continuous path traversing a fictitious background lattice . . .	112
7.1	Navier–Stokes rising bubble I pressure	146
7.2	Navier–Stokes rising bubble I velocity	147
7.3	Navier–Stokes rising bubble I sphericity	147
7.4	Navier–Stokes rising bubble I rising velocity	148
7.5	Navier–Stokes rising bubble I barycentre	148
7.6	Navier–Stokes rising bubble I inner area	148
7.7	Navier–Stokes rising bubble II pressure	151
7.8	Navier–Stokes rising bubble II velocity	152
7.9	Navier–Stokes rising bubble II sphericity	152
7.10	Navier–Stokes rising bubble II rising velocity	153
7.11	Navier–Stokes rising bubble II barycentre	153
7.12	Navier–Stokes rising bubble II inner area	153

LIST OF TABLES

4.1	Stokes 2d stationary bubble errors P ₂ –P ₀	69
4.2	Stokes 2d stationary bubble errors P ₂ –P ₁	69
4.3	Stokes 2d stationary bubble errors P ₂ –P ₁ ^{dgr}	69
4.4	Stokes 2d stationary bubble errors P ₂ –(P ₁ +P ₀)	69
4.5	Stokes expanding bubble uniform meshes parameters	71
4.6	Stokes expanding bubble uniform mesh errors P ₂ –P ₀	72
4.7	Stokes expanding bubble uniform mesh errors P ₂ –P ₁ ^{dgr}	72
4.8	Stokes expanding bubble uniform mesh errors P ₂ –(P ₁ +P ₀) . .	73
4.9	Stokes expanding bubble adaptive meshes parameters	75
4.10	Stokes expanding bubble adaptive mesh errors P ₂ –P ₀	75
4.11	Stokes expanding bubble adaptive mesh errors P ₂ –P ₁ ^{dgr}	76
4.12	Stokes expanding bubble adaptive mesh errors P ₂ –(P ₁ +P ₀) . .	76
4.13	Stokes 2d shear flow preconditioners comparison	84
4.14	Stokes 3d stationary bubble errors P ₂ –P ₀	89
4.15	Stokes 3d stationary bubble errors P ₂ –P ₁	89
4.16	Stokes 3d stationary bubble errors P ₂ –P ₁ ^{dgr}	90
4.17	Stokes 3d stationary bubble errors P ₂ –(P ₁ +P ₀)	90
4.18	Stokes 3d shear flow preconditioners comparison	93
7.1	Navier–Stokes expanding bubble meshes parameters	134
7.2	Navier–Stokes expanding bubble I errors P ₂ –P ₀	135
7.3	Navier–Stokes expanding bubble I errors P ₂ –P ₁ ^{dgr}	136
7.4	Navier–Stokes expanding bubble I errors P ₂ –(P ₁ +P ₀)	137

7.5	Navier–Stokes expanding bubble II errors P2–P0	138
7.6	Navier–Stokes expanding bubble II errors P2–P1 ^{dgr}	139
7.7	Navier–Stokes expanding bubble II errors P2–(P1+P0)	140
7.8	Navier–Stokes rising bubble I meshes parameters	141
7.9	Navier–Stokes rising bubble I benchmark values P2–P0	142
7.10	Navier–Stokes rising bubble I benchmark values P2–P1 ^{dgr} . . .	143
7.11	Navier–Stokes rising bubble I benchmark values P2–(P1+P0) .	144
7.12	Navier–Stokes rising bubble II benchmark values	149

CONTENTS

1	INTRODUCTION	1
1.1	Free-boundary fluid flows	2
1.2	One-phase Navier–Stokes model	3
1.3	Two-phase Navier–Stokes model	6
1.4	Interface treatment	10
1.5	Numerical challenges	12
1.6	Numerical implementation	13
2	GEOMETRIC EVOLUTION EQUATIONS	15
2.1	Geometric PDEs	16
2.2	Geometric analysis	17
2.3	Properties of geometric flows	20
2.4	Front tracking approach	23
2.5	Finite element approximation	24
2.6	Semidiscrete scheme	27
2.7	Algebraic formulation	29
2.8	Numerical results	30
2.8.1	Mean curvature flow with a sphere as initial condition .	31
2.8.2	Equidistribution property	33
2.8.3	Surface diffusion with a cage as initial condition	33
3	TWO-PHASE STOKES FLOW FEM	37
3.1	Mathematical model	38
3.2	Weak formulation	39

3.3	Energy bound and volume conservation	41
3.4	Finite element approximation	42
3.5	Fitted and unfitted approach	44
3.6	Existence and uniqueness of a discrete solution	46
3.7	Stability	48
3.8	Discrete stationary solutions	49
3.9	Semidiscrete scheme	51
3.10	Algebraic formulation	53
3.11	Solution method	55
3.12	Mesh generation and smoothing	60
4	TWO-PHASE STOKES FLOW NUMERICAL RESULTS	63
4.1	Exact solutions	64
4.1.1	Stationary bubble	64
4.1.2	Expanding bubble	65
4.2	Settings and error estimators	67
4.3	Convergence tests in 2d	68
4.4	Equidistribution property in 2d	77
4.5	Energy decay and area conservation in 2d	80
4.6	Shear flow experiment in 2d	82
4.7	Convergence test in 3d	88
4.8	Shear flow experiment in 3d	90
5	TWO-PHASE NAVIER–STOKES FLOW STANDARD FEMs	94
5.1	Mathematical model	95
5.2	Weak formulation	96
5.3	Antisymmetric finite element approximation	100
5.3.1	Existence and uniqueness of a discrete solution	103

5.3.2	Stability	104
5.4	Standard finite element approximation	106
5.5	Solution methods	108
5.6	Velocity interpolation	110
6	TWO-PHASE NAVIER–STOKES FLOW ALE FEM	113
6.1	Mathematical model	114
6.2	Weak formulation	117
6.3	Semidiscrete finite element approximation	118
6.4	Fully discrete finite element approximation	122
6.5	Solution method	124
7	TWO-PHASE NAVIER–STOKES FLOW NUMERICAL RESULTS	127
7.1	Exact solutions	127
7.1.1	Expanding bubble I	128
7.1.2	Expanding bubble II	129
7.2	Non divergence-free scheme modifications	130
7.3	Benchmark quantities	133
7.4	Convergence tests	134
7.5	Rising bubble experiments	141
8	CONCLUSION	154
	REFERENCES	163

1

INTRODUCTION

Fluid flow problems with an unknown interface are ubiquitous in physics and engineering. This introductory chapter is devoted to a description of the mathematical model used to model this type of systems together with a brief overview of the possible approaches to describe the unknown interface.

The chapter is organised as follows: in §1.1 we define what a free-boundary fluid flow is and we introduce a generic setting for the problem; in §1.2 we present the one-phase Navier–Stokes equations and their physical meaning; in §1.3 we discuss the two-phase Navier–Stokes case and the interface conditions needed for the well posedness of the problem; in §1.4 we briefly overview the different ways to treat the unknown interface; in §1.5 we detail the various numerical challenges posed by these types of flows; in §1.6 we finally list the libraries used to implement the numerical schemes described in this thesis and we provide the links to the code developed in order to make all the results presented in this work reproducible.

1.1 FREE-BOUNDARY FLUID FLOWS

Fluid flow problems with a moving interface are encountered in many applications in physics, engineering and biophysics. Typical applications are drops and bubbles, die swell, dam break, liquid storage tanks, dendritic growth, ink-jet printing, fuel injection. For this reason, developing robust and efficient numerical methods for these flows is an important problem and has attracted tremendous interest over the last decade.

In these type of problems, apart from the flow solution in the bulk domain, the position of a portion of the boundary is also unknown. This boundary can either be an external boundary or an interface between sub-domains. At the boundary/interface, certain boundary conditions need to be fulfilled, which specify the position of the boundary. These conditions relate the variables of the flow, velocity and pressure, across the domains under consideration of external influences, such as for example surface tension. Numerically, in order to be able to compute the flow solution as well as the boundary/interface geometry, a measure to track the boundary starting from an initial position needs to be incorporated.

The scenario we consider are two-phase flows, liquid-liquid or liquid-gas, in a d -dimensional computational domain $\Omega \subset \mathbb{R}^d$. This domain Ω contains two different immiscible fluids which, for all $t \in [0, T]$, occupy time dependent regions $\Omega_+(t)$ and $\Omega_-(t) := \Omega \setminus \overline{\Omega}_+(t)$ and which are separated by an interface $(\Gamma(t))_{t \in [0, T]}$, $\Gamma(t) \subset \Omega$. For later use, we always assume that $(\Gamma(t))_{t \in [0, T]}$ is a sufficiently smooth evolving hypersurface without boundary. See Figure 1.1 for an illustration. Therefore both the sub-domains themselves and the flow field are part of the solution. Indeed the main task in this context is to account for the interface $\Gamma(t)$, which separates the distinct fluid domains and is generally in motion. Apart from its exact position, the computation of geometrical quantities of $\Gamma(t)$ such as its normal vector $\vec{\nu}$ and its mean curvature κ are of interest.

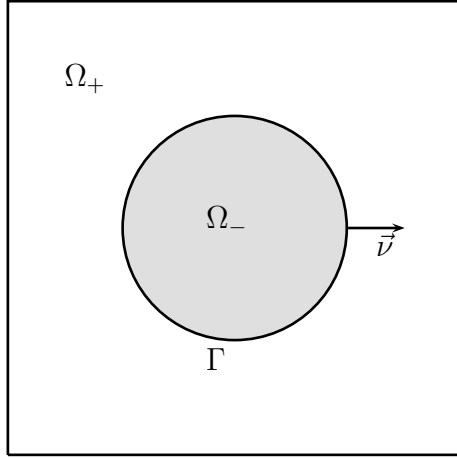


Figure 1.1: Two-phase flow setting.

1.2 ONE-PHASE NAVIER–STOKES MODEL

Before describing the full two-phase Navier–Stokes model, we start introducing the simpler one-phase case where the full domain Ω is occupied by one fluid only. We restrict ourselves to isothermal conditions, incompressible fluids and we assume that there is no change of phase. For more details see [37].

Denoting the velocity and pressure by \vec{u} and p , respectively, we introduce the Newtonian stress tensor

$$\underline{\sigma} = \mu (\nabla \vec{u} + (\nabla \vec{u})^T) - p \underline{\text{id}} = 2\mu \underline{D}(\vec{u}) - p \underline{\text{id}}, \quad (1.1)$$

where $\underline{\text{id}} \in \mathbb{R}^{d \times d}$ is the identity matrix and $\underline{D}(\vec{u}) := \frac{1}{2} (\nabla \vec{u} + (\nabla \vec{u})^T)$ is the rate-of-deformation tensor with $[\nabla \vec{u}]_{ij} = \frac{\partial u_i}{\partial z_j}$, $1 \leq i, j \leq d$. Moreover, let μ , with $\mu \in \mathbb{R}_{>0}$, be the fluid dynamic viscosity and let ρ , with $\rho \in \mathbb{R}_{>0}$, be the fluid density.

Imposing the conservation of momentum and mass, the following standard

Navier–Stokes governing equations can be derived:

$$\rho (\vec{u}_t + (\vec{u} \cdot \nabla) \vec{u}) - \nabla \cdot \underline{\underline{\sigma}} = \vec{f} \quad \text{in } \Omega, \quad (1.2a)$$

$$\nabla \cdot \vec{u} = 0 \quad \text{in } \Omega, \quad (1.2b)$$

where \vec{f} includes all external body forces referred to the unit mass of fluid. For later use, we define the divergence of a tensor $\underline{\underline{H}} : \mathbb{R}^d \rightarrow \mathbb{R}^{d \times d}$ as the vector with entries

$$[\nabla \cdot \underline{\underline{H}}]_i = \sum_{j=1}^d \frac{\partial [\underline{\underline{H}}]_{ij}}{\partial z_j}, \quad 1 \leq i \leq d. \quad (1.3)$$

Substituting (1.1) in (1.2a), we obtain the well known one-phase incompressible Navier–Stokes model:

$$\rho (\vec{u}_t + (\vec{u} \cdot \nabla) \vec{u}) - 2\mu \nabla \cdot \underline{\underline{D}}(\vec{u}) + \nabla p = \vec{f} \quad \text{in } \Omega, \quad (1.4a)$$

$$\nabla \cdot \vec{u} = 0 \quad \text{in } \Omega. \quad (1.4b)$$

To better grasp the physical meaning of the terms appearing in the momentum equation (1.4a) we briefly describe them. The inertia term $(\vec{u} \cdot \nabla) \vec{u}$ is a convection term arising from the conservation of momentum. The momentum of each portion of fluid needs to be conserved therefore it needs to move with the fluid which means that it is convected with the fluid. The pressure term ∇p is originated by the Newtonian constitutive equation (1.1) and it represent all the forces resulting from pressure differences within the fluid. Finally, the friction term $\nabla \cdot \underline{\underline{D}}(\vec{u})$, which again arises from the Newtonian constitutive equation (1.1), is a diffusion operator equalizing the velocity of neighbouring elements. The more viscous the fluid, the stronger is the friction between neighbouring particles and thus the equalizing effect.

The Reynolds number Re is an important dimensionless quantity in fluid mechanics and it is defined as

$$Re = \frac{\rho u_c L_c}{\mu}, \quad (1.5)$$

where L_c is the characteristic dimension of the problem and u_c is the characteristic velocity of the fluid. It quantifies the ratio of inertial forces to viscous forces within the fluid, therefore it is used to predict flow patterns in different fluid flow situations. When $Re \ll 1$ the flow is laminar due to the fact that viscous forces are dominant and it is characterized by smooth, constant fluid motion. Instead, when $Re \gg 1$ the flow is turbulent due to the fact that inertial forces are dominant and it tends to produce chaotic eddies, vortices and other flow instabilities.

In the case of laminar flow, the advective term in the momentum equation (1.2a) can be neglected, giving rise to the so called Stokes equations

$$-\nabla \cdot \underline{\underline{\sigma}} = \vec{f} \quad \text{in } \Omega, \quad (1.6a)$$

$$\nabla \cdot \vec{u} = 0 \quad \text{in } \Omega, \quad (1.6b)$$

which for Newtonian fluids are expressed as

$$-2\mu \nabla \cdot \underline{\underline{D}}(\vec{u}) + \nabla p = \vec{f} \quad \text{in } \Omega, \quad (1.7a)$$

$$\nabla \cdot \vec{u} = 0 \quad \text{in } \Omega. \quad (1.7b)$$

We finally observe that, using the incompressibility condition (1.4b) we have that

$$2\nabla \cdot \underline{\underline{D}}(\vec{u}) = \nabla \cdot (\nabla \vec{u} + (\nabla \vec{u})^T) = \Delta \vec{u} + \nabla(\nabla \cdot \vec{u}) = \Delta \vec{u}. \quad (1.8)$$

Therefore the system (1.4a–b) can be rewritten as

$$\rho(\vec{u}_t + (\vec{u} \cdot \nabla) \vec{u}) - \mu \Delta \vec{u} + \nabla p = \vec{f} \quad \text{in } \Omega, \quad (1.9a)$$

$$\nabla \cdot \vec{u} = 0 \quad \text{in } \Omega, \quad (1.9b)$$

which is the canonical form of the one-phase Navier–Stokes problem and the system (1.7a–b) can be rewritten as

$$-\mu \Delta \vec{u} + \nabla p = \vec{f} \quad \text{in } \Omega, \quad (1.10a)$$

$$\nabla \cdot \vec{u} = 0 \quad \text{in } \Omega, \quad (1.10b)$$

which is the canonical form of the one-phase Stokes problem.

For the full Navier–Stokes problem (1.4a–b), a divergence-free velocity field for the whole computational domain is needed as an initial condition. Therefore we impose

$$\vec{u}(0) = \vec{u}_0 \quad \text{in } \Omega. \quad (1.11)$$

The initial condition is not needed in the Stokes case (1.7a–b) since it is a stationary problem.

In order to obtain a well-posed system, boundary conditions have to be imposed on the bulk domain boundary $\partial\Omega$. Let $\partial\Omega$ be partitioned as $\partial\Omega = \partial_1\Omega \cup \partial_2\Omega$ with $\partial_1\Omega \cap \partial_2\Omega = \emptyset$. On $\partial_1\Omega$ we use the Dirichlet condition

$$\vec{u} = \vec{g} \quad \text{on } \partial_1\Omega, \quad (1.12)$$

and we notice that the case $\vec{g} = \vec{0}$ corresponds to the so called no-slip condition. Instead, on $\partial_2\Omega$ we prescribe the free-slip condition

$$\vec{u} \cdot \vec{n} = 0, \quad \underline{\sigma} \vec{n} \cdot \vec{t} = 0 \quad \forall \vec{t} \in \{\vec{n}\}^\perp \quad \text{on } \partial_2\Omega, \quad (1.13)$$

with \vec{n} denoting the outer unit normal of $\partial\Omega$ and $\{\vec{n}\}^\perp := \{\vec{t} \in \mathbb{R}^d : \vec{t} \cdot \vec{n} = 0\}$. The second term in (1.13) can be derived from the balance of kinetic energy prescribing a null power transfer through $\partial_2\Omega$. Therefore, (1.13) is an energy preserving boundary condition, see [18] for more details.

1.3 TWO-PHASE NAVIER–STOKES MODEL

We now consider two-phase flows, i.e., the domain Ω contains two different immiscible incompressible phases which may move in time and have different densities and dynamic viscosities. As mentioned before, we assume isothermal conditions and both phases to be pure substances. Furthermore, we do not consider reaction, mass transfer or phase transition. For more details see again [37].

Each fluid phase is governed by the Navier–Stokes equations (1.4a–b), or by the Stokes equations (1.7a–b). Therefore the two-phase Navier–Stokes model

is simply

$$\rho(\vec{u}_t + (\vec{u} \cdot \nabla) \vec{u}) - 2\mu \nabla \cdot \underline{\underline{D}}(\vec{u}) + \nabla p = \vec{f} \quad \text{in } \Omega_{\pm}(t), \quad (1.14a)$$

$$\nabla \cdot \vec{u} = 0 \quad \text{in } \Omega_{\pm}(t), \quad (1.14b)$$

where $\mu(t) = \mu_+ \mathcal{X}_{\Omega_+(t)} + \mu_- \mathcal{X}_{\Omega_-(t)}$, with $\mu_{\pm} \in \mathbb{R}_{>0}$, is the dynamic viscosity and $\rho(t) = \rho_+ \mathcal{X}_{\Omega_+(t)} + \rho_- \mathcal{X}_{\Omega_-(t)}$, with $\rho_{\pm} \in \mathbb{R}_{>0}$, is the fluid density. Here and throughout, $\mathcal{X}_{\mathcal{D}}$ denotes the characteristic function for a set \mathcal{D} . Analogously, the two-phase Stokes model is

$$-2\mu \nabla \cdot \underline{\underline{D}}(\vec{u}) + \nabla p = \vec{f} \quad \text{in } \Omega_{\pm}(t), \quad (1.15a)$$

$$\nabla \cdot \vec{u} = 0 \quad \text{in } \Omega_{\pm}(t). \quad (1.15b)$$

In addition to the initial condition (1.11), which is needed only in the Navier–Stokes case, and to the boundary conditions (1.12) and (1.13), some interface conditions are also needed on the unknown interface $\Gamma(t)$, which couple the velocity and stress between the two domains. Viscosity of the fluids leads to the continuity condition

$$[\vec{u}]_{-}^{+} = \vec{0} \quad \text{on } \Gamma(t), \quad (1.16)$$

where $[\vec{u}]_{-}^{+} := \vec{u}_+ - \vec{u}_-$ denote the jump in velocity across the interface $\Gamma(t)$. Here and throughout, we employ the shorthand notation $\vec{h}_{\pm} := \vec{h}|_{\Omega_{\pm}(t)}$ for a function $\vec{h} : \Omega \times [0, T] \rightarrow \mathbb{R}^d$; and similarly for scalar and matrix-valued functions.

The assumption that there is no change of phase leads to the dynamic interface condition

$$\vec{\mathcal{V}} \cdot \vec{\nu} = \vec{u} \cdot \vec{\nu} \quad \text{on } \Gamma(t), \quad (1.17)$$

given that $\vec{\mathcal{V}}$ is the velocity of the evolving interface $\Gamma(t)$ and where $\vec{\nu}(t)$ is the unit normal on $\Gamma(t)$ pointing into $\Omega_+(t)$. Thus the normal velocity of the interface needs to match the flow normal velocity across the interface $\Gamma(t)$ which means that no particle of fluid can cross the interface. Therefore, given that the interface separates the two phases, 1.17 is equivalent to imposing no change of phase.

The momentum conservation in a small material volume that intersects the interface leads to the stress balance condition

$$[\underline{\sigma} \vec{\nu}]_-^+ = -\nabla_s \cdot \underline{\sigma}_\Gamma \quad \text{on } \Gamma(t), \quad (1.18)$$

where $\underline{\sigma}_\Gamma$ is the interface stress tensor and $\nabla_s \cdot$ is the surface divergence on $\Gamma(t)$, see [37] for more details. The operator ∇_s is the surface gradient on $\Gamma(t)$ and it is the orthogonal projection of the usual gradient operator ∇ on the tangent space of the surface $\Gamma(t)$. Therefore, given a smooth function h defined on a neighbourhood of $\Gamma(t)$, it is defined as

$$\nabla_s h(\vec{z}) = \underline{\underline{P}}(\vec{z}) \nabla h(\vec{z}) = \nabla h(\vec{z}) - \nabla h(\vec{z}) \cdot \vec{\nu}(\vec{z}) \vec{\nu}(\vec{z}), \quad \vec{z} \in \Gamma(t), \quad (1.19)$$

with the usual projection operator $\underline{\underline{P}}$ defined as

$$\underline{\underline{P}} = \underline{\underline{\text{id}}} - \vec{\nu} \vec{\nu}^T \quad \text{on } \Gamma(t). \quad (1.20)$$

It can be shown that the definition of $\nabla_s h$ does not depend on the chosen extension of h , but only on the value of h on $\Gamma(t)$. See e.g. [21, §2.1] for details. For later use, we also define the surface Laplacian, also known as Laplace–Beltrami operator, Δ_s on $\Gamma(t)$ as

$$\Delta_s = \nabla_s \cdot \nabla_s. \quad (1.21)$$

We restrict ourselves to the case that the only force acting on the interface is the surface tension contact force. Therefore the interface stress tensor $\underline{\sigma}_\Gamma$ has the following constitutive equation

$$\underline{\sigma}_\Gamma = \gamma \underline{\underline{P}}, \quad (1.22)$$

where γ is the surface tension coefficient. Substituting (1.22) in (1.18) we

obtain

$$\begin{aligned}
[\underline{\sigma} \vec{\nu}]_-^+ &= -\nabla_s \cdot (\gamma \underline{P}) = -\gamma \nabla_s \cdot \underline{P} - \nabla_s \gamma = \gamma \nabla_s \cdot (\vec{\nu} \vec{\nu}^T) - \nabla_s \gamma \\
&= \gamma \nabla_s \cdot \vec{\nu} \vec{\nu} + \gamma \nabla_s \vec{\nu} \cdot \vec{\nu} - \nabla_s \gamma = \gamma \nabla_s \cdot \vec{\nu} \vec{\nu} - \nabla_s \gamma \\
&= -\gamma \kappa \vec{\nu} - \nabla_s \gamma \quad \text{on } \Gamma(t),
\end{aligned} \tag{1.23}$$

where we have used the fact that the surface gradient ∇_s is, by definition, always orthogonal to the surface normal $\vec{\nu}$ and that $\kappa = -\nabla_s \cdot \vec{\nu}$ is the mean curvature of $\Gamma(t)$. The projection \underline{P} is used, since $\underline{\sigma}_\Gamma$ should represent only contact forces that are tangential to the surface. We assume that γ is constant and therefore, from (1.23), we obtain the so called clean interface model for the interfacial forces

$$[\underline{\sigma} \vec{\nu}]_-^+ = -\gamma \kappa \vec{\nu} \quad \text{on } \Gamma(t), \tag{1.24}$$

which, in the case of Newtonian stress tensor (1.1), assumes the form

$$[2\mu \underline{D}(\vec{u}) \cdot \vec{\nu} - p \vec{\nu}]_-^+ = -\gamma \kappa \vec{\nu} \quad \text{on } \Gamma(t). \tag{1.25}$$

Moreover, in order to have a well-posed problem, one needs suitable initial conditions for the interface. Therefore we set $\Gamma(0) = \Gamma_0$.

Finally, we can formulate the two-phase Navier–Stokes model, with the necessary initial, boundary and interface conditions, as

$$\rho (\vec{u}_t + (\vec{u} \cdot \nabla) \vec{u}) - 2\mu \nabla \cdot \underline{D}(\vec{u}) + \nabla p = \vec{f} \quad \text{in } \Omega_\pm(t), \tag{1.26a}$$

$$\nabla \cdot \vec{u} = 0 \quad \text{in } \Omega_\pm(t), \tag{1.26b}$$

$$\vec{u} = \vec{g} \quad \text{on } \partial_1 \Omega, \tag{1.26c}$$

$$\vec{u} \cdot \vec{n} = 0, \quad \underline{\sigma} \vec{n} \cdot \vec{t} = 0 \quad \forall \vec{t} \in \{\vec{n}\}^\perp \quad \text{on } \partial_2 \Omega, \tag{1.26d}$$

$$[\vec{u}]_-^+ = \vec{0} \quad \text{on } \Gamma(t), \tag{1.26e}$$

$$[2\mu \underline{D}(\vec{u}) \cdot \vec{\nu} - p \vec{\nu}]_-^+ = -\gamma \kappa \vec{\nu} \quad \text{on } \Gamma(t), \tag{1.26f}$$

$$(\vec{\mathcal{V}} - \vec{u}) \cdot \vec{\nu} = 0 \quad \text{on } \Gamma(t), \tag{1.26g}$$

$$\Gamma(0) = \Gamma_0, \tag{1.26h}$$

$$\vec{u}(0) = \vec{u}_0. \tag{1.26i}$$

1.4 INTERFACE TREATMENT

The dynamics of the interface are determined by the condition (1.17) which, however, describes the dynamics in a strongly implicit way since the velocity field \vec{u} depends on the position of the interface itself. In numerical simulations, there are several strategies to deal with this problem, which can be divided into two categories depending on the viewpoint: interface capturing and interface tracking.

Interface capturing methods use an Eulerian description of the interface, which is defined implicitly. A characteristic scalar field ψ is used to identify the two phases as well as the interface along the boundaries of the individual fluid domains. Depending on the method, this scalar field may be, for example, a discontinuous Heaviside function or a signed-distance function. The interface motion is taken into account using a standard advection equation

$$\frac{\partial \psi}{\partial t} + \vec{u} \cdot \nabla \psi = 0 \quad \text{in } \Omega, \quad (1.27)$$

which transports the scalar field with the fluid velocity \vec{u} . The most important methods, which belong to this category, are the particle method, the volume-of-fluid method, the level-set method and the phase-field method. The particle method utilizes mass-less particles distributed in an Eulerian mesh to capture the fluid flow and in particular the interface position, see e.g [34]. In the volume-of-fluid method, the characteristic function of one of the phases is approximated numerically, see e.g. [39, 54, 53]. In the level-set method, the interface is given as the level set of a function, which has to be determined, see e.g. [58, 57, 51, 36, 59]. Instead, the phase-field method works with diffuse interfaces, and therefore the transition layer between the phases has a finite size. There is no tracking mechanism for the interface, but the phase state is included implicitly in the governing equations. The interface is associated with a smooth, but highly localized variation of the so-called phase-field variable. We refer to [40, 3, 46, 27, 44, 1, 38] for details. In general, the great advantage of the interface capturing approaches is that they are inherently able to deal with topological changes of the interface. This allows a much more flexible interface description than in interface tracking

approaches. On the other hand, it is challenging to treat accurately discontinuous quantities across the interface, to have mass conservation within each phase and to apply boundary conditions along the interface.

Interface tracking approaches, instead, use a Lagrangian description of the interface which is described explicitly. The idea is to take a (virtual) particle on the interface at time $t = t_0$ with Eulerian coordinates $\vec{z}(0) \in \Gamma_0$. Let $\vec{z}(t)$ be the Eulerian coordinates of this particle at time t , with $t \geq t_0$. The particles on the interface are transported by the flow velocity \vec{u} , therefore it satisfies the equation

$$\frac{\partial \vec{z}(t)}{\partial t} = \vec{u}(\vec{z}(t), t), \quad (1.28)$$

which determines the path of a material particle and consequently it characterizes the evolution of the interface. This interface representation forms the basis of the interface tracking methods. In these methods a collection of markers is put on a given interface Γ_0 and then transported (numerically) by the flow velocity \vec{u} to obtain the markers on the interface $\Gamma(t)$. Usually, the collection of markers on Γ_0 are the set of vertices of the triangulation of Γ_0 . The great advantage of interface tracking approaches is that they offer an accurate and computationally efficient approximation of the evolving interface. Moreover, the imposition of boundary conditions at the interface is simple since the mesh nodes lie on the interface itself. However, firstly the mesh quality will usually degrade quickly in the case of large deformations and secondly topological changes require a special treatment. In order to keep an acceptable mesh quality throughout the simulation, mesh smoothing techniques are applied and, when they are not enough, a full remeshing is used. If topological changes occur, the only way to tackle the issue is to perform a remeshing with respect to the new interface. The main consequence of remeshing is the need to project the field values from the old to the new mesh, a ceaseless source for errors, and at the same time computationally costly especially in dimension 3. Therefore, it is desirable to keep the frequency of remeshing as low as possible. We refer e.g. to [61, 5, 60, 30, 31, 10, 12] for further details, and to [45, 52] for the related immersed boundary method, which is used to simulate fluid-structure interactions using Eulerian coordinates for the fluid and Lagrangian coordinates for the structure.

In the following chapters, we always use an interface tracking approach to describe the interface evolution. In particular, we adopt a fitted mesh approach which means that the discrete interface is composed by bulk element faces. Consequently there is a strong coupling between the bulk mesh and the interface mesh.

1.5 NUMERICAL CHALLENGES

Two-phase flows pose enormous challenges to numerical simulation tools and they can not be solved reliably and accurately by the commercial software that are available nowadays. Therefore, compared to one-phase flow solvers, special tailor-made numerical schemes have to be developed. Below we address some causes of the very high numerical complexity of this problem class.

The evolution of the unknown interface is determined by the simple dynamic condition (1.17). Unfortunately, it turns out that an accurate numerical approximation of the geometric object representing the interface and its evolution is a very difficult task. This task become even more complicated in cases of geometric singularities such as droplet break up or collision. Although several techniques have been developed, an accurate interface approximation remains a challenging task.

For high Reynolds number, the flow model is strongly nonlinear. Therefore the coupling between fluid dynamics and interface evolution turns out to be strongly nonlinear. This nonlinearity cause difficulties for the construction of accurate numerical schemes for time discretization.

Usually several quantities are discontinuous across the interface. Indeed, for example, the value of density and viscosity have jumps across the interface, since the interface separates two different fluids. Moreover, due to surface tension forces, also the pressure is discontinuous across the interface. In most applications the stress balance (1.18) and a jump in the viscosity across the interface typically induce a discontinuity across the interface of the normal derivative of the velocity. Of particular importance is the precise inclusion

of surface tension terms, and the correct handling of discontinuity jumps in the material properties and in the pressure at the interface, in order to suppress spurious velocities, which are also called parasitic currents. Apart from stationary problems, the unknown interface is changing as a function of time and therefore these discontinuities are moving. The numerical treatment of moving discontinuities often causes severe difficulties.

The full discretization in space and in time results in a very large nonlinear system of equations at each time step. Most of the total computing time is spent solving these large nonlinear systems and therefore it is crucial to use efficient iterative solvers. The efficiency can be largely improved by using special techniques that are adapted to the problem class, in the sense that the solver makes use of certain structural properties of the problem.

1.6 NUMERICAL IMPLEMENTATION

We implement all numerical schemes from scratch in C++ within the DUNE framework, see [15, 14]. DUNE, the Distributed and Unified Numerics Environment is a modular and extensible toolbox for solving partial differential equations with grid-based methods. It supports different schemes based on finite elements, finite volumes and finite differences. We use the following DUNE modules: `dune-common` (build system, infrastructure and foundation classes), `dune-istl` (algebraic solvers), `dune-geometry` (geometric entities), `dune-grid` (grid manager interface) and `dune-fem` (FEM toolbox), see [22]. More information on the library can be found on the official website <https://www.dune-project.org/>.

We actively contributed to the various modules of the library providing upstream patches for new features and bug fixing with more than $4 \cdot 10^4$ lines of changes.

As grid manager we use ALBERTA, see [56], available here <http://www.alberta-fem.de/>. We also use the sparse factorization package SuiteSparse, see [19], available here <http://faculty.cse.tamu.edu/davis/suitesparse.html>.

We implement the scheme described in Chapter 2 as a DUNE module named `dune-geometric-pde`, available here

<https://github.com/magnese/dune-geometric-pde>, while the schemes described in Chapter 3 and Chapter 5 are implemented as a DUNE module called `dune-navier-stokes-two-phase`, available here

<https://github.com/magnese/dune-navier-stokes-two-phase>.

All the meshes are created with the library `Gmsh`, see [32], available here <http://gmsh.info/> and the plots are generated with either `ParaView`, available here <http://www.paraview.org/>, or `Gnuplot`, available here <http://www.gnuplot.info/>.

All the simulations we report on are performed as single thread computations on a Linux cluster equipped with `Ubuntu 14.04.1 LTS` and compiled with `g++ 5.3.0`. The cluster is heterogeneous and consist of 32 computing nodes. Each node is equipped with dual Xeon CPUs containing either 4 or 6 processor cores with frequency ranging from 2.40GHz to 3.00GHz and memory between 16GB and 48GB.

2

GEOMETRIC EVOLUTION EQUATIONS

As starting point, in order to describe the key ideas of the front tracking approach, we consider the simple problem of purely geometric evolution equations. The overall goal of this chapter is to give the reader a brief overview of these time-dependent interface problems, report some useful definitions and theorems from differential geometry and present an efficient numerical method to simulate the evolution of closed hypersurfaces in the setting of the parametric approach. These techniques will be used extensively in the following chapters in order to simulate the unknown interface in the two-phase flow context.

The chapter is organised as follows: in §2.1 we give the definition of geometric evolution equation and in particular we confine our attention to the so called mean curvature flow and surface diffusion; in §2.2 we present some definitions and known results from differential geometry which will be employed throughout the thesis; in §2.3 we report on some fundamental properties of geometric flows, recalling theoretical results already proven in the literature; in §2.4 we introduce, in order to describe the unknown surface, the

front tracking method which is the technique used in all our schemes; in §2.5 we discuss the fully practical finite element approximation for the interface equations which will be used throughout this thesis and we recall, from the literature, the main results about existence, uniqueness and stability; in §2.6 we investigate the equidistribution property and the volume conservation of a semidiscrete variant of the surface diffusion discretization; in §2.7 we reformulate the discrete schemes as algebraic systems of equations and we briefly describe the solution technique adopted; in §2.8 we report on three different experiments in order to show the property of the schemes and of the flows.

2.1 GEOMETRIC PDEs

A geometric evolution equation defines the motion of a hypersurface by prescribing its normal velocity in terms of its geometric quantities. These problems are part of the more general time-dependent interface evolution problems category, where the normal velocity depends also on field quantities evaluated on the analysed hypersurface. A detailed description and analysis can be found in the review article [21].

Interface evolution problems are everywhere in modern physics and engineering. Several typical applications can be found in materials science, such as the mathematical modelling of the morphology of microstructure in order to correctly evaluate the mechanical properties of the material, or in void electro-stress migration, where small voids or cracks contained in metallic materials can change their location and shape according to the presence of surface diffusion and electro-stress loading. Other typical applications, which can be modelled as time-dependent interface evolution problems, are the motion of grain boundaries which separate differing orientations of the same crystalline phase, or solid-liquid interfaces exhibiting dendritic structures in under-cooled solidification. Another research field where these models can be applied is image processing to detect the separation of dark regions from a brighter background and to identify separating contours in order to correctly cluster the objects in the image. Instead, as explained in Chapter 1, we apply these techniques to incompressible two-phase flow problems.

A general geometric evolution equation has the following formulation

$$\vec{\mathcal{V}} \cdot \vec{\nu} = f(\vec{z}, \vec{\nu}, \varkappa) \quad \text{on } \Gamma(t), \quad (2.1)$$

which prescribes the normal velocity $\vec{\mathcal{V}} \cdot \vec{\nu}$ of the interface $\Gamma(t)$ as a function depending on the position \vec{z} , its normal direction $\vec{\nu}$ and the sum of its principal curvatures \varkappa . The evolution equation (2.1) prescribes only the normal velocity therefore the overall goal is to find a family of solutions $\{\Gamma(t)\}_{t \in [0, T]}$ of closed compact and orientable hypersurfaces in \mathbb{R}^d ($d = 2$ for curves, $d = 3$ for surfaces).

The simplest geometric PDE is the one which arises from motion by mean curvature,

$$\vec{\mathcal{V}} \cdot \vec{\nu} = \varkappa \quad \text{on } \Gamma(t). \quad (2.2)$$

This equation describes a surface evolving in such a way that its own normal velocity is equal to the sum of the $d - 1$ principal curvatures of $\Gamma(t)$.

Another important geometric PDE is the one which arises from motion by surface diffusion

$$\vec{\mathcal{V}} \cdot \vec{\nu} = -\Delta_s \varkappa \quad \text{on } \Gamma(t), \quad (2.3)$$

where we use the Laplace–Beltrami operator Δ_s defined by (1.21). In this case the surface normal velocity matches the surface Laplacian of the mean curvature.

For both models, (2.2) and (2.3), it is necessary to prescribe the initial interface $\Gamma(0) = \Gamma_0$ in order to have a well posed problem.

2.2 GEOMETRIC ANALYSIS

The aim of this section is to collect some useful definitions and results from differential geometry. Again we refer to [21], which covers the subject in depth.

A subset $\Gamma \subset \mathbb{R}^d$ is called a C^2 -hypersurface if for each point $\vec{z}_0 \in \Gamma$ there

exists an open set $G \subset \mathbb{R}^d$ containing \vec{z}_0 and a function $g \in C^2(G)$ such that

$$G \cap \Gamma = \{\vec{z} \in G \mid g(\vec{z}) = 0\} \quad \text{and} \quad \nabla g(\vec{z}) \neq 0, \quad \forall \vec{z} \in G \cap \Gamma. \quad (2.4)$$

The tangent space $T_{\vec{z}}\Gamma$ is then the $(d - 1)$ -dimensional linear subspace of \mathbb{R}^d that is orthogonal to $\nabla g(\vec{z})$. It does not depend on the particular function g which is chosen to describe Γ . A C^2 -hypersurface $\Gamma \in \mathbb{R}^d$ is called orientable if there exists a vector-valued function $\vec{\nu} \in C^1(\Gamma, \mathbb{R}^d)$, i.e. $\vec{\nu} \in C^1$ in an open neighbourhood of Γ , such that $\vec{\nu}(\vec{z}) \perp T_{\vec{z}}\Gamma$ and $|\vec{\nu}(\vec{z})| = 1$ for all $\vec{z} \in \Gamma$. In what follows, we shall assume that $\Gamma \subset \mathbb{R}^d$ is an orientable C^2 -hypersurface.

In order to prove some property of the surface gradient (1.19), we employ the notation

$$\nabla_s g(\vec{z}) = (\underline{D}_1 g(\vec{z}), \dots, \underline{D}_d g(\vec{z})) \quad (2.5)$$

for the d components of the surface gradient. Since $\nabla_s g(\vec{z})$ is the orthogonal projection of $\nabla g(\vec{z})$ onto $T_{\vec{z}}\Gamma$, it depends only on the values of g on Γ , and from (1.19) it follows that

$$\nabla_s g(\vec{z}) \cdot \vec{\nu}(\vec{z}) = 0, \quad \vec{z} \in \Gamma. \quad (2.6)$$

Moreover, if \vec{g} is a differentiable vector field, the surface divergence can be written as

$$\nabla_s \cdot \vec{g}(\vec{z}) = \sum_{j=1}^d \underline{D}_j g_j(\vec{z}), \quad \vec{z} \in \Gamma, \quad (2.7)$$

while, if g is twice differentiable in an open neighbourhood of Γ , the surface Laplacian (1.21) can be written as

$$\Delta_s g(\vec{z}) = \nabla_s \cdot \nabla_s g(\vec{z}) = \sum_{i=1}^d \underline{D}_i \underline{D}_i g(\vec{z}), \quad \vec{z} \in \Gamma. \quad (2.8)$$

We assume $\vec{\nu} \in C^1$ in a neighbourhood of Γ so that we may introduce the matrix $\underline{\underline{H}}(\vec{z})$ with components

$$[\underline{\underline{H}}(\vec{z})]_{jk} = -\underline{D}_j \nu_k(\vec{z}), \quad \vec{z} \in \Gamma, \quad (2.9)$$

with $1 \leq j, k \leq n$. It can be shown that $\underline{\underline{H}}(\vec{z})$ is symmetric. Furthermore,

$$\sum_{k=1}^d [\underline{\underline{H}}(\vec{z})]_{jk} \nu_k(\vec{z}) = \sum_{k=1}^d -\underline{D}_j \nu_k(\vec{z}) \nu_k(\vec{z}) = -\frac{1}{2} \underline{D}_j |\vec{\nu}|^2(\vec{z}) = 0, \quad (2.10)$$

since $|\vec{\nu}| = 1$ on Γ . Thus, $\underline{\underline{H}}(\vec{z})$ has one eigenvalue which is equal to zero with corresponding eigenvector $\vec{\nu}(\vec{z})$. The remaining $d - 1$ eigenvalues $\varkappa_1(\vec{z}), \dots, \varkappa_{d-1}(\vec{z})$ are called the principal curvatures of Γ at the point \vec{z} . The mean curvature of Γ at \vec{z} can then be defined as the trace of the matrix $\underline{\underline{H}}(\vec{z})$, that is

$$\varkappa(\vec{z}) = \sum_{j=1}^d [\underline{\underline{H}}(\vec{z})]_{jj} = \sum_{j=1}^{d-1} \varkappa_j(\vec{z}). \quad (2.11)$$

Note that (2.11) differs from the more common definition of mean curvature $\frac{1}{d-1} \sum_{j=1}^{d-1} \varkappa_j$. From (2.9) we derive the following expression for mean curvature:

$$\varkappa(\vec{z}) = -\nabla_s \cdot \vec{\nu}(\vec{z}) \quad \vec{z} \in \Gamma. \quad (2.12)$$

In particular, if Γ is the unit sphere, $\Gamma = \{\vec{z} \in \mathbb{R}^d : |\vec{z}| = 1\}$, and the unit normal field is chosen to point away from Γ , i.e. $\vec{\nu}(\vec{z}) = \vec{z}$, we obtain that $\varkappa = -(d - 1)$, on considering the particular function $g(\vec{z}) = z_j$, with $1 \leq j \leq d$, and observing that $\underline{D}_i z_j = \delta_{ij} - \nu_j \nu_i$. This shows that the mean curvature \varkappa is positive if Γ is curved in the direction of the normal.

Moreover, while the sign of \varkappa depends on the choice of the normal $\vec{\nu}$, the mean curvature vector $\varkappa \vec{\nu}$ is an invariant. By choosing again the particular function $g(\vec{z}) = z_j$, with $1 \leq j \leq d$, in (2.8) and recalling the application of the Laplace-Beltrami operator to each independent variable z_j , we deduce that

$$\Delta_s z_j = - \sum_{i=1}^d \underline{D}_i (\nu_j \nu_i) = -(\nabla_s \cdot \vec{\nu}) \nu_j - \nabla_s \nu_j \cdot \vec{\nu} = \varkappa \nu_j, \quad (2.13)$$

which leads to the identity

$$\Delta_s \vec{\text{id}} = \varkappa \vec{\nu} \quad \text{on } \Gamma(t). \quad (2.14)$$

This identity of differential geometry will be useful at a later stage to obtain

a weak formulation of the surface diffusion and mean curvature problems.

For later use, we also introduce the integration by part formula

Lemma 1. *Let Γ be a hypersurface without boundary. Moreover, let h and g continuously differentiable in a neighbourhood of Γ . Then it holds*

$$\int_{\Gamma} \nabla_s h \cdot \nabla_s g \, d\mathcal{H}^{d-1} = - \int_{\Gamma} h \Delta_s g \, d\mathcal{H}^{d-1}. \quad (2.15)$$

Proof. It holds, from [33, Lemma 16.1],

$$\int_{\Gamma} \underline{D}_i \eta \, d\mathcal{H}^{d-1} = \int_{\Gamma} \eta \varkappa \nu_i \, d\mathcal{H}^{d-1}, \quad 1 \leq i \leq d.$$

Applying it with $\eta = h \underline{D}_i g$, summing for all i and taking into account that $\nabla_s g \cdot \vec{\nu} = 0$ we obtain the desired result. \square

2.3 PROPERTIES OF GEOMETRIC FLOWS

Here we report some fundamental properties of the mean curvature flow and surface diffusion. In order to derive these properties, we need a transport theorem for integrals. Consider a family $\{\Gamma(t)\}_{t \in [0, T]}$ of hypersurfaces that evolve over time. Such a family is called a $C^{2,1}$ -family of hypersurfaces if, for each point $(\vec{z}_0, t_0) \in \mathbb{R}^d \times (0, T)$ with $\vec{z}_0 \in \Gamma_0$, there exists an open set $G \subset \mathbb{R}^d$, $\delta > 0$ and a function $g \in C^{2,1}(G \times (t_0 - \delta, t_0 + \delta))$ such that

$$G \cap \Gamma(t) = \{\vec{z} \in G \mid g(\vec{z}, t) = 0\} \quad \text{and} \quad \nabla g(\vec{z}, t) \neq 0 \quad \forall \vec{z} \in G \cap \Gamma(t). \quad (2.16)$$

Moreover, suppose that each $\Gamma(t)$ is oriented by a unit normal field $\vec{\nu}(\cdot, t) \in C^1(\Gamma(t), \mathbb{R}^d)$ and that $\vec{\nu} \in C^0(\cup_{0 < t < T} \Gamma(t) \times \{t\}, \mathbb{R}^d)$.

We define the velocity at a point (\vec{z}_0, t_0) , with $\vec{z}_0 \in \Gamma(t_0)$, as

$$\vec{\mathcal{V}}(\vec{z}_0, t_0) = \vec{\phi}_t(t_0), \quad \text{with } \vec{\phi}(t_0) = \vec{z}_0, \quad (2.17)$$

where $\vec{\phi} \in C^1((t_0 - \delta, t_0 + \delta), \mathbb{R}^d)$ and $\vec{\phi}(t) \in \Gamma(t)$ for $|t - t_0| < \delta$. It can be shown that $\vec{\mathcal{V}}(\vec{z}_0, t_0)$ is independent of the particular choice of $\vec{\phi}$.

Now take a family $\{\Gamma(t)\}_{t \in [0,T]}$ of evolving hypersurfaces which satisfies the above assumptions and, moreover, suppose that each surface $\Gamma(t)$ is compact. We are interested in the time derivative of certain volume and area integrals. As usual, \mathcal{H}^{d-1} is the $(d-1)$ -dimensional Hausdorff measure and \mathcal{L}^d is the Lebesgue measure in \mathbb{R}^d .

Lemma 2. *Let $g \in C^1(Q)$, where Q is an open set containing*

$$\bigcup_{0 < t < T} \Gamma(t) \times \{t\}. \quad (2.18)$$

Suppose in addition that each surface $\Gamma(t)$ is the boundary of an open bounded subset $\Omega(t) \subset \mathbb{R}^d$. Then

$$\frac{d}{dt} \int_{\Omega(t)} g \, d\mathcal{L}^d = \int_{\Omega(t)} \frac{\partial g}{\partial t} \, d\mathcal{L}^d + \int_{\Gamma(t)} g \vec{\mathcal{V}} \cdot \vec{\nu} \, d\mathcal{H}^{d-1}, \quad (2.19)$$

$$\begin{aligned} \frac{d}{dt} \int_{\Gamma(t)} g \, d\mathcal{H}^{d-1} &= \int_{\Gamma(t)} \frac{\partial g}{\partial t} \, d\mathcal{H}^{d-1} - \int_{\Gamma(t)} g \vec{\mathcal{V}} \cdot \vec{\nu} \kappa \, d\mathcal{H}^{d-1} \\ &\quad + \int_{\Gamma(t)} \frac{\partial g}{\partial \vec{\nu}} \vec{\mathcal{V}} \cdot \vec{\nu} \, d\mathcal{H}^{d-1}. \end{aligned} \quad (2.20)$$

Proof. For a proof, see [21, §2.6, Lemma 2.1]. □

The evolution of an hypersurface subject to the mean curvature flow (2.2) exhibits the interesting area-decreasing property, which is obtained from the following lemma.

Lemma 3. *Let $\Gamma(t)$ be a family of evolving hypersurfaces satisfying (2.2) and assume that each $\Gamma(t)$ is compact. Then*

$$\int_{\Gamma(t)} \kappa^2 \, d\mathcal{H}^{d-1} + \frac{d}{dt} \mathcal{H}^{d-1}(\Gamma(t)) = 0. \quad (2.21)$$

Proof. Choosing $g \equiv 1$ in (2.20) and the evolution law (2.2) yields

$$\int_{\Gamma(t)} (\vec{\mathcal{V}} \cdot \vec{\nu})^2 \, d\mathcal{H}^{d-1} + \frac{d}{dt} \mathcal{H}^{d-1}(\Gamma(t)) = 0,$$

and hence the desired result follows immediately from (2.2). \square

The case $d = 2$ is usually referred to as curve shortening flow.

On the other hand, the evolution of an hypersurface subject to surface diffusion (2.3) conserves, for closed hypersurfaces, the enclosed volume and decreases the area as obtained from the following lemma

Lemma 4. *Let $\Gamma(t)$ be a family of evolving hypersurfaces satisfying (2.3) and assume that each $\Gamma(t)$ is compact and closed. Then*

$$\frac{d}{dt} \mathcal{L}^d(\Omega(t)) = 0, \quad (2.22)$$

$$\int_{\Gamma(t)} |\nabla_s \varkappa|^2 d\mathcal{H}^{d-1} + \frac{d}{dt} \mathcal{H}^{d-1}(\Gamma(t)) = 0. \quad (2.23)$$

Proof. For (2.22), choosing $g \equiv 1$ in (2.19) and the evolution law (2.3) yields that

$$\begin{aligned} \frac{d}{dt} \mathcal{L}^d(\Omega(t)) &= - \int_{\Gamma(t)} \vec{\mathcal{V}} \cdot \vec{\nu} d\mathcal{H}^{d-1} = \int_{\Gamma(t)} \Delta_s \varkappa d\mathcal{H}^{d-1} \\ &= - \int_{\Gamma(t)} \nabla_s \varkappa \cdot \nabla_s 1 d\mathcal{H}^{d-1} = 0, \end{aligned}$$

where the third equality is obtained with the integration by part formula (2.15).

Similarly for (2.23), choosing $g \equiv 1$ in (2.20) and the evolution law (2.3) yields to

$$\frac{d}{dt} \mathcal{H}^{d-1}(\Gamma(t)) = - \int_{\Gamma(t)} \vec{\mathcal{V}} \cdot \vec{\nu} \varkappa d\mathcal{H}^{d-1} = - \int_{\Gamma(t)} |\nabla_s \varkappa|^2 d\mathcal{H}^{d-1}.$$

\square

From a physical point of view, equation (2.21) and (2.23) are associated to the minimization of the surface energy with constant energy density 1 which is defined as

$$E(\Gamma(t)) = \int_{\Gamma(t)} 1 d\mathcal{H}^{d-1}. \quad (2.24)$$

We will see that surface diffusion is not dissimilar to two-phase Stokes flow, in that in the absence of external forces the surface energy (2.24) is decreased and the enclosed volume is conserved.

2.4 FRONT TRACKING APPROACH

We always treat the interface using a front tracking approach, which involves seeking a parametrization of the unknown interface over a reference manifold. More formally, we assume that $(\Gamma(t))_{t \in [0,T]}$ is a sufficiently smooth evolving hypersurface without boundary which is parametrized by $\vec{x}(\cdot, t) : \Upsilon \rightarrow \mathbb{R}^d$, where $\Upsilon \subset \mathbb{R}^d$ is a given reference manifold of the same topological type of the evolving hypersurface $\Gamma(t)$, therefore

$$\Gamma(t) = \vec{x}(\Upsilon, t). \quad (2.25)$$

The position vector $\vec{x}(\cdot, t)$, for every time t , maps a certain point \vec{q} of the reference manifold Υ to its actual position \vec{z} on $\Gamma(t)$. Therefore, using (2.25), we can define the surface velocity (2.17) alternatively as

$$\vec{\mathcal{V}}(\vec{z}, t) := \vec{x}_t(\vec{q}, t) \quad \forall \vec{z} = \vec{x}(\vec{q}, t) \in \Gamma(t). \quad (2.26)$$

The position vector $\vec{x}(\cdot, t)$ is one unknown of the problem and, once computed, the evolution of $\Gamma(t)$ is fully determined. Moreover, all the geometrical quantities of the hypersurface, e.g. curvature, can be expressed as derivatives of the parametrization.

It is worth to notice that, at the discrete level, the reference manifold Υ is never used. Indeed, instead of computing the position vector $\vec{x}(\cdot, t)$, the unknown variable is the displacement that the previous discrete interface is subject to. This can be viewed as setting, at every time step, a new reference manifold which correspond to the actual hypersurface configuration.

2.5 FINITE ELEMENT APPROXIMATION

The finite element discretization which we use is based on the seminal paper [25] and we refer to the ones described in [6, 7, 8]. We use a different notation in order to be consistent with [10] and [2].

Putting together the mean curvature flow (2.2) with the identity (2.14) we obtain the following system of PDEs

$$\vec{\mathcal{V}} \cdot \vec{\nu} = \kappa \quad \text{on } \Gamma(t), \quad (2.27\text{a})$$

$$\kappa \vec{\nu} = \Delta_s \text{id} \quad \text{on } \Gamma(t). \quad (2.27\text{b})$$

Analogously, the surface diffusion problem (2.3) can be rewritten as a system of second order equations

$$\vec{\mathcal{V}} \cdot \vec{\nu} = -\Delta_s \kappa \quad \text{on } \Gamma(t), \quad (2.28\text{a})$$

$$\kappa \vec{\nu} = \Delta_s \text{id} \quad \text{on } \Gamma(t). \quad (2.28\text{b})$$

In both problems (2.27a–b) and (2.28a–b) we impose the initial condition $\Gamma(0) = \Gamma_0$.

We consider the partitioning $0 = t_0 < t_1 < \dots < t_{M-1} < t_M = T$ of $[0, T]$ into possibly variable time steps $\tau_m := t_{m+1} - t_m$, $m = 0, \dots, M - 1$.

In order to define the parametric finite element spaces on Γ^m , we assume that $\Gamma^m = \bigcup_{j=1}^{J_\Gamma} \overline{\sigma_j^m}$, where $\{\sigma_j^m\}_{j=1}^{J_\Gamma}$ is a family of mutually disjoint open $(d - 1)$ -simplices with vertices $\{\vec{q}_k^m\}_{k=1}^{K_\Gamma}$. We also define the function space

$$\underline{V}(\Gamma^m) := \{\vec{\chi} \in [C(\Gamma^m)]^d : \vec{\chi}|_{\sigma_j^m} \in \mathcal{P}_1(\sigma_j^m), j = 1, \dots, J_\Gamma\} =: [W(\Gamma^m)]^d, \quad (2.29)$$

where $W(\Gamma^m) \subset H^1(\Gamma^m)$ is the space of scalar continuous piecewise linear functions on Γ^m , with $\{\chi_k^m\}_{k=1}^{K_\Gamma}$ denoting the standard basis of $W(\Gamma^m)$ and with $\mathcal{P}_k(\sigma^m)$ denoting the space of polynomials of degree k on σ^m .

The new surface Γ^{m+1} is parametrized with respect to Γ^m using the parametrization $\vec{X}^{m+1} \in \underline{V}(\Gamma^m)$, so that $\Gamma^{m+1} = \vec{X}^{m+1}(\Gamma^m)$.

Then the finite element approximation from [6, 8] of the mean curvature flow, which is based on the variational formulation (2.27a–b), is given as follows. Let Γ^0 be an approximation to $\Gamma(0)$. For $m = 0, \dots, M - 1$, find $(\vec{X}^{m+1}, \kappa^{m+1}) \in \underline{V}(\Gamma^m) \times W(\Gamma^m)$ such that

$$\left\langle \frac{\vec{X}^{m+1} - \vec{X}^m}{\tau_m}, \chi \vec{\nu}^m \right\rangle_{\Gamma^m}^h - \left\langle \kappa^{m+1}, \chi \right\rangle_{\Gamma^m}^h = 0 \quad \forall \chi \in W(\Gamma^m), \quad (2.30a)$$

$$\left\langle \kappa^{m+1} \vec{\nu}^m, \vec{\eta} \right\rangle_{\Gamma^m}^h + \left\langle \nabla_s \vec{X}^{m+1}, \nabla_s \vec{\eta} \right\rangle_{\Gamma^m} = 0 \quad \forall \vec{\eta} \in \underline{V}(\Gamma^m), \quad (2.30b)$$

and set $\Gamma^{m+1} = \vec{X}^{m+1}(\Gamma^m)$. We observe that (2.30a–b) is a linear scheme in that it leads to a linear system of equations for the unknowns $(\vec{X}^{m+1}, \kappa^{m+1})$ at each time level. Here $\langle \cdot, \cdot \rangle_{\Gamma^m}$ is the L^2 inner product over the current polyhedral surface

$$\langle u, v \rangle_{\Gamma^m} = \int_{\Gamma^m} uv \, d\mathcal{H}^{d-1}, \quad \forall u, v \in L^2(\Gamma^m), \quad (2.31)$$

and similarly for $\vec{u}, \vec{v} \in [L^2(\Gamma^m)]^d$. In addition, $\langle \cdot, \cdot \rangle_{\Gamma^m}^h$ is a mass lumped inner product with the vertices of each triangle of the mesh as quadrature points. If $v, w \in L^\infty(\Gamma^m)$ are piecewise continuous, with possible jumps across the edges of $\{\sigma_j^m\}_{j=1}^{J_\Gamma}$, we define the mass lumped inner product $\langle \cdot, \cdot \rangle_{\Gamma^m}^h$ as

$$\langle v, w \rangle_{\Gamma^m}^h := \frac{1}{d} \sum_{j=1}^{J_\Gamma} \mathcal{H}^{d-1}(\sigma_j^m) \sum_{k=1}^d (v w)((\vec{q}_{j_k}^m)^-), \quad (2.32)$$

where $\{\vec{q}_{j_k}^m\}_{k=1}^d$ are the vertices of σ_j^m , and where we define the limit $v((\vec{q}_{j_k}^m)^-) := \lim_{\sigma_j^m \ni \vec{p} \rightarrow \vec{q}_{j_k}^m} v(\vec{p})$. We naturally extend (2.32) to vector valued functions. The mass lumped inner product is used in (2.30b) to obtain good mesh properties, see §2.6 below. For stability it is then necessary to use mass lumping on the first term in (2.30a), which makes it the natural choice also for the second term. In fact, choosing $\chi = \kappa^{m+1}$ in (2.30a) and $\vec{\eta} = \vec{X}^{m+1} - \vec{X}^m|_{\Gamma^m}$ in (2.30b), and summing the two equations, yields that

$$\left\langle \nabla_s \vec{X}^{m+1}, \nabla_s (\vec{X}^{m+1} - \vec{X}^m) \right\rangle_{\Gamma^m} + \tau_m \langle \kappa^{m+1}, \kappa^{m+1} \rangle_{\Gamma^m}^h = 0.$$

Using the inequality

$$\left\langle \nabla_s \vec{X}^{m+1}, \nabla_s (\vec{X}^{m+1} - \vec{X}^m) \right\rangle_{\Gamma^m} \geq \mathcal{H}^{d-1}(\Gamma^{m+1}) - \mathcal{H}^{d-1}(\Gamma^m), \quad (2.33)$$

see e.g. [7, Proof of Theorem 2.3] and [8, Proof of Theorem 2.2] for the proofs for $d = 2$ and $d = 3$, respectively, we obtain

$$\mathcal{H}^{d-1}(\Gamma^{m+1}) + \tau_m \langle \kappa^{m+1}, \kappa^{m+1} \rangle_{\Gamma^m}^h \leq \mathcal{H}^{d-1}(\Gamma^m),$$

and, summing for $m = 0, \dots, k-1$, we finally obtain

$$\mathcal{H}^{d-1}(\Gamma^k) + \sum_{m=0}^{k-1} \tau_m \langle \kappa^{m+1}, \kappa^{m+1} \rangle_{\Gamma^m}^h \leq \mathcal{H}^{d-1}(\Gamma^0),$$

for $k = 1, \dots, M$. Hence the scheme (2.30a–b) is unconditionally stable.

Similarly, the finite element approximation for the surface diffusion problem (2.28a–b) is analogous to the one obtained for the mean curvature flow with the linear system (2.30a–b) changed to

$$\left\langle \frac{\vec{X}^{m+1} - \vec{X}^m}{\tau_m}, \chi \vec{\nu}^m \right\rangle_{\Gamma^m}^h - \left\langle \nabla_s \kappa^{m+1}, \nabla_s \chi \right\rangle_{\Gamma^m} = 0 \quad \forall \chi \in W(\Gamma^m), \quad (2.34a)$$

$$\left\langle \kappa^{m+1} \vec{\nu}^m, \vec{\eta} \right\rangle_{\Gamma^m}^h + \left\langle \nabla_s \vec{X}^{m+1}, \nabla_s \vec{\eta} \right\rangle_{\Gamma^m} = 0 \quad \forall \vec{\eta} \in \underline{V}(\Gamma^m). \quad (2.34b)$$

If Γ^m is an hypersurface without self-intersections, then there exists a unique solution $(\vec{X}^{m+1}, \kappa^{m+1}) \in \underline{V}(\Gamma^m) \times W(\Gamma^m)$ to the systems (2.30a–b) and (2.34a–b). See [8, Theorem 2.1] for the complete proof. Moreover, similarly to before, choosing $\chi = \kappa^{m+1}$ in (2.34a) and $\vec{\eta} = \vec{X}^{m+1} - \text{id}|_{\Gamma^m}$ in (2.34b), yields that

$$\mathcal{H}^{d-1}(\Gamma^k) + \sum_{m=0}^{k-1} \tau_m \langle \nabla_s \kappa^{m+1}, \nabla_s \kappa^{m+1} \rangle_{\Gamma^m} \leq \mathcal{H}^{d-1}(\Gamma^0),$$

for $k = 1, \dots, M$. Hence also the scheme (2.34a–b) is unconditionally stable.

2.6 SEMIDISCRETE SCHEME

As shown in [7, Remark 2.3] and [8, §4], it is worthwhile to consider continuous-in-time semidiscrete versions of the aforementioned finite element schemes.

Firstly, let $(\Gamma^h(t))_{t \in [0, T]}$ be a family of polyhedral surfaces, with outer normal $\vec{\nu}^h(t)$. We also define the piecewise linear finite element spaces $W(\Gamma^h(t))$ and $\underline{V}(\Gamma^h(t))$, with $\{\chi_k^h(\cdot, t)\}_{k=1}^{K_\Gamma}$ denoting the standard basis of the former. Hence $\chi_k^h(\vec{q}_l^h(t), t) = \delta_{kl}$ for all $k, l \in \{1, \dots, K_\Gamma\}$ and $t \in [0, T]$, where $\{\vec{q}_k^h(t)\}_{k=1}^{K_\Gamma}$ are the vertices of $\Gamma^h(t)$. Similarly to (2.26), we can then define the discrete velocity

$$\vec{\mathcal{V}}^h(\vec{z}, t) := \sum_{k=1}^{K_\Gamma} \left[\frac{d}{dt} \vec{q}_k^h(t) \right] \chi_k^h(\vec{z}, t) \in \underline{V}(\Gamma^h(t)), \quad (2.35)$$

see e.g. [11, (3.3)].

Then, the finite element approximation of the surface diffusion problem (2.34a–b) can be replaced by the following one. Given $\Gamma^h(0)$, for $t \in (0, T]$ find $\Gamma^h(t)$ and $\kappa^h \in W(\Gamma^h(t))$ such that

$$\langle \vec{\mathcal{V}}^h, \chi \vec{\nu}^h \rangle_{\Gamma^h(t)} - \langle \nabla_s \kappa^h, \nabla_s \chi \rangle_{\Gamma^h(t)} = 0 \quad \forall \chi \in W(\Gamma^h(t)), \quad (2.36a)$$

$$\langle \kappa^h \vec{\nu}^h, \vec{\eta} \rangle_{\Gamma^h(t)} + \langle \nabla_s \text{id}, \nabla_s \vec{\eta} \rangle_{\Gamma^h(t)} = 0 \quad \forall \vec{\eta} \in \underline{V}(\Gamma^h(t)), \quad (2.36b)$$

where we always integrate over the current surface $\Gamma^h(t)$, with normal $\vec{\nu}^h(t)$. In addition, $\langle \cdot, \cdot \rangle_{\Gamma^h(t)}^{(h)}$ is the continuous-in-time counterpart of $\langle \cdot, \cdot \rangle_{\Gamma^m}^{(h)}$ where Γ^m is replaced by $\Gamma^h(t)$.

Firstly, choosing $\chi \equiv 1$ in (2.36a) and recalling the mass lumped inner product (2.32), we have that

$$0 = \langle \vec{\mathcal{V}}^h, \vec{\nu}^h \rangle_{\Gamma^h(t)}^h = \int_{\Gamma^h(t)} \vec{\mathcal{V}}^h \cdot \vec{\nu}^h \, d\mathcal{H}^{d-1} = \frac{d}{dt} \mathcal{L}^d(\Omega^h(t)), \quad (2.37)$$

where $\Omega^h(t) \subset \mathbb{R}^d$ is open bounded set whose boundary is given by $\Gamma^h(t)$. Therefore, the continuous-in-time semidiscrete version of the aforementioned surface diffusion finite element scheme conserves the enclosed volume exactly. It does not appear possible to prove the conservation of the enclosed volume

for the fully discrete scheme but, from all the numerical simulations performed in this thesis, we experimentally observe that the enclosed volume is approximately preserved, and that the volume loss tends to zero as $\tau \rightarrow 0$.

We now investigate an equidistribution property for the scheme (2.34a–b), see [7, Remark 2.4] and [50, Theorem 3.2] for more details.

Theorem 5. *Let $d = 2$ and let $\{\vec{q}_k^h\}_{k=1}^{K_\Gamma^h}$ denote the sequentially ordered vertices on $\Gamma^h(t)$. Let $(\Gamma^h(t), \kappa^h(t))$ be a solution to the system (2.36a–b), and set $\vec{h}_k(t) := \vec{q}_k^h(t) - \vec{q}_{k-1}^h(t)$. Then it holds that*

$$|\vec{h}_k(t)| = |\vec{h}_{k-1}(t)| \quad \text{if } \vec{h}_k(t) \nparallel \vec{h}_{k-1}(t) \quad k = 1, \dots, K_\Gamma^h. \quad (2.38)$$

Proof. Choosing $\vec{\eta} = (\vec{h}_{k+1} + \vec{h}_k) \phi_k \in \underline{V}(\Gamma^h(t))$ in (2.36b), where $\{\phi_l\}_{l=1}^{K_\Gamma^h}$ denote the basis functions of $W(\Gamma^h(t))$, and recalling 2.32, we obtain that for $k = 1, \dots, K_\Gamma^h$

$$0 = \langle \nabla_s \vec{\text{id}}, \nabla_s [(\vec{h}_{k+1} + \vec{h}_k) \phi_k] \rangle_{\Gamma^h(t)}. \quad (2.39)$$

The integral in (2.39) can now be easily computed by hand, since the support of ϕ_k is given by $[\vec{q}_{k-1}, \vec{q}_k] \cup [\vec{q}_k, \vec{q}_{k+1}]$. On noting that $\nabla_s \phi_k = \frac{1}{|\vec{h}_k|}$ on $[\vec{q}_{k-1}, \vec{q}_k]$ and $\nabla_s \phi_k = -\frac{1}{|\vec{h}_{k+1}|}$ on $[\vec{q}_k, \vec{q}_{k+1}]$, we then deduce that

$$\left[\frac{\vec{h}_{k+1}}{|\vec{h}_{k+1}|} - \frac{\vec{h}_k}{|\vec{h}_k|} \right] \cdot (\vec{h}_{k+1} + \vec{h}_k) = 0. \quad (2.40)$$

It immediately follows from (2.40) that

$$(|\vec{h}_{k+1}| - |\vec{h}_k|)(|\vec{h}_{k+1}| |\vec{h}_k| - \vec{h}_{k+1} \cdot \vec{h}_k) = 0, \quad (2.41)$$

which implies either $|\vec{h}_k(t)| = |\vec{h}_{k-1}(t)|$ or $\vec{h}_k(t) \parallel \vec{h}_{k-1}(t)$. \square

Therefore, in the $d = 2$ case, the continuous-in-time semidiscrete version of (2.34a–b) will always equidistribute the vertices provided that they are not locally parallel. Only a fully implicit scheme can achieve that also on the fully discrete level, see [9], but a fully implicit scheme is very expensive without

providing better accuracy for the solution. Nevertheless, in practice we see that for the semi-implicit schemes (2.27a–b) and (2.28a–b) over a number of time steps, the vertices are moved tangentially so that they will eventually be equidistributed.

Instead in [8, §4] the case $d = 3$ has been thoroughly investigated showing that the continuous-in-time semidiscrete versions of (2.30a–b) and (2.34a–b) guarantee good mesh properties. Again, in practice, we notice that it is true for the fully discrete schemes.

We want to stress the fact that this equidistribution property is only achievable because (2.2) and (2.3) prescribe the velocity only in the normal direction while, in the tangential direction, the mesh vertices are free to move. Moreover, if instead of the mass lumped inner product (2.32) it is used an exact quadrature, an analogue of the equidistribution properties cannot be established.

2.7 ALGEBRAIC FORMULATION

As regards the mean curvature flow, (2.30a–b), the corresponding algebraic system of equations can be written as

$$\begin{pmatrix} M_\Gamma & -\frac{1}{\tau_m} \vec{N}_\Gamma^T \\ \vec{N}_\Gamma & \vec{A}_\Gamma \end{pmatrix} \begin{pmatrix} \kappa^{m+1} \\ \delta \vec{X}^{m+1} \end{pmatrix} = \begin{pmatrix} 0 \\ -\vec{A}_\Gamma \vec{X}^m \end{pmatrix}, \quad (2.42)$$

while, for the system of equations describing the surface diffusion, (2.34a–b), the algebraic system is

$$\begin{pmatrix} A_\Gamma & -\frac{1}{\tau_m} \vec{N}_\Gamma^T \\ \vec{N}_\Gamma & \vec{A}_\Gamma \end{pmatrix} \begin{pmatrix} \kappa^{m+1} \\ \delta \vec{X}^{m+1} \end{pmatrix} = \begin{pmatrix} 0 \\ -\vec{A}_\Gamma \vec{X}^m \end{pmatrix}, \quad (2.43)$$

where we define the interface displacement $\delta \vec{X}^{m+1} = \vec{X}^{m+1} - \vec{X}^m$ and we have used the trivial identity $\vec{A}_\Gamma \vec{X}^{m+1} = \vec{A}_\Gamma \vec{X}^m + \vec{A}_\Gamma \delta \vec{X}^{m+1}$. We can notice that the only difference between the above systems occurs in the upper-left entry of the matrix.

The entries of the matrix are defined as

$$[M_\Gamma]_{kl} := \langle \chi_k^m, \chi_l^m \rangle_{\Gamma^m}^h, \quad (2.44)$$

$$[\vec{N}_\Gamma]_{kl} := \langle \chi_k^m \vec{\nu}^m, \chi_l^m \rangle_{\Gamma^m}^h, \quad (2.45)$$

$$[A_\Gamma]_{kl} := \langle \nabla_s \chi_k^m, \nabla_s \chi_l^m \rangle_{\Gamma^m}, \quad (2.46)$$

where $\{\chi_k^m\}$ are the basis functions of the finite element space of piecewise linear continuous functions $W(\Gamma^m)$ and

$$[\vec{A}_\Gamma]_{kl} := [A_\Gamma]_{kl} \underline{\underline{\text{id}}}. \quad (2.47)$$

Since the entries of A_Γ can be assembled by summing up the contributions to (2.46) over all the elements, and since each contribution is a planar integral in \mathbb{R}^d with the integrand being a constant, we notice that (2.46) can be assembled in a straightforward way.

The linear systems (2.42) and (2.43) are invertible under a suitable assumption on the triangulation at each time step, see [8]. The algebraic systems (2.42) and (2.43) are very small also for fine meshes. Therefore they can be solved very efficiently with a sparse factorization package such as UMFPACK, see [19]. Instead, in [8], the authors use a more involving Schur complement approach to solve the linear systems (2.42) and (2.43).

2.8 NUMERICAL RESULTS

Here we report on several numerical examples to benchmark the schemes (2.30a–b) and (2.34a–b).

With a view towards our numerical simulations, we want to be able to compute the initial mean curvature κ^0 of an initial surface Γ^0 in order to plot it. This initial mean curvature κ^0 can be computed by solving the algebraic system

$$\begin{pmatrix} 0 & -\vec{N}_\Gamma^T \\ \vec{N}_\Gamma & \vec{A}_\Gamma \end{pmatrix} \begin{pmatrix} \kappa^0 \\ \delta \vec{X}^0 \end{pmatrix} = \begin{pmatrix} 0 \\ -\vec{A}_\Gamma \vec{X}^0 \end{pmatrix}, \quad (2.48)$$

which is a discretization of the stationary geometric PDE

$$\vec{\mathcal{V}} \cdot \vec{\nu} = 0 \quad \text{on } \Gamma(t), \quad (2.49)$$

in the flavour of (2.30a–b) for the mean curvature flow (2.2).

2.8.1 MEAN CURVATURE FLOW WITH A SPHERE AS INITIAL CONDITION

As regards the mean curvature flow, the simplest case is to use a sphere as the initial condition, see [43]. In this case, the solution to the geometric evolution equation is known in closed form and it is a shrinking sphere. Let $\Gamma(t) = \{\vec{z} \in \mathbb{R}^d : |\vec{z} - \vec{z}_0| = r(t)\}$ be a sphere centred in \vec{z}_0 with radius $r(t)$ and mean curvature $\kappa(t) = -\frac{d-1}{r(t)}$. Its unit outer normal is given by $\vec{\nu}(\vec{z}) = \frac{\vec{z} - \vec{z}_0}{r(t)}$. It is straightforward to derive that $\vec{\mathcal{V}} \cdot \vec{\nu} = r'(t)$ on $\Gamma(t)$, so that $\Gamma(t)$ moves by mean curvature provided that $r'(t) = -\frac{d-1}{r(t)}$. The solution of this separable variable ODE is easily given by

$$r(t) = \sqrt{r_0^2 - 2(d-1)t}, \quad t \in [0, t_e], \quad (2.50)$$

where $\Gamma(0) = \{\vec{z} \in \mathbb{R}^d : |\vec{z} - \vec{z}_0| = r_0\}$ and

$$t_e = \frac{r_0^2}{2(d-1)} \quad (2.51)$$

is the so called extinction time. It is worth noting that the surface $\Gamma(t)$ shrinks to a point as $t \rightarrow t_e$.

Figure 2.1 shows the evolution of a sphere with initial radius $r_0 = 5$ at time $t = 0$, $t = 2$, $t = 4$ and $t = 6$ respectively. In this case, the extinction time, is $t_e = 6.25$. The number of mesh elements is $J_\Gamma = 3026$ and the time step is constant and equal to $\tau = 10^{-3}$.

Figure 2.2 shows in red the average radius length over time of the discrete spheres Γ^m , while the blue plot is the exact radius computed from the analytical solution.

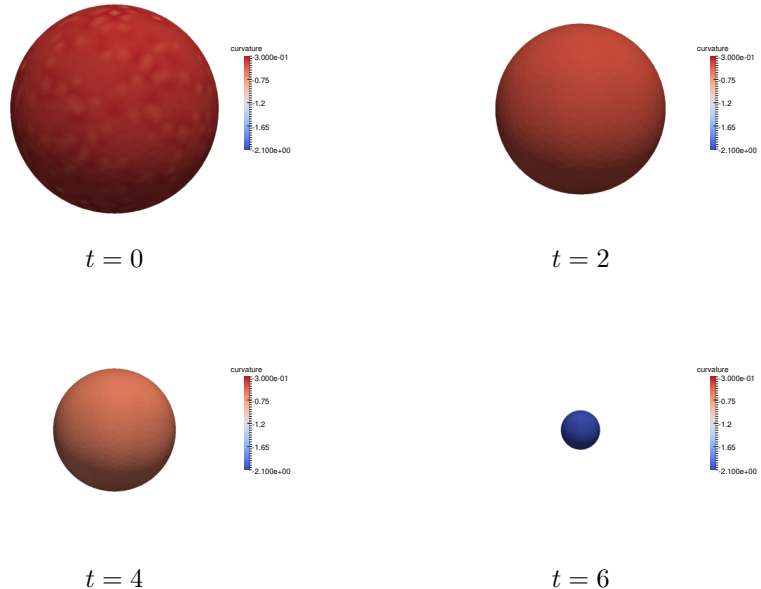


Figure 2.1: Surface evolution of a sphere of initial radius $r_0 = 5$ subject to mean curvature flow.

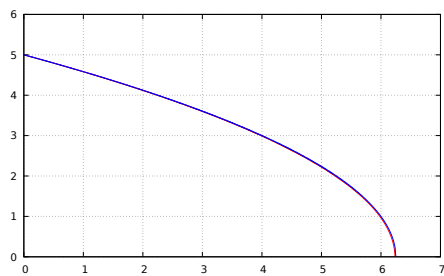


Figure 2.2: Average radius of a sphere of initial radius $r_0 = 5$ subject to mean curvature flow. In blue the analytical solution while in red the computed one.

2.8.2 EQUIDISTRIBUTION PROPERTY

In order to show the equidistribution property of the scheme, we simulate the evolution, under surface diffusion, of a circle of radius $r_0 = 0.5$ with a very poor initial mesh quality. Indeed, the initial curve consists of a semi-circle and a single additional node on the periphery of the circle for a total number of mesh elements equal to $J_\Gamma = 32$.

Figure 2.3 shows the mesh evolution at time $t = 0$, $t = 0.05$, $t = 0.25$ and $t = 10$ respectively with a constant time step equal to $\tau = 10^{-2}$. One can clearly see that although the true solution, which is a circle, is reached very quickly, in the remaining time the vertices are continually moved tangentially, which results in a further decrease in the ratio

$$\frac{\max_{\sigma \in \Gamma^m} \mathcal{H}^{d-1}(\sigma)}{\min_{\sigma \in \Gamma^m} \mathcal{H}^{d-1}(\sigma)}, \quad (2.52)$$

which approaches the optimal value 1. This mesh quality indicator is simply the ratio between the maximum and minimum segment of the hypersurface.

In Figure 2.4 we see that the equidistribution velocity is varying inversely with the size of τ . For example, when $\tau = 10^{-4}$, the equidistribution is reached almost instantaneously.

2.8.3 SURFACE DIFFUSION WITH A CAGE AS INITIAL CONDITION

Our last simulation is inspired by the test in [8, Fig. 15]. We investigate the evolution of a cage subject to surface diffusion. The dimensions of the initial surface are $4 \times 4 \times 4$, with the region enclosed by $\Gamma(0)$ given as the union of 12 cuboids of dimension $4 \times 1 \times 1$.

Figure 2.5 shows the cage evolution at time $t = 0$, $t = 0.2$, $t = 0.4$ and $t = 0.6$ respectively. The number of mesh elements is $J_\Gamma = 3816$ and the time step is constant and equal to $\tau = 10^{-2}$.

At time $t = 0.6$ a topological change is encountered when the six holes of the surface are about to close to form a hollow ball. Figure 2.6 shows a section

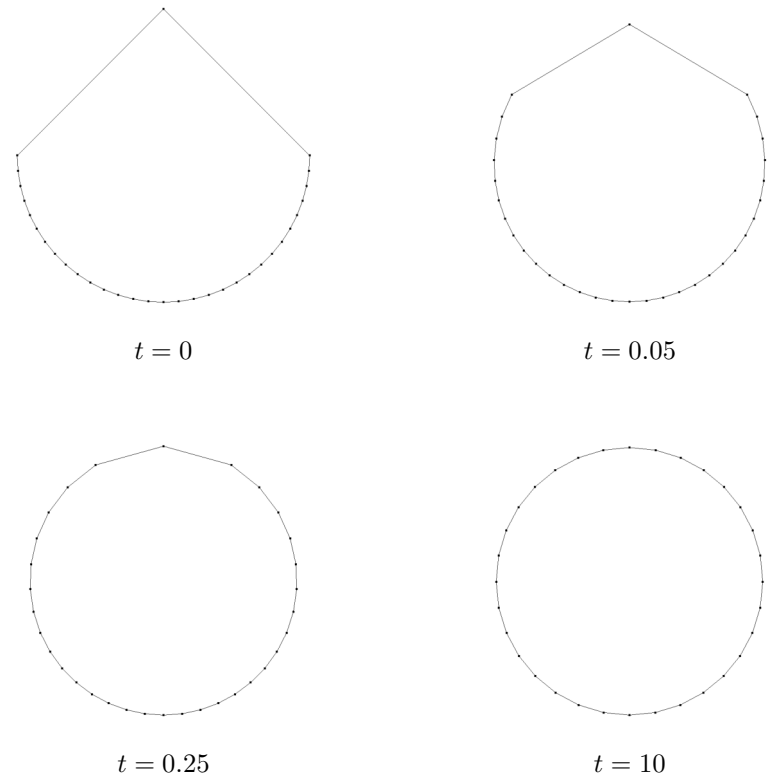


Figure 2.3: Surface evolution of a circle of initial radius $r_0 = 0.5$ subject to surface diffusion.

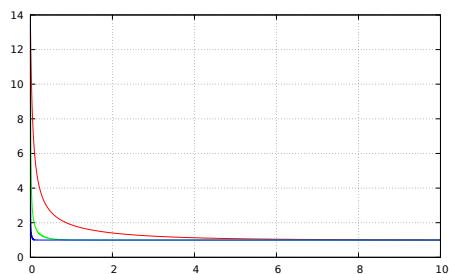


Figure 2.4: Time evolution of the ratio $\frac{\max_{\sigma \in \Gamma^m} \mathcal{H}^{d-1}(\sigma)}{\min_{\sigma \in \Gamma^m} \mathcal{H}^{d-1}(\sigma)}$ for a circle of initial radius $r_0 = 0.5$ subject to surface diffusion. In red $\tau = 10^{-2}$, in green $\tau = 10^{-3}$ and in blue $\tau = 10^{-4}$.

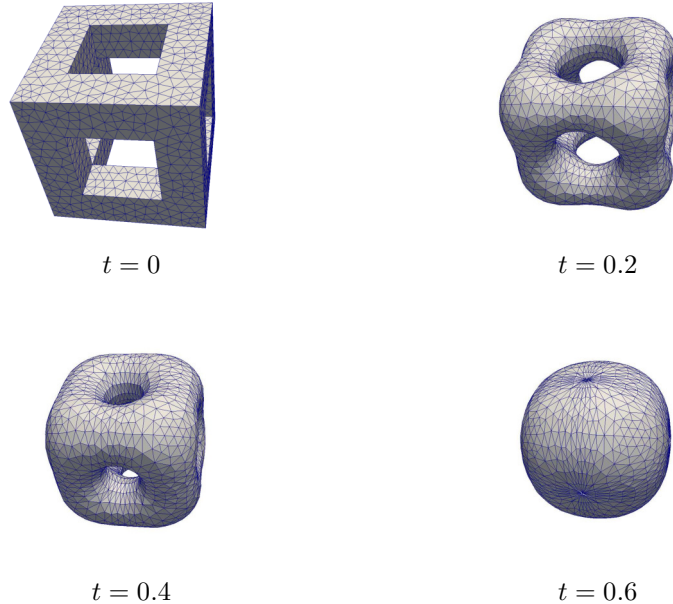


Figure 2.5: Surface evolution of a cage $4 \times 4 \times 4$ subject to surface diffusion.

of this hollow ball. This hollow ball is still topological equivalent with the cage, i.e. genus is 5. Indeed we can see 6 very long and thin strands of elements, which connect the inner ball with the outer ball. A topological change breaks the front tracking approach since the reference manifold Γ^m is not topological compatible with the unknown surface Γ^{m+1} . In practice, it is possible to apply some heuristic algorithms for the detection of topological changes, such as the merging of surfaces into one or the pinching-off of one surface from another, which can lead to a modified surface mesh that can be handled again with the parametric approach, see [55].

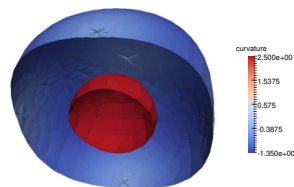


Figure 2.6: Section at $t = 0.6$ of a cage $4 \times 4 \times 4$ subject to surface diffusion.

Finally, Figure 2.7 shows the evolution of the surface energy (2.24) over time. As expected, see (2.23), this energy is monotonically decreasing.

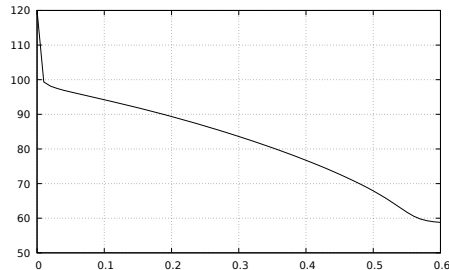


Figure 2.7: Surface energy evolution $\mathcal{H}^{d-1}(\Gamma^m)$ of a cage $4 \times 4 \times 4$ subject to surface diffusion.

3

FINITE ELEMENT APPROXIMATION FOR TWO-PHASE STOKES FLOW

We now propose a novel finite element approximation for incompressible two-phase Stokes flow that naturally avoids spurious velocities. Our scheme uses a fitted approach with piecewise linear parametric finite elements to describe the moving discrete interface and employs standard velocity and pressure finite element spaces in the bulk. This chapter is extensively based on a paper we wrote, see [2].

The chapter is organised as follows: in §3.1 we state the mathematical model for the incompressible two-phase Stokes flow; in §3.2 we derive the weak formulation on which our finite element approximation is going to be based; in §3.3 we show an energy bound and the volume conservation for the weak problem; in §3.4 we present our fitted finite element discretization; in §3.5 we outline the main differences between a fitted and an unfitted approach; in §3.6 we prove the existence and uniqueness of the discrete approximation; in §3.7 we demonstrate that our scheme is unconditionally stable; in §3.8 we show some properties of stationary solutions which will be investigated in the numerical experiments; in §3.9 we investigate the equidistribution property

and the volume conservation of a semidiscrete variant of the scheme; in §3.10 we describe the arising linear systems; in §3.11 we explain the Schur complement approach used to solve the algebraic system and the preconditioners adopted; in §3.12 we discuss the mesh generation process together with the smoothing and remeshing procedures used to preserve the mesh quality.

3.1 MATHEMATICAL MODEL

We consider two-phase Stokes flow in a given domain $\Omega \subset \mathbb{R}^d$, where $d = 2$ or $d = 3$. As already described in §1.1, the domain Ω contains two different immiscible, incompressible, viscous fluids (liquid-liquid or liquid-gas) which for all $t \in [0, T]$ occupy time dependent regions $\Omega_+(t)$ and $\Omega_-(t) := \Omega \setminus \overline{\Omega}_+(t)$ and which are separated by an interface $(\Gamma(t))_{t \in [0, T]}$, $\Gamma(t) \subset \Omega$. In this thesis, we always treat interfaces formed by closed hypersurfaces, as illustrated in Figure 1.1 for dimension $d = 2$.

The interface $\Gamma(t)$ is described with the same technique used in the approximation of mean curvature flow and surface diffusion, see Chapter 2. More precisely, we use a front tracking approach, see §2.4, which parametrize the unknown interface $\Gamma(t)$ as $\vec{x}(\cdot, t) : \Upsilon \rightarrow \mathbb{R}^d$ where $\Upsilon \subset \mathbb{R}^d$ is a given reference manifold such that $\Gamma(t) = \vec{x}(\Upsilon, t)$. We always require that the evolving hypersurface is sufficiently smooth and without boundary. Therefore, the velocity $\vec{\mathcal{V}}$ of $\Gamma(t)$ is defined by the equation (2.26) which we report here for the benefit of the reader

$$\vec{\mathcal{V}}(\vec{z}, t) := \vec{x}_t(\vec{q}, t) \quad \forall \vec{z} = \vec{x}(\vec{q}, t) \in \Gamma(t),$$

where $\vec{\mathcal{V}} \cdot \vec{\nu}$ is the normal velocity of the evolving hypersurface $\Gamma(t)$ and $\vec{\nu}(t)$ is the unit normal on $\Gamma(t)$ pointing into $\Omega_+(t)$.

The fluid dynamics in the bulk domain Ω is governed by the two-phase Stokes model (1.15a–b) which describes the velocity \vec{u} and pressure p fields of the fluid. The velocity and stress tensor, see (1.1), needs to be coupled across the free surface $\Gamma(t)$ and therefore we impose the interface conditions (1.16), (1.25) and (1.17). Let $\partial\Omega$ be partitioned as $\partial\Omega = \partial_1\Omega \cup \partial_2\Omega$ with

$\partial_1\Omega \cap \partial_2\Omega = \emptyset$. We impose, on $\partial_1\Omega$, the Dirichlet condition $\vec{u} = \vec{g}$ and, on $\partial_2\Omega$, the free-slip condition $\vec{u} \cdot \vec{n} = 0$ and $\underline{\sigma} \vec{n} \cdot \vec{t} = 0$, $\forall \vec{t} \in \{\vec{n}\}^\perp$, with \vec{n} denoting the outer unit normal of $\partial\Omega$ and $\{\vec{n}\}^\perp := \{\vec{t} \in \mathbb{R}^d : \vec{t} \cdot \vec{n} = 0\}$. Finally, to close the system, we prescribe the initial data $\Gamma(0) = \Gamma_0$. Therefore the total system can be rewritten as follows:

$$-2\mu \nabla \cdot \underline{D}(\vec{u}) + \nabla p = \vec{f} \quad \text{in } \Omega_\pm(t), \quad (3.1a)$$

$$\nabla \cdot \vec{u} = 0 \quad \text{in } \Omega_\pm(t), \quad (3.1b)$$

$$\vec{u} = \vec{g} \quad \text{on } \partial_1\Omega, \quad (3.1c)$$

$$\vec{u} \cdot \vec{n} = 0, \quad \underline{\sigma} \vec{n} \cdot \vec{t} = 0 \quad \forall \vec{t} \in \{\vec{n}\}^\perp \quad \text{on } \partial_2\Omega, \quad (3.1d)$$

$$[\vec{u}]_-^+ = \vec{0} \quad \text{on } \Gamma(t), \quad (3.1e)$$

$$[2\mu \underline{D}(\vec{u}) \cdot \vec{\nu} - p \vec{\nu}]_-^+ = -\gamma \varkappa \vec{\nu} \quad \text{on } \Gamma(t), \quad (3.1f)$$

$$(\vec{\mathcal{V}} - \vec{u}) \cdot \vec{\nu} = 0 \quad \text{on } \Gamma(t), \quad (3.1g)$$

$$\Gamma(0) = \Gamma_0, \quad (3.1h)$$

where $\mu(t) = \mu_+ \mathcal{X}_{\Omega_+(t)} + \mu_- \mathcal{X}_{\Omega_-(t)}$, with $\mu_\pm \in \mathbb{R}_{>0}$, denotes the dynamic viscosities in the two phases, $\underline{D}(\vec{u}) := \frac{1}{2} (\nabla \vec{u} + (\nabla \vec{u})^T)$ is the rate-of-deformation tensor, \vec{f} is a possible forcing term, $\gamma > 0$ is the surface tension coefficient and \varkappa denotes the mean curvature of $\Gamma(t)$. See Chapter 1 for more details.

3.2 WEAK FORMULATION

In order to obtain a weak formulation, we define the function spaces, for a given $\vec{b} \in [H^1(\Omega)]^d$,

$$\mathbb{U}(\vec{b}) := \{\vec{\phi} \in [H^1(\Omega)]^d : \vec{\phi} = \vec{b} \quad \text{on } \partial_1\Omega, \quad \vec{\phi} \cdot \vec{n} = 0 \quad \text{on } \partial_2\Omega\},$$

$$\mathbb{P} := L^2(\Omega),$$

$$\tilde{\mathbb{P}} := \{\eta \in \mathbb{P} : \int_{\Omega} \eta \, d\mathcal{L}^d = 0\},$$

and let, as usual, (\cdot, \cdot) and $\langle \cdot, \cdot \rangle_{\Gamma(t)}$ denote the L^2 -inner products on Ω and $\Gamma(t)$, respectively. In addition, we let \mathcal{L}^d and \mathcal{H}^{d-1} denote the Lebesgue measure in \mathbb{R}^d and the $(d-1)$ -dimensional Hausdorff measure, respectively.

We also need a weak form of the differential geometry identity (2.14), which can be obtained by multiplying (2.14) with a test function and performing integration by parts, recall (2.15), leading to

$$\langle \varkappa \vec{\nu}, \vec{\eta} \rangle_{\Gamma(t)} + \langle \nabla_s \text{id}, \nabla_s \vec{\eta} \rangle_{\Gamma(t)} = 0 \quad \forall \vec{\eta} \in [H^1(\Gamma(t))]^d. \quad (3.2)$$

Moreover, on noting (1.1) and (1.25), we have that

$$\begin{aligned} \int_{\Omega_+(t) \cup \Omega_-(t)} (\nabla \cdot \underline{\underline{\sigma}}) \cdot \vec{\xi} \, d\mathcal{L}^d &= - (\underline{\underline{\sigma}}, \nabla \vec{\xi}) - \langle [\underline{\underline{\sigma}} \vec{\nu}]_+^\perp, \vec{\xi} \rangle_{\Gamma(t)} \\ &= - (2\mu \underline{\underline{D}}(\vec{u}) - p \text{id}, \nabla \vec{\xi}) - \langle [2\mu \underline{\underline{D}}(\vec{u}) \cdot \vec{\nu} - p \vec{\nu}]_+^\perp, \vec{\xi} \rangle_{\Gamma(t)} \\ &= (p \text{id}, \nabla \vec{\xi}) - 2(\mu \underline{\underline{D}}(\vec{u}), \nabla \vec{\xi}) + \gamma \langle \varkappa \vec{\nu}, \vec{\xi} \rangle_{\Gamma(t)} \\ &= (p, \nabla \cdot \vec{\xi}) - 2(\mu \underline{\underline{D}}(\vec{u}), \underline{\underline{D}}(\vec{\xi})) + \gamma \langle \varkappa \vec{\nu}, \vec{\xi} \rangle_{\Gamma(t)} \end{aligned} \quad (3.3)$$

for all $\vec{\xi} \in \mathbb{U}(\vec{0})$. We notice that in the first equality we used the standard integration by parts on $\Omega_+(t)$ and $\Omega_-(t)$ separately. Hence a possible weak formulation of (3.1a–h) is given as follows. Given $\Gamma(0) = \Gamma_0$, for almost all $t \in (0, T)$ find $\Gamma(t)$ and $(\vec{u}, p, \varkappa) \in \mathbb{U}(\vec{g}) \times \tilde{\mathbb{P}} \times H^1(\Gamma(t))$ such that

$$2(\mu \underline{\underline{D}}(\vec{u}), \underline{\underline{D}}(\vec{\xi})) - (p, \nabla \cdot \vec{\xi}) - \gamma \langle \varkappa \vec{\nu}, \vec{\xi} \rangle_{\Gamma(t)} = (\vec{f}, \vec{\xi}) \quad \forall \vec{\xi} \in \mathbb{U}(\vec{0}), \quad (3.4a)$$

$$(\nabla \cdot \vec{u}, \varphi) = 0 \quad \forall \varphi \in \tilde{\mathbb{P}}, \quad (3.4b)$$

$$\langle \vec{\mathcal{V}} - \vec{u}, \chi \vec{\nu} \rangle_{\Gamma(t)} = 0 \quad \forall \chi \in H^1(\Gamma(t)), \quad (3.4c)$$

$$\langle \varkappa \vec{\nu}, \vec{\eta} \rangle_{\Gamma(t)} + \langle \nabla_s \text{id}, \nabla_s \vec{\eta} \rangle_{\Gamma(t)} = 0 \quad \forall \vec{\eta} \in [H^1(\Gamma(t))]^d \quad (3.4d)$$

holds for almost all times $t \in (0, T]$. Here we have observed that if $p \in \mathbb{P}$ is part of a solution to (3.1a–h), then so is $p+c$ for an arbitrary $c \in \mathbb{R}$. We also note the natural compatibility condition $\int_{\partial_1 \Omega} \vec{g} \cdot \vec{n} \, d\mathcal{H}^{d-1} = 0$ for a solution to (3.4a–d) to exist.

We finally observe that an alternative weak formulation can be obtained using directly the vector quantity $\vec{\kappa} := \varkappa \vec{\nu}$ in the identity (2.14), see [25, 5, 30]. Instead, consistently with Chapter 2, we follow the approach introduced in [7] for $d = 2$ and in [8] for $d = 3$, which treats the mean curvature as a scalar and we treat it separately from the normal $\vec{\nu}$, because this approach leads to

good mesh properties and to smaller algebraic systems.

3.3 ENERGY BOUND AND VOLUME CONSERVATION

It is straightforward to show an a priori energy bound, in the absence of external forces, and a volume conservation property for the system (3.4a–d). For the former, we use (2.20) and we obtain

$$\frac{d}{dt} \mathcal{H}^{d-1}(\Gamma(t)) = - \left\langle \boldsymbol{\varkappa}, \vec{\mathcal{V}} \cdot \vec{\nu} \right\rangle_{\Gamma(t)}. \quad (3.5)$$

Hence, in the case $\vec{g} = \vec{0}$, on choosing $\vec{\xi} = \vec{u} \in \mathbb{U}(\vec{0})$ in (3.4a), and noting (3.4b,c), we obtain that

$$\gamma \frac{d}{dt} \mathcal{H}^{d-1}(\Gamma(t)) = -\gamma \left\langle \boldsymbol{\varkappa} \vec{\nu}, \vec{u} \right\rangle_{\Gamma(t)} = -2 \left(\mu \underline{D}(\vec{u}), \underline{D}(\vec{u}) \right) + (\vec{f}, \vec{u}), \quad (3.6)$$

and so in the absence of outer forces, the interfacial energy is monotonically decreasing.

In order to show the volume conservation property, we use (2.19) to have that

$$\frac{d}{dt} \mathcal{L}^d(\Omega_-(t)) = \left\langle \vec{\mathcal{V}}, \vec{\nu} \right\rangle_{\Gamma(t)}. \quad (3.7)$$

Hence it follows immediately from the incompressibility condition (3.4b) and (3.4c), using the divergence theorem, that

$$\frac{d}{dt} \mathcal{L}^d(\Omega_-(t)) = \left\langle \vec{u}, \vec{\nu} \right\rangle_{\Gamma(t)} = \int_{\Omega_-(t)} \nabla \cdot \vec{u} \, d\mathcal{L}^d = 0. \quad (3.8)$$

It will be our aim to introduce a fitted finite element approximation for two-phase Stokes flow that satisfies discrete analogous of (3.6) and (3.8).

3.4 FINITE ELEMENT APPROXIMATION

We consider the partitioning $0 = t_0 < t_1 < \dots < t_{M-1} < t_M = T$ of $[0, T]$ into possibly variable time steps $\tau_m := t_{m+1} - t_m$, $m = 0, \dots, M - 1$. Moreover, let \mathcal{T}^m , $\forall m \geq 0$, be a regular partitioning of the domain Ω into disjoint open simplices o_j^m , $j = 1, \dots, J_\Omega^m$. From now on, the domain Ω which we consider is the polyhedral domain defined by the triangulation \mathcal{T}^m . On \mathcal{T}^m we define the finite element spaces

$$S_k^m := \{\chi \in C(\bar{\Omega}) : \chi|_{o^m} \in \mathcal{P}_k(o^m) \quad \forall o^m \in \mathcal{T}^m\}, \quad k \in \mathbb{N},$$

where $\mathcal{P}_k(o^m)$ denotes the space of polynomials of degree k on o^m . Moreover, S_0^m is the space of piecewise constant functions on \mathcal{T}^m . For later use, we also define \vec{I}_k^m to be the standard interpolation operator onto $[S_k^m]^d$.

Let $\mathbb{U}^m(\vec{g}) \subset \mathbb{U}(\vec{I}_k^m \vec{g})$ and $\mathbb{P}^m \subset \mathbb{P}$ be the finite element spaces we use for the approximation of velocity and pressure, and let $\tilde{\mathbb{P}}^m := \mathbb{P}^m \cap \tilde{\mathbb{P}}$. The spaces $(\mathbb{U}^m(\vec{0}), \mathbb{P}^m)$ satisfy the LBB inf-sup condition if there exists a constant $C_0 \in \mathbb{R}_{>0}$, independent of \mathcal{T}^m , such that

$$\inf_{\varphi \in \tilde{\mathbb{P}}^m} \sup_{\vec{\xi} \in \mathbb{U}^m(\vec{0})} \frac{(\varphi, \nabla \cdot \vec{\xi})}{\|\varphi\|_0 \|\vec{\xi}\|_1} \geq C_0 > 0, \quad (3.9)$$

see [35, p. 114]. Here $\|\cdot\|_0 := (\cdot, \cdot)^{\frac{1}{2}}$ and $\|\cdot\|_1 := \|\cdot\|_0 + \|\nabla \cdot \|\|_0$ denote the L^2 -norm and the H^1 -norm on Ω , respectively. Throughout this thesis, if not otherwise stated, we will assume that $\mathcal{X}_{\Omega_-^m} \in \mathbb{P}^m$. Then, for $d = 2$, possible pairs $(\mathbb{U}^m(\vec{0}), \mathbb{P}^m)$ that satisfy (3.9) are P2–P0 and P2–(P1+P0), i.e. we set $\mathbb{U}^m(\vec{0}) = [S_2^m]^d \cap \mathbb{U}(\vec{0})$ and either $\mathbb{P}^m = S_0^m$ or $S_1^m + S_0^m$. We note that the choice P2–(P1+P0) requires the weak constraint that all simplices have a vertex in Ω , see [17]. For $d = 3$, pairs of spaces that satisfy $\mathcal{X}_{\Omega_-^m} \in \mathbb{P}^m$ and (3.9) are the P3–(P2+P0) element, see [17], or stabilized spaces such as P1_{face bubble}–P0, see [16, Remark 8.7.1], which is also called the SMALL element. With a view towards our numerical simulations, we also introduce the pairs P2–P1^{dgr}, where the space P1^{dgr} is a space of polynomials of order 1 defined in the two subdomains Ω_-^m and Ω_+^m . This space is equivalent to

a P1 space which is continuous everywhere except across the interface Γ^m . With this choice of space, the discrete scheme falls in the category of XFEM, extended FEM, since the pressure space is enriched by adding additional degrees of freedom for the nodes on the interface in order to better capture the discontinuity of the pressure.

In this thesis we consider a fitted finite element approximation for the evolution of the interface $\Gamma(t)$. Let $\Gamma^m \subset \mathbb{R}^d$ be a $(d - 1)$ -dimensional polyhedral surface approximating the closed surface $\Gamma(t_m)$, $m = 0, \dots, M$. Let Ω_+^m denote the exterior of Γ^m and let Ω_-^m be the interior of Γ^m , where we assume that Γ^m has no self-intersections. Then $\Omega = \Omega_-^m \cup \Gamma^m \cup \Omega_+^m$, and the fitted nature of our method implies that

$$\overline{\Omega_+^m} = \bigcup_{o \in \mathcal{T}_+^m} \overline{o} \quad \text{and} \quad \overline{\Omega_-^m} = \bigcup_{o \in \mathcal{T}_-^m} \overline{o}, \quad (3.10)$$

where $\mathcal{T}^m = \mathcal{T}_+^m \cup \mathcal{T}_-^m$ and $\mathcal{T}_+^m \cap \mathcal{T}_-^m = \emptyset$. Let $\vec{\nu}^m$ denote the piecewise constant unit normal to Γ^m such that $\vec{\nu}^m$ points into Ω_+^m .

In order to define the parametric finite element spaces on Γ^m , we proceed analogously to the mean curvature flow and surface diffusion problems, see §2.5. Therefore we assume that $\Gamma^m = \bigcup_{j=1}^{J_\Gamma} \overline{\sigma_j^m}$, where $\{\sigma_j^m\}_{j=1}^{J_\Gamma}$ is a family of mutually disjoint open $(d - 1)$ -simplices with vertices $\{\vec{q}_k^m\}_{k=1}^{K_\Gamma}$. Then we define $\underline{V}(\Gamma^m) := \{\vec{\chi} \in [C(\Gamma^m)]^d : \vec{\chi}|_{\sigma_j^m} \in \mathcal{P}_1(\sigma_j^m), j = 1, \dots, J_\Gamma\} =: [W(\Gamma^m)]^d$, where $W(\Gamma^m) \subset H^1(\Gamma^m)$ is the space of scalar continuous piecewise linear functions on Γ^m , with $\{\chi_k^m\}_{k=1}^{K_\Gamma}$ denoting the standard basis of $W(\Gamma^m)$. As usual, we parametrize the new surface Γ^{m+1} over Γ^m using a parametrization $\vec{X}^{m+1} \in \underline{V}(\Gamma^m)$, so that $\Gamma^{m+1} = \vec{X}^{m+1}(\Gamma^m)$. Finally, let $\langle \cdot, \cdot \rangle_{\Gamma^m}^h$ be the mass lumped inner product on Γ^m , see (2.32), and let $\langle \cdot, \cdot \rangle_{\Gamma^m}$ denote the standard L^2 -inner product on Γ^m .

Then our finite element approximation, which is based on the variational formulation (3.4a–d), assumes the following formulation. Let Γ^0 be an approximation to the initial interface $\Gamma(0)$. For $m = 0, \dots, M - 1$, find

$(\vec{U}^{m+1}, P^{m+1}, \vec{X}^{m+1}, \kappa^{m+1}) \in \mathbb{U}^m(\vec{g}) \times \widetilde{\mathbb{P}}^m \times \underline{V}(\Gamma^m) \times W(\Gamma^m)$ such that

$$2 \left(\mu^m \underline{\underline{D}}(\vec{U}^{m+1}), \underline{\underline{D}}(\vec{\xi}) \right) - \left(P^{m+1}, \nabla \cdot \vec{\xi} \right) \\ - \gamma \left\langle \kappa^{m+1} \vec{\nu}^m, \vec{\xi} \right\rangle_{\Gamma^m} = \left(\vec{f}^{m+1}, \vec{\xi} \right) \quad \forall \vec{\xi} \in \mathbb{U}^m(\vec{0}), \quad (3.11a)$$

$$\left(\nabla \cdot \vec{U}^{m+1}, \varphi \right) = 0 \quad \forall \varphi \in \widetilde{\mathbb{P}}^m, \quad (3.11b)$$

$$\left\langle \frac{\vec{X}^{m+1} - \text{id}}{\tau_m}, \chi \vec{\nu}^m \right\rangle_{\Gamma^m}^h - \left\langle \vec{U}^{m+1}, \chi \vec{\nu}^m \right\rangle_{\Gamma^m} = 0 \quad \forall \chi \in W(\Gamma^m), \quad (3.11c)$$

$$\left\langle \kappa^{m+1} \vec{\nu}^m, \vec{\eta} \right\rangle_{\Gamma^m}^h + \left\langle \nabla_s \vec{X}^{m+1}, \nabla_s \vec{\eta} \right\rangle_{\Gamma^m} = 0 \quad \forall \vec{\eta} \in \underline{V}(\Gamma^m) \quad (3.11d)$$

and set $\Gamma^{m+1} = \vec{X}^{m+1}(\Gamma^m)$. Here we have defined $\vec{f}^{m+1}(\cdot) := \vec{I}_2^m \vec{f}(\cdot, t_{m+1})$ and

$$\mu^m = \mu_+ \mathcal{X}_{\Omega_+^m} + \mu_- \mathcal{X}_{\Omega_-^m} \in S_0^m. \quad (3.12)$$

We observe that (3.11a–d) is a linear scheme in that it leads to a coupled linear system of equations for the unknowns $(\vec{U}^{m+1}, P^{m+1}, \vec{X}^{m+1}, \kappa^{m+1})$ at each time level. We also note that the scheme (3.11a–d), in the context of an unfitted finite element approximation, has been considered in [10]. In particular, most of the theoretical results presented in the following are a direct consequence of the results in [10].

3.5 FITTED AND UNFITTED APPROACH

The key difference between [10] and our approach is that the former uses an unfitted approach while the latter adopts a fitted one. In Figure 3.1, from [10, Fig. 1], is shown an example of fitted and unfitted interface meshes for a circular interface. In the fitted approach, the interface mesh is made up of edges, in 2d, or faces, in 3d, of elements belonging to the bulk mesh. This means that there is a strong coupling between the bulk mesh and interface mesh. This is a very intuitive approach to treat the problem. Discontinuity jumps in the material properties and in the pressure are captured naturally. In particular, we do not need to employ an XFEM-type extension of standard bulk pressure spaces. Moreover, there is no need to transport quantities from the interface to the bulk, or vice versa. On the other hand, it is not possible

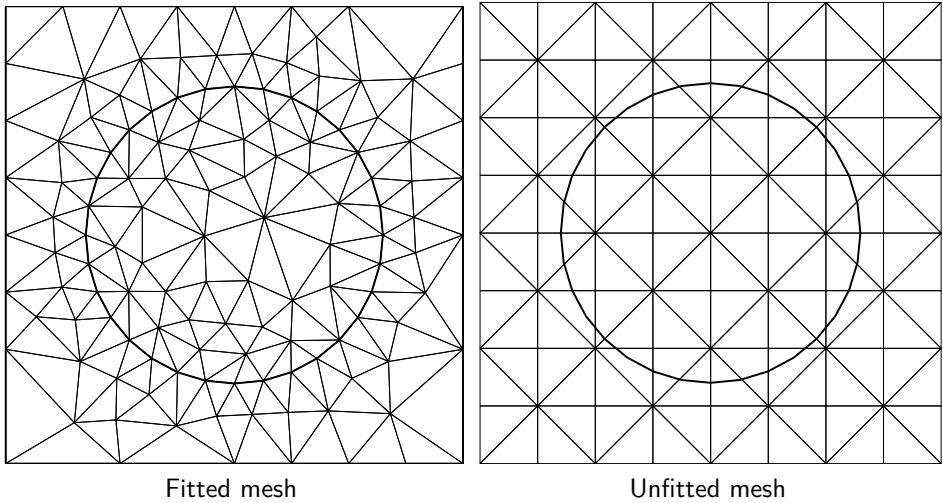


Figure 3.1: Fitted and unfitted meshes for a circular interface.

to locally refine the bulk mesh close to the interface without modifying the number of elements of the interface. Also, every interface deformation corresponds to a bulk deformation, which means that smoothing and remeshing techniques need to be employed in order to preserve the bulk mesh quality.

Instead, in the unfitted approach, the interface mesh is completely independent from the bulk mesh. In particular, there exist bulk elements which are cut by the interface elements. For this reason there is no need to remesh or deform the bulk mesh in order to preserve the correspondence with the interface. Moreover, standard strategies for refinement and coarsening can be employed for the bulk mesh. Since the bulk mesh is immutable, its quality is preserved without the need of smoothing techniques. The downside of this approach is that the quantities computed on the bulk mesh, such as velocity and pressure, need to be interpolated in order to have their values on the interface. This also requires finding the intersections between the interface mesh and the bulk mesh at every time step. Finally, it is necessary to use some XFEM-type extension in order to capture the discontinuity of quantities of interest across the interface.

3.6 EXISTENCE AND UNIQUENESS OF A DISCRETE SOLUTION

Theorem 6. Let $m \in \{0, \dots, M - 1\}$ and let $(\mathbb{U}^m(\vec{0}), \mathbb{P}^m)$ satisfy the LBB condition (3.9). Then there exists a unique solution $(\vec{U}^{m+1}, P^{m+1}, \vec{X}^{m+1}, \kappa^{m+1}) \in \mathbb{U}^m(\vec{g}) \times \tilde{\mathbb{P}}^m \times \underline{V}(\Gamma^m) \times W(\Gamma^m)$ to (3.11a-d).

Proof. As the system (3.11a-d) is linear, existence follows from uniqueness. In order to establish the latter, we consider the system: Find $(\vec{U}, P, \vec{X}, \kappa) \in \mathbb{U}^m(\vec{0}) \times \tilde{\mathbb{P}}^m \times \underline{V}(\Gamma^m) \times W(\Gamma^m)$ such that

$$2 \left(\mu^m \underline{\underline{D}}(\vec{U}), \underline{\underline{D}}(\vec{\xi}) \right) - \left(P, \nabla \cdot \vec{\xi} \right) - \gamma \left\langle \kappa \vec{\nu}^m, \vec{\xi} \right\rangle_{\Gamma^m} = 0 \quad \forall \vec{\xi} \in \mathbb{U}^m(\vec{0}), \quad (3.13a)$$

$$\left(\nabla \cdot \vec{U}, \varphi \right) = 0 \quad \forall \varphi \in \tilde{\mathbb{P}}^m, \quad (3.13b)$$

$$\left\langle \vec{X}, \chi \vec{\nu}^m \right\rangle_{\Gamma^m}^h - \tau_m \left\langle \vec{U}, \chi \vec{\nu}^m \right\rangle_{\Gamma^m} = 0 \quad \forall \chi \in W(\Gamma^m), \quad (3.13c)$$

$$\left\langle \kappa \vec{\nu}^m, \vec{\eta} \right\rangle_{\Gamma^m}^h + \left\langle \nabla_s \vec{X}, \nabla_s \vec{\eta} \right\rangle_{\Gamma^m} = 0 \quad \forall \vec{\eta} \in \underline{V}(\Gamma^m). \quad (3.13d)$$

Choosing $\vec{\xi} = \vec{U}$ in (3.13a), $\varphi = P$ in (3.13b), $\chi = \gamma \kappa$ in (3.13c) and $\vec{\eta} = \gamma \vec{X}$ in (3.13d) yields that

$$2 \tau_m \left(\mu^m \underline{\underline{D}}(\vec{U}), \underline{\underline{D}}(\vec{U}) \right) + \gamma \left\langle \nabla_s \vec{X}, \nabla_s \vec{X} \right\rangle_{\Gamma^m} = 0, \quad (3.14)$$

which implies that $\underline{\underline{D}}(\vec{U}) = \underline{\underline{0}}$. We know that the kernel of $\underline{\underline{D}}$ is the space of rigid motions

$$RM = \{ \vec{\alpha} + \mathcal{A} \vec{z} : \vec{\alpha} \in \mathbb{R}^d, \mathcal{A} \text{ antisymmetric matrix in } \mathbb{R}^{d \times d} \}, \quad (3.15)$$

see [47]. Given that $\vec{U} \in RM$, in particular we have that $\vec{U}(\vec{z})$ is linear in \vec{z} . Moreover, $\vec{U} \in \mathbb{U}^m(\vec{0})$ means that $\vec{U}(\vec{z}) = \vec{0}$ for every corner \vec{z} of Ω . Therefore $\vec{U}(\vec{z}) = \vec{0}$ for all $\vec{z} \in \Omega$. In addition, it holds that \vec{X} is equal to a constant on Γ^m , which satisfies, on recalling (3.13c) and $\vec{U} = \vec{0}$, that

$$\left\langle \vec{X}, \chi \vec{\nu}^m \right\rangle_{\Gamma^m}^h = 0 \quad \forall \chi \in W(\Gamma^m). \quad (3.16)$$

It was shown in [8, Proof of Theorem 2.1] that if Γ^m has no self-intersections,

then (3.16) immediately yields that $\vec{X} = \vec{0}$. As $\Gamma^m = \partial\Omega_-^m$ is the boundary of an open domain, we always assume that it does not self-intersect, and hence we obtain that $\vec{X} = \vec{0}$. This means that (3.13d) reduces to

$$\langle \kappa \vec{\nu}^m, \vec{\eta} \rangle_{\Gamma^m}^h = 0 \quad \forall \vec{\eta} \in \underline{V}(\Gamma^m). \quad (3.17)$$

Let $\vec{\omega}^m \in \underline{V}(\Gamma^m)$ be the mass-lumped L^2 -projection of $\vec{\nu}^m$ onto $\underline{V}(\Gamma^m)$, i.e. $\langle \vec{\omega}^m, \vec{\varphi} \rangle_{\Gamma^m}^h = \langle \vec{\nu}^m, \vec{\varphi} \rangle_{\Gamma^m}^h = \langle \vec{\nu}^m, \vec{\varphi} \rangle_{\Gamma^m}$ for all $\vec{\varphi} \in \underline{V}(\Gamma^m)$. It is easy to see that $\vec{\omega}^m(\vec{q}_k^m) \neq \vec{0}$ for all $k = 1, \dots, K_\Gamma$, because Γ^m does not self-intersect. Then it follows from choosing $\vec{\eta} = \vec{\omega}^m$ in (3.17) that

$$0 = \langle \kappa \vec{\nu}^m, \vec{\omega}^m \rangle_{\Gamma^m}^h = \langle \vec{\nu}^m, \vec{\pi}^m[\kappa \vec{\omega}^m] \rangle_{\Gamma^m} = \langle \vec{\omega}^m, \vec{\pi}^m[\kappa \vec{\omega}^m] \rangle_{\Gamma^m}^h = \left\langle \kappa, |\vec{\omega}^m|^2 \right\rangle_{\Gamma^m}^h,$$

and so $\kappa = 0 \in W(\Gamma^m)$. Finally, it follows from (3.13a) with $\vec{U} = \vec{0}$ and $\kappa = 0$, on recalling (3.9), that $P = 0$. Hence there exists a unique solution $(\vec{U}^{m+1}, P^{m+1}, \vec{X}^{m+1}, \kappa^{m+1}) \in \mathbb{U}^m(\vec{g}) \times \tilde{\mathbb{P}}^m \times \underline{V}(\Gamma^m) \times W(\Gamma^m)$ to (3.11a–d). \square

We note that if $(\mathbb{U}^m(\vec{0}), \mathbb{P}^m)$ does not satisfy the LBB condition (3.9), then existence and uniqueness of the solution $(\vec{U}^{m+1}, \vec{X}^{m+1}, \kappa^{m+1})$ to a reduced system, where the pressure P^{m+1} is eliminated, can be shown. More precisely, let

$$\mathbb{U}_0^m(\vec{g}) := \{ \vec{U} \in \mathbb{U}^m(\vec{g}) : (\nabla \cdot \vec{U}, \varphi) = 0 \quad \forall \varphi \in \mathbb{P}^m \}. \quad (3.18)$$

Then any solution $(\vec{U}^{m+1}, P^{m+1}, \vec{X}^{m+1}, \kappa^{m+1}) \in \mathbb{U}^m(\vec{g}) \times \tilde{\mathbb{P}}^m \times \underline{V}(\Gamma^m) \times W(\Gamma^m)$ to (3.11a–d) is such that $(\vec{U}^{m+1}, \vec{X}^{m+1}, \kappa^{m+1}) \in \mathbb{U}_0^m(\vec{g}) \times \underline{V}(\Gamma^m) \times W(\Gamma^m)$ with

$$2 \left(\mu^m \underline{D}(\vec{U}^{m+1}), \underline{D}(\vec{\xi}) \right) - \gamma \left\langle \kappa^{m+1} \vec{\nu}^m, \vec{\xi} \right\rangle_{\Gamma^m} = \left(\vec{f}^{m+1}, \vec{\xi} \right) \quad \forall \vec{\xi} \in \mathbb{U}_0^m(\vec{0}), \quad (3.19a)$$

$$\left\langle \frac{\vec{X}^{m+1} - \text{id}}{\tau_m}, \chi \vec{\nu}^m \right\rangle_{\Gamma^m}^h - \left\langle \vec{U}^{m+1}, \chi \vec{\nu}^m \right\rangle_{\Gamma^m} = 0 \quad \forall \chi \in W(\Gamma^m), \quad (3.19b)$$

$$\left\langle \kappa^{m+1} \vec{\nu}^m, \vec{\eta} \right\rangle_{\Gamma^m}^h + \left\langle \nabla_s \vec{X}^{m+1}, \nabla_s \vec{\eta} \right\rangle_{\Gamma^m} = 0 \quad \forall \vec{\eta} \in \underline{V}(\Gamma^m) \quad (3.19c)$$

Theorem 7. Let $m \in \{0, \dots, M-1\}$ and let $\mathbb{U}_0^m(\vec{g})$ be non-empty. Then

there exists a unique solution $(\vec{U}^{m+1}, \vec{X}^{m+1}, \kappa^{m+1}) \in \mathbb{U}_0^m(\vec{g}) \times \underline{V}(\Gamma^m) \times W(\Gamma^m)$ to (3.19a–c).

Proof. As $\mathbb{U}_0^m(\vec{0})$ is a subspace of $\mathbb{U}^m(\vec{0})$, existence to the linear system (3.19a–c) follows from uniqueness, which is easy to show. In fact, similarly to the proof of Theorem 6 we obtain (3.14) and hence the desired uniqueness result. \square

3.7 STABILITY

We now demonstrate that the scheme (3.11a–d) satisfies an energy estimate, which corresponds to the bound (3.6) in the continuous case. In particular, we obtain an unconditional stability result for our scheme.

Theorem 8. *Let $\vec{g} = \vec{0}$. Moreover let $m \in \{0, \dots, M - 1\}$ and let $(\vec{U}^{m+1}, P^{m+1}, \vec{X}^{m+1}, \kappa^{m+1}) \in \mathbb{U}^m(\vec{0}) \times \tilde{\mathbb{P}}^m \times \underline{V}(\Gamma^m) \times W(\Gamma^m)$ be a solution to (3.11a–d). Then*

$$\begin{aligned} & \gamma \mathcal{H}^{d-1}(\Gamma^{m+1}) + 2 \tau_m (\mu^m \underline{\underline{D}}(\vec{U}^{m+1}), \underline{\underline{D}}(\vec{U}^{m+1})) \\ & \leq \gamma \mathcal{H}^{d-1}(\Gamma^m) + \tau_m (\vec{f}^{m+1}, \vec{U}^{m+1}). \end{aligned} \quad (3.20)$$

In addition, let $\{t_k\}_{k=0}^M$ be an arbitrary partitioning of $[0, T]$.

Then it holds that

$$\begin{aligned} & \gamma \mathcal{H}^{d-1}(\Gamma^{m+1}) + 2 \sum_{k=0}^m \tau_k (\mu^k \underline{\underline{D}}(\vec{U}^{k+1}), \underline{\underline{D}}(\vec{U}^{k+1})) \\ & \leq \gamma \mathcal{H}^{d-1}(\Gamma^0) + \sum_{k=0}^m \tau_k (\vec{f}^{k+1}, \vec{U}^{k+1}) \end{aligned} \quad (3.21)$$

for $m = 0, \dots, M - 1$.

Proof. Choosing $\vec{\xi} = \vec{U}^{m+1} \in \mathbb{U}^m(\vec{0})$ in (3.11a), $\varphi = P^{m+1} \in \tilde{\mathbb{P}}^m$ in (3.11b),

$\chi = \gamma \kappa^{m+1}$ in (3.11c) and $\vec{\eta} = \gamma (\vec{X}^{m+1} - \vec{\text{id}}|_{\Gamma^m})$ in (3.11d) yields that

$$\begin{aligned} 2\tau_m & \left(\mu^m \underline{\underline{D}}(\vec{U}^{m+1}), \underline{\underline{D}}(\vec{U}^{m+1}) \right) + \gamma \left\langle \nabla_s \vec{X}^{m+1}, \nabla_s (\vec{X}^{m+1} - \vec{X}^m) \right\rangle_{\Gamma^m} \\ & = \tau_m \left(\vec{f}^{m+1}, \vec{U}^{m+1} \right). \end{aligned}$$

Hence (3.20) follows immediately, where we have used (2.33). The desired result (3.21) immediately follows from (3.20). \square

3.8 DISCRETE STATIONARY SOLUTIONS

If the solution $(\vec{U}^{m+1}, P^{m+1}, \vec{X}^{m+1}, \kappa^{m+1})$ to (3.11a–d) is such that the interface has not moved, $\Gamma^{m+1} = \Gamma^m$, then it holds that

$$\exists \zeta \in W(\Gamma^m) : \quad \langle \zeta \vec{\nu}^m, \vec{\eta} \rangle_{\Gamma^m}^h + \left\langle \nabla_s \vec{\text{id}}, \nabla_s \vec{\eta} \right\rangle_{\Gamma^m} = 0 \quad \forall \vec{\eta} \in \underline{V}(\Gamma^m). \quad (3.22)$$

We recall that the proof of Theorem 5 shows that (3.22), in the case $d = 2$, implies that Γ^m is equidistributed, with the possible exception of elements σ_j^m that are locally parallel to each other; see also [9, Theorem 2.2]. Moreover, we recall from [8, §4.1] that surfaces $\Gamma^m \subset \mathbb{R}^3$ that satisfy (3.22) are called conformal polyhedral surfaces.

Next we consider discrete stationary states when no outer forces act, i.e. when $\vec{f} = \vec{0}$. Here, independently of the choice of μ_{\pm} , no spurious velocities appear for discrete stationary solutions. Indeed, Theorem 8 has an immediate consequence.

Theorem 9. *Let $\vec{g} = \vec{0}$. Let $(\vec{U}^{m+1}, P^{m+1}, \vec{X}^{m+1}, \kappa^{m+1}) \in \mathbb{U}^m(\vec{0}) \times \tilde{\mathbb{P}}^m \times \underline{V}(\Gamma^m) \times W(\Gamma^m)$ be a solution to (3.11a–d) with $\vec{f}^{m+1} = \vec{0}$. If $\vec{X}^{m+1} = \vec{X}^m$, then $\vec{U}^{m+1} = \vec{0}$.*

Proof. The solution $(\vec{U}^{m+1}, \vec{X}^{m+1})$ fulfills (3.20) with Γ^{m+1} replaced by Γ^m and $\vec{f}^{m+1} = \vec{0}$. Hence we obtain $(\mu^m \underline{\underline{D}}(\vec{U}^{m+1}), \underline{\underline{D}}(\vec{U}^{m+1})) = 0$ which implies $\underline{\underline{D}}(\vec{U}^{m+1}) = \underline{0}$. Therefore, as shown in the proof of Theorem 6, it implies $\vec{U}^{m+1} = \vec{0}$. \square

Finally, it holds that polyhedral surfaces with constant discrete mean curvature and zero velocity are stationary solutions

Theorem 10. *Let $\vec{g} = \vec{0}$. Let $(\mathbb{U}^m(\vec{0}), \mathbb{P}^m)$ satisfy the LBB condition (3.9) and let $\mathcal{X}_{\Omega_-^m} \in \mathbb{P}^m$. Let $\vec{f}^{m+1} = \vec{0}$. Moreover, let Γ^m be a polyhedral surface with constant discrete mean curvature, i.e. there exists a constant $\bar{\kappa} \in \mathbb{R}$ such that*

$$\bar{\kappa} \langle \vec{\nu}^m, \vec{\eta} \rangle_{\Gamma^m} + \left\langle \nabla_s \vec{\text{id}}, \nabla_s \vec{\eta} \right\rangle_{\Gamma^m} = 0 \quad \forall \vec{\eta} \in \underline{V}(\Gamma^m). \quad (3.23)$$

Then Γ^m satisfies (3.22) and

$$(\vec{U}^{m+1}, P^{m+1}, \vec{X}^{m+1}, \kappa^{m+1}) = (\vec{0}, -\gamma \bar{\kappa} \left[\mathcal{X}_{\Omega_-^m} - \frac{\mathcal{L}^d(\Omega_-^m)}{\mathcal{L}^d(\Omega)} \right], \vec{\text{id}}|_{\Gamma^m}, \bar{\kappa}) \quad (3.24)$$

is the unique solution to (3.11a–d).

Proof. It immediately follows from (3.23) that (3.22) holds. We now show that the solution stated in (3.24) solves (3.11a–d). Since $\mathcal{X}_{\Omega_-^m} \in \mathbb{P}^m$, we have that $P^{m+1} \in \tilde{\mathbb{P}}^m$, and so (3.24) is admissible. Clearly, the three equations (3.11b), (3.11c) and (3.11d) hold trivially. In order to show that (3.11a) holds, we observe that the divergence theorem implies that

$$-\gamma \left\langle \kappa^{m+1} \vec{\nu}^m, \vec{\xi} \right\rangle_{\Gamma^m} = -\gamma \bar{\kappa} \left\langle \vec{\nu}^m, \vec{\xi} \right\rangle_{\Gamma^m} = -\gamma \bar{\kappa} (\nabla \cdot \vec{\xi}, \mathcal{X}_{\Omega_-^m}) = (\nabla \cdot \vec{\xi}, P^{m+1})$$

for all $\vec{\xi} \in \mathbb{U}^m(\vec{0})$, where we have observed that P^{m+1} differs from $-\gamma \bar{\kappa} \mathcal{X}_{\Omega_-^m}$ only by a constant. Hence (3.11a) also holds, and so (3.24) is the unique solution to (3.11a–d) \square

A stationary solution to the continuous problem with $\vec{f} = \vec{0}$ is a circle, $d = 2$, or a sphere, $d = 3$, with zero velocity and a piecewise constant pressure with a discontinuity across the interface, see (4.1a–b).

For $d = 2$, one can choose Γ^m with equidistributed points on a circle as an approximation of this circle, i.e. a closed regular polygon. Such a Γ^m has constant discrete curvature, i.e. there exists a $\bar{\kappa} \in \mathbb{R}$ such that (3.23) is satisfied. Hence Theorem 10 yields that in this situation

$(\vec{U}^{m+1}, \vec{X}^{m+1}, \kappa^{m+1}) = (\vec{0}, \vec{X}^m, \vec{\kappa})$ is the unique solution to the reduced system with $\vec{f}^{m+1} = \vec{0}$. See §4.3 for details.

For $d = 3$, we observe in practice that conformal approximations of the sphere, i.e. spherical Γ^m satisfying (3.22), also satisfy (3.23). See §4.7 for details.

3.9 SEMIDISCRETE SCHEME

We briefly investigate a semidiscrete variant of the scheme (3.11a–d) in order to highlight two additional important properties of the scheme: a good tangential distribution of mesh points, and good volume conservation. For simplicity, we assume $\vec{g} = \vec{0}$ throughout this section.

Consistently with §2.6, let $(\Gamma^h(t))_{t \in [0, T]}$ be a family of polyhedral surfaces, with outer normal $\vec{\nu}^h(t)$. We also define the piecewise linear finite element spaces $W(\Gamma^h(t))$ and $\underline{V}(\Gamma^h(t))$, with $\{\chi_k^h(\cdot, t)\}_{k=1}^{K_\Gamma}$ denoting the standard basis of the former. Hence $\chi_k^h(\vec{q}_l^h(t), t) = \delta_{kl}$ for all $k, l \in \{1, \dots, K_\Gamma\}$ and $t \in [0, T]$, where $\{\vec{q}_k^h(t)\}_{k=1}^{K_\Gamma}$ are the vertices of $\Gamma^h(t)$. We also recall the discrete velocity

$$\vec{v}^h(\vec{z}, t) := \sum_{k=1}^{K_\Gamma} \left[\frac{d}{dt} \vec{q}_k^h(t) \right] \chi_k^h(\vec{z}, t) \in \underline{V}(\Gamma^h(t)).$$

For $t \in [0, T]$, let $\mathcal{T}^h(t)$ be a regular partitioning of Ω into disjoint open simplices and define the finite element spaces $S_k^h(t)$, $\mathbb{U}^h(t)$ and $\mathbb{P}^h(t)$ similarly to S_k^m , $\mathbb{U}^m(\vec{0})$ and \mathbb{P}^m , with the corresponding interpolation operators I_k^h and discrete approximations $\mu^h(t) \in S_0^h(t)$. Here we recall that we assume $\mathcal{X}_{\Omega_-^h(t)} \in \mathbb{P}^h(t)$. Then, given $\Gamma^h(0)$, for $t \in (0, T]$ find $\Gamma^h(t)$ and

$(\vec{U}^h(t), P^h(t), \vec{\mathcal{V}}^h(t), \kappa^h(t)) \in \mathbb{U}^h(t) \times \tilde{\mathbb{P}}^h(t) \times \underline{V}(\Gamma^h(t)) \times W(\Gamma^h(t))$ such that

$$2 \left(\mu^h \underline{\underline{D}}(\vec{U}^h), \underline{\underline{D}}(\vec{\xi}) \right) - \left(P^h, \nabla \cdot \vec{\xi} \right) - \gamma \left\langle \kappa^h \vec{\nu}^h, \vec{\xi} \right\rangle_{\Gamma^h(t)} = \left(\vec{f}^h, \vec{\xi} \right) \forall \vec{\xi} \in \mathbb{U}^h(t), \quad (3.25a)$$

$$\left(\nabla \cdot \vec{U}^h, \varphi \right) = 0 \quad \forall \varphi \in \tilde{\mathbb{P}}^h(t), \quad (3.25b)$$

$$\left\langle \vec{\mathcal{V}}^h, \chi \vec{\nu}^h \right\rangle_{\Gamma^h(t)}^h - \left\langle \vec{U}^h, \chi \vec{\nu}^h \right\rangle_{\Gamma^h(t)} = 0 \quad \forall \chi \in W(\Gamma^h(t)), \quad (3.25c)$$

$$\left\langle \kappa^h \vec{\nu}^h, \vec{\eta} \right\rangle_{\Gamma^h(t)}^h + \left\langle \nabla_s \text{id}, \nabla_s \vec{\eta} \right\rangle_{\Gamma^h(t)} = 0 \quad \forall \vec{\eta} \in \underline{V}(\Gamma^h(t)), \quad (3.25d)$$

where $\vec{f}^h := \vec{I}_2^h \vec{f}(t)$.

First of all we note that a solution $\Gamma^h(t)$ to (3.25a–d) clearly satisfies (3.22), with Γ^m replaced by $\Gamma^h(t)$. This means that in 2d the polygonal curve $\Gamma^h(t)$ is equidistributed, and asymptotically this property is inherited by our fully discrete scheme (3.11a–d); see e.g. Figure 4.6 below. In 3d the property (3.22) means that $\Gamma^h(t)$ is a conformal polyhedral surface, which implies that the mesh quality is good. Once again, we observe in practice that the fully discrete solutions to (3.11a–d) also exhibit nice meshes, without coalescence or other mesh defects occurring.

Secondly, we can show that solutions to (3.25a–d) satisfy a discrete analogue of (3.8). To see this, choose $\chi = 1$ in (3.25c) and $\varphi = (\mathcal{X}_{\Omega_-^h(t)} - \frac{\mathcal{L}^d(\Omega_-^h(t))}{\mathcal{L}^d(\Omega)}) \in \tilde{\mathbb{P}}^h(t)$ in (3.25b), to obtain

$$\begin{aligned} \frac{d}{dt} \mathcal{L}^d(\Omega_-^h(t)) &= \left\langle \vec{\mathcal{V}}^h, \vec{\nu}^h \right\rangle_{\Gamma^h(t)} = \left\langle \vec{\mathcal{V}}^h, \vec{\nu}^h \right\rangle_{\Gamma^h(t)}^h = \left\langle \vec{U}^h, \vec{\nu}^h \right\rangle_{\Gamma^h(t)} \\ &= \int_{\Omega_-^h(t)} \nabla \cdot \vec{U}^h \, d\mathcal{L}^d = \left(\nabla \cdot \vec{U}^h, \mathcal{X}_{\Omega_-^h(t)} \right) \\ &= \left(\nabla \cdot \vec{U}^h, \mathcal{X}_{\Omega_-^h(t)} \right) - \frac{\mathcal{L}^d(\Omega_-^h(t))}{\mathcal{L}^d(\Omega)} \left(\nabla \cdot \vec{U}^h, 1 \right) = 0, \end{aligned} \quad (3.26)$$

given that

$$\left(\nabla \cdot \vec{U}^h, 1 \right) = \int_{\partial\Omega} \vec{U}^h \cdot \vec{n} \, d\mathcal{H}^{d-1} = 0. \quad (3.27)$$

Hence solution to (3.25a–d) conserve the enclosed volume. Once again, the fully discrete scheme (3.11a–d) inherits this property in the sense that in our simulations the volumes are always well maintained, with the observed

relative volume loss tending to zero as $\tau \rightarrow 0$.

3.10 ALGEBRAIC FORMULATION

As is standard practice for the solution of linear systems arising from discretizations of (Navier–)Stokes equations, we avoid the complications of the constrained pressure space $\tilde{\mathbb{P}}^m$ in practice by considering an overdetermined linear system with \mathbb{P}^m instead. In a post-processing step the computed pressure is then projected into the space of zero mean functions. The adoption of the unconstrained pressure space \mathbb{P}^m requires particular care when the Dirichlet boundary data \vec{g} is different from zero. Indeed, let $\varphi \in \mathbb{P}^m$, then we can rewrite φ as

$$\varphi = \varphi - \frac{(\varphi, 1)}{(1, 1)} + \frac{(\varphi, 1)}{(1, 1)}, \quad (3.28)$$

where $\varphi - \frac{(\varphi, 1)}{(1, 1)} \in \tilde{\mathbb{P}}^m$ and $\frac{(\varphi, 1)}{(1, 1)} \in \mathbb{R}$. Substituting (3.28) in (3.11b) we obtain

$$(\nabla \cdot \vec{U}^{m+1}, \varphi) = \left(\nabla \cdot \vec{U}^{m+1}, \varphi - \frac{(\varphi, 1)}{(1, 1)} \right) + \left(\nabla \cdot \vec{U}^{m+1}, 1 \right) \frac{(\varphi, 1)}{(1, 1)}, \quad (3.29)$$

but, from (3.11b), we have

$$\left(\nabla \cdot \vec{U}^{m+1}, \varphi - \frac{(\varphi, 1)}{(1, 1)} \right) = 0, \quad (3.30)$$

and, noting that

$$\left(\nabla \cdot \vec{U}^{m+1}, 1 \right) = \int_{\partial\Omega} \vec{U}^{m+1} \cdot \vec{n} \, d\mathcal{H}^{d-1} = \int_{\partial_1\Omega} (\vec{I}_2^m \vec{g}) \cdot \vec{n} \, d\mathcal{H}^{d-1}, \quad (3.31)$$

we finally deduce

$$(\nabla \cdot \vec{U}^{m+1}, \varphi) = \frac{(\varphi, 1)}{\mathcal{L}^d(\Omega)} \int_{\partial_1\Omega} (\vec{I}_2^m \vec{g}) \cdot \vec{n} \, d\mathcal{H}^{d-1} \quad \forall \varphi \in \mathbb{P}^m. \quad (3.32)$$

Therefore, as in our case, when the pressure space used is the unconstrained space \mathbb{P}^m instead of $\tilde{\mathbb{P}}^m$, then the equation (3.32) replaces (3.11b) and the resulting finite element approximation is: For $m = 0, \dots, M-1$, find

$(\vec{U}^{m+1}, P^{m+1}, \vec{X}^{m+1}, \kappa^{m+1}) \in \mathbb{U}^m(\vec{g}) \times \mathbb{P}^m \times \underline{V}(\Gamma^m) \times W(\Gamma^m)$ such that

$$\begin{aligned} & 2 \left(\mu^m \underline{\underline{D}}(\vec{U}^{m+1}), \underline{\underline{D}}(\vec{\xi}) \right) - \left(P^{m+1}, \nabla \cdot \vec{\xi} \right) \\ & - \gamma \left\langle \kappa^{m+1} \vec{\nu}^m, \vec{\xi} \right\rangle_{\Gamma^m} = \left(\vec{f}^{m+1}, \vec{\xi} \right) \quad \forall \vec{\xi} \in \mathbb{U}^m(\vec{0}), \end{aligned} \quad (3.33a)$$

$$\left(\nabla \cdot \vec{U}^{m+1}, \varphi \right) = \frac{(\varphi, 1)}{\mathcal{L}^d(\Omega)} \int_{\partial_1 \Omega} (\vec{I}_2^m \vec{g}) \cdot \vec{n} \, d\mathcal{H}^{d-1} \quad \forall \varphi \in \mathbb{P}^m, \quad (3.33b)$$

$$\left\langle \frac{\vec{X}^{m+1} - \text{id}}{\tau_m}, \chi \vec{\nu}^m \right\rangle_{\Gamma^m}^h - \left\langle \vec{U}^{m+1}, \chi \vec{\nu}^m \right\rangle_{\Gamma^m} = 0 \quad \forall \chi \in W(\Gamma^m), \quad (3.33c)$$

$$\left\langle \kappa^{m+1} \vec{\nu}^m, \vec{\eta} \right\rangle_{\Gamma^m}^h + \left\langle \nabla_s \vec{X}^{m+1}, \nabla_s \vec{\eta} \right\rangle_{\Gamma^m} = 0 \quad \forall \vec{\eta} \in \underline{V}(\Gamma^m) \quad (3.33d)$$

and set $\Gamma^{m+1} = \vec{X}^{m+1}(\Gamma^m)$.

Let \mathbb{U}^m be the unconstrained velocity space, with basis $\{\phi_i^{\mathbb{U}^m}\}_{i=1}^{K_{\mathbb{U}}^m}$. Moreover, let $\{\phi_i^{\mathbb{P}^m}\}_{i=1}^{K_{\mathbb{P}}^m}$ span the unconstrained pressure space \mathbb{P}^m and let $\{\chi_i^m\}_{i=1}^{K_{\Gamma}^m}$ be the basis of $W(\Gamma^m)$. Then, ignoring for now the Dirichlet and free-slip boundary conditions, the resulting linear system can be formulated as: Find $(\vec{U}^{m+1}, P^{m+1}, \kappa^{m+1}, \delta \vec{X}^{m+1}) \in (\mathbb{R}^d)^{K_{\mathbb{U}}^m} \times \mathbb{R}^{K_{\mathbb{P}}^m} \times \mathbb{R}^{K_{\Gamma}^m} \times (\mathbb{R}^d)^{K_{\Gamma}^m}$, where $\vec{X}^{m+1} = \vec{X}^m + \delta \vec{X}^{m+1}$, such that

$$\begin{pmatrix} \vec{B}_{\Omega} & \vec{C}_{\Omega} & -\gamma \vec{N}_{\Gamma, \Omega} & 0 \\ \vec{C}_{\Omega}^T & 0 & 0 & 0 \\ \vec{N}_{\Gamma, \Omega}^T & 0 & 0 & -\frac{1}{\tau_m} \vec{N}_{\Gamma}^T \\ 0 & 0 & \vec{N}_{\Gamma} & \vec{A}_{\Gamma} \end{pmatrix} \begin{pmatrix} \vec{U}^{m+1} \\ P^{m+1} \\ \kappa^{m+1} \\ \delta \vec{X}^{m+1} \end{pmatrix} = \begin{pmatrix} \vec{c} \\ \vec{\beta} \\ 0 \\ -\vec{A}_{\Gamma} \vec{X}^m \end{pmatrix}, \quad (3.34)$$

where $(\vec{U}^{m+1}, P^{m+1}, \kappa^{m+1}, \delta \vec{X}^{m+1})$ here denote the coefficients of these finite element functions with respect to the aforementioned (basis) functions. Moreover, \vec{X}^m denotes the coefficients of $\text{id}|_{\Gamma^m}$ with respect to the basis of $\underline{V}(\Gamma^m)$. The definitions of the matrices and vectors in (3.34) directly follow

from (3.33a–d) and are:

$$\begin{aligned} [\vec{B}_\Omega]_{ij} &:= 2 \left((\mu^m \underline{\underline{D}}(\phi_j^{\mathbb{U}^m} \vec{e}_q), \underline{\underline{D}}(\phi_i^{\mathbb{U}^m} \vec{e}_r)) \right)_{q,r=1}^d, \quad \vec{c}_i := \left(\vec{f}^{m+1}, \phi_i^{\mathbb{U}^m} \right), \\ [\vec{C}_\Omega]_{ip} &:= - \left((\nabla \cdot (\phi_i^{\mathbb{U}^m} \vec{e}_q), \phi_p^{\mathbb{P}^m}) \right)_{q=1}^d, \quad [\vec{N}_{\Gamma,\Omega}]_{il} := \left\langle \phi_i^{\mathbb{U}^m}, \chi_l^m \vec{\nu}^m \right\rangle_{\Gamma^m}, \\ \vec{\beta}_i &:= \frac{(\phi_i^{\mathbb{P}^m}, 1)}{(1, 1)} \left\langle \vec{I}_2^m \vec{g}, \vec{n} \right\rangle_{\partial_1 \Omega}, \quad [\vec{N}_\Gamma]_{kl} := \langle \chi_l^m, \chi_k^m \vec{\nu}^m \rangle_{\Gamma^m}^h, \\ [\vec{A}_\Gamma]_{kl} &:= \langle \nabla_s \chi_l^m, \nabla_s \chi_k^m \rangle_{\Gamma^m} \text{id}, \end{aligned}$$

where $\{\vec{e}_q\}_{q=1}^d$ denotes the standard basis in \mathbb{R}^d . Note that for the submatrices we have used the convention that the subscripts refer to the test and trial domains, respectively. A single subscript is used where the two domains are the same.

The Dirichlet boundary condition can be imposed by doctoring the matrix and the right-hand side of the algebraic system (3.34). The matrix doctoring process consists on zeroing the rows which correspond to the Dirichlet boundary degrees of freedom in \vec{B}_Ω , \vec{C}_Ω and $\vec{N}_{\Gamma,\Omega}$ in the first block row of (3.34) and setting a unitary value on the correspondent diagonal entries in \vec{B}_Ω . The vector doctoring process consists on setting the Dirichlet boundary data on the correspondent right-hand side entries in \vec{c} . Similarly, the free-slip boundary condition is enforced by doctoring the matrix entries corresponding to the degrees of freedom of the basis functions $\phi_i^{\mathbb{U}^m} \vec{e}_q$ associated with vertices that lie on parts of $\partial_2 \Omega$ that satisfy $\vec{e}_q = \vec{n}$. Of course, the corresponding entries in the right-hand side vector \vec{c} are set to zero.

We observe the analogy of the interface part of the algebraic system, namely the matrices $[\vec{A}_\Gamma]$ and $[\vec{N}_\Gamma]$ and the right-hand side term $-\vec{A}_\Gamma \vec{X}^m$, with the algebraic system arising from the mean curvature flow (2.42) and surface diffusion (2.43).

3.11 SOLUTION METHOD

For the solution of (3.34) we use a Schur complement approach that eliminates $(\kappa^{m+1}, \delta \vec{X}^{m+1})$ from (3.34), and then use an iterative solver for the

remaining system in (\vec{U}^{m+1}, P^{m+1}) . This approach has the advantage that for the reduced system well-known solution methods for finite element discretizations for standard (Navier–)Stokes discretizations may be employed. The desired Schur complement can be obtained as follows. Let

$$\Xi_\Gamma := \begin{pmatrix} 0 & -\frac{1}{\tau_m} \vec{N}_\Gamma^T \\ \vec{N}_\Gamma & \vec{A}_\Gamma \end{pmatrix}, \quad (3.35)$$

be the interface condensed operator, which is exactly the same operator (2.48) arising from the discretization of the stationary geometric PDE. Then (3.34) can be reduced to

$$\begin{pmatrix} \vec{B}_\Omega + \gamma (\vec{N}_{\Gamma,\Omega} \ 0) \Xi_\Gamma^{-1} \begin{pmatrix} \vec{N}_{\Gamma,\Omega}^T \\ 0 \end{pmatrix} & \vec{C}_\Omega \\ \vec{C}_\Omega^T & 0 \end{pmatrix} \begin{pmatrix} \vec{U}^{m+1} \\ P^{m+1} \end{pmatrix} = \begin{pmatrix} \vec{c} + \gamma (\vec{N}_{\Gamma,\Omega} \ 0) \Xi_\Gamma^{-1} \begin{pmatrix} 0 \\ -\vec{A}_\Gamma \vec{X}^m \end{pmatrix} \\ \vec{\beta} \end{pmatrix} \quad (3.36a)$$

and

$$\begin{pmatrix} \kappa^{m+1} \\ \delta \vec{X}^{m+1} \end{pmatrix} = \Xi_\Gamma^{-1} \begin{pmatrix} -\vec{N}_{\Gamma,\Omega}^T \vec{U}^{m+1} \\ -\vec{A}_\Gamma \vec{X}^m \end{pmatrix}. \quad (3.36b)$$

We notice that when $\gamma = 0$ the linear system (3.36a) becomes

$$\begin{pmatrix} \vec{B}_\Omega & \vec{C}_\Omega \\ \vec{C}_\Omega^T & 0 \end{pmatrix} \begin{pmatrix} \vec{U}^{m+1} \\ P^{m+1} \end{pmatrix} = \begin{pmatrix} \vec{c} \\ \vec{\beta} \end{pmatrix}, \quad (3.37)$$

which for $\mu_+ = \mu_-$ corresponds to a discretization of the one-phase Stokes problem. This system is well known and a classical way to solve it is to use a preconditioned GMRES iteration. The generalized minimal residual method (GMRES) is an iterative method for non-symmetric systems. It generates a sequence of orthogonal vectors using the Arnoldi method which is a modified Gram-Schmidt orthogonalization applied to a Krylov subspace with minimal residual. See [13] for more details. Therefore, we solve (3.36a), which is a slight modification of (3.37), employing a preconditioned GMRES iterative solver. For the inverse Ξ_Γ^{-1} we employ a sparse $L U$ decomposition, which we obtain with the help of the sparse factorization package UMFPACK, see

[19], in order to reuse the factorization. Having obtained (\vec{U}^{m+1}, P^{m+1}) from (3.36a), we solve (3.36b) for $(\kappa^{m+1}, \delta\vec{X}^{m+1})$.

As regarding the preconditioner, see [26] for more details, a possible choice is to use the preconditioner

$$\mathcal{P} = \begin{pmatrix} \vec{\mathcal{P}}_{\vec{B}} & \vec{C}_{\Omega} \\ 0 & -\mathcal{P}_S \end{pmatrix}, \quad (3.38)$$

where $\vec{\mathcal{P}}_{\vec{B}}$ is some preconditioner for the matrix \vec{B}_{Ω} , and \mathcal{P}_S acts as a preconditioner for the bulk Schur complement operator $S_{\Omega} = \vec{C}_{\Omega}^T \vec{B}_{\Omega}^{-1} \vec{C}_{\Omega}$.

An application of the preconditioner (3.38) amounts to solving the equations

$$\begin{pmatrix} \vec{\mathcal{P}}_{\vec{B}} & \vec{C}_{\Omega} \\ 0 & -\mathcal{P}_S \end{pmatrix} \begin{pmatrix} \vec{U} \\ P \end{pmatrix} = \begin{pmatrix} \vec{v} \\ q \end{pmatrix}$$

which, by backward substitution, is equivalent to

$$\mathcal{P}_S P = -q, \quad \vec{\mathcal{P}}_{\vec{B}} \vec{U} = \vec{v} - \vec{C}_{\Omega} P. \quad (3.39)$$

We choose \vec{B}_{Ω} for $\vec{\mathcal{P}}_{\vec{B}}$ and the pressure mass matrix M_{Ω} defined as

$$[M_{\Omega}]_{ij} = (\phi_j^{\mathbb{P}^m}, \phi_i^{\mathbb{P}^m}).$$

for \mathcal{P}_S . Again, in order to reuse the factorization, we employ a sparse $L U$ decomposition to factorize the matrices \vec{B} and M_{Ω} .

Alternatively, it is possible to use the standard Stokes matrix, see (3.37),

$$\begin{pmatrix} \vec{B}_{\Omega} & \vec{C}_{\Omega} \\ \vec{C}_{\Omega}^T & 0 \end{pmatrix} \quad (3.40)$$

as a preconditioner for (3.36a) and factorize it directly with a sparse $L U$ decomposition. Since in the Stokes problem the pressure solution is only unique up to a constant, the matrix (3.40) is singular. In particular, if LBB holds, the matrix has rank deficiency 1. Therefore, in order to use UMFPACK to factorize the matrix, the rank deficiency needs to be reduced to 0. This can

be achieved by fixing a degree of freedom in the discrete pressure. For example, by using a matrix doctoring which replaces the first row of the second block row of (3.40) with the corresponding row of the identity matrix. This doctoring process can be avoided if SPQR is used to factorize the preconditioner since SPQR can decompose also singular matrices. Indeed, SPQR is a sparse factorization package, see [20], performing a QR decomposition which can be used to solve the least squares problem.

The algebraic system (3.34) can be rewritten when we use (P1+P0) or P1^{dgr} as pressure space. Indeed it assumes the following form

$$\begin{pmatrix} \vec{B}_\Omega & \vec{C}_\spadesuit & \vec{C}_\clubsuit & -\gamma \vec{N}_{\Gamma,\Omega} & 0 \\ \vec{C}_\spadesuit^T & 0 & 0 & 0 & 0 \\ \vec{C}_\clubsuit^T & 0 & 0 & 0 & 0 \\ \vec{N}_{\Gamma,\Omega}^T & 0 & 0 & 0 & -\frac{1}{\tau_m} \vec{N}_\Gamma^T \\ 0 & 0 & 0 & \vec{N}_\Gamma & \vec{A}_\Gamma \end{pmatrix} \begin{pmatrix} \vec{U}^{m+1} \\ P_\spadesuit^{m+1} \\ P_\clubsuit^{m+1} \\ \kappa^{m+1} \\ \delta \vec{X}^{m+1} \end{pmatrix} = \begin{pmatrix} \vec{c} \\ \vec{\beta}_\spadesuit \\ \vec{\beta}_\clubsuit \\ 0 \\ -\vec{A}_\Gamma \vec{X}^m \end{pmatrix}, \quad (3.41)$$

where \vec{C}_\spadesuit and \vec{C}_\clubsuit have the same definition of \vec{C}_Ω in (3.34) but now in terms of bases of different spaces. More precisely, in the case (P1+P0), there are two independent spaces for the pressure of polynomial order 1 and 0, respectively. Instead, in the case P1^{dgr}, both spaces have polynomial degree 1 but the basis functions support is restricted to Ω_-^m and Ω_+^m , respectively.

A suitable preconditioner for the algebraic system (3.41) is then

$$\mathcal{P} = \begin{pmatrix} \vec{\mathcal{P}}_{\vec{B}} & \vec{C}_\spadesuit & \vec{C}_\clubsuit \\ 0 & -\mathcal{P}_{S,\spadesuit} & 0 \\ 0 & 0 & -\mathcal{P}_{S,\clubsuit} \end{pmatrix}, \quad (3.42)$$

while the reduced system (3.36a) becomes

$$\begin{pmatrix} \vec{B}_\Omega + \gamma (\vec{N}_{\Gamma,\Omega} \ 0) \Xi_\Gamma^{-1} \begin{pmatrix} \vec{N}_{\Gamma,\Omega}^T \\ 0 \end{pmatrix} & \vec{C}_\spadesuit & \vec{C}_clubs \\ \vec{C}_\spadesuit^T & 0 & 0 \\ \vec{C}_clubs^T & 0 & 0 \end{pmatrix} \begin{pmatrix} \vec{U}^{m+1} \\ P_\spadesuit^{m+1} \\ P_{clubs}^{m+1} \end{pmatrix} = \\ \begin{pmatrix} \vec{c} + \gamma (\vec{N}_{\Gamma,\Omega} \ 0) \Xi_\Gamma^{-1} \begin{pmatrix} 0 \\ -\vec{A}_\Gamma \vec{X}^m \end{pmatrix} \\ \vec{\beta}_\spadesuit \\ \vec{\beta}_{clubs} \end{pmatrix}. \quad (3.43)$$

An application of the preconditioner (3.42) amounts to solving the equations

$$\begin{pmatrix} \vec{\mathcal{P}}_{\vec{B}} & \vec{C}_\spadesuit & \vec{C}_clubs \\ 0 & -\mathcal{P}_{S,\spadesuit} & 0 \\ 0 & 0 & -\mathcal{P}_{S,clubs} \end{pmatrix} \begin{pmatrix} \vec{U} \\ P_\spadesuit \\ P_{clubs} \end{pmatrix} = \begin{pmatrix} \vec{v} \\ q \\ p \end{pmatrix}$$

which, by backward substitution, is equivalent to

$$\mathcal{P}_{S,\spadesuit} P_\spadesuit = -q, \quad \mathcal{P}_{S,clubs} P_{clubs} = -p, \quad \vec{\mathcal{P}}_{\vec{B}} \vec{U} = \vec{v} - \vec{C}_\spadesuit P_\spadesuit - \vec{C}_clubs P_{clubs}. \quad (3.44)$$

Alternatively, as before, it is possible to use the standard Stokes matrix

$$\begin{pmatrix} \vec{B}_\Omega & \vec{C}_\spadesuit & \vec{C}_clubs \\ \vec{C}_\spadesuit^T & 0 & 0 \\ \vec{C}_clubs^T & 0 & 0 \end{pmatrix} \quad (3.45)$$

as a preconditioner for (3.43) and factorize them directly with a sparse LU decomposition. The matrix (3.45), if LBB holds, has rank deficiency 1 for the P2–P1^{dgr} element and 2 for the P2–(P1+P0) element. Therefore, in the case P2–P1^{dgr}, only the block entry in position (2, 2) of (3.45) is doctored while, in the case P2–(P1+P0), the block entries in position (2, 2) and (3, 3) of (3.45) are doctored. Again, we point out that the doctoring is not needed when SPQR is used to factorize the preconditioner.

3.12 MESH GENERATION AND SMOOTHING

Given the initial polyhedral surface Γ^0 , we create a triangulation \mathcal{T}^0 of Ω that is fitted to Γ^0 with the help of the package **Gmsh**, see [32].

The mesh generation process is controlled by the characteristic lengths of the points describing the geometry of the domain boundary $\partial\Omega$. Each point has associated a characteristic length which prescribes the size of the mesh elements. For example, a segment of length L , which defines an edge of the domain boundary, delimited by two points of characteristic length c_l will be subdivided into several segments of lengths $\frac{L}{c_l}$ during the mesh generation. Therefore, the smaller is the characteristic length, the finer is the resulting mesh. When the characteristic lengths of two points defining an edge are different, **Gmsh** performs an interpolation process. In general we use either nearly uniform or adaptive bulk meshes. In the former case, the characteristic length c_l is set to be equal to the characteristic length of the interface $c_{l,\Gamma}$, while in the latter case the characteristic length is $c_l(\vec{z}) = \min\{8c_{l,\Gamma}, \text{dist}(\vec{z}, \Gamma)\}$. Therefore, in the adaptive case, if the interface is far enough from the boundary, the resulting bulk mesh will be coarse. We define the characteristic length of the interface $c_{l,\Gamma}$, in the 2d case, as the average length of the segments describing the discrete interface Γ^m or, in the 3d case, as the length of an equilateral triangle with area equal to the average of the areas of the triangles describing the discrete interface Γ^m .

Then, for $m \geq 0$, having computed the new interface Γ^{m+1} , we would like to obtain a bulk triangulation \mathcal{T}^{m+1} that is fitted to Γ^{m+1} , and ideally is close to \mathcal{T}^m . This is to avoid unnecessary overhead from remeshing the domain Ω completely.

To this end, we perform the following smoothing step on \mathcal{T}^m , which is inspired by the method proposed in [29], see also [31]. Having obtained $\delta\vec{X}^{m+1}$ from the solution of (3.34), we solve the linear elasticity problem: Find a

displacement $\vec{\psi} \in [H^1(\Omega)]^d$ such that

$$\nabla \cdot \underline{\underline{S}} = \vec{0} \quad \text{in } \Omega_{\pm}^m, \quad (3.46a)$$

$$\vec{\psi} = \delta \vec{X} \quad \text{on } \Gamma^m, \quad (3.46b)$$

$$\vec{\psi} \cdot \vec{n} = 0 \quad \text{on } \partial\Omega, \quad (3.46c)$$

where the stress tensor $\underline{\underline{S}}$ is defined as

$$\underline{\underline{S}} = 2 \underline{\underline{D}}(\vec{\psi}) + (\nabla \cdot \vec{\psi}) \underline{\underline{\text{id}}}. \quad (3.47)$$

In practice we approximate (3.46a–c) with piecewise linear elements and solve the resulting system of linear equations with the UMPFACK package, see [19]. The obtained discrete variant of $\vec{\psi}$, at every vertex of the current bulk grid \mathcal{T}^m , then represents the variation in their position that we compute in order to obtain \mathcal{T}^{m+1} .

Occasionally the deformation of the mesh becomes too large, for instance when the bubble making up the inner phase undergoes strong deformations, and so a complete remeshing of Ω becomes necessary. In order to detect the need for a complete remeshing, we define the volume criterion

$$\frac{\max_{o \in \mathcal{T}^{m+1}} \mathcal{L}^d(o)}{\min_{o \in \mathcal{T}^{m+1}} \mathcal{L}^d(o)} \geq C_v \geq 1, \quad (3.48)$$

where C_v is a fixed constant. Of course, if we choose $C_v = 1$, then a remeshing would be triggered after every time step, while, if we choose $C_v = \infty$, then no remeshing would ever be triggered. Obviously, the volume criterion (3.48) cannot be used for adaptive meshes therefore we also define the angle criterion

$$\min_{o \in \mathcal{T}^{m+1}} \min_{\alpha \in \angle(o)} \alpha \leq C_a, \quad (3.49)$$

where $\angle(o)$ is the set of all the angles of the simplex o which can be computed as $\alpha_{ij} = \cos^{-1}(-\vec{n}_i \cdot \vec{n}_j)$, $\forall i, j \in \{0, \dots, d\}$, with \vec{n}_i the unitary normal to the simplex face i . Of course, if we chose $C_a = 60^\circ$, then a remeshing is triggered after every time step, while, if we choose $C_a = 0^\circ$, then no remeshing would ever be triggered.

We stress that in all our numerical simulations we never need to remesh the interface Γ^m itself. Hence the stability results from Theorem 8 hold throughout. Of course, a remeshing of Γ^m would mean that (3.20) in Theorem 8 is no longer valid because the re-meshed interface $\hat{\Gamma}^m$ differs from the computed Γ^m .

4

TWO-PHASE STOKES FLOW NUMERICAL RESULTS

In order to test our method, and to allow comparisons with the unfitted finite element approximation in [10], we now present several numerical experiments in 2d and 3d. This chapter is extensively based on a paper we wrote, see [2].

The chapter is organised as follows: in §4.1 we state two exact solutions to the two-phase Stokes problem and we verify that they are indeed solutions; in §4.2 we describe the general settings for the simulations and we define the error estimators used; in §4.3 we report on the convergence test in 2d; in §4.4 we show that interface mesh points are naturally equidistributed by our scheme; in §4.5 we show that our scheme conserve the enclosed volume and that the surface energy monotonically decays; in §4.6 we present a shear flow experiment in 2d; in §4.7 we report on the convergence test in 3d; in §4.8 we finally present a shear flow experiment in 3d.

4.1 EXACT SOLUTIONS

We recall the following stationary and expanding spherical solutions from [10]. Let $\Gamma(t) = \{\vec{z} \in \mathbb{R}^d : |\vec{z}| = r(t)\}$ be a sphere of radius $r(t)$ and mean curvature $\varkappa(t) = -\frac{d-1}{r(t)}$. Moreover let $\alpha, \gamma \in \mathbb{R}_{\geq 0}$ be given. We will refer to (4.1a,b) as the stationary bubble solution, and to (4.2a,b) as the expanding bubble solution.

4.1.1 STATIONARY BUBBLE

The stationary sphere where

$$r(t) = r(0), \quad (4.1a)$$

together with

$$\vec{u}(\vec{z}, t) = \vec{0}, \quad p(\vec{z}, t) = -\gamma\varkappa(0) \left[\mathcal{X}_{\Omega_{-(0)}} - \frac{\mathcal{L}^d(\Omega_{-(0)})}{\mathcal{L}^d(\Omega)} \right], \quad (4.1b)$$

is an exact solution to the problem (3.1a–h) on e.g. $\Omega = (-1, 1)^d$ with $\vec{f} = \vec{0}$ and $\vec{g} = \vec{0}$ on $\partial_1\Omega = \partial\Omega$. This solution is the continuous version of (3.24).

It is trivial to verify that (4.1a,b) is indeed an exact solution. Firstly, given that the velocity \vec{u} is zero and the pressure p is constant in each phase, the momentum equation (3.1a) automatically holds if $\vec{f} = \vec{0}$ and the continuity equation (3.1b) is satisfied. Moreover, also the stress balance (3.1f) holds since, substituting (4.1b) in (3.1f), we obtain

$$\begin{aligned} [2\mu\mathbf{\underline{D}}(\vec{u}) \cdot \vec{\nu} - p\vec{\nu}]_-^+ &= [-p\vec{\nu}]_-^+ \\ &= -\gamma\varkappa(0) \frac{\mathcal{L}^d(\Omega_{-(0)})}{\mathcal{L}^d(\Omega)} \vec{\nu} - \gamma\varkappa(0)\vec{\nu} + \gamma\varkappa(0) \frac{\mathcal{L}^d(\Omega_{-(0)})}{\mathcal{L}^d(\Omega)} \vec{\nu} \\ &= -\gamma\varkappa(0)\vec{\nu} = -\gamma\varkappa\vec{\nu}. \end{aligned}$$

Finally, the dynamic interface condition (3.1g) is trivially satisfied since the interface is stationary and \vec{u} is zero.

4.1.2 EXPANDING BUBBLE

A nontrivial divergence free and radially symmetric solution \vec{u} can be constructed on a domain that does not contain the origin. To this end, consider e.g. $\Omega = (-1, 1)^d \setminus [-\frac{1}{3}, \frac{1}{3}]^d$. Then, the expanding sphere where

$$r(t) = ([r(0)]^d + \alpha t d)^{\frac{1}{d}}, \quad (4.2a)$$

together with

$$\vec{u}(\vec{z}, t) = \alpha \frac{\vec{z}}{|\vec{z}|^d}, \quad p(\vec{z}, t) = - \left(\gamma + 2\alpha \frac{\mu_+ - \mu_-}{r(t)^{d-1}} \right) \varkappa(t) \left[\mathcal{X}_{\Omega_-(t)} - \frac{\mathcal{L}^d(\Omega_-(t))}{\mathcal{L}^d(\Omega)} \right], \quad (4.2b)$$

is an exact solution to the problem (3.1a–h) with $\vec{f} = \vec{0}$ and $\vec{g}(\vec{z}) = \alpha |\vec{z}|^{-d} \vec{z}$ on $\partial_1 \Omega = \partial \Omega$.

We now verify that (4.2a,b) is indeed an exact solution. Firstly, we have that

$$\frac{\partial u_i}{\partial z_j} = \alpha \frac{\delta_{ij} - dz_i z_j |\vec{z}|^{-2}}{|\vec{z}|^d}$$

and

$$\frac{\partial^2 u_i}{\partial z_j^2} = \alpha d \frac{-2\delta_{ij} z_j - z_i + (d+2)z_i z_j^2 |\vec{z}|^{-2}}{|\vec{z}|^{d+2}}.$$

Since $\frac{\partial u_i}{\partial z_j} = \frac{\partial u_j}{\partial z_i}$, the components of the rate-of-deformation tensor are simply

$$[\underline{\underline{D}}(\vec{u})]_{ij} = \frac{1}{2} \left(\frac{\partial u_i}{\partial z_j} + \frac{\partial u_j}{\partial z_i} \right) = \frac{\partial u_i}{\partial z_j}.$$

Then, it holds

$$\begin{aligned} [\nabla \cdot \underline{\underline{D}}(\vec{u})]_i &= \sum_{j=1}^d \frac{\partial}{\partial z_j} \frac{\partial u_i}{\partial z_j} = \frac{\alpha d}{|\vec{z}|^{d+2}} \sum_{j=1}^d \left(-2\delta_{ij} z_j - z_i + (d+2)z_i z_j^2 |\vec{z}|^{-2} \right) \\ &= \frac{\alpha d}{|\vec{z}|^{d+2}} \left(-2z_i - dz_i + (d+2)z_i \right) = 0. \end{aligned}$$

Therefore, given that the pressure p is constant in each phase, the momentum equation (3.1a) holds if $\vec{f} = \vec{0}$. Also the continuity equation (3.1b) is satisfied

since we have

$$\nabla \cdot \vec{u} = \sum_{j=1}^d \frac{\partial u_j}{\partial z_j} = \sum_{j=1}^d \alpha \frac{1 - dz_j^2 |\vec{z}|^{-2}}{|\vec{z}|^d} = \frac{\alpha}{|\vec{z}|^d} (d - d|\vec{z}|^2 |\vec{z}|^{-2}) = 0.$$

Moreover, also the stress balance (3.1f) holds since, substituting (4.2b) in (3.1f), we obtain for the i component

$$\begin{aligned} \left[[2\mu \underline{D}(\vec{u}) \cdot \vec{\nu} - p \vec{\nu}]_i \right]_-^+ &= \left[2\mu \sum_{j=1}^d \frac{\partial u_i}{\partial z_j} \nu_j - p \nu_i \right]_-^+ = \left[2\mu \sum_{j=1}^d \frac{\partial u_i}{\partial z_j} \frac{z_j}{|\vec{z}|} \right]_-^+ - [p \nu_i]_-^+ \\ &= \left[2\mu \sum_{j=1}^d \left(\alpha \frac{\delta_{ij} z_j - dz_i z_j^2 |\vec{z}|^{-2}}{|\vec{z}|^{d+1}} \right) \right]_-^+ - \left(\gamma + 2\alpha \frac{\mu_+ - \mu_-}{r^{d-1}} \right) \varkappa \nu_i \\ &= \left[2\mu \alpha \frac{z_i - dz_i}{|\vec{z}|^{d+1}} \right]_-^+ - \gamma \varkappa \nu_i - 2\alpha \frac{\mu_+ - \mu_-}{|\vec{z}|^{d-1}} \frac{1-d}{|\vec{z}|} \frac{z_i}{|\vec{z}|} \\ &= 2\alpha \frac{(\mu_+ - \mu_-)(1-d)z_i}{|\vec{z}|^{d+1}} - \gamma \varkappa \nu_i - 2\alpha \frac{(\mu_+ - \mu_-)(1-d)z_i}{|\vec{z}|^{d+1}} = -\gamma \varkappa \nu_i. \end{aligned}$$

Finally, the dynamic interface condition (3.1g) is satisfied since the fluid velocity on the interface along the normal direction is

$$\vec{u} \cdot \vec{\nu}|_\Gamma = \alpha \frac{\vec{z}}{|\vec{z}|^d} \cdot \frac{\vec{z}}{|\vec{z}|} = \alpha \frac{r^2}{r^{d+1}} = \alpha r^{1-d},$$

while the interface velocity along the normal direction is

$$\vec{\mathcal{V}} \cdot \vec{\nu} = r' = \alpha r^{1-d},$$

where we have used

$$r^d = r_0^d + \alpha t d \iff dr^{d-1} r' = \alpha d \iff r' = \alpha r^{1-d},$$

with $r_0 = r(0)$.

4.2 SETTINGS AND ERROR ESTIMATORS

In our numerical simulations, unless otherwise stated, we use the following settings. We choose the initial surface $\Gamma(0) = \{\vec{z} \in \mathbb{R}^d : |\vec{z}| = \frac{1}{2}\}$, the domain $\Omega = (-1, 1)^d$ and we employ uniform time steps $\tau_m = \tau$, $m = 0, \dots, M - 1$. We compute the discrete solutions over the time interval $[0, 1]$. Moreover, we set the GMRES tolerance to $\text{tol} = 10^{-12}$ and the restart value to 50. We use the Stokes matrix (3.40) or, depending on the pressure space, (3.45) as a preconditioner factorizing it with UMFPACK. We point out that the restart value corresponds to the size of the Krylov subspace used by the GMRES method while the tolerance is the value for the stopping criterion. More precisely, the GMRES iteration ends when the ratio between the norm of the preconditioned actual residual and the norm of the preconditioned initial residual is smaller than the required tolerance.

We define the errors

$$\|\Gamma^h - \Gamma\|_{L^\infty} := \max_{m=1, \dots, M} \|\Gamma^m - \Gamma(t_m)\|_{L^\infty}, \quad (4.3)$$

where $\|\Gamma^m - \Gamma(t_m)\|_{L^\infty} := \max_{k=1, \dots, K_\Gamma} \text{dist}(\vec{q}_k^m, \Gamma(t_m))$,

$$\|\vec{U} - I_2^h \vec{u}\|_{L^2} := \left[\tau \sum_{m=1}^M \|\vec{U}^m - I_2^m \vec{u}(\cdot, t_m)\|_{L^2(\Omega)}^2 \right]^{\frac{1}{2}}, \quad (4.4)$$

$$\|\vec{U} - I_2^h \vec{u}\|_{L^2(H^1)} := \left[\tau \sum_{m=1}^M \|\vec{U}^m - I_2^m \vec{u}(\cdot, t_m)\|_{H^1(\Omega)}^2 \right]^{\frac{1}{2}}, \quad (4.5)$$

and

$$\|P - p\|_{L^2} := \left[\tau \sum_{m=1}^M \|P^m - p(\cdot, t_m)\|_{L^2(\Omega)}^2 \right]^{\frac{1}{2}}. \quad (4.6)$$

In (4.6) we employ a quadrature rule of degree k , with $k = 13$ in 2d and $k = 10$ in 3d, to compute the L^2 -norms over Ω .

Finally, we also define the estimated order of convergence EOC as

$$\text{EOC} = \frac{\ln \frac{\text{error}_1}{\text{error}_0}}{\ln \frac{h_1}{h_0}}, \quad (4.7)$$

where error_1 is the error computed on a triangulation finer than the one used to compute error_0 while h_1 and h_0 are the respective characteristic lengths.

4.3 CONVERGENCE TESTS IN 2D

For the true solution (4.1a,b) we choose $\mu = \gamma = 1$. Therefore, the solution reduces to $r(t) = \frac{1}{2}$, $\vec{u}(\cdot, t) = \vec{0}$ and $p(t) = 2\mathcal{X}_{\Omega-(0)} - \frac{\pi}{8}$ for all $t \geq 0$. We approximate this stationary solution on nearly uniform meshes that feature $J_\Gamma = 2^i$, $i = 4, \dots, 7$, uniform interface elements and $J_\Omega^0 = 224, 1076, 4240, 17194$ bulk elements, respectively. We show the initial mesh for $J_\Gamma = 32$ in Figure 4.1. In addition, we use a uniform time step size $\tau = 10^{-2}$. We report

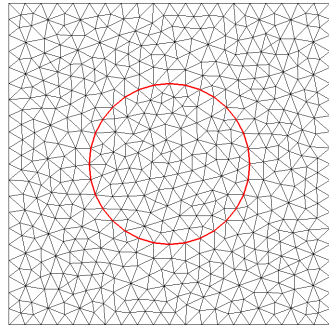


Figure 4.1: Initial mesh for the 2d stationary bubble problem with $J_\Gamma = 32$ interface elements.

on the errors for the P2–P0, P2–P1, P2–P1^{dgr} and P2–(P1+P0) elements in Tables 4.1, 4.2, 4.3 and 4.4, respectively.

We can clearly see that the stationary nature of the true solution (4.1a,b) is captured exactly by our numerical method with the P2–P0, the P2–P1^{dgr} and the P2–(P1+P0) element, see also Figure 4.2 for a visualization of the discrete pressure in the case $J_\Gamma = 32$. This is not surprising given the result of

J_Γ	$\ \Gamma^h - \Gamma\ _{L^\infty}$	$\ \vec{U} - I_2^h \vec{u}\ _{L^2}$	$\ P - p\ _{L^2}$	EOC	CPU[s]
16	0	0	3.22254e-01	-	9
32	0	0	1.41195e-01	0.90	54
64	0	0	4.06438e-02	1.80	292
128	0	0	2.60448e-02	0.64	1443

Table 4.1: ($\mu = \gamma = 1$) Stationary bubble problem on $(-1, 1)^2$ over the time interval $[0, 1]$ for the P2–P0 element.

J_Γ	$\ \Gamma^h - \Gamma\ _{L^\infty}$	$\ \vec{U} - I_2^h \vec{u}\ _{L^2}$	$\ P - p\ _{L^2}$	EOC	CPU[s]
16	2.41133e-02	9.35478e-03	5.75614e-01	-	5
32	1.21789e-02	3.44473e-03	3.99457e-01	0.40	36
64	6.17055e-03	1.24629e-03	2.77632e-01	0.52	170
128	2.97451e-03	4.41980e-04	1.96901e-01	0.50	1343

Table 4.2: ($\mu = \gamma = 1$) Stationary bubble problem on $(-1, 1)^2$ over the time interval $[0, 1]$ for the P2–P1 element.

J_Γ	$\ \Gamma^h - \Gamma\ _{L^\infty}$	$\ \vec{U} - I_2^h \vec{u}\ _{L^2}$	$\ P - p\ _{L^2}$	EOC	CPU[s]
16	0	0	3.22254e-01	-	8
32	0	0	1.41195e-01	0.90	42
64	0	0	4.06438e-02	1.80	181
128	0	0	2.60448e-02	0.64	1006

Table 4.3: ($\mu = \gamma = 1$) Stationary bubble problem on $(-1, 1)^2$ over the time interval $[0, 1]$ for the P2–P1 $^{dg_\Gamma}$ element.

J_Γ	$\ \Gamma^h - \Gamma\ _{L^\infty}$	$\ \vec{U} - I_2^h \vec{u}\ _{L^2}$	$\ P - p\ _{L^2}$	EOC	CPU[s]
16	0	0	3.22254e-01	-	13
32	0	0	1.41195e-01	0.90	44
64	0	0	4.06438e-02	1.80	203
128	0	0	2.60448e-02	0.64	2151

Table 4.4: ($\mu = \gamma = 1$) Stationary bubble problem on $(-1, 1)^2$ over the time interval $[0, 1]$ for the P2–(P1+P0) element.

Theorem 10, and the fact that we use an equidistributed approximation Γ^0 , which means that (3.23) is satisfied. Instead the element P2–P1 does not satisfy the hypothesis that $\mathcal{X}_{\Omega_-^m} \in \mathbb{P}^m$ of Theorem 10 and therefore the true solution is not captured exactly. Moreover, since $\mathcal{X}_{\Omega_-^h(t)} \notin \text{P1}$, the volume conservation property of the semidiscrete scheme (3.26) does not hold which implies that the P2–P1 element does not conserve the enclosed volume. Of course, since the discrete solution is stationary, neither smoothing nor remeshing is performed for the simulations in Tables 4.1, 4.2, 4.3 and 4.4. We also observe that the error for the three approximations with the P2–P0, the P2–P1^{dgr} and the P2–(P1+P0) element, respectively, produce identical errors. Again, that is to be expected, since the pressure solution (3.24)

$$P^{m+1} = -\gamma \bar{\kappa} \left[\mathcal{X}_{\Omega_-^m} - \frac{\mathcal{L}^d(\Omega_-^m)}{\mathcal{L}^d(\Omega)} \right]$$

is such that P^{m+1} is independent of \mathbb{P}^m , and so the additional degrees of freedom are not utilized by the pressure approximation.

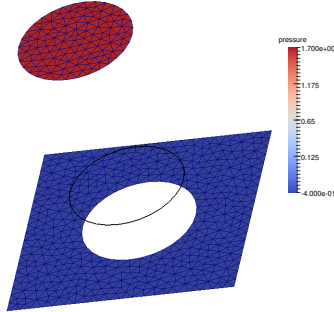


Figure 4.2: ($\mu = \gamma = 1$) Pressure of the 2d stationary bubble at time $t = 1$ for the P2–P0 element with $J_T = 32$ interface elements.

For the expanding bubble test, we fix $\Omega = (-1, 1)^2 \setminus [-\frac{1}{3}, \frac{1}{3}]^2$ and we choose the parameters $\alpha = 0.15$ and $\mu_+ = 10\mu_- = \gamma = 1$ for the true solution (4.2a,b). Here we consider two different bulk mesh strategies. Either we use a nearly uniform mesh, as shown on the left of Figure 4.3, or an adaptive mesh that uses a finer resolution close to the interface, see the example mesh on the right-hand side of Figure 4.3.

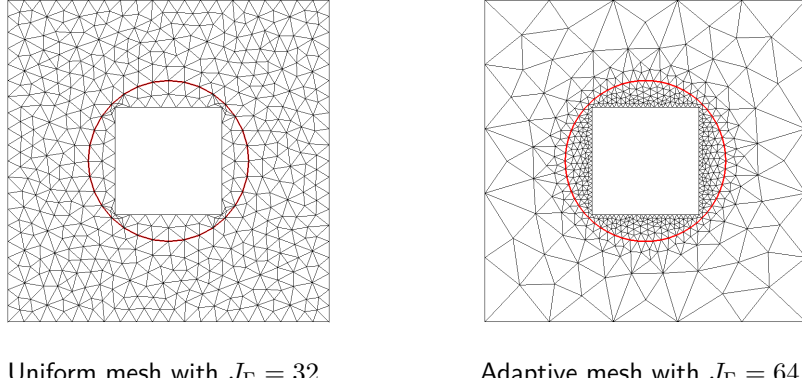


Figure 4.3: Initial meshes for the expanding bubble problem.

J_Γ	J_Ω^0	τ	J_Ω^M for $C_v = 1$	J_Ω^M for $C_v = 3$
16	316	$1.6 \cdot 10^{-2}$	120	184
32	1016	$4 \cdot 10^{-3}$	452	468
64	3916	10^{-3}	1864	1858
128	15784	$2.5 \cdot 10^{-4}$	7264	7263

Table 4.5: Discretization parameters for the 2d expanding bubble problem, nearly uniform meshes.

Details on the discretization parameters for the nearly uniform meshes are given in Table 4.5. Here we explicitly state the final number of bulk elements, J_Ω^M , in the case $C_v = 1$ and $C_v = 3$, recall the volume criterion (3.48), for the P2–P0 element. In the former the bulk is remeshed after every time step while in the latter the bulk is remeshed when the max–min entity volume ratio is bigger than 3. Of course, when only smoothing is employed, then the number of bulk mesh elements is invariant, and so $J_\Omega^M = J_\Omega^0$. We report on the error for the P2–P0, the P2–P1^{dg Γ} and the P2–(P1+P0) element in Table 4.6, 4.7 and 4.8, respectively. On the top part of the tables only mesh smoothings are applied, in the central part the bulk mesh is remeshed after every time step while at the bottom the bulk mesh is remeshed only when the volume criterion (3.48), with $C_v = 3$, is not satisfied. Due to the expanding motion of the interface, if no remesh is used, we observe that over time bulk mesh elements strongly deform. This leads to large CPU times and additional approximation errors. In particular, the strong mesh

J_Γ	$\ \Gamma^h - \Gamma\ _{L^\infty}$	$\ \vec{U} - I_2^h \vec{u}\ _{L^2}$	EOC	$\ \vec{U} - I_2^h \vec{u}\ _{L^2(H^1)}$	$\ P - p\ _{L^2}$	EOC	CPU[s]
no remeshing							
16	5.94637e-03	7.26038e-04	-	1.98118e-02	4.30560e-01	-	9
32	1.47959e-03	3.39540e-04	0.83	1.17665e-02	2.27294e-01	0.70	98
64	3.68960e-04	8.66188e-05	1.97	5.82989e-03	1.05041e-01	1.11	1709
128	9.20414e-05	5.87165e-05	0.56	6.24063e-03	3.18072e-02	1.72	37539
$C_v = 1$							
16	5.92441e-03	5.27627e-04	-	1.57505e-02	4.43442e-01	-	59
32	1.46657e-03	1.05800e-04	1.75	5.26275e-03	2.14680e-01	0.79	100
64	3.65433e-04	1.48680e-05	2.83	1.50695e-03	8.14177e-02	1.40	2785
128	9.12526e-05	1.81107e-06	3.04	3.59374e-04	3.69593e-02	1.14	23465
$C_v = 3$							
16	5.94589e-03	5.71201e-04	-	1.51195e-02	4.44395e-01	-	41
32	1.47176e-03	1.02091e-04	1.88	4.86975e-03	2.13617e-01	0.80	92
64	3.65488e-04	1.50366e-05	2.76	1.50058e-03	8.22797e-02	1.38	1847
128	9.12406e-05	1.81327e-06	3.05	3.59347e-04	3.69473e-02	1.16	26973

Table 4.6: ($\mu_+ = 10, \mu_- = \gamma = 1, \alpha = 0.15$) Expanding bubble problem on $(-1, 1)^2 \setminus [-\frac{1}{3}, \frac{1}{3}]^2$ over the time interval $[0, 1]$ for the P2–P0 element with nearly uniform mesh.

J_Γ	$\ \Gamma^h - \Gamma\ _{L^\infty}$	$\ \vec{U} - I_2^h \vec{u}\ _{L^2}$	EOC	$\ \vec{U} - I_2^h \vec{u}\ _{L^2(H^1)}$	$\ P - p\ _{L^2}$	EOC	CPU[s]
no remeshing							
16	5.99881e-03	1.42557e-03	-	3.45859e-02	4.31784e-01	-	9
32	1.47936e-03	4.11514e-04	1.36	1.28088e-02	2.27350e-01	0.70	82
64	3.69030e-04	1.03424e-04	1.99	6.17291e-03	1.05060e-01	1.11	1391
128	9.21619e-05	6.12532e-05	0.76	6.21616e-03	3.17967e-02	1.72	31042
$C_v = 1$							
16	5.95848e-03	8.38757e-04	-	2.23968e-02	4.44061e-01	-	100
32	1.47123e-03	2.22736e-04	1.45	7.70628e-03	2.15081e-01	0.79	728
64	3.65750e-04	2.16681e-05	3.36	1.76987e-03	8.15608e-02	1.40	3050
128	9.12893e-05	2.33116e-06	3.22	3.96930e-04	3.69418e-02	1.14	25348
$C_v = 3$							
16	5.99703e-03	8.59166e-04	-	2.23227e-02	4.44656e-01	-	47
32	1.47622e-03	2.03051e-04	1.57	7.04524e-03	2.13800e-01	0.80	145
64	3.65886e-04	2.21067e-05	3.20	1.77973e-03	8.20109e-02	1.38	2325
128	9.12664e-05	2.33913e-06	3.24	3.97020e-04	3.69351e-02	1.15	26045

Table 4.7: ($\mu_+ = 10, \mu_- = \gamma = 1, \alpha = 0.15$) Expanding bubble problem on $(-1, 1)^2 \setminus [-\frac{1}{3}, \frac{1}{3}]^2$ over the time interval $[0, 1]$ for the P2–P1^{dgr} element with nearly uniform mesh.

J_Γ	$\ \Gamma^h - \Gamma\ _{L^\infty}$	$\ \vec{U} - I_2^h \vec{u}\ _{L^2}$	EOC	$\ \vec{U} - I_2^h \vec{u}\ _{L^2(H^1)}$	$\ P - p\ _{L^2}$	EOC	CPU[s]
no remeshing							
16	5.99532e-03	1.55402e-03	-	4.09186e-02	4.31782e-01	-	9
32	1.48145e-03	4.40335e-04	1.38	1.35501e-02	2.27375e-01	0.70	80
64	3.68601e-04	1.08675e-04	2.02	6.48883e-03	1.05064e-01	1.11	1316
128	9.22254e-05	6.25696e-05	0.80	6.07813e-03	3.17870e-02	1.72	39375
$C_v = 1$							
16	5.96235e-03	8.94203e-04	-	2.61842e-02	4.44306e-01	-	159
32	1.47265e-03	2.41779e-04	1.43	1.03858e-02	2.15011e-01	0.79	619
64	3.65605e-04	2.33308e-05	3.37	2.02208e-03	8.11222e-02	1.41	3014
128	9.12693e-05	2.42966e-06	3.26	4.31820e-04	3.69632e-02	1.13	22128
$C_v = 3$							
16	5.97343e-03	8.91171e-04	-	2.46402e-02	4.45063e-01	-	95
32	1.47254e-03	2.20844e-04	1.52	9.55901e-03	2.13809e-01	0.80	178
64	3.65587e-04	2.33348e-05	3.24	2.00192e-03	8.17655e-02	1.39	2225
128	9.12663e-05	2.44147e-06	3.26	4.32699e-04	3.69512e-02	1.15	23265

Table 4.8: ($\mu_+ = 10 \mu_- = \gamma = 1, \alpha = 0.15$) Expanding bubble problem on $(-1, 1)^2 \setminus [-\frac{1}{3}, \frac{1}{3}]^2$ over the time interval $[0, 1]$ for the P2–(P1+P0) element with nearly uniform mesh.

deformations for the finest run, with $J_\Omega^0 = J_\Omega^M = 15212$, leads to a breakdown of the convergence rate for the L^2 -velocity error, and, for the elements P2–P0 and P2–P1^{dgr}, an actual increase in the H^1 -velocity error. Instead, if remesh is applied, we observe a dramatic improvement in the CPU times, and a significant reduction in the error quantities. In particular, there is no deterioration of the observed convergence rates. Comparing the errors in Tables 4.6, 4.7 and 4.8 we note that element P2–P1^{dgr} and element P2–(P1+P0) performs, in term of CPU times and errors, almost the same and they are slightly outperformed by element P2–P0, which, together with a remesh performed at every time step, gives the best overall results.

The evolution of the discrete pressure solution in the case $J_\Gamma = 32$, for the run with $C_v = 1$, can be seen in Figure 4.4. Here we note that the discontinuous jump in the pressure at the interface is captured very well, with no oscillations being present. This is a significant improvement on the oscillations observed in the discrete pressures for the unfitted finite element approximation from [10], see e.g. Figure 6 in that paper.

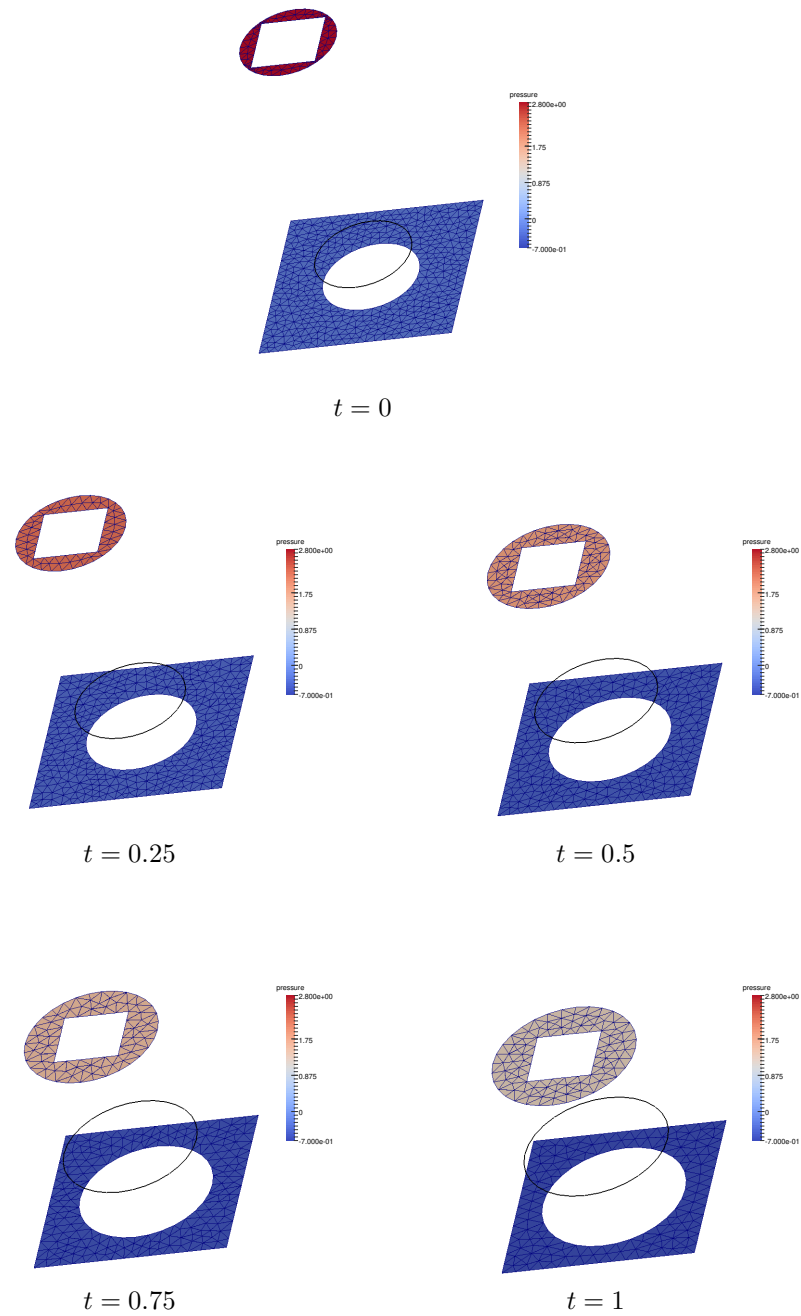


Figure 4.4: ($\mu_+ = 10 \mu_- = \gamma = 1, \alpha = 0.15$) Pressure evolution of the 2d expanding bubble for the P2–P0 element, nearly uniform mesh with $J_\Gamma = 32$ interface elements and $C_v = 1$.

J_Γ	J_Ω^0	τ	J_Ω^M for $C_a = 60^\circ$	J_Ω^M for $C_a = 20^\circ$
32	460	$6.4 \cdot 10^{-2}$	216	216
64	1040	$1.6 \cdot 10^{-2}$	452	440
128	2628	$4 \cdot 10^{-3}$	1084	1384
256	7460	10^{-3}	3840	4004

Table 4.9: Discretization parameters for the 2d expanding bubble problem, adaptive meshes.

J_Γ	$\ \Gamma^h - \Gamma\ _{L^\infty}$	$\ \vec{U} - I_2^h \vec{u}\ _{L^2}$	EOC	$\ \vec{U} - I_2^h \vec{u}\ _{L^2(H^1)}$	$\ P - p\ _{L^2}$	EOC	CPU[s]
no remeshing							
32	4.37607e-03	8.78021e-04	-	1.81156e-02	5.74936e-01	-	3
64	9.85447e-04	1.01294e-04	3.12	5.67749e-03	2.79462e-01	1.04	18
128	2.42678e-04	2.92289e-05	1.79	2.75563e-03	1.48572e-01	0.91	221
256	6.09781e-05	2.55111e-05	0.19	2.58915e-03	7.95637e-02	0.88	3652
$C_a = 60^\circ$							
32	3.91561e-03	7.10756e-04	-	1.60401e-02	5.58280e-01	-	18
64	1.00456e-03	3.71590e-04	0.94	1.11137e-02	2.94466e-01	0.92	113
128	2.48565e-04	2.67810e-04	0.47	9.27231e-03	1.50823e-01	0.97	644
256	6.04620e-05	7.00763e-05	1.89	3.87511e-03	6.32475e-02	1.23	3877
$C_a = 20^\circ$							
32	3.96937e-03	7.08593e-04	-	1.55497e-02	5.62013e-01	-	4
64	1.00880e-03	2.93799e-04	1.27	8.94937e-03	2.87566e-01	0.97	15
128	2.43658e-04	1.44371e-04	1.03	5.72647e-03	1.53910e-01	0.90	154
256	6.10778e-05	6.57476e-05	1.11	3.81816e-03	6.73295e-02	1.17	1441

Table 4.10: ($\mu_+ = 10 \mu_- = \gamma = 1, \alpha = 0.15$) Expanding bubble problem on $(-1, 1)^2 \setminus [-\frac{1}{3}, \frac{1}{3}]^2$ over the time interval $[0, 1]$ for the P2-P0 element with adaptive mesh.

Finally, we would also like to investigate the effect of using adaptive bulk meshes, that are refined close to the interface. An example mesh is shown on the right-hand side of Figure 4.3, and we list our employed discretization parameters in Table 4.9. Obviously the volume criterion (3.48) cannot be used for an adaptive mesh since it would be always violated therefore we use the angle criterion (3.49) with $C_a = 20^\circ$. The observed errors for our numerical approximation are shown in Table 4.10, 4.11 and 4.12. Comparing the error quantities in Tables 4.6, 4.7 and 4.8 against the ones in Tables 4.10, 4.11 and 4.12 we note that there appears to be no advantage in using a highly refined mesh near the moving interface. Again the element which performs

J_Γ	$\ \Gamma^h - \Gamma\ _{L^\infty}$	$\ \vec{U} - I_2^h \vec{u}\ _{L^2}$	EOC	$\ \vec{U} - I_2^h \vec{u}\ _{L^2(H^1)}$	$\ P - p\ _{L^2}$	EOC	CPU[s]
no remeshing							
32	4.44770e-03	1.03835e-03	-	2.09015e-02	5.74058e-01	-	2
64	9.96385e-04	1.24152e-04	3.06	5.85650e-03	2.79564e-01	1.04	22
128	2.43860e-04	3.43865e-05	1.85	2.92915e-03	1.48563e-01	0.91	209
256	6.09133e-05	2.85605e-05	0.26	2.71585e-03	7.95602e-02	0.88	4281
$C_a = 60^\circ$							
32	4.04836e-03	1.03041e-03	-	2.11862e-02	5.58428e-01	-	13
64	1.06336e-03	5.81260e-04	0.83	1.47843e-02	2.94451e-01	0.92	52
128	2.64772e-04	4.48334e-04	0.37	1.27870e-02	1.50552e-01	0.97	364
256	6.39800e-05	1.38724e-04	1.65	5.44161e-03	6.32714e-02	1.22	3743
$C_a = 20^\circ$							
32	4.08914e-03	9.75075e-04	-	1.98793e-02	5.63360e-01	-	5
64	1.05303e-03	4.43826e-04	1.14	1.14591e-02	2.87514e-01	0.97	13
128	2.50894e-04	2.89007e-04	0.62	8.72470e-03	1.54031e-01	0.90	148
256	6.40185e-05	1.15617e-04	1.29	5.10565e-03	6.98979e-02	1.11	2143

Table 4.11: ($\mu_+ = 10, \mu_- = \gamma = 1, \alpha = 0.15$) Expanding bubble problem on $(-1, 1)^2 \setminus [-\frac{1}{3}, \frac{1}{3}]^2$ over the time interval $[0, 1]$ for the P2–P1^{dgr} element with adaptive mesh.

J_Γ	$\ \Gamma^h - \Gamma\ _{L^\infty}$	$\ \vec{U} - I_2^h \vec{u}\ _{L^2}$	EOC	$\ \vec{U} - I_2^h \vec{u}\ _{L^2(H^1)}$	$\ P - p\ _{L^2}$	EOC	CPU[s]
no remeshing							
32	4.39967e-03	1.14087e-03	-	2.26396e-02	5.73270e-01	-	6
64	9.94365e-04	1.34986e-04	3.08	6.01358e-03	2.79584e-01	1.04	25
128	2.43769e-04	3.91547e-05	1.79	3.13728e-03	1.48565e-01	0.91	210
256	6.08641e-05	3.20203e-05	0.28	2.77934e-03	7.95609e-02	0.88	3798
$C_a = 60^\circ$							
32	3.97673e-03	1.16740e-03	-	2.54389e-02	5.59015e-01	-	18
64	1.04465e-03	6.57166e-04	0.83	1.84165e-02	2.94657e-01	0.92	81
128	2.64078e-04	5.07829e-04	0.37	1.60658e-02	1.50595e-01	0.97	385
256	6.39339e-05	1.55008e-04	1.67	7.26636e-03	6.33057e-02	1.22	3274
$C_a = 20^\circ$							
32	4.02881e-03	1.12100e-03	-	2.32002e-02	5.63527e-01	-	4
64	1.04388e-03	5.00129e-04	1.16	1.39060e-02	2.85520e-01	0.98	18
128	2.49831e-04	3.25755e-04	0.62	1.17532e-02	1.54026e-01	0.89	172
256	6.45554e-05	1.34537e-04	1.25	6.48976e-03	6.98821e-02	1.11	2701

Table 4.12: ($\mu_+ = 10, \mu_- = \gamma = 1, \alpha = 0.15$) Expanding bubble problem on $(-1, 1)^2 \setminus [-\frac{1}{3}, \frac{1}{3}]^2$ over the time interval $[0, 1]$ for the P2–(P1+P0) element with adaptive mesh.

better in term of errors is the P2–P0 element which, together with the choice of $C_a = 20^\circ$, gives the best result in terms of accuracy and performance.

The evolution of the discrete pressure solution in the case $J_\Gamma = 64$, for the run with $C_a = 60^\circ$, can be seen in Figure 4.5.

4.4 EQUIDISTRIBUTION PROPERTY IN 2D

We now demonstrate the remarkable equidistribution property of our method showing that the circular, equidistributed numerical steady state solution is recovered by our method even if we choose a very nonuniform initial interface Γ^0 . This is the analogue of what shown in §2.8.2 for a pure geometric PDE. In particular, for the presented numerical simulation, we take Γ^0 to be a very nonuniform approximation of a unit circle, where we represent the upper half of the circle by a single vertex, while the lower half resembles a semicircle. In total we use $J_\Gamma = 32$ elements for Γ^0 and we start with a very nonuniform bulk mesh with $J_\Omega^0 = 670$ elements. Of course, the initial bulk mesh has to respect the nonuniform approximation of the interface, and so is very nonuniform itself. However, we see from the evolution in Figure 4.6 that as the interface gets closer and closer to an equidistributed approximation of a circle, the bulk mesh also becomes more uniform. For the presented simulation we used the physical parameters $\mu = \gamma = 1$. The uniform time step size is chosen as $\tau = 10^{-4}$ and we set $C_v = 3$, recall (3.48). In Figure 4.7 is shown the evolution of $\|\vec{U}^m\|_{L^\infty(\Omega)}$ which, as expected, converges to zero.

Finally, we would also like to investigate the effect of using an adaptive bulk mesh, which is more refined close to the interface, and performing only mesh smoothing. We use $J_\Gamma = 64$ elements for Γ^0 and $J_\Omega^0 = 954$ elements for the bulk. We see from the evolution in Figure 4.8 that, again, we obtain an equidistributed approximation of a circle. Obviously, since we never perform a remesh, the final bulk mesh quality is very poor. In Figure 4.9 is shown the evolution of $\|\vec{U}^m\|_{L^\infty(\Omega)}$ which, again, converges to zero. We notice that the evolution of the quantity $\|\vec{U}^m\|_{L^\infty(\Omega)}$ is now very smooth in comparison to the one reported in Figure 4.7 but this is not surprising since we never perform a remesh.

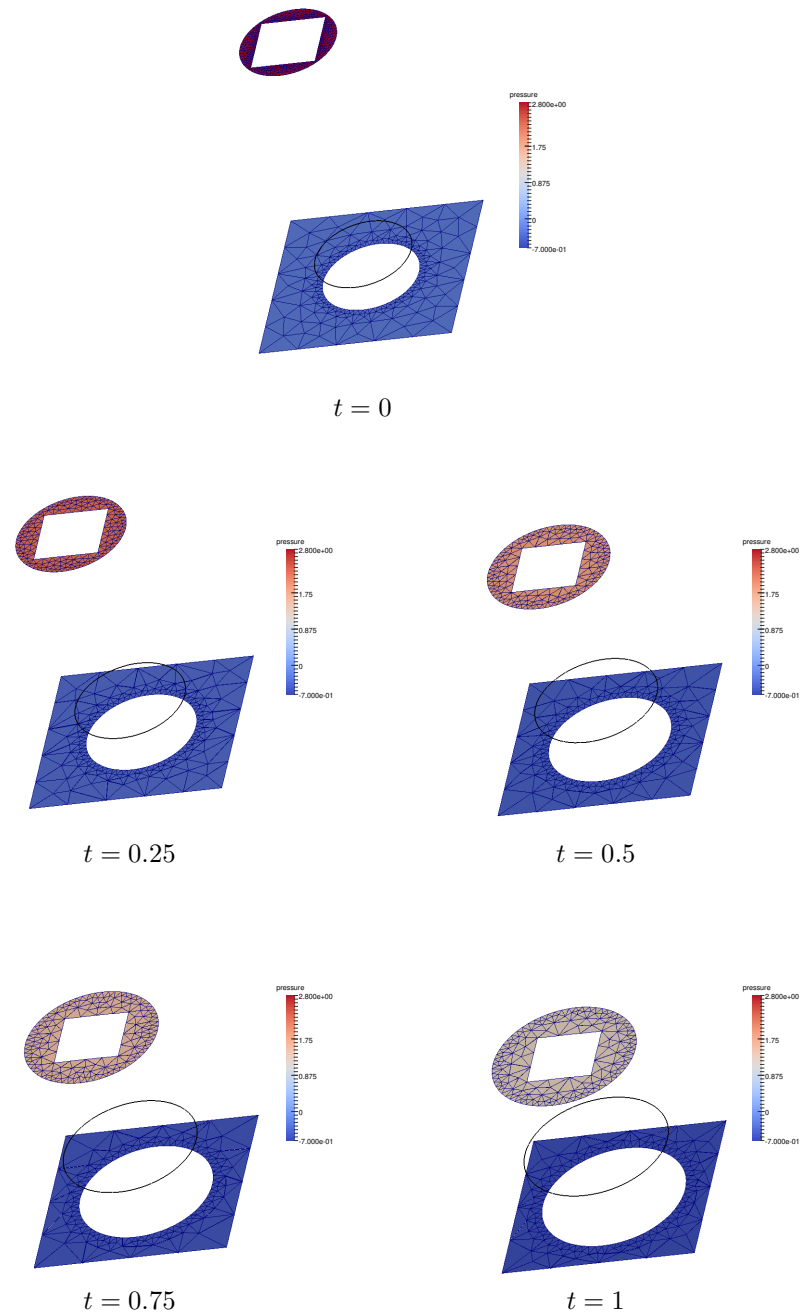


Figure 4.5: ($\mu_+ = 10 \mu_- = \gamma = 1, \alpha = 0.15$) Pressure evolution of the 2d expanding bubble for the P2–P0 element, adaptive mesh with $J_\Gamma = 64$ interface elements and $C_a = 60^\circ$.

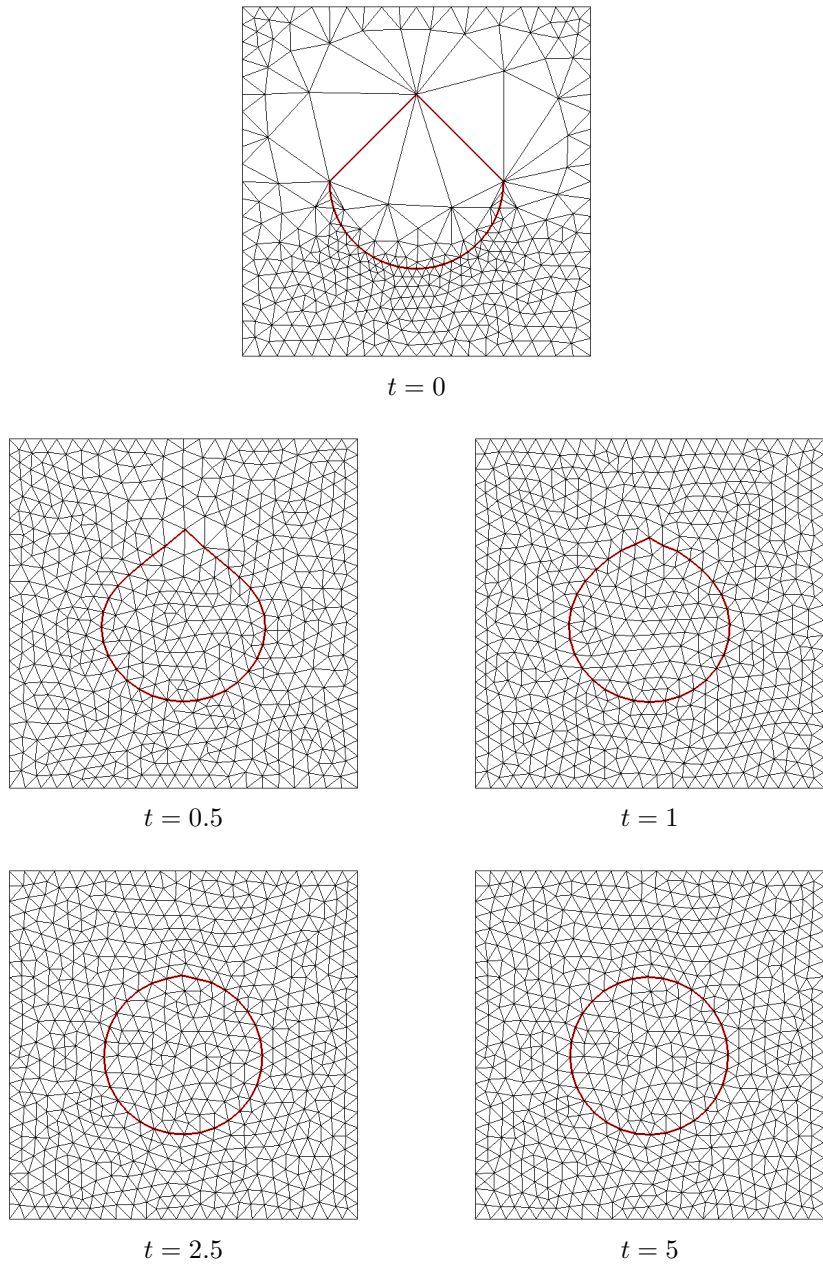


Figure 4.6: ($\mu = \gamma = 1$) Mesh evolution of a nonuniform circle formed by $J_\Gamma = 32$ elements. Here we use the P2–P0 element, and let $C_v = 3$.

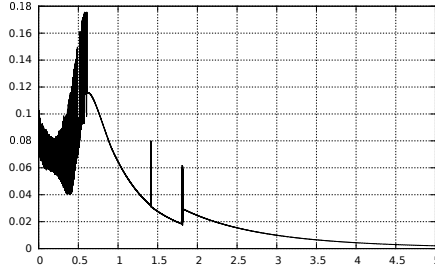


Figure 4.7: $\|\vec{U}^m\|_{L^\infty(\Omega)}$ evolution for the simulation in Figure 4.6.

4.5 ENERGY DECAY AND AREA CONSERVATION IN 2D

In Figure 4.10 we show the pressure evolution for a simulation that starts with an initial ellipse, with major and minor axes of 1.6 and 0.75. We use the parameters $\mu = \gamma = 1$, $\tau = 10^{-2}$ and $T = 10$. The initial interface is discretized with $J_\Gamma = 40$ surface elements while the initial bulk mesh is nearly uniform and it has $J_\Omega^0 = 1112$ elements. We employ the P2–P0 element and use the remeshing parameter $C_v = 3$ during the evolution. Figure 4.11 shows the evolution of the relative inner area $\frac{\mathcal{L}^2(\Omega_-^m)}{\mathcal{L}^2(\Omega_-^0)}$ and the evolution of the interface energy $\gamma \mathcal{H}^1(\Gamma^m)$. The graphs show that the inner area is nearly conserved, and that the interface energy is monotonically decreasing. We point out that, since there is no exact solution to the problem, we cannot show the pressure state at time $t = 0$ therefore we show the pressure state at $t = 10^{-5}$, which is computed with the help of our scheme with one time step of size $\tau = 10^{-5}$.

As a comparison, we show in Figure 4.12 and 4.13 the same simulation when no remeshings are performed. We clearly see that due to the strong deformation of the interface, this leads to elongated elements in the inner and in the outer phase of the bulk finite element mesh.

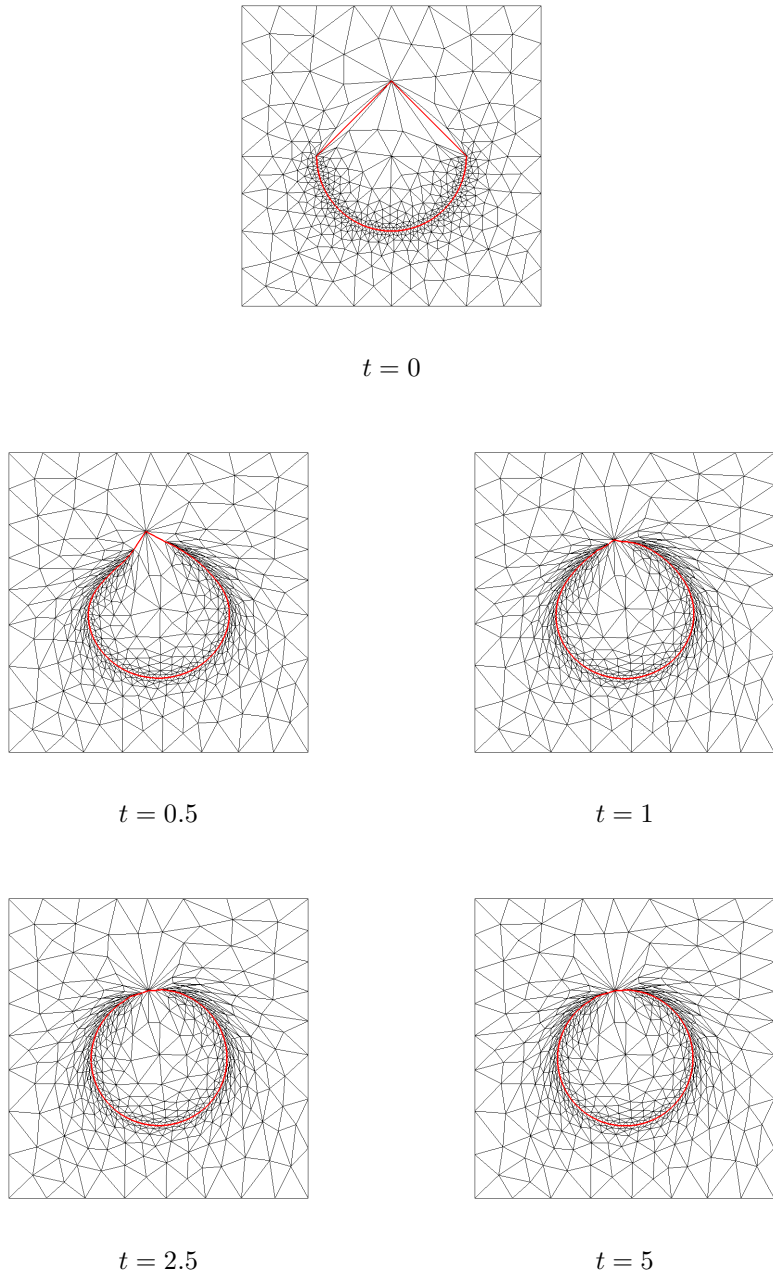


Figure 4.8: ($\mu = \gamma = 1$) Mesh evolution of a nonuniform circle formed by $J_\Gamma = 64$ elements and adaptive bulk mesh. Here we use the P2–P0 element, and no remeshing.

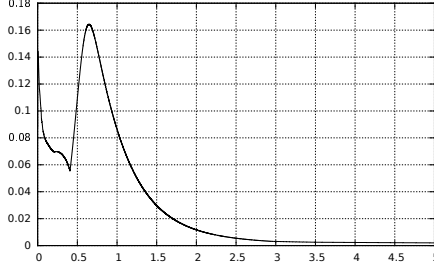


Figure 4.9: $\|\vec{U}^m\|_{L^\infty(\Omega)}$ evolution for the simulation in Figure 4.8.

4.6 SHEAR FLOW EXPERIMENT IN 2D

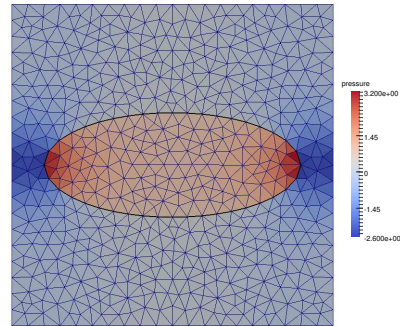
As the final 2d numerical simulation we present a shear flow experiment. Here we prescribe the inhomogeneous Dirichlet boundary condition

$$\vec{g}(\vec{z}) = (z_2, 0)^T \quad \text{on } \partial_1 \Omega = \partial \Omega,$$

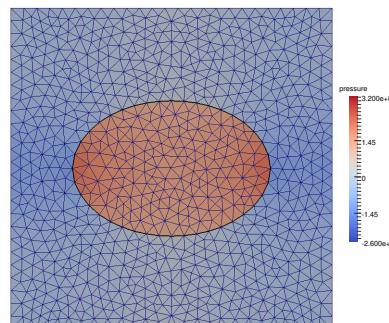
and we use the parameters $\mu = 1$, $\gamma = 3$, $\tau = 10^{-2}$ and $T = 5$. The initial interface is discretized with $J_\Gamma = 64$ surface elements, and the initial bulk mesh is nearly uniform with $J_\Omega^0 = 4240$ elements. In Figure 4.14 we show the evolution of the discrete pressures for a simulation with $C_v = 3$ for the P2–P0 element, while the velocities are visualized in Figure 4.15.

A plot of the relative inner area over time is shown in Figure 4.16, where we again observe that our numerical method maintains the enclosed volume well.

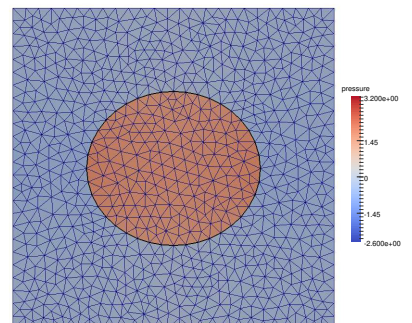
Finally we want to compare the performance of different preconditioners for the preconditioned GMRES used to solve the reduce system (3.36a) or, depending on the pressure space, (3.43). In Table 4.13 we report the CPU time, in seconds, and the number of GMRES iteration to solve the algebraic system (3.43) at the first time step, $m = 0$. We employ nearly uniform bulk meshes and the P2–(P1+P0) element. We test the direct preconditioner (3.45) factorizing it alternatively with either UMFPACK or SPQR and the block preconditioner (3.42) with restart value either 50 or 1000. We can notice that the direct preconditioner, whose matrix is equivalent to the standard Stokes discretization (3.37) perform extremely well in terms of CPU time and



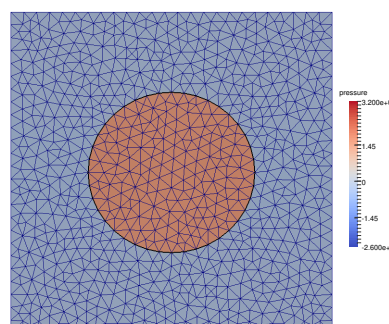
$t = 10^{-5}$



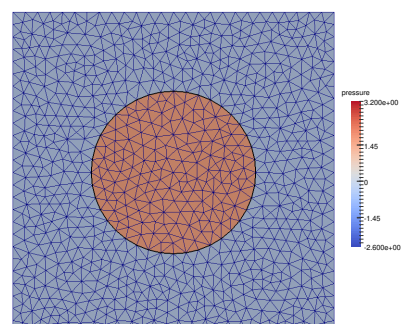
$t = 2.5$



$t = 5$



$t = 7.5$



$t = 10$

Figure 4.10: ($\mu = \gamma = 1$) Pressure evolution of an ellipse that evolves towards a circle. Here we use the P2–P0 element with $J_\Gamma = 40$ interface elements and $C_v = 3$.

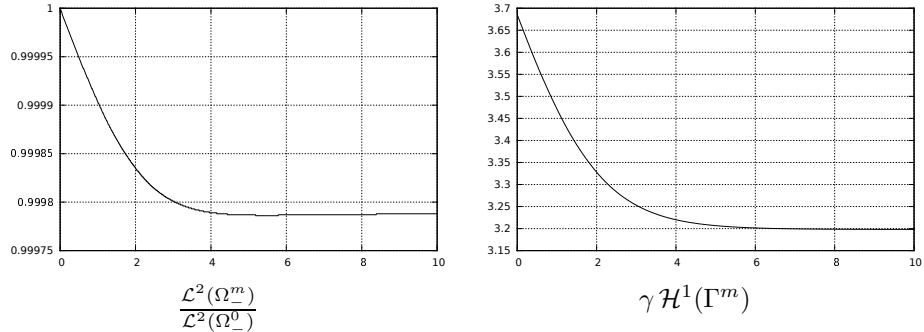
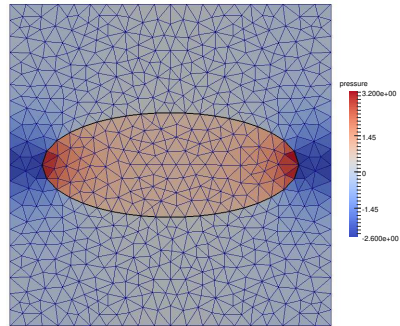


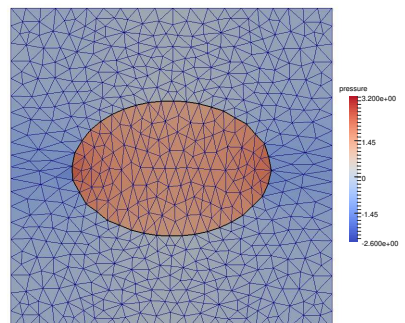
Figure 4.11: Evolutions of the relative inner area and the interface energy for the simulation in Figure 4.10.

J_Γ	Direct UMFPACK		Direct SPQR		Block restart 50		Block restart 1000	
	CPU[s]	iterations	CPU[s]	iterations	CPU[s]	iterations	CPU[s]	iterations
16	0.06	6	0.13	5	0.94	349	1.16	221
32	0.33	7	0.68	6	11.33	839	11.51	441
64	1.83	8	4.16	8	138.58	2026	136.99	772
128	10.05	9	25.71	9	2079.82	6436	1442.76	1745

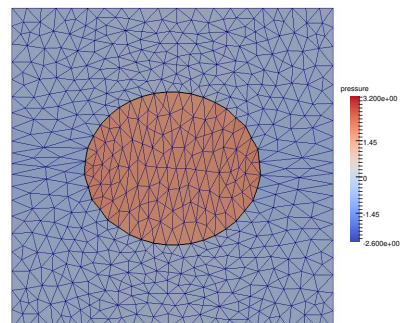
Table 4.13: ($\mu = 1, \gamma = 3$) Time and number of GMRES iterations to solve the algebraic system (3.43) adopting different preconditioners for the 2d shear flow using P2-(P1+P0) element, nearly uniform mesh and $m = 0$.



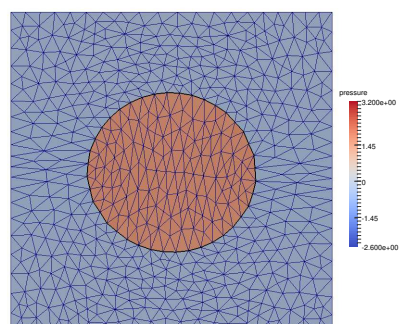
$t = 10^{-5}$



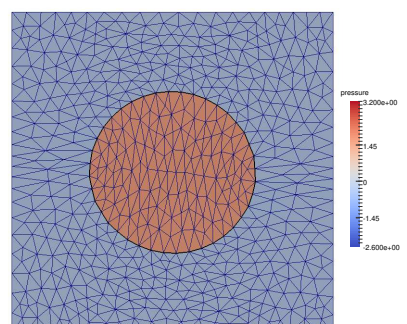
$t = 2.5$



$t = 5$



$t = 7.5$



$t = 10$

Figure 4.12: ($\mu = \gamma = 1$) Pressure evolution of an ellipse that evolves towards a circle. Here we use the P2–P0 element with $J_\Gamma = 40$ interface elements and no remeshing.

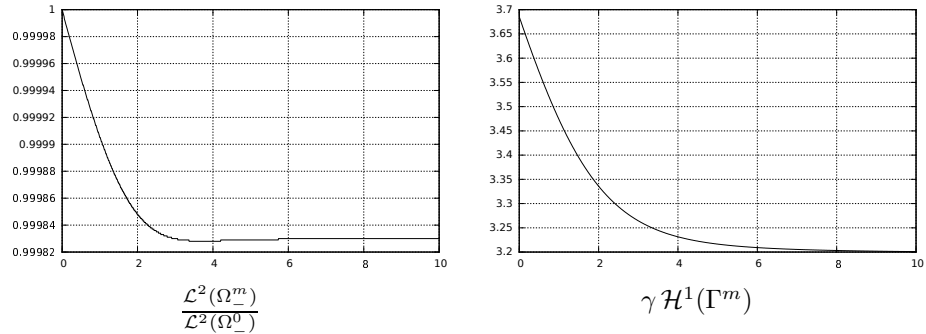


Figure 4.13: Evolutions of the relative inner area and the interface energy for the simulation in Figure 4.12.

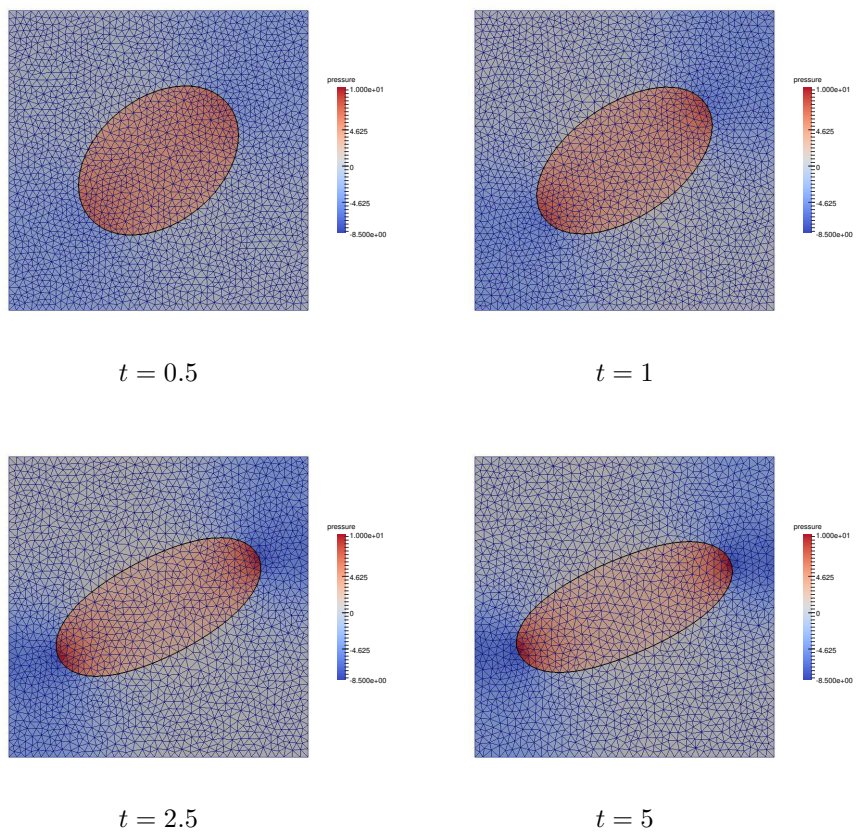


Figure 4.14: ($\mu = 1, \gamma = 3$) Pressure evolution for the 2d shear flow with $C_v = 3$ for the P2-P0 element, nearly uniform mesh with $J_\Gamma = 64$ interface elements.

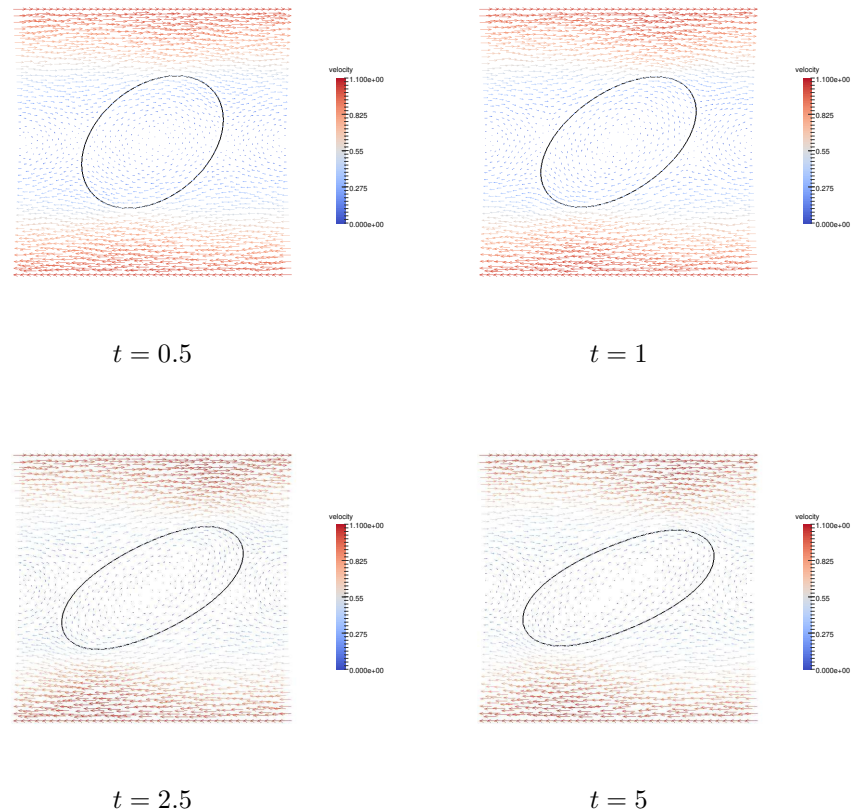


Figure 4.15: Velocity vector field for the simulation in Figure 4.14.

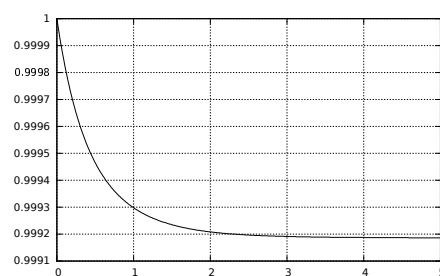


Figure 4.16: A plot of the relative inner area $\frac{\mathcal{L}^2(\Omega_-^m)}{\mathcal{L}^2(\Omega_-^0)}$ over time for the simulation in Figure 4.14.

number of GMRES iterations. This is not very surprising since the preconditioner and the reduced two-phase stokes system have almost the same matrix. Therefore the number of GMRES iterations is very low. Moreover, the factorization is computed only once with both SPQR and UMFPACK so it is extremely efficient to apply the preconditioner at every GMRES iteration. On the other hand, the block preconditioner perform very poorly requiring a very high number of GMRES iterations in order to converge. An increase of the restart value obviously reduces the number of GMRES iterations but also drastically increases the memory footprint. Moreover, the application of the preconditioner consists of doing the backward substitution (3.44) which is expensive.

4.7 CONVERGENCE TEST IN 3D

Similarly to §4.3, we perform the following convergence test for a stationary spherical bubble in 3d. Let $\mu = \gamma = 1$. Then the true solution (4.1a,b) reduces to $r(t) = \frac{1}{2}$, $\vec{u}(\cdot, t) = \vec{0}$ and $p(t) = 4\mathcal{X}_{\Omega_{-(0)}} - \frac{\pi}{12}$ for all $t \geq 0$. We approximate this stationary solution on nearly uniform meshes that feature $J_\Gamma = 32, 220$ and 596 interface elements, and $J_\Omega^0 = 408, 3590$ and 20473 bulk elements, respectively. Here, in contrast to the situation in 2d, we are not able to define Γ^0 such that the vertices of Γ^0 lie on $\Gamma(0)$ and such that (3.23) is satisfied. As we would like to demonstrate the ability of our method to recover the discrete stationary solution (3.24) also in 3d, we choose the initial interface Γ^0 such that (3.23) holds, at the expense of a nonzero initial error $\|\Gamma^0 - \Gamma(0)\|_{L^\infty}$, recall (4.3). We obtain such an initial triangulation with the help of the numerical scheme (2.34a–b) from Chapter 2 for surface diffusion, which is a gradient flow for surface area that maintains the enclosed volume. See Figure 4.17, or [8, Fig. 11], for an evolution towards a polyhedral approximation of a sphere that satisfies (3.23), and hence also (3.22). The sphere in Figure 4.17 has $J_\Gamma = 596$ elements.

We report on the errors for the P2–P0, P2–P1, P2–P1^{dgr} and P2–(P1+P0) elements in Tables 4.14, 4.15, 4.16 and 4.17, respectively. Here we note that, as yet, for the pairs P2–P0, P2–P1^{dgr} and P2–(P1+P0) there exist no proofs

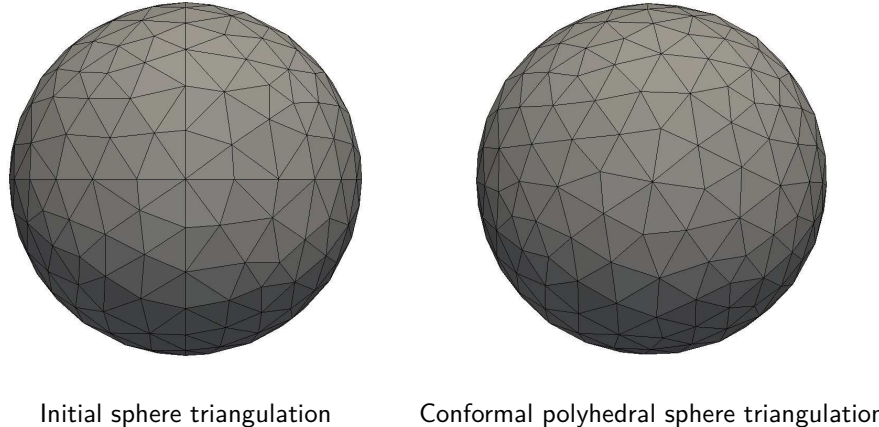


Figure 4.17: Initial triangulation of a sphere and conformal polyhedral sphere after surface diffusion, with $J_\Gamma = 596$.

J_Γ	$\ \Gamma^h - \Gamma\ _{L^\infty}$	$\ \vec{U} - I_2^h \vec{u}\ _{L^2}$	$\ P - p\ _{L^2}$	EOC	CPU[s]
32	2.97986e-02	0	1.65555e-00	-	385
220	5.80971e-03	0	7.14269e-01	1.21	4699
596	2.42857e-03	0	3.58466e-01	0.99	51604

Table 4.14: ($\mu = \gamma = 1$) Stationary bubble problem on $(-1, 1)^3$ over the time interval $[0, 1]$ for the P2–P0 element.

in the literature that the LBB condition (3.9) holds, see e.g. the discussion in [16, Remark 8.4.3]. However, in practice we encountered no problems when using these spaces, and our iterative solver always converged to a solution of the scheme (3.11a–d). For both sets of simulations we use the uniform time step size $\tau = 10^{-2}$.

We note that we again recover the discrete stationary solutions (3.24) for the P2–P0, P2–P1^{dgr} and P2–(P1+P0) elements while, as before, the P2–P1

J_Γ	$\ \Gamma^h - \Gamma\ _{L^\infty}$	$\ \vec{U} - I_2^h \vec{u}\ _{L^2}$	$\ P - p\ _{L^2}$	EOC	CPU[s]
32	1.56938e-01	6.01956e-02	2.10996e-00	-	315
220	7.28946e-02	3.13992e-02	1.47595e-00	0.52	4231
596	4.04291e-02	1.34276e-02	1.09674e-00	0.43	51287

Table 4.15: ($\mu = \gamma = 1$) Stationary bubble problem on $(-1, 1)^3$ over the time interval $[0, 1]$ for the P2–P1 element.

J_Γ	$\ \Gamma^h - \Gamma\ _{L^\infty}$	$\ \vec{U} - I_2^h \vec{u}\ _{L^2}$	$\ P - p\ _{L^2}$	EOC	CPU[s]
32	2.97986e-02	0	1.65555e-00	-	73
220	5.80971e-03	0	7.14269e-01	1.21	1018
596	2.42857e-03	0	3.58466e-01	0.99	17814

Table 4.16: ($\mu = \gamma = 1$) Stationary bubble problem on $(-1, 1)^3$ over the time interval $[0, 1]$ for the P2–P1^{dgr} element.

J_Γ	$\ \Gamma^h - \Gamma\ _{L^\infty}$	$\ \vec{U} - I_2^h \vec{u}\ _{L^2}$	$\ P - p\ _{L^2}$	EOC	CPU[s]
32	2.97986e-02	0	1.65749e-00	-	568
220	5.80971e-03	0	7.15353e-01	1.21	9174
596	2.42857e-03	0	3.59181e-01	0.99	121110

Table 4.17: ($\mu = \gamma = 1$) Stationary bubble problem on $(-1, 1)^3$ over the time interval $[0, 1]$ for the P2–(P1+P0) element.

element does not capture exactly the true solution since this element does not satisfy the hypothesis that $\mathcal{X}_{\Omega_m} \in \mathbb{P}^m$ of Theorem 10. Here this leads to a nonzero error in the position of the discrete interface, because the vertices of the initial interface Γ^0 do not lie on $\Gamma(0)$.

4.8 SHEAR FLOW EXPERIMENT IN 3D

Finally, we also report on a 3d shear flow experiment. The initial interface mesh has $J_\Gamma = 596$ elements, while the nearly uniform bulk mesh is made up of $J_\Omega^0 = 19641$ elements. We prescribe the inhomogeneous Dirichlet boundary condition

$$\vec{g}(\vec{z}) = (z_3, 0, 0)^T \quad \text{on } \partial_1 \Omega = \partial \Omega,$$

and we use the parameters $\mu = 1$, $\gamma = 3$, $\tau = 10^{-2}$ and $T = 5$. In Figure 4.18 we show the evolution of the discrete interface for a simulation with $C_v = 3$ for the P2–P0 element, while the velocities are visualized in Figure 4.19.

A plot of the relative inner volume over time is shown in Figure 4.20, where we again observe that our numerical method maintains the enclosed volume well.

Finally, as in the 2d case, see Table 4.13, we want to compare the perfor-

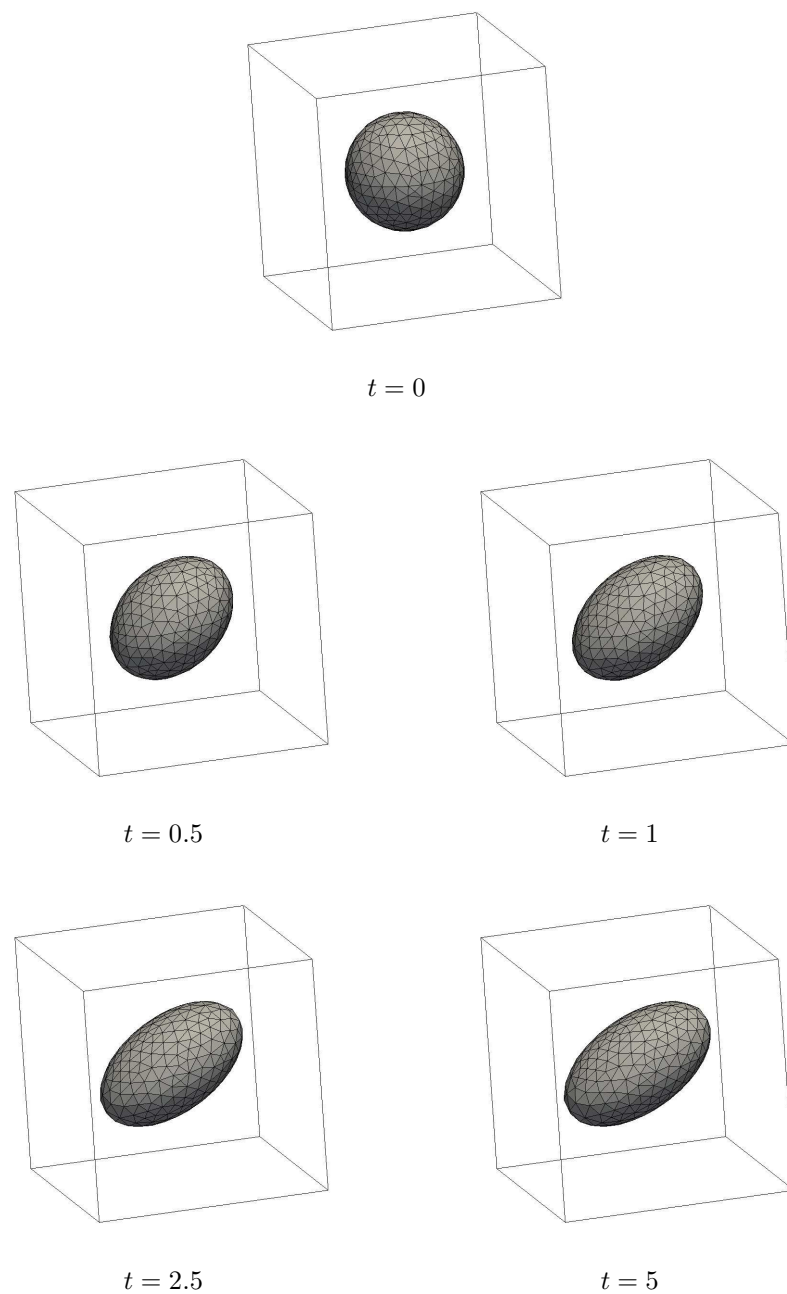


Figure 4.18: ($\mu = 1, \gamma = 3$) Interface evolution for the 3d shear flow with $C_v = 3$ for the P2–P0 element, nearly uniform mesh with $J_\Gamma = 596$ interface elements.

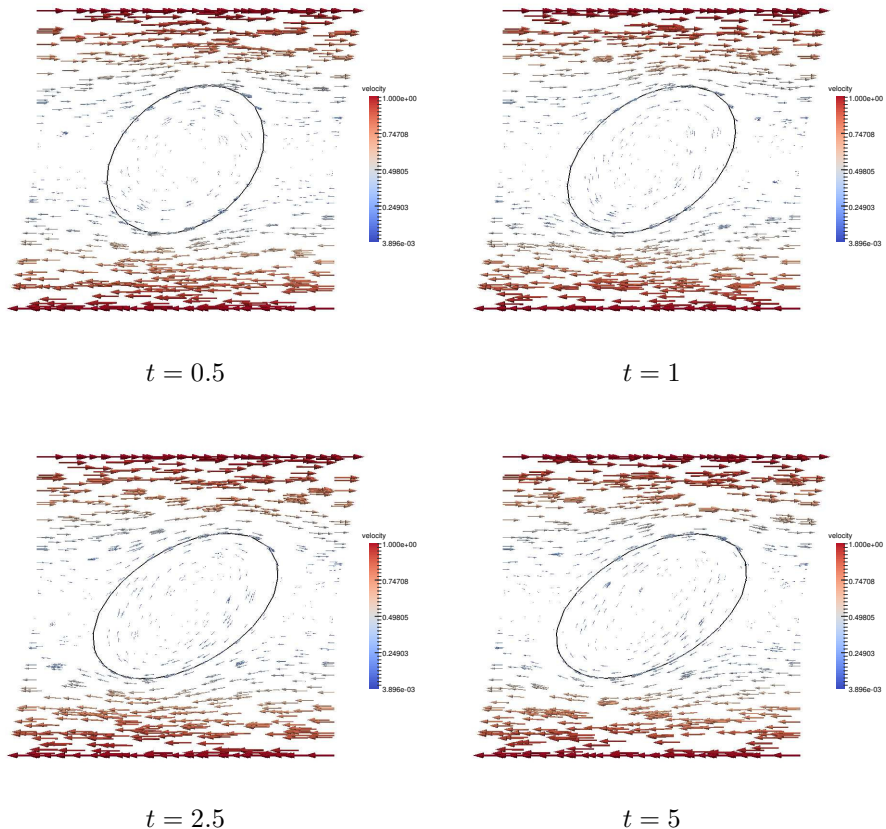


Figure 4.19: Velocity vector field in the plane normal to $(0, 1, 0)^T$ and passing through the origin for the simulation in Figure 4.18.

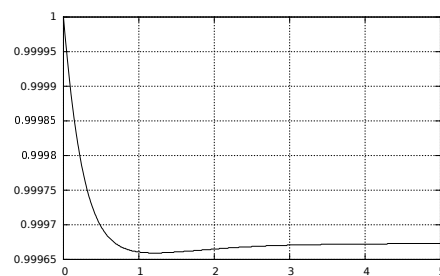


Figure 4.20: A plot of the relative inner volume $\frac{\mathcal{L}^3(\Omega^m)}{\mathcal{L}^3(\Omega^0)}$ over time for the simulation in Figure 4.18.

J_Γ	Direct UMFPACK		Direct SPQR		Block restart 50		Block restart 1000	
	CPU[s]	iterations	CPU[s]	iterations	CPU[s]	iterations	CPU[s]	iterations
32	0.16	8	0.26	5	1.10	158	1.17	130
220	3.56	7	4.91	6	15.31	234	14.53	193
596	13.77	6	44.44	6	101.53	328	93.00	266

Table 4.18: ($\mu = 1, \gamma = 3$) Time and number of GMRES iterations to solve the algebraic system (3.43) adopting different preconditioners for the 3d shear flow using P2–(P1+P0) element, adaptive mesh and $m = 0$.

mance of different preconditioners. In Table 4.18 we report the CPU time, in seconds, and the number of GMRES iteration to solve the algebraic system (3.43) at the first time step, $m = 0$. We employ adaptive bulk meshes and the P2–(P1+P0) element. We test the direct preconditioner (3.45) factorizing it alternatively with either UMFPACK or SPQR and the block preconditioner (3.42) with restart value either 50 or 1000. We observe that also in 3d the direct preconditioners outperform the block preconditioner both in term of GMRES iterations and CPU time.

5

STANDARD FINITE ELEMENT APPROXIMATIONS FOR TWO-PHASE NAVIER–STOKES FLOW

We now present two novel finite element approximations for incompressible two-phase Navier–Stokes flow that use a fitted approach with piecewise linear parametric finite elements to describe the moving discrete interface, and that employ standard velocity and pressure finite element spaces in the bulk.

The chapter is organised as follows: in §5.1 we state the mathematical model for the incompressible two-phase Navier–Stokes flow; in §5.2 we derive a standard weak formulation and an alternative weak formulation based on an antisymmetric rewrite on which our finite element approximations are going to be based; in §5.3 we present our antisymmetric fitted finite element discretization, we prove the existence and uniqueness of a discrete solution and we demonstrate that this scheme has certain stability properties; in §5.4 we present our standard fitted finite element discretization; in §5.5 we explain

the various solutions methods used to solve the algebraic system; in §5.6 we examine the techniques used to interpolate the velocity.

5.1 MATHEMATICAL MODEL

We now consider two-phase Navier–Stokes flow in a given domain $\Omega \subset \mathbb{R}^d$, where $d = 2$ or $d = 3$. As already described in §1.1 and §3.1, the domain Ω contains two different immiscible, incompressible fluids (liquid-liquid or liquid-gas) which for all $t \in [0, T]$ occupy time dependent regions $\Omega_+(t)$ and $\Omega_-(t) := \Omega \setminus \overline{\Omega}_+(t)$ and which are separated by an interface $(\Gamma(t))_{t \in [0, T]}$, $\Gamma(t) \subset \Omega$. Consistently with two-phase Stokes flow, we limit ourselves to interfaces formed by closed hypersurfaces, see Figure 1.1 for a pictorial representation in dimension $d = 2$.

We treat the interface $\Gamma(t)$ with the same technique used for the two-phase Stokes, see Chapter 3. Therefore we use a front tracking approach, see §2.4, which parametrizes the unknown interface $\Gamma(t)$ as $\vec{x}(\cdot, t) : \Upsilon \rightarrow \mathbb{R}^d$ where $\Upsilon \subset \mathbb{R}^d$ is a given reference manifold such that $\Gamma(t) = \vec{x}(\Upsilon, t)$. As usual, we require that the evolving hypersurface is sufficiently smooth and without boundary. The velocity $\vec{\mathcal{V}}$ of $\Gamma(t)$ is defined by the equation (2.26) which we report here for the sake of completeness

$$\vec{\mathcal{V}}(\vec{z}, t) := \vec{x}_t(\vec{q}, t) \quad \forall \vec{z} = \vec{x}(\vec{q}, t) \in \Gamma(t),$$

where $\vec{\mathcal{V}} \cdot \vec{\nu}$ is the normal velocity of the evolving hypersurface $\Gamma(t)$, and $\vec{\nu}(t)$ is the unit normal on $\Gamma(t)$ pointing into $\Omega_+(t)$.

The fluid dynamics in the bulk domain Ω is governed by the two-phase Navier–Stokes model (1.14a–b), which describes the velocity \vec{u} and pressure p fields of the fluid. The velocity and stress tensor, see (1.1), need to be coupled across the free surface $\Gamma(t)$. Therefore we impose the interface conditions (1.16), (1.25) and (1.17). In order to close the system, we prescribe the initial data $\Gamma(0) = \Gamma_0$ and the initial velocity $\vec{u}(0) = \vec{u}_0$. Finally, we impose the Dirichlet condition $\vec{u} = \vec{g}$ on $\partial_1 \Omega$ and the free-slip condition $\vec{u} \cdot \vec{n} = 0$ and $\underline{\sigma} \vec{n} \cdot \vec{t} = 0$, $\forall \vec{t} \in \{\vec{n}\}^\perp$, on $\partial_2 \Omega$, with \vec{n} denoting the outer unit normal of $\partial \Omega$

and $\{\vec{n}\}^\perp := \{\vec{t} \in \mathbb{R}^d : \vec{t} \cdot \vec{n} = 0\}$. As usual, it holds that $\partial\Omega = \partial_1\Omega \cup \partial_2\Omega$ and $\partial_1\Omega \cap \partial_2\Omega = \emptyset$. Therefore the total system of equations can be rewritten as follows:

$$\begin{aligned} \rho(\vec{u}_t + (\vec{u} \cdot \nabla)\vec{u}) - 2\mu \nabla \cdot \underline{D}(\vec{u}) + \nabla p &= \vec{f} && \text{in } \Omega_\pm(t), \quad (5.1a) \\ \nabla \cdot \vec{u} &= 0 && \text{in } \Omega_\pm(t), \quad (5.1b) \\ \vec{u} &= \vec{g} && \text{on } \partial_1\Omega, \quad (5.1c) \\ \vec{u} \cdot \vec{n} = 0, \quad \underline{\sigma} \vec{n} \cdot \vec{t} &= 0 \quad \forall \vec{t} \in \{\vec{n}\}^\perp && \text{on } \partial_2\Omega, \quad (5.1d) \\ [\vec{u}]_-^+ &= \vec{0} && \text{on } \Gamma(t), \quad (5.1e) \\ [2\mu \underline{D}(\vec{u}) \cdot \vec{\nu} - p \vec{\nu}]_-^+ &= -\gamma \varkappa \vec{\nu} && \text{on } \Gamma(t), \quad (5.1f) \\ (\vec{\mathcal{V}} - \vec{u}) \cdot \vec{\nu} &= 0 && \text{on } \Gamma(t), \quad (5.1g) \\ \Gamma(0) &= \Gamma_0, && \quad (5.1h) \\ \vec{u}(0) &= \vec{u}_0. && \quad (5.1i) \end{aligned}$$

As usual, let $\rho(t) = \rho_+ \mathcal{X}_{\Omega_+(t)} + \rho_- \mathcal{X}_{\Omega_-(t)}$, with $\rho_\pm \in \mathbb{R}_{>0}$, be the fluid density in the two phases, let $\mu(t) = \mu_+ \mathcal{X}_{\Omega_+(t)} + \mu_- \mathcal{X}_{\Omega_-(t)}$, with $\mu_\pm \in \mathbb{R}_{>0}$, be the dynamic viscosities in the two phases, let $\underline{D}(\vec{u}) := \frac{1}{2}(\nabla \vec{u} + (\nabla \vec{u})^T)$ be the rate-of-deformation tensor, let $\vec{f} := \rho \vec{f}_1 + \vec{f}_2$ be a possible forcing term, let $\gamma > 0$ be the surface tension coefficient and let \varkappa be the mean curvature of $\Gamma(t)$. See Chapter 1 for more details.

5.2 WEAK FORMULATION

A standard weak formulation of (5.1a–i) can be obtained by proceeding analogously to the Stokes case, see §3.2. We define the same function spaces

$$\begin{aligned} \mathbb{U}(\vec{b}) &:= \{\vec{\phi} \in [H^1(\Omega)]^d : \vec{\phi} = \vec{b} \text{ on } \partial_1\Omega, \quad \vec{\phi} \cdot \vec{n} = 0 \text{ on } \partial_2\Omega\}, \\ \mathbb{P} &:= L^2(\Omega), \\ \tilde{\mathbb{P}} &:= \{\eta \in \mathbb{P} : \int_{\Omega} \eta \, d\mathcal{L}^d = 0\}, \end{aligned}$$

for a given $\vec{b} \in [H^1(\Omega)]^d$. As usual, let (\cdot, \cdot) and $\langle \cdot, \cdot \rangle_{\Gamma(t)}$ denote the L^2 -inner products on Ω and $\Gamma(t)$, respectively. In addition, we let \mathcal{L}^d and \mathcal{H}^{d-1} denote

the Lebesgue measure in \mathbb{R}^d and the $(d - 1)$ -dimensional Hausdorff measure, respectively.

Using (3.2) and (3.3), we can write the standard weak formulation of (5.1a–i) as follows. Given $\Gamma(0) = \Gamma_0$ and $\vec{u}(0) = \vec{u}_0$, for almost all $t \in (0, T)$ find $\Gamma(t)$ and $(\vec{u}, p, \boldsymbol{\varkappa}) \in \mathbb{U}(\vec{g}) \times \tilde{\mathbb{P}} \times H^1(\Gamma(t))$ such that

$$\begin{aligned} & (\rho \vec{u}_t, \vec{\xi}) + (\rho (\vec{u} \cdot \nabla) \vec{u}, \vec{\xi}) + 2 (\mu \underline{D}(\vec{u}), \underline{D}(\vec{\xi})) \\ & - (p, \nabla \cdot \vec{\xi}) - \gamma \langle \boldsymbol{\varkappa} \vec{\nu}, \vec{\xi} \rangle_{\Gamma(t)} = (\vec{f}, \vec{\xi}) \quad \forall \vec{\xi} \in \mathbb{U}(\vec{0}), \end{aligned} \quad (5.2a)$$

$$(\nabla \cdot \vec{u}, \varphi) = 0 \quad \forall \varphi \in \tilde{\mathbb{P}}, \quad (5.2b)$$

$$\langle \vec{\nu} - \vec{u}, \chi \vec{\nu} \rangle_{\Gamma(t)} = 0 \quad \forall \chi \in H^1(\Gamma(t)), \quad (5.2c)$$

$$\langle \boldsymbol{\varkappa} \vec{\nu}, \vec{\eta} \rangle_{\Gamma(t)} + \langle \nabla_s \text{id}, \nabla_s \vec{\eta} \rangle_{\Gamma(t)} = 0 \quad \forall \vec{\eta} \in [H^1(\Gamma(t))]^d \quad (5.2d)$$

holds for almost all times $t \in (0, T]$. Again, we notice that if $p \in \mathbb{P}$ is part of a solution to (5.1a–i), then so is $p + c$ for an arbitrary $c \in \mathbb{R}$.

An alternative to the weak formulation (5.2a–d) can be obtained following the paper [12]. The authors show that it is easy to derive an energy bound not only on the continuous level but also on the discrete level. Moreover, they are able to show existence/uniqueness results for the discrete solution. In order to obtain this alternative weak formulation, we want to rewrite the term $(\rho \vec{u}_t, \vec{\xi}) + (\rho (\vec{u} \cdot \nabla) \vec{u}, \vec{\xi})$ in (5.2a) in such a way that certain undesirable terms vanish when choosing $\vec{\xi} = \vec{u}$. Due to the resulting structure of the equation, we will refer to this form as the antisymmetric weak formulation.

First, we observe that for arbitrary functions $\vec{v}, \vec{\omega}, \vec{\xi} \in [H^1(\Omega)]^d$ it holds that

$$\begin{aligned} & [(\vec{v} \cdot \nabla) \vec{\omega}] \cdot \vec{\xi} = (\vec{v} \cdot \nabla) (\vec{\omega} \cdot \vec{\xi}) - [(\vec{v} \cdot \nabla) \vec{\xi}] \cdot \vec{\omega} \\ & = \frac{1}{2} (\vec{v} \cdot \nabla) (\vec{\omega} \cdot \vec{\xi}) + \frac{1}{2} (\vec{v} \cdot \nabla) (\vec{\omega} \cdot \vec{\xi}) - \frac{1}{2} [(\vec{v} \cdot \nabla) \vec{\xi}] \cdot \vec{\omega} - \frac{1}{2} [(\vec{v} \cdot \nabla) \vec{\xi}] \cdot \vec{\omega} \\ & = \frac{1}{2} (\vec{v} \cdot \nabla) (\vec{\omega} \cdot \vec{\xi}) + \frac{1}{2} [(\vec{v} \cdot \nabla) \vec{\omega}] \cdot \vec{\xi} - \frac{1}{2} [(\vec{v} \cdot \nabla) \vec{\xi}] \cdot \vec{\omega}. \end{aligned} \quad (5.3)$$

Choosing $\vec{v} = \vec{\omega} = \vec{u}$ in (5.3) and substituting it in the convection term

$(\rho(\vec{u} \cdot \nabla) \vec{u}, \vec{\xi})$, we obtain

$$(\rho(\vec{u} \cdot \nabla) \vec{u}, \vec{\xi}) = \frac{1}{2}(\rho, (\vec{u} \cdot \nabla)(\vec{u} \cdot \vec{\xi})) + \frac{1}{2}(\rho(\vec{u} \cdot \nabla) \vec{u}, \vec{\xi}) - \frac{1}{2}(\rho(\vec{u} \cdot \nabla) \vec{\xi}, \vec{u}). \quad (5.4)$$

Then we have for any $\vec{v} \in [H^1(\Omega)]^d$ and $\phi \in W_0^{1,\frac{3}{2}}(\Omega)$ that

$$\begin{aligned} (\rho, (\vec{v} \cdot \nabla) \phi) &= (\rho, \nabla \cdot (\phi \vec{v})) - (\rho(\nabla \cdot \vec{v}), \phi) \\ &= \langle [\rho]_-^+ \vec{v} \cdot \vec{\nu}, \phi \rangle_{\Gamma(t)} - (\rho(\nabla \cdot \vec{v}), \phi). \end{aligned} \quad (5.5)$$

Here we notice that (5.5) is well defined. Indeed, $\phi \in W_0^{1,\frac{3}{2}}(\Omega)$ implies that its trace is in $L^{\frac{3}{2}}(\partial\Omega)$. Moreover, given that $\vec{v} \in [H^1(\Omega)]^d$, it holds that $\vec{v} \cdot \vec{\nu} \in H^{\frac{1}{2}}(\partial\Omega)$, which implies, thanks to the continuous embedding theorems [23, Theorem 6.5 and 6.7], that $\vec{v} \cdot \vec{\nu} \in L^4(\partial\Omega)$. But we know, using the Hölder inequality, that the term $\langle [\rho]_-^+ \vec{v} \cdot \vec{\nu}, \phi \rangle_{\Gamma(t)}$ is well defined if $\vec{v} \cdot \vec{\nu}$ is at least in $L^3(\partial\Omega)$, which is indeed the case.

Moreover, if $\vec{u} \in [H^1(\Omega)]^d$ and $\vec{\xi} \in \mathbb{U}(\vec{0})$ then $\vec{u} \cdot \vec{\xi} \in W_0^{1,\frac{3}{2}}(\Omega)$. Indeed, $H^1(\Omega)$ is compactly embedded in $L^6(\Omega)$, for $d = 2$ or $d = 3$. By the generalized Hölder inequality we know that $(\nabla h)\omega \in [L^{\frac{3}{2}}(\Omega)]^d$ if $h \in H^1(\Omega)$ and $\omega \in L^6(\Omega)$. Therefore $\nabla(\vec{u} \cdot \vec{\xi}) \in [L^{\frac{3}{2}}(\Omega)]^d$, which implies $\vec{u} \cdot \vec{\xi} \in W_0^{1,\frac{3}{2}}(\Omega)$. Hence, it follows from taking $\phi = \vec{u} \cdot \vec{\xi}$ and $\vec{v} = \vec{u}$ in (5.5) and applying it to the first term on the right-hand side of (5.4) that

$$\begin{aligned} (\rho(\vec{u} \cdot \nabla) \vec{u}, \vec{\xi}) &= -\frac{1}{2} \langle [\rho]_-^+ \vec{u} \cdot \vec{\nu}, \vec{u} \cdot \vec{\xi} \rangle_{\Gamma(t)} - \frac{1}{2}(\rho(\nabla \cdot \vec{u}), \vec{u} \cdot \vec{\xi}) \\ &\quad + \frac{1}{2}(\rho(\vec{u} \cdot \nabla) \vec{u}, \vec{\xi}) - \frac{1}{2}(\rho(\vec{u} \cdot \nabla) \vec{\xi}, \vec{u}) \quad \forall \vec{\xi} \in \mathbb{U}(\vec{0}), \end{aligned} \quad (5.6)$$

and, using the incompressibility condition (5.1b), we obtain

$$\begin{aligned} (\rho(\vec{u} \cdot \nabla) \vec{u}, \vec{\xi}) &= \frac{1}{2}[(\rho(\vec{u} \cdot \nabla) \vec{u}, \vec{\xi}) - (\rho(\vec{u} \cdot \nabla) \vec{\xi}, \vec{u}) \\ &\quad - \langle [\rho]_-^+ \vec{u} \cdot \vec{\nu}, \vec{u} \cdot \vec{\xi} \rangle_{\Gamma(t)}] \quad \forall \vec{\xi} \in \mathbb{U}(\vec{0}). \end{aligned} \quad (5.7)$$

Next, we recall the Reynolds transport theorem

$$\frac{d}{dt} \int_{\Omega(t)} h \, d\mathcal{L}^d = \int_{\Omega(t)} h_t \, d\mathcal{L}^d + \int_{\Omega(t)} \nabla \cdot (h \vec{\mathcal{W}}) \, d\mathcal{L}^d, \quad (5.8)$$

where $\Omega(t)$ is a moving domain with velocity $\vec{\mathcal{W}}$ and $h : \mathbb{R}^d \rightarrow \mathbb{R}$ is a continuously differentiable function, see [4]. Then we can use (5.8) together with (5.1g), to rewrite the time derivative term $(\rho \vec{u}_t, \vec{\xi})$ and obtain

$$\begin{aligned} \frac{d}{dt}(\rho \vec{u}, \vec{\xi}) &= \frac{d}{dt} \left(\rho_+ \int_{\Omega_+(t)} \vec{u} \cdot \vec{\xi} \, d\mathcal{L}^d + \rho_- \int_{\Omega_-(t)} \vec{u} \cdot \vec{\xi} \, d\mathcal{L}^d \right) \\ &= (\rho \vec{u}_t, \vec{\xi}) - \langle [\rho]_+^+ \vec{\mathcal{V}} \cdot \vec{\nu}, \vec{u} \cdot \vec{\xi} \rangle_{\Gamma(t)} \\ &= (\rho \vec{u}_t, \vec{\xi}) - \langle [\rho]_-^+ \vec{u} \cdot \vec{\nu}, \vec{u} \cdot \vec{\xi} \rangle_{\Gamma(t)} \quad \forall \vec{\xi} \in \mathbb{U}(\vec{0}). \end{aligned} \quad (5.9)$$

Therefore, it follows from (5.9) that

$$(\rho \vec{u}_t, \vec{\xi}) = \frac{1}{2} \left[\frac{d}{dt}(\rho \vec{u}, \vec{\xi}) + (\rho \vec{u}_t, \vec{\xi}) + \langle [\rho]_-^+ \vec{u} \cdot \vec{\nu}, \vec{u} \cdot \vec{\xi} \rangle_{\Gamma(t)} \right] \quad \forall \vec{\xi} \in \mathbb{U}(\vec{0}),$$

which on combining with (5.7) yields that

$$\begin{aligned} &(\rho [\vec{u}_t + (\vec{u} \cdot \nabla) \vec{u}], \vec{\xi}) \\ &= \frac{1}{2} \left[\frac{d}{dt}(\rho \vec{u}, \vec{\xi}) + (\rho \vec{u}_t, \vec{\xi}) + (\rho, [(\vec{u} \cdot \nabla) \vec{u}] \cdot \vec{\xi} - [(\vec{u} \cdot \nabla) \vec{\xi}] \cdot \vec{u}) \right] \quad \forall \vec{\xi} \in \mathbb{U}(\vec{0}). \end{aligned} \quad (5.10)$$

Hence, the antisymmetric weak formulation of (5.1a–i) is given as follows. Given $\Gamma(0) = \Gamma_0$ and $\vec{u}(0) = \vec{u}_0$, for almost all $t \in (0, T)$ find $\Gamma(t)$ and

$(\vec{u}, p, \boldsymbol{\varkappa}) \in \mathbb{U}(\vec{g}) \times \tilde{\mathbb{P}} \times H^1(\Gamma(t))$ such that

$$\begin{aligned} & \frac{1}{2} \left[\frac{d}{dt} (\rho \vec{u}, \vec{\xi}) + (\rho \vec{u}_t, \vec{\xi}) + (\rho, [(\vec{u} \cdot \nabla) \vec{u}] \cdot \vec{\xi} - [(\vec{u} \cdot \nabla) \vec{\xi}] \cdot \vec{u}) \right] \\ & + 2 \left(\mu \underline{D}(\vec{u}), \underline{D}(\vec{\xi}) \right) - (p, \nabla \cdot \vec{\xi}) \\ & - \gamma \langle \boldsymbol{\varkappa} \vec{\nu}, \vec{\xi} \rangle_{\Gamma(t)} = (\vec{f}, \vec{\xi}) \quad \forall \vec{\xi} \in \mathbb{U}(\vec{0}), \end{aligned} \quad (5.11a)$$

$$(\nabla \cdot \vec{u}, \varphi) = 0 \quad \forall \varphi \in \tilde{\mathbb{P}}, \quad (5.11b)$$

$$\langle \vec{\mathcal{V}} - \vec{u}, \chi \vec{\nu} \rangle_{\Gamma(t)} = 0 \quad \forall \chi \in H^1(\Gamma(t)), \quad (5.11c)$$

$$\langle \boldsymbol{\varkappa} \vec{\nu}, \vec{\eta} \rangle_{\Gamma(t)} + \langle \nabla_s \text{id}, \nabla_s \vec{\eta} \rangle_{\Gamma(t)} = 0 \quad \forall \vec{\eta} \in [H^1(\Gamma(t))]^d \quad (5.11d)$$

holds for almost all times $t \in (0, T]$.

5.3 ANTISYMMETRIC FINITE ELEMENT APPROXIMATION

In order to obtain a fully practical finite element approximation of the anti-symmetric weak formulation (5.11a–d) we proceed analogously to the Stokes case, see §3.4. For the benefit of the reader, we state again all the hypothesis and the notations used.

Here, in order to have a consistent finite element approximation, we consider the partitioning $t_m = m \tau$, $m = 0, \dots, M$, of $[0, T]$ into uniform time steps $\tau = \frac{T}{M}$, see [12]. The uniform time step size is needed to ensure that the discrete time derivative approximation is consistent. Moreover, let \mathcal{T}^m , $\forall m \geq 0$, be a regular partitioning of the domain Ω into disjoint open simplices o_j^m , $j = 1, \dots, J_\Omega^m$. From now on, the domain Ω which we consider is the polyhedral domain defined by the triangulation \mathcal{T}^m . On \mathcal{T}^m we define the finite element spaces

$$S_k^m := \{ \chi \in C(\overline{\Omega}) : \chi|_{o^m} \in \mathcal{P}_k(o^m) \quad \forall o^m \in \mathcal{T}^m \}, \quad k \in \mathbb{N},$$

where $\mathcal{P}_k(o^m)$ denotes the space of polynomials of degree k on o^m . Moreover, S_0^m is the space of piecewise constant functions on \mathcal{T}^m and let \vec{I}_k^m be the standard interpolation operator onto $[S_k^m]^d$.

Let $\mathbb{U}^m(\vec{g}) \subset \mathbb{U}(\vec{I}_k^m \vec{g})$ and $\mathbb{P}^m \subset \mathbb{P}$ be the finite element spaces we use for the approximation of velocity and pressure, and let $\tilde{\mathbb{P}}^m := \mathbb{P}^m \cap \tilde{\mathbb{P}}$. Then, for $d = 2$, possible pairs $(\mathbb{U}^m(\vec{0}), \mathbb{P}^m)$ that satisfy the LBB inf-sup condition (3.9) are P2–P0 and P2–(P1+P0), i.e. we set $\mathbb{U}^m(\vec{0}) = [S_2^m]^d \cap \mathbb{U}(\vec{0})$ and either $\mathbb{P}^m = S_0^m$ or $S_1^m + S_0^m$, while for $d = 3$ are the P3–(P2+P0) element and P1^{face bubble}–P0. See §3.4 for more details.

We consider a fitted finite element approximation for the evolution of the interface $\Gamma(t)$. Let $\Gamma^m \subset \mathbb{R}^d$ be a $(d - 1)$ -dimensional polyhedral surface approximating the closed surface $\Gamma(t_m)$, $m = 0, \dots, M$. Let Ω_+^m denote the exterior of Γ^m and let Ω_-^m be the interior of Γ^m , where we assume that Γ^m has no self-intersections. Then $\Omega = \Omega_-^m \cup \Gamma^m \cup \Omega_+^m$, and the fitted nature of our method implies that

$$\overline{\Omega_+^m} = \bigcup_{o \in \mathcal{T}_+^m} \overline{o} \quad \text{and} \quad \overline{\Omega_-^m} = \bigcup_{o \in \mathcal{T}_-^m} \overline{o},$$

where $\mathcal{T}^m = \mathcal{T}_+^m \cup \mathcal{T}_-^m$ and $\mathcal{T}_+^m \cap \mathcal{T}_-^m = \emptyset$. Let $\vec{\nu}^m$ denote the piecewise constant unit normal to Γ^m such that $\vec{\nu}^m$ points into Ω_+^m .

In order to define the parametric finite element spaces on Γ^m , we proceed analogously to the mean curvature flow and surface diffusion problems, see §2.5. Therefore we assume that $\Gamma^m = \bigcup_{j=1}^{J_\Gamma} \overline{\sigma_j^m}$, where $\{\sigma_j^m\}_{j=1}^{J_\Gamma}$ is a family of mutually disjoint open $(d - 1)$ -simplices with vertices $\{\vec{q}_k^m\}_{k=1}^{K_\Gamma}$. Then we define $\underline{V}(\Gamma^m) := \{\vec{\chi} \in [C(\Gamma^m)]^d : \vec{\chi}|_{\sigma_j^m} \in \mathcal{P}_1(\sigma_j^m), j = 1, \dots, J_\Gamma\} =: [W(\Gamma^m)]^d$, where $W(\Gamma^m) \subset H^1(\Gamma^m)$ is the space of scalar continuous piecewise linear functions on Γ^m , with $\{\chi_k^m\}_{k=1}^{K_\Gamma}$ denoting the standard basis of $W(\Gamma^m)$. As usual, we parametrize the new surface Γ^{m+1} over Γ^m using a parametrization $\vec{X}^{m+1} \in \underline{V}(\Gamma^m)$, so that $\Gamma^{m+1} = \vec{X}^{m+1}(\Gamma^m)$. Finally, let $\langle \cdot, \cdot \rangle_{\Gamma^m}^h$ be the mass lumped inner product on Γ^m , see (2.32), and let $\langle \cdot, \cdot \rangle_{\Gamma^m}$ denote the standard L^2 -inner product on Γ^m .

We need to pay particular attention to the discretization of the time derivative in (5.11a). Indeed, for the discrete counterpart of $\frac{1}{2} \frac{d}{dt}(\rho \vec{u}, \vec{\xi})$ we use

$$\frac{1}{2} \left(\frac{\rho^m \vec{U}^{m+1} - I_0^m \rho^{m-1} \vec{I}_2^m \vec{U}^m}{\tau}, \vec{\xi} \right), \quad (5.12)$$

while for the discrete version of $\frac{1}{2}(\rho \vec{u}_t, \vec{\xi})$ we employ

$$\frac{1}{2} \left(I_0^m \rho^{m-1} \frac{\vec{U}^{m+1} - \vec{I}_2^m \vec{U}^m}{\tau}, \vec{\xi} \right). \quad (5.13)$$

We notice that in (5.13), instead of using the actual density ρ^m , we use the density at the previous time step ρ^{m-1} and we interpolate it on the current bulk grid Ω_\pm^m . This is needed to prove stability over one time step. Since $\rho^m = \rho_+ \mathcal{X}_{\Omega_+^m} + \rho_- \mathcal{X}_{\Omega_-^m} \in S_0^m$, we can rewrite the discretization of the weak time derivative $\frac{1}{2} \left[\frac{d}{dt} (\rho \vec{u}, \vec{\xi}) + (\rho \vec{u}_t, \vec{\xi}) \right]$ in the simpler form

$$\left(\frac{\frac{1}{2}(I_0^m \rho^{m-1} + \rho^m) \vec{U}^{m+1} - I_0^m \rho^{m-1} \vec{I}_2^m \vec{U}^m}{\tau}, \vec{\xi} \right). \quad (5.14)$$

Then our antisymmetric finite element approximation is given as follows. Let Γ^0 , an approximation to $\Gamma(0)$, and $\vec{U}^0 \in \mathbb{U}^0(\vec{g})$ be given. For $m = 0, \dots, M-1$, find $(\vec{U}^{m+1}, P^{m+1}, \vec{X}^{m+1}, \kappa^{m+1}) \in \mathbb{U}^m(\vec{g}) \times \tilde{\mathbb{P}}^m \times \underline{V}(\Gamma^m) \times W(\Gamma^m)$ such that

$$\begin{aligned} & \left(\frac{\frac{1}{2}(I_0^m \rho^{m-1} + \rho^m) \vec{U}^{m+1} - I_0^m \rho^{m-1} \vec{I}_2^m \vec{U}^m}{\tau}, \vec{\xi} \right) \\ & + \frac{1}{2} \left((\rho^m \vec{I}_2^m \vec{U}^m \cdot \nabla) \vec{U}^{m+1}, \vec{\xi} \right) - \frac{1}{2} \left((\rho^m \vec{I}_2^m \vec{U}^m \cdot \nabla) \vec{\xi}, \vec{U}^{m+1} \right) \\ & + 2 \left(\mu^m \underline{\underline{D}}(\vec{U}^{m+1}), \underline{\underline{D}}(\vec{\xi}) \right) - \left(P^{m+1}, \nabla \cdot \vec{\xi} \right) \\ & - \gamma \left\langle \kappa^{m+1} \vec{\nu}^m, \vec{\xi} \right\rangle_{\Gamma^m} = \left(\rho^m \vec{f}_1^{m+1} + \vec{f}_2^{m+1}, \vec{\xi} \right) \quad \forall \vec{\xi} \in \mathbb{U}^m(\vec{0}), \end{aligned} \quad (5.15a)$$

$$\left(\nabla \cdot \vec{U}^{m+1}, \varphi \right) = 0 \quad \forall \varphi \in \tilde{\mathbb{P}}^m, \quad (5.15b)$$

$$\left\langle \frac{\vec{X}^{m+1} - \vec{\text{id}}}{\tau}, \chi \vec{\nu}^m \right\rangle_{\Gamma^m}^h - \left\langle \vec{U}^{m+1}, \chi \vec{\nu}^m \right\rangle_{\Gamma^m} = 0 \quad \forall \chi \in W(\Gamma^m), \quad (5.15c)$$

$$\left\langle \kappa^{m+1} \vec{\nu}^m, \vec{\eta} \right\rangle_{\Gamma^m}^h + \left\langle \nabla_s \vec{X}^{m+1}, \nabla_s \vec{\eta} \right\rangle_{\Gamma^m} = 0 \quad \forall \vec{\eta} \in \underline{V}(\Gamma^m) \quad (5.15d)$$

and set $\Gamma^{m+1} = \vec{X}^{m+1}(\Gamma^m)$. Here we have defined $\vec{f}_i^{m+1}(\cdot) := \vec{I}_2^m \vec{f}_i(\cdot, t_{m+1})$, $i = 1, 2$,

$$\mu^m = \mu_+ \mathcal{X}_{\Omega_+^m} + \mu_- \mathcal{X}_{\Omega_-^m} \in S_0^m \quad (5.16)$$

and

$$\rho^m = \rho_+ \mathcal{X}_{\Omega_+^m} + \rho_- \mathcal{X}_{\Omega_-^m} \in S_0^m. \quad (5.17)$$

5.3.1 EXISTENCE AND UNIQUENESS OF A DISCRETE SOLUTION

The existence and uniqueness proof of a discrete solution for the scheme (5.15a–d) is analogous to the Stokes case presented in §3.6.

Theorem 11. *Let $m \in \{0, \dots, M - 1\}$ and let $(\mathbb{U}^m(\vec{0}), \mathbb{P}^m)$ satisfy the LBB condition (3.9). Then there exists a unique solution $(\vec{U}^{m+1}, P^{m+1}, \vec{X}^{m+1}, \kappa^{m+1}) \in \mathbb{U}^m(\vec{g}) \times \tilde{\mathbb{P}}^m \times \underline{\mathbb{V}}(\Gamma^m) \times W(\Gamma^m)$ to (5.15a–d).*

Proof. As the system (5.15a–d) is linear, existence follows from uniqueness. In order to establish the latter, we consider the system: Find $(\vec{U}, P, \vec{X}, \kappa) \in \mathbb{U}^m(\vec{0}) \times \tilde{\mathbb{P}}^m \times \underline{\mathbb{V}}(\Gamma^m) \times W(\Gamma^m)$ such that

$$\begin{aligned} & \frac{1}{2\tau} \left((I_0^m \rho^{m-1} + \rho^m) \vec{U}, \vec{\xi} \right) \\ & + \frac{1}{2} \left((\rho^m \vec{I}_2^m \vec{U}^m \cdot \nabla) \vec{U}, \vec{\xi} \right) - \frac{1}{2} \left((\rho^m \vec{I}_2^m \vec{U}^m \cdot \nabla) \vec{\xi}, \vec{U} \right) \\ & + 2 \left(\mu^m \underline{\underline{D}}(\vec{U}), \underline{\underline{D}}(\vec{\xi}) \right) - \left(P, \nabla \cdot \vec{\xi} \right) - \gamma \left\langle \kappa \vec{\nu}^m, \vec{\xi} \right\rangle_{\Gamma^m} = 0 \quad \forall \vec{\xi} \in \mathbb{U}^m(\vec{0}), \end{aligned} \quad (5.18a)$$

$$(\nabla \cdot \vec{U}, \varphi) = 0 \quad \forall \varphi \in \tilde{\mathbb{P}}^m, \quad (5.18b)$$

$$\left\langle \vec{X}, \chi \vec{\nu}^m \right\rangle_{\Gamma^m}^h - \tau \left\langle \vec{U}, \chi \vec{\nu}^m \right\rangle_{\Gamma^m} = 0 \quad \forall \chi \in W(\Gamma^m), \quad (5.18c)$$

$$\left\langle \kappa \vec{\nu}^m, \vec{\eta} \right\rangle_{\Gamma^m}^h + \left\langle \nabla_s \vec{X}, \nabla_s \vec{\eta} \right\rangle_{\Gamma^m} = 0 \quad \forall \vec{\eta} \in \underline{\mathbb{V}}(\Gamma^m). \quad (5.18d)$$

Choosing $\vec{\xi} = \vec{U}$ in (5.18a), $\varphi = P$ in (5.18b), $\chi = \gamma \kappa$ in (5.18c) and $\vec{\eta} = \gamma \vec{X}$ in (5.18d) yields that

$$\frac{1}{2} \left((I_0^m \rho^{m-1} + \rho^m) \vec{U}, \vec{U} \right) + 2\tau \left(\mu^m \underline{\underline{D}}(\vec{U}), \underline{\underline{D}}(\vec{U}) \right) + \gamma \left\langle \nabla_s \vec{X}, \nabla_s \vec{X} \right\rangle_{\Gamma^m} = 0. \quad (5.19)$$

If $\rho > 0$, we immediately obtain that $\vec{U} = \vec{0}$. Otherwise we still get that $\underline{\underline{D}}(\vec{U}) = \underline{\underline{0}}$, and arguing as in the proof of Theorem 6 in §3.6 then yields that $\vec{U} = \vec{0}$. For the remainder of the proof we may proceed as in the proof

of Theorem 6. Hence there exists a unique solution $(\vec{U}^{m+1}, P^{m+1}, \vec{X}^{m+1}, \kappa^{m+1}) \in \mathbb{U}^m(\vec{g}) \times \tilde{\mathbb{P}}^m \times \underline{\mathcal{V}}(\Gamma^m) \times W(\Gamma^m)$ to (5.15a–d). \square

We note that if $(\mathbb{U}^m(\vec{0}), \mathbb{P}^m)$ does not satisfy the LBB condition (3.9), then existence and uniqueness of the solution $(\vec{U}^{m+1}, \vec{X}^{m+1}, \kappa^{m+1})$ to a reduced system, where the pressure P^{m+1} is eliminated, can be shown. More precisely, let $\mathbb{U}_0^m(\vec{g})$ be the divergence-free velocity space, see (3.18). Then any solution $(\vec{U}^{m+1}, P^{m+1}, \vec{X}^{m+1}, \kappa^{m+1}) \in \mathbb{U}^m(\vec{g}) \times \tilde{\mathbb{P}}^m \times \underline{\mathcal{V}}(\Gamma^m) \times W(\Gamma^m)$ to (5.15a–d) is such that $(\vec{U}^{m+1}, \vec{X}^{m+1}, \kappa^{m+1}) \in \mathbb{U}_0^m(\vec{g}) \times \underline{\mathcal{V}}(\Gamma^m) \times W(\Gamma^m)$ with

$$\begin{aligned} & \left(\frac{\frac{1}{2}(I_0^m \rho^{m-1} + \rho^m) \vec{U}^{m+1} - I_0^m \rho^{m-1} \vec{I}_2^m \vec{U}^m}{\tau}, \vec{\xi} \right) \\ & + \frac{1}{2} \left((\rho^m \vec{I}_2^m \vec{U}^m \cdot \nabla) \vec{U}^{m+1}, \vec{\xi} \right) - \frac{1}{2} \left((\rho^m \vec{I}_2^m \vec{U}^m \cdot \nabla) \vec{\xi}, \vec{U}^{m+1} \right) \\ & + 2 \left(\mu^m \underline{\mathcal{D}}(\vec{U}^{m+1}), \underline{\mathcal{D}}(\vec{\xi}) \right) - \gamma \left\langle \kappa^{m+1} \vec{\nu}^m, \vec{\xi} \right\rangle_{\Gamma^m} \\ & = \left(\rho^m \vec{f}_1^{m+1} + \vec{f}_2^{m+1}, \vec{\xi} \right) \quad \forall \vec{\xi} \in \mathbb{U}_0^m(\vec{0}), \end{aligned} \quad (5.20a)$$

$$\left\langle \frac{\vec{X}^{m+1} - \text{id}}{\tau}, \chi \vec{\nu}^m \right\rangle_{\Gamma^m}^h - \left\langle \vec{U}^{m+1}, \chi \vec{\nu}^m \right\rangle_{\Gamma^m} = 0 \quad \forall \chi \in W(\Gamma^m), \quad (5.20b)$$

$$\left\langle \kappa^{m+1} \vec{\nu}^m, \vec{\eta} \right\rangle_{\Gamma^m}^h + \left\langle \nabla_s \vec{X}^{m+1}, \nabla_s \vec{\eta} \right\rangle_{\Gamma^m} = 0 \quad \forall \vec{\eta} \in \underline{\mathcal{V}}(\Gamma^m) \quad (5.20c)$$

Theorem 12. Let $m \in \{0, \dots, M-1\}$ and let $\mathbb{U}_0^m(\vec{g})$ be non-empty. Then there exists a unique solution $(\vec{U}^{m+1}, \vec{X}^{m+1}, \kappa^{m+1}) \in \mathbb{U}_0^m(\vec{g}) \times \underline{\mathcal{V}}(\Gamma^m) \times W(\Gamma^m)$ to (5.20a–c).

Proof. As $\mathbb{U}_0^m(\vec{0})$ is a subspace of $\mathbb{U}^m(\vec{0})$, existence to the linear system (5.20a–c) follows from uniqueness, which is easy to show. In fact, similarly to the proof of Theorem 11 we obtain (5.19) and hence the desired uniqueness result. \square

5.3.2 STABILITY

We now demonstrate that the scheme (5.15a–d) in a loose sense is stable over a single time step. The proof is similar to the Stokes case presented in §3.7 and follows closely the paper [12].

Theorem 13. Let $\vec{g} = \vec{0}$. Moreover let $m \in \{0, \dots, M-1\}$ and let $(\vec{U}^{m+1}, P^{m+1}, \vec{X}^{m+1}, \kappa^{m+1}) \in \mathbb{U}^m(\vec{0}) \times \tilde{\mathbb{P}}^m \times \underline{V}(\Gamma^m) \times W(\Gamma^m)$ be a solution to (5.15a-d). Then

$$\begin{aligned} & \gamma \mathcal{H}^{d-1}(\Gamma^{m+1}) + \frac{1}{2} (\rho^m \vec{U}^{m+1}, \vec{U}^{m+1}) + 2 \tau (\mu^m \underline{\underline{D}}(\vec{U}^{m+1}), \underline{\underline{D}}(\vec{U}^{m+1})) \\ & \quad + \frac{1}{2} ((I_0^m \rho^{m-1}) (\vec{U}^{m+1} - \vec{I}_2^m \vec{U}^m), \vec{U}^{m+1} - \vec{I}_2^m \vec{U}^m) \\ & \leq \gamma \mathcal{H}^{d-1}(\Gamma^m) + \frac{1}{2} ((I_0^m \rho^{m-1}) \vec{I}_2^m \vec{U}^m, \vec{I}_2^m \vec{U}^m) \\ & \quad + \tau (\rho^m \vec{f}_1^{m+1} + \vec{f}_2^{m+1}, \vec{U}^{m+1}). \end{aligned} \quad (5.21)$$

Proof. Choosing $\vec{\xi} = \vec{U}^{m+1} \in \mathbb{U}^m(\vec{0})$ in (5.15a), $\varphi = P^{m+1} \in \tilde{\mathbb{P}}^m$ in (5.15b), $\chi = \gamma \kappa^{m+1}$ in (5.15c) and $\vec{\eta} = \gamma (\vec{X}^{m+1} - \text{id}|_{\Gamma^m})$ in (5.15d) yields that

$$\begin{aligned} & \left(\frac{1}{2} (I_0^m \rho^{m-1} + \rho^m) \vec{U}^{m+1} - I_0^m \rho^{m-1} \vec{I}_2^m \vec{U}^m, \vec{U}^{m+1} \right) \\ & \quad + 2 \tau (\mu^m \underline{\underline{D}}(\vec{U}^{m+1}), \underline{\underline{D}}(\vec{U}^{m+1})) + \gamma \langle \nabla_s \vec{X}^{m+1}, \nabla_s (\vec{X}^{m+1} - \vec{X}^m) \rangle_{\Gamma^m} \\ & = \tau (\rho^m \vec{f}_1^{m+1} + \vec{f}_2^{m+1}, \vec{U}^{m+1}), \end{aligned}$$

and, rearranging the terms,

$$\begin{aligned} & \frac{1}{2} (\rho^m \vec{U}^{m+1}, \vec{U}^{m+1}) + \frac{1}{2} ((I_0^m \rho^{m-1}) (\vec{U}^{m+1} - \vec{I}_2^m \vec{U}^m), \vec{U}^{m+1} - \vec{I}_2^m \vec{U}^m) \\ & \quad + 2 \tau (\mu^m \underline{\underline{D}}(\vec{U}^{m+1}), \underline{\underline{D}}(\vec{U}^{m+1})) + \gamma \langle \nabla_s \vec{X}^{m+1}, \nabla_s (\vec{X}^{m+1} - \vec{X}^m) \rangle_{\Gamma^m} \\ & = \frac{1}{2} ((I_0^m \rho^{m-1}) \vec{I}_2^m \vec{U}^m, \vec{I}_2^m \vec{U}^m) + \tau (\rho^m \vec{f}_1^{m+1} + \vec{f}_2^{m+1}, \vec{U}^{m+1}). \end{aligned}$$

Hence (5.21) follows immediately, where we have used (2.33). \square

We remark that on assuming that the bound

$$((I_0^m \rho^{m-1}) \vec{I}_2^m \vec{U}^m, \vec{I}_2^m \vec{U}^m) \leq (\rho^{m-1} \vec{U}^m, \vec{U}^m) \quad (5.22)$$

holds for $m = 1, \dots, M - 1$, it is possible to prove that

$$\begin{aligned} & \gamma \mathcal{H}^{d-1}(\Gamma^{m+1}) + \frac{1}{2} (\rho^m \vec{U}^{m+1}, \vec{U}^{m+1}) + 2 \sum_{k=0}^m \tau (\mu^k \underline{\underline{D}}(\vec{U}^{k+1}), \underline{\underline{D}}(\vec{U}^{k+1})) \\ & + \frac{1}{2} \sum_{k=0}^m ((I_0^k \rho^{k-1}) (\vec{U}^{k+1} - \vec{I}_2^k \vec{U}^k), \vec{U}^{k+1} - \vec{I}_2^k \vec{U}^k) \\ & \leq \gamma \mathcal{H}^{d-1}(\Gamma^0) + \frac{1}{2} (\rho^{-1} \vec{U}^0, \vec{U}^0) + \tau \sum_{k=0}^m (\rho^k \vec{f}_1^{k+1} + \vec{f}_2^{k+1}, \vec{U}^{k+1}), \quad (5.23) \end{aligned}$$

for $m = 0, \dots, M - 1$, which implies the stability of the scheme. In fact, the assumption (5.22) always holds in the unfitted case for (a) a fixed background mesh, or for (b) adaptive meshes where no coarsening is employed during the evolution. See [12] for details.

Instead, for a fitted finite element approach, as considered in this thesis, the condition (5.22) will in general not hold, because the underlying bulk triangulation changes at every time step, unless the position of the discrete interface remains unchanged. Therefore for the fitted approach it does not appear possible to prove a stability bound in the spirit of (5.23).

5.4 STANDARD FINITE ELEMENT APPROXIMATION

An alternative to the antisymmetric discrete finite element approximation (5.15a–d) can be obtained by using the standard weak formulation (5.2a–d). We use the same hypothesis and definitions employed in §5.3. Then the only difference is that we consider the more general partitioning $0 = t_0 < t_1 < \dots < t_{M-1} < t_M = T$ of $[0, T]$ into possibly variable time steps $\tau_m := t_{m+1} - t_m$, $m = 0, \dots, M - 1$.

Then our explicit standard finite element approximation, which is based on the variational formulation (5.2a–d), is given as follows. Let Γ^0 , an approximation to $\Gamma(0)$, and $\vec{U}^0 \in \mathbb{U}^0(\vec{g})$ be given. For $m = 0, \dots, M - 1$, find

$(\vec{U}^{m+1}, P^{m+1}, \vec{X}^{m+1}, \kappa^{m+1}) \in \mathbb{U}^m(\vec{g}) \times \tilde{\mathbb{P}}^m \times \underline{V}(\Gamma^m) \times W(\Gamma^m)$ such that

$$\begin{aligned} & \left(\rho^m \frac{\vec{U}^{m+1} - \vec{I}_2^m \vec{U}^m}{\tau_m}, \vec{\xi} \right) + \left(\rho^m (\vec{I}_2^m \vec{U}^m \cdot \nabla) \vec{U}^{m+1}, \vec{\xi} \right) \\ & + 2 \left(\mu^m \underline{D}(\vec{U}^{m+1}), \underline{D}(\vec{\xi}) \right) - \left(P^{m+1}, \nabla \cdot \vec{\xi} \right) \\ & - \gamma \left\langle \kappa^{m+1} \vec{\nu}^m, \vec{\xi} \right\rangle_{\Gamma^m} = \left(\rho^m \vec{f}_1^{m+1} + \vec{f}_2^{m+1}, \vec{\xi} \right) \quad \forall \vec{\xi} \in \mathbb{U}^m(\vec{0}), \end{aligned} \quad (5.24a)$$

$$(\nabla \cdot \vec{U}^{m+1}, \varphi) = 0 \quad \forall \varphi \in \tilde{\mathbb{P}}^m, \quad (5.24b)$$

$$\left\langle \frac{\vec{X}^{m+1} - \text{id}}{\tau_m}, \chi \vec{\nu}^m \right\rangle_{\Gamma^m}^h - \left\langle \vec{U}^{m+1}, \chi \vec{\nu}^m \right\rangle_{\Gamma^m} = 0 \quad \forall \chi \in W(\Gamma^m), \quad (5.24c)$$

$$\left\langle \kappa^{m+1} \vec{\nu}^m, \vec{\eta} \right\rangle_{\Gamma^m}^h + \left\langle \nabla_s \vec{X}^{m+1}, \nabla_s \vec{\eta} \right\rangle_{\Gamma^m} = 0 \quad \forall \vec{\eta} \in \underline{V}(\Gamma^m) \quad (5.24d)$$

and set $\Gamma^{m+1} = \vec{X}^{m+1}(\Gamma^m)$. Again, we have defined $\vec{f}_i^{m+1}(\cdot) := \vec{I}_2^m \vec{f}_i(\cdot, t_{m+1})$, $i = 1, 2$,

$$\mu^m = \mu_+ \mathcal{X}_{\Omega_+^m} + \mu_- \mathcal{X}_{\Omega_-^m} \in S_0^m \quad (5.25)$$

and

$$\rho^m = \rho_+ \mathcal{X}_{\Omega_+^m} + \rho_- \mathcal{X}_{\Omega_-^m} \in S_0^m. \quad (5.26)$$

Since the convective term is treated explicitly, the scheme (5.24a–d) is a linear scheme that leads to a coupled linear system of equations for the unknowns $(\vec{U}^{m+1}, P^{m+1}, \vec{X}^{m+1}, \kappa^{m+1})$ at each time level.

We notice that the antisymmetric scheme (5.15a–d) and the explicit standard scheme (5.24a–d) only differ in the approximation of the convective term and in the density coefficients used in the time derivative approximation. Indeed, instead of using the actual density ρ^m , it uses an average between the actual density and the interpolation of the density at the previous time step $\frac{1}{2}(I_0^m \rho^{m-1} + \rho^m)$ for what concern \vec{U}^{m+1} and it uses directly the density interpolation $I_0^m \rho^{m-1}$ for $\vec{I}_2^m \vec{U}^m$.

Alternatively, the convective term in (5.24a) can be treated implicitly and

the finite element approximation (5.24a–d) becomes

$$\begin{aligned} & \left(\rho^m \frac{\vec{U}^{m+1} - \vec{I}_2^m \vec{U}^m}{\tau_m}, \vec{\xi} \right) + \left(\rho^m (\vec{U}^{m+1} \cdot \nabla) \vec{U}^{m+1}, \vec{\xi} \right) \\ & + 2 \left(\mu^m \underline{\underline{D}}(\vec{U}^{m+1}), \underline{\underline{D}}(\vec{\xi}) \right) - \left(P^{m+1}, \nabla \cdot \vec{\xi} \right) \\ & - \gamma \left\langle \kappa^{m+1} \vec{\nu}^m, \vec{\xi} \right\rangle_{\Gamma^m} = \left(\rho^m \vec{f}_1^{m+1} + \vec{f}_2^{m+1}, \vec{\xi} \right) \quad \forall \vec{\xi} \in \mathbb{U}^m(\vec{0}), \end{aligned} \quad (5.27a)$$

$$(\nabla \cdot \vec{U}^{m+1}, \varphi) = 0 \quad \forall \varphi \in \tilde{\mathbb{P}}^m, \quad (5.27b)$$

$$\left\langle \frac{\vec{X}^{m+1} - \text{id}}{\tau_m}, \chi \vec{\nu}^m \right\rangle_{\Gamma^m}^h - \left\langle \vec{U}^{m+1}, \chi \vec{\nu}^m \right\rangle_{\Gamma^m} = 0 \quad \forall \chi \in W(\Gamma^m), \quad (5.27c)$$

$$\left\langle \kappa^{m+1} \vec{\nu}^m, \vec{\eta} \right\rangle_{\Gamma^m}^h + \left\langle \nabla_s \vec{X}^{m+1}, \nabla_s \vec{\eta} \right\rangle_{\Gamma^m} = 0 \quad \forall \vec{\eta} \in \underline{\mathcal{V}}(\Gamma^m). \quad (5.27d)$$

The scheme (5.27a–d) is a nonlinear scheme that leads to a coupled nonlinear system of equations for the unknowns $(\vec{U}^{m+1}, P^{m+1}, \vec{X}^{m+1}, \kappa^{m+1})$ at each time level.

5.5 SOLUTION METHODS

The linear algebraic systems arising from (5.24a–d) and (5.15a–d) are identical to the two-phase Stokes algebraic system (3.34) with the only modification in the terms \vec{B}_Ω and \vec{c} . Indeed, for the explicit standard scheme (5.24a–d) these terms become

$$\begin{aligned} [\vec{B}_\Omega]_{ij} &:= \left(\frac{\rho^m}{\tau_m} \phi_j^{\mathbb{U}^m}, \phi_i^{\mathbb{U}^m} \right) \underline{\underline{\text{id}}} + 2 \left(\left(\mu^m \underline{\underline{D}}(\phi_j^{\mathbb{U}^m} \vec{e}_q), \underline{\underline{D}}(\phi_i^{\mathbb{U}^m} \vec{e}_r) \right) \right)_{q,r=1}^d \\ &+ \left(\left(\rho^m \vec{I}_2^m \vec{U}^m \cdot \nabla \right) \phi_j^{\mathbb{U}^m}, \phi_i^{\mathbb{U}^m} \right) \underline{\underline{\text{id}}}, \\ \vec{c}_i &:= \left(\frac{\rho^m}{\tau_m} \vec{I}_2^m \vec{U}^m + \rho^m \vec{f}_1^{m+1} + \vec{f}_2^{m+1}, \phi_i^{\mathbb{U}^m} \right), \end{aligned}$$

while for the antisymmetric scheme (5.15a–d) these terms become

$$\begin{aligned} [\vec{B}_\Omega]_{ij} &:= \left(\frac{\rho^m}{\tau_m} \phi_j^{\mathbb{U}^m}, \phi_i^{\mathbb{U}^m} \right) \underline{\underline{\text{id}}} + 2 \left(\left(\mu^m \underline{\underline{D}}(\phi_j^{\mathbb{U}^m} \vec{e}_q), \underline{\underline{D}}(\phi_i^{\mathbb{U}^m} \vec{e}_r) \right) \right)_{q,r=1}^d \\ &\quad + \frac{1}{2} \left(\left(\rho^m \vec{I}_2^m \vec{U}^m \cdot \nabla \right) \phi_j^{\mathbb{U}^m}, \phi_i^{\mathbb{U}^m} \right) \underline{\underline{\text{id}}} - \frac{1}{2} \left(\left(\rho^m \vec{I}_2^m \vec{U}^m \cdot \nabla \right) \phi_i^{\mathbb{U}^m}, \phi_j^{\mathbb{U}^m} \right) \underline{\underline{\text{id}}}, \\ \vec{c}_i &:= \left(\frac{I_0^m \rho^{m-1} + \rho^m}{2\tau_m} \vec{I}_2^m \vec{U}^m + \rho^m \vec{f}_1^{m+1} + \vec{f}_2^{m+1}, \phi_i^{\mathbb{U}^m} \right). \end{aligned}$$

Then the resulting algebraic system can be solved using the same technique introduced in §3.11.

Instead, in order to solve the implicit standard scheme (5.27a–d) we use a fixed point iteration. In particular, we can find a solution to the scheme (5.27a–d) as follow. Let Γ^m and $\vec{U}^m \in \mathbb{U}^{m-1}(\vec{g})$ be given. Let $\vec{U}^{m+1,0} = \vec{I}_2^m \vec{U}^m$ and fix $\epsilon_f > 0$. Then, for $s \geq 0$, find $(\vec{U}^{m+1,s+1}, P^{m+1,s+1}, \vec{X}^{m+1,s+1}, \kappa^{m+1,s+1}) \in \mathbb{U}^m(\vec{g}) \times \tilde{\mathbb{P}}^m \times \underline{\mathcal{V}}(\Gamma^m) \times W(\Gamma^m)$ such that

$$\begin{aligned} &\left(\rho^m \frac{\vec{U}^{m+1,s+1} - \vec{I}_2^m \vec{U}^m}{\tau_m}, \vec{\xi} \right) + \left((\rho^m \vec{U}^{m+1,s} \cdot \nabla) \vec{U}^{m+1,s+1}, \vec{\xi} \right) \\ &\quad + 2 \left(\mu^m \underline{\underline{D}}(\vec{U}^{m+1,s+1}), \underline{\underline{D}}(\vec{\xi}) \right) - \left(P^{m+1,s+1}, \nabla \cdot \vec{\xi} \right) \\ &\quad - \gamma \left\langle \kappa^{m+1,s+1} \vec{\nu}^m, \vec{\xi} \right\rangle_{\Gamma^m} = \left(\rho^m \vec{f}_1^{m+1} + \vec{f}_2^{m+1}, \vec{\xi} \right) \quad \forall \vec{\xi} \in \mathbb{U}^m(\vec{0}), \end{aligned} \tag{5.28a}$$

$$(\nabla \cdot \vec{U}^{m+1,s+1}, \varphi) = 0 \quad \forall \varphi \in \tilde{\mathbb{P}}^m, \tag{5.28b}$$

$$\left\langle \frac{\vec{X}^{m+1,s+1} - \vec{\text{id}}}{\tau_m}, \chi \vec{\nu}^m \right\rangle_{\Gamma^m}^h - \left\langle \vec{U}^{m+1,s+1}, \chi \vec{\nu}^m \right\rangle_{\Gamma^m} = 0 \quad \forall \chi \in W(\Gamma^m), \tag{5.28c}$$

$$\left\langle \kappa^{m+1,s+1} \vec{\nu}^m, \vec{\eta} \right\rangle_{\Gamma^m}^h + \left\langle \nabla_s \vec{X}^{m+1,s+1}, \nabla_s \vec{\eta} \right\rangle_{\Gamma^m} = 0 \quad \forall \vec{\eta} \in \underline{\mathcal{V}}(\Gamma^m), \tag{5.28d}$$

and repeat the iteration until $\|\vec{U}^{m+1,s+1} - \vec{U}^{m+1,s}\|_{L^\infty} \leq \epsilon_f$. Finally, set $\Gamma^{m+1} = \vec{X}^{m+1,s+1}(\Gamma^m)$ and $(\vec{U}^{m+1}, P^{m+1}, \kappa^{m+1}) = (\vec{U}^{m+1,s+1}, P^{m+1,s+1}, \kappa^{m+1,s+1})$. The scheme (5.28a–d), at each time level m , is a fixed point iteration that consists of solving a coupled linear system of equations for the unknowns $(\vec{U}^{m+1,s+1}, P^{m+1,s+1}, \vec{X}^{m+1,s+1}, \kappa^{m+1,s+1})$ at each

step s until the L^∞ -error of the velocity $\|U^{m+1,s+1} - U^{m+1,s}\|_{L^\infty}$ is smaller than the required tolerance ϵ_f . Obviously, in the case that the fixed point iteration performs only one step, (5.28a–d) reduces to the explicit standard scheme (5.24a–d). In practice, we also require $s > 1$, which means that we do at least two full iterations of the fixed point scheme. Again, at every step, the linear algebraic system arising from (5.28a–d) is identical to the two-phase Stokes algebraic system (3.34) with the only modification in the terms \vec{B}_Ω and \vec{c} , which now become

$$\begin{aligned} [\vec{B}_\Omega]_{ij} &:= \left(\frac{\rho^m}{\tau_m} \phi_j^{\mathbb{U}^m}, \phi_i^{\mathbb{U}^m} \right) \underline{\underline{\text{id}}} + 2 \left((\mu^m \underline{\underline{D}}(\phi_j^{\mathbb{U}^m} \vec{e}_q), \underline{\underline{D}}(\phi_i^{\mathbb{U}^m} \vec{e}_r)) \right)_{q,r=1}^d \\ &\quad + \left((\rho^m \vec{U}^{m+1,s} \cdot \nabla) \phi_j^{\mathbb{U}^m}, \phi_i^{\mathbb{U}^m} \right) \underline{\underline{\text{id}}}, \\ \vec{c}_i &:= \left(\frac{\rho^m}{\tau_m} \vec{I}_2^m \vec{U}^m + \rho^m \vec{f}_1^{m+1} + \vec{f}_2^{m+1}, \phi_i^{\mathbb{U}^m} \right). \end{aligned}$$

5.6 VELOCITY INTERPOLATION

We can notice that all the Navier–Stokes schemes presented so far, namely (5.15a–d), (5.24a–d) and (5.28a–d), have at least one term containing the interpolated velocity $\vec{I}_2^m \vec{U}^m$. The interpolation operator is needed because the velocity \vec{U}^m , which has been computed at time level $m - 1$, is defined on \mathcal{T}^{m-1} . Therefore, at the next time level m , the previous velocity \vec{U}^m needs to be interpolated on \mathcal{T}^m in order to be used. Obviously this is not necessary for the Stokes scheme (3.11a–d), since there the previous velocity is never utilized.

The interpolation routine simply consists in evaluating the discrete function \vec{U}^m in all the degrees of freedom of a P2 discrete function defined on \mathcal{T}^m . These values will then define the interpolated velocity $\vec{I}_2^m \vec{U}^m$. From a computational point of view, since all the discrete functions are defined locally, it consists, for each degree of freedom defined on \mathcal{T}^m , of finding the element in \mathcal{T}^{m-1} which contains the coordinate of the degree of freedom. Once the element is found, the discrete function \vec{U}^m at this degree of freedom can be evaluated locally, and hence cheaply.

All the computational complexity lies in the algorithm that, given a point, finds the element which contains it. Since, after a full remeshing, the meshes \mathcal{T}^{m-1} and \mathcal{T}^m are completely unrelated, and since the meshes are unstructured, there is no one-to-one relation between elements of \mathcal{T}^{m-1} and elements of \mathcal{T}^m . The simplest, but very expensive, routine is to, for each point, perform a linear search over all the elements of \mathcal{T}^{m-1} until the element which contains the point is found. This linear search, since it is repeated for every degree of freedom, is extremely slow and, for large meshes, can be orders of magnitudes slower than the assembly and the solution of the algebraic system.

The linear search is very inefficient because, for each point, it traverses the mesh from the first element to the correct one. A simple optimization consists in starting the search from the last correctly found element and, if it does not contain the new point, move to a neighbouring element. Here the neighbouring element chosen is the one that corresponds to the face opposite to the vertex with the maximal distance to the new point. The maximal distance corresponds to the minimal weight in the barycentric coordinates of the new point with respect to the vertices of the current element. The barycentric coordinate system is a coordinate system in which the location of a point of a simplex is specified as the centre of mass of unequal masses placed at its vertices.

In the first instance, the simple optimization described above is restricted to convex domains, as otherwise the face opposite to the vertex with maximal distance to the new point might be a boundary face, and so there is no desired neighbouring element. But of course for nonconvex domains this optimized search can be combined with a linear search whenever a boundary face is encountered in the local search for the next neighbour.

In order to further optimize the algorithm, it would be very beneficial to have a continuous path of elements, which visits, only once, all the elements of \mathcal{T}^m . This ensures that successive degrees of freedom on the new mesh are spatially close, and so the local optimized search for the next element of \mathcal{T}^{m-1} to visit is likely to be very short. In particular, following the given sequence of elements of \mathcal{T}^m , all the points corresponding to the local degrees of freedom

are searched. But, since the path is continuous, the element of \mathcal{T}^{m-1} where the search starts will be always very close to the correct one. Unfortunately, since we use unstructured meshes, such a path, in general, is difficult to construct. Hence, instead of explicitly constructing such a path, we create a fictitious background lattice that covers the domain $\bar{\Omega}$. Then, at each element of \mathcal{T}^m is assigned the point of the lattice which is closest to its barycentre. Depending on the size of the lattice, multiple entities can be mapped to the same point. Since the lattice is structured, it is straightforward to build a continuous path which visits all its points. For example, for a rectangular domain in 2d we can use a snaking path that traverses the lattice alternating left-to-right and right-to-left, see Figure 5.1.

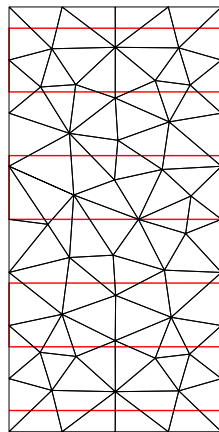


Figure 5.1: Continuous path (red) traversing a fictitious background lattice.

In practice, the elements of \mathcal{T}^m are visited following the given lattice path. This means that, for each lattice point traversed, the associated entities are visited. Obviously, the lattice size should not be too big, as otherwise too many entities will be associated to the same lattice point. On the other hand, it should not be too small either, as otherwise many lattice points would not have any entity associated with them, making the path very slow to traverse. A good rule of thumb, which works well in practice, is to use the characteristic length of the mesh as the lattice size.

6

ALE FINITE ELEMENT APPROXIMATION FOR TWO-PHASE NAVIER–STOKES FLOW

We now present an alternative finite element approximation for incompressible two-phase Navier–Stokes flow which uses the Arbitrary Lagrangian Eulerian (ALE) method. This technique allows to rewrite the velocity time derivative with respect to a fixed reference manifold. The system of PDEs describing the two-phase fluid, after space discretization, becomes the evolution of the solution along trajectories. Thus the velocity does not need to be interpolated anymore, with the exception of when a full bulk remeshing is performed. This is a great advantage of ALE methods compared to non-ALE methods, because the interpolation process is expensive in terms of CPU time and introduces interpolation errors. Moreover, the interpolated velocity is no longer, in a discrete weakly sense, divergence-free which could possibly lead to unphysical solutions.

The chapter is organised as follows: in §6.1 we reformulate the mathematical model for the incompressible two-phase Navier–Stokes flow using the

ALE method; in §6.2 we derive the weak formulation on which our finite element approximation is going to be based; in §6.3 we derive a semidiscrete continuous-in-time finite element approximation, which leads to a system of ODEs describing the solution along trajectories; in §6.4 we present the fully discrete finite element discretization; in §6.5 we explain the the solution method employed to solve the algebraic system.

6.1 MATHEMATICAL MODEL

The Arbitrary Lagrangian Eulerian (ALE) method is an alternative technique to numerically approximate equations on a moving domain. It was first proposed in the papers [24, 41]. In our presentation we follow closely [49, 28, 48]. The ALE technique consists in reformulating the partial time derivative by expressing it with respect to a fixed reference configuration. A special homeomorphic map, called the ALE map, associates, at each time t , a point in the current computational domain $\Omega(t)$ to a point in the reference domain \mathcal{D} . Therefore, the system of ODEs resulting after space discretization actually describes the evolution of the solution along trajectories that are at all times contained in the computational domain.

More precisely, we want to reformulate the two-phase Navier–Stokes system (5.1a–i), which is expressed in terms of Eulerian coordinates $\vec{z} \in \Omega(t)$, by rewriting the velocity time derivative \vec{u}_t with respect to the so called ALE coordinate $\vec{q} \in \mathcal{D}$. Analogously to what is done in §2.4 to parametrize the interface $\Gamma(t)$, we can define the fixed reference manifold \mathcal{D} and extend the map (2.25) to parametrize $\Omega(t)$ as $\Omega(t) = \vec{x}(\mathcal{D}, t)$. This extended map clearly still satisfies $\Gamma(t) = \vec{x}(\Upsilon, t)$, given that $\Upsilon \subset \mathcal{D}$. Moreover, we let $\partial\mathcal{D}$ be partitioned as $\partial\mathcal{D} = \partial_1\mathcal{D} \cup \partial_2\mathcal{D}$ with $\partial_1\mathcal{D} \cap \partial_2\mathcal{D} = \emptyset$.

Now, let $h : \Omega(t) \times [0, T] \rightarrow \mathbb{R}$ be a function defined on the Eulerian frame. The corresponding function on the ALE frame \hat{h} is defined as

$$\hat{h} : \mathcal{D} \times [0, T] \rightarrow \mathbb{R}, \quad \hat{h}(\vec{q}, t) = h(\vec{x}(\vec{q}, t), t). \quad (6.1)$$

In order to compute the time derivative of (6.1) with respect to the ALE

frame, using the chain rule, we have

$$\frac{\partial \hat{h}(\vec{q}, t)}{\partial t} = \frac{\partial h(\vec{x}(\vec{q}, t), t)}{\partial t} = \frac{\partial h(\vec{z}, t)}{\partial t} + \vec{x}_t(\vec{q}, t) \cdot \nabla h(\vec{z}, t), \quad (6.2)$$

therefore it holds that

$$\frac{\partial h(\vec{z}, t)}{\partial t} = \frac{\partial \hat{h}(\vec{q}, t)}{\partial t} - \vec{x}_t(\vec{q}, t) \cdot \nabla h(\vec{z}, t). \quad (6.3)$$

Finally, introducing the domain velocity

$$\vec{\mathcal{W}}(\vec{z}, t) := \vec{x}_t(\vec{q}, t) \quad \forall \vec{z} = \vec{x}(\vec{q}, t) \in \Omega(t) \quad (6.4)$$

and the time derivative in the ALE frame

$$\left. \frac{\partial h(\vec{z}, t)}{\partial t} \right|_{\mathcal{D}} := \frac{\partial \hat{h}(\vec{q}, t)}{\partial t} \quad \forall \vec{z} = \vec{x}(\vec{q}, t) \in \Omega(t), \quad (6.5)$$

we obtain

$$h_t = h_t|_{\mathcal{D}} - \vec{\mathcal{W}} \cdot \nabla h. \quad (6.6)$$

The identity (6.6) is naturally extended to vector valued functions. We stress the fact that the domain velocity $\vec{\mathcal{W}}$ for the interface points is consistent with the interface velocity $\vec{\mathcal{V}}$. Therefore it holds

$$\vec{\mathcal{W}}|_{\Gamma(t)} = \vec{\mathcal{V}}. \quad (6.7)$$

We also point out that the ALE mapping is somehow arbitrary, apart from the requirement of conforming to the evolution of the domain boundary. Indeed the map of the boundary $\partial_i \mathcal{D}$ of the reference domain has then to provide, at all t , the boundary $\partial_i \Omega(t)$ of the current configuration, with $i = 1, 2$.

Using (6.6) in the momentum equation (5.1a), we can rewrite (5.1a–i) in the

ALE frame as:

$$\rho (\vec{u}_t|_{\mathcal{D}} + ((\vec{u} - \vec{\mathcal{W}}) \cdot \nabla) \vec{u}) - 2\mu \nabla \cdot \underline{\underline{D}}(\vec{u}) + \nabla p = \vec{f} \quad \text{in } \Omega_{\pm}(t), \quad (6.8a)$$

$$\nabla \cdot \vec{u} = 0 \quad \text{in } \Omega_{\pm}(t), \quad (6.8b)$$

$$\vec{u} = \vec{g} \quad \text{on } \partial_1 \Omega(t), \quad (6.8c)$$

$$\vec{u} \cdot \vec{n} = 0, \quad \underline{\underline{\sigma}} \vec{n} \cdot \vec{t} = 0 \quad \forall \vec{t} \in \{\vec{n}\}^{\perp} \quad \text{on } \partial_2 \Omega(t), \quad (6.8d)$$

$$[\vec{u}]_{-}^{+} = \vec{0} \quad \text{on } \Gamma(t), \quad (6.8e)$$

$$[2\mu \underline{\underline{D}}(\vec{u}) \cdot \vec{\nu} - p \vec{\nu}]_{-}^{+} = -\gamma \varkappa \vec{\nu} \quad \text{on } \Gamma(t), \quad (6.8f)$$

$$(\vec{\mathcal{V}} - \vec{u}) \cdot \vec{\nu} = 0 \quad \text{on } \Gamma(t), \quad (6.8g)$$

$$\Gamma(0) = \Gamma_0, \quad (6.8h)$$

$$\vec{u}(0) = \vec{u}_0. \quad (6.8i)$$

As usual, let $\rho(t) = \rho_{+} \mathcal{X}_{\Omega_{+}(t)} + \rho_{-} \mathcal{X}_{\Omega_{-}(t)}$, with $\rho_{\pm} \in \mathbb{R}_{>0}$, be the fluid density in the two phases, let $\mu(t) = \mu_{+} \mathcal{X}_{\Omega_{+}(t)} + \mu_{-} \mathcal{X}_{\Omega_{-}(t)}$, with $\mu_{\pm} \in \mathbb{R}_{>0}$, be the dynamic viscosities in the two phases, let $\underline{\underline{D}}(\vec{u}) := \frac{1}{2} (\nabla \vec{u} + (\nabla \vec{u})^T)$ be the rate-of-deformation tensor, let $\vec{f} := \rho \vec{f}_1 + \vec{f}_2$ be a possible forcing term, let $\gamma > 0$ be the surface tension coefficient and let \varkappa be the mean curvature of $\Gamma(t)$. See Chapter 1 for more details. We can notice that, with respect to the original formulation, there is a convective-type term due to the domain movement and the time derivative is computed in the fixed reference frame \mathcal{D} . Moreover, contrary to the original system, not only the regions $\Omega_{\pm}(t)$ are time dependent but also the whole domain $\Omega(t)$ is time dependent.

Obviously, if the domain is fixed, the additional convective term is zero and the time derivative in the ALE frame coincides with the usual time derivative in the Eulerian frame. This means that $\vec{\mathcal{W}} = \vec{0}$ corresponds to a pure Eulerian method, while $\vec{\mathcal{W}} = \vec{u}$ corresponds to a fully Lagrangian scheme. In our case, since we have a fixed domain Ω , the ALE formulation might not seem very useful. But, at the discrete level, we are concerned with the evolution of the discrete triangulated domains. Therefore the discrete ALE map describes the evolution of the grid during the domain movement. It is indeed at the discrete level that the advantage of the ALE formulation emerges, as in an

ALE setting the time advancing scheme provides directly the evolution of the unknowns at mesh nodes and thus that of the degrees of freedom of the discrete solutions.

6.2 WEAK FORMULATION

In order to define the ALE weak formulation, we need to use a different functional setting for the test functions with respect to the one used for the standard and antisymmetric weak formulation, recall §5.2. The reason is that here it needs to be defined on the moving domain $\Omega(t)$. Therefore we introduce the admissible spaces of test functions on the reference domain \mathcal{D}

$$\begin{aligned}\mathcal{U}(\vec{b}) &:= \{\vec{\phi} \in [H^1(\mathcal{D})]^d : \vec{\phi} = \vec{b} \quad \text{on } \partial_1 \mathcal{D}, \quad \vec{\phi} \cdot \vec{n} = 0 \quad \text{on } \partial_2 \mathcal{D}\}, \\ \mathcal{P} &:= L^2(\mathcal{D}), \\ \tilde{\mathcal{P}} &:= \{\eta \in \mathcal{P} : \int_{\mathcal{D}} \eta \, d\mathcal{L}^d = 0\},\end{aligned}$$

for a given $\vec{b} \in [H^1(\mathcal{D})]^d$. Then, using the ALE mapping, we can define the admissible spaces of test functions on the moving domain $\Omega(t)$ by setting

$$\begin{aligned}\mathfrak{U}(\vec{b}) &:= \{\vec{\phi} : \bigcup_{t \in [0, T]} \Omega(t) \times \{t\} \rightarrow \mathbb{R}^d, \quad \vec{\phi} = \hat{\vec{\phi}} \circ \vec{x}^{-1}, \quad \hat{\vec{\phi}} \in \mathcal{U}(\vec{b}) \quad \forall t \in [0, T]\}, \\ \mathfrak{P} &:= \{\eta : \bigcup_{t \in [0, T]} \Omega(t) \times \{t\} \rightarrow \mathbb{R}, \quad \eta = \hat{\eta} \circ \vec{x}^{-1}, \quad \hat{\eta} \in \mathcal{P} \quad \forall t \in [0, T]\}, \\ \tilde{\mathfrak{P}} &:= \{\eta : \bigcup_{t \in [0, T]} \Omega(t) \times \{t\} \rightarrow \mathbb{R}, \quad \eta = \hat{\eta} \circ \vec{x}^{-1}, \quad \hat{\eta} \in \tilde{\mathcal{P}} \quad \forall t \in [0, T]\}.\end{aligned}$$

Note that all the functions in $\mathfrak{U}(\vec{b})$, \mathfrak{P} and $\tilde{\mathfrak{P}}$ are space and time dependent. Moreover, let $(\cdot, \cdot)_{\Omega(t)}$ and $\langle \cdot, \cdot \rangle_{\Gamma(t)}$ denote the L^2 -inner products on $\Omega(t)$ and $\Gamma(t)$, respectively. In addition, we let \mathcal{L}^d and \mathcal{H}^{d-1} denote the Lebesgue measure in \mathbb{R}^d and the $(d-1)$ -dimensional Hausdorff measure, respectively.

Hence, the ALE weak formulation of (6.8a–i) is given as follows. Given $\Gamma(0) = \Gamma_0$ and $\vec{u}(0) = \vec{u}_0$, find $(\Gamma(t))_{t \in [0, T]}$ and $(\vec{u}, p, \boldsymbol{\varkappa}) \in \mathfrak{U}(\vec{g}) \times \tilde{\mathfrak{P}} \times$

$H^1(\cup_{t \in [0, T]} \Gamma(t) \times \{t\})$ such that

$$\begin{aligned} & (\rho |\vec{u}_t|_{\mathcal{D}}, \vec{\xi})_{\Omega(t)} + (\rho ((\vec{u} - \vec{W}) \cdot \nabla) \vec{u}, \vec{\xi})_{\Omega(t)} + 2 (\mu \underline{\underline{D}}(\vec{u}), \underline{\underline{D}}(\vec{\xi}))_{\Omega(t)} \\ & - (p, \nabla \cdot \vec{\xi})_{\Omega(t)} - \gamma \langle \boldsymbol{\varkappa} \vec{\nu}, \vec{\xi} \rangle_{\Gamma(t)} = (\vec{f}, \vec{\xi})_{\Omega(t)} \quad \forall \vec{\xi} \in \mathfrak{U}(\vec{0}), \end{aligned} \quad (6.9a)$$

$$(\nabla \cdot \vec{u}, \varphi)_{\Omega(t)} = 0 \quad \forall \varphi \in \tilde{\mathfrak{P}}, \quad (6.9b)$$

$$\langle \vec{V} - \vec{u}, \chi \vec{\nu} \rangle_{\Gamma(t)} = 0 \quad \forall \chi \in H^1(\Gamma(t)), \quad (6.9c)$$

$$\langle \boldsymbol{\varkappa} \vec{\nu}, \vec{\eta} \rangle_{\Gamma(t)} + \langle \nabla_s \text{id}, \nabla_s \vec{\eta} \rangle_{\Gamma(t)} = 0 \quad \forall \vec{\eta} \in [H^1(\Gamma(t))]^d \quad (6.9d)$$

holds for almost all times $t \in (0, T]$.

6.3 SEMIDISCRETE FINITE ELEMENT APPROXIMATION

We want to derive a semidiscrete continuous-in-time fitted finite element approximation of (6.9a–d). Let \mathfrak{T}^h be a regular partitioning of the reference domain \mathcal{D} into disjoint open simplices o_j^h , $j = 1, \dots, J_{\mathcal{D}}^h$. From now on, the reference domain \mathcal{D} , which we consider, is the polyhedral domain defined by the triangulation \mathfrak{T}^h . On \mathfrak{T}^h we define the finite element spaces

$$S_k^h(\mathcal{D}) := \{\chi \in C(\overline{\mathcal{D}}) : \chi|_{o^h} \in \mathcal{P}_k(o^h) \quad \forall o^h \in \mathfrak{T}^h\}, \quad k \in \mathbb{N},$$

where $\mathcal{P}_k(o^h)$ denotes the space of polynomials of degree k on o^h . Moreover, S_0^h is the space of piecewise constant functions on \mathfrak{T}^h .

Then, using the discrete ALE mapping \vec{x}_h , we can define the finite element spaces on the discretized moving domains $\Omega^h(t) = \vec{x}_h(\mathcal{D}, t)$ by

$$S_k^h(\Omega^h(t)) := \{\eta : \Omega^h(t) \rightarrow \mathbb{R}, \quad \eta = \hat{\eta} \circ \vec{x}_h^{-1}, \quad \hat{\eta} \in S_k^h(\mathcal{D})\}, \quad k \in \mathbb{N} \cup \{0\}.$$

Here $\vec{x}_h \in [S_1^h]^d$ maps each simplex with straight faces in \mathfrak{T}^h to a simplex with straight faces belonging to the triangulation $\mathcal{T}^h(t)$ of the discretized moving domain $\Omega^h(t)$. For later use, we let $\mathfrak{U}^h(\vec{g}, t) \subset [S_2^h(\Omega^h(t))]^d$ and $\tilde{\mathfrak{P}}^h(t) \subset S_1^h(\Omega^h(t)) + S_0^h(\Omega^h(t))$, or $\tilde{\mathfrak{P}}^h(t) \subset S_1^h(\Omega_-^h(t)) + S_1^h(\Omega_+^h(t))$, denote the appropriate spaces for the discrete velocities and pressure.

We also define the discrete domain velocity as

$$\vec{\mathcal{W}}^h(\vec{z}, t) := \sum_{k=1}^{K_\Omega} \left[\frac{d}{dt} \vec{p}_k^h(t) \right] \varphi_k^h(\vec{z}, t) \in [S_1^h(\Omega^h(t))]^d, \quad (6.10)$$

with $\{\varphi_k^h(\cdot, t)\}_{k=1}^{K_\Omega}$ denoting the standard basis of $S_1^h(\Omega^h(t))$, and $\{\vec{p}_k^h(t)\}_{k=1}^{K_\Omega}$ denoting the vertices of $\mathcal{T}^h(t)$. Moreover, we also introduce the L^2 -inner product $(\cdot, \cdot)_{\Omega^h(t)}$.

For what concerns the interface, let $(\Gamma^h(t))_{t \in [0, T]}$ be a family of $(d - 1)$ -dimensional polyhedral surfaces approximating the closed surface $\Gamma(t)$. Let $\Omega_+^h(t)$ denote the exterior of $\Gamma^h(t)$ and let $\Omega_-^h(t)$ be the interior of $\Gamma^h(t)$, where we assume that $\Gamma^h(t)$ has no self-intersections. Then $\Omega^h(t) = \Omega_-^h(t) \cup \Gamma^h(t) \cup \Omega_+^h(t)$, and the fitted nature of our method implies that

$$\overline{\Omega_+^h(t)} = \bigcup_{o \in \mathcal{T}_+^h(t)} \overline{o} \quad \text{and} \quad \overline{\Omega_-^h(t)} = \bigcup_{o \in \mathcal{T}_-^h(t)} \overline{o}, \quad (6.11)$$

where $\mathcal{T}^h(t) = \mathcal{T}_+^h(t) \cup \mathcal{T}_-^h(t)$ and $\mathcal{T}_+^h(t) \cap \mathcal{T}_-^h(t) = \emptyset$. Let $\vec{\nu}^h(t)$ denote the piecewise constant unit normal to $\Gamma^h(t)$ such that $\vec{\nu}^h(t)$ points into $\Omega_+^h(t)$. We also define the piecewise linear finite element spaces $W(\Gamma^h(t))$ and $\underline{V}(\Gamma^h(t))$, with $\{\chi_k^h(\cdot, t)\}_{k=1}^{K_\Gamma}$ denoting the standard basis of the former. Hence $\chi_k^h(\vec{q}_l^h(t), t) = \delta_{kl}$ for all $k, l \in \{1, \dots, K_\Gamma\}$ and $t \in [0, T]$, where $\{\vec{q}_k^h(t)\}_{k=1}^{K_\Gamma}$ are the vertices of $\Gamma^h(t)$. We also notice that the discrete interface velocity $\vec{\mathcal{V}}^h$, see (2.35), is simply the trace of $\vec{\mathcal{W}}^h$ on Γ^h . Finally, let $\langle \cdot, \cdot \rangle_{\Gamma^h(t)}^h$ be the mass lumped inner product on $\Gamma^h(t)$, see (2.32), and let $\langle \cdot, \cdot \rangle_{\Gamma^h(t)}$ denote the standard L^2 -inner product on $\Gamma^h(t)$.

Then, given $\Gamma^h(0)$ and $\vec{U}^h(0) \in \mathfrak{U}^h(\vec{g}, 0)$, for $t \in (0, T]$ find $\Gamma^h(t)$ and $(\vec{U}^h(t), P^h(t), \vec{\mathcal{V}}^h(t), \kappa^h(t)) \in \mathfrak{U}^h(\vec{g}, t) \times \tilde{\mathfrak{P}}^h(t) \times \underline{V}(\Gamma^h(t)) \times W(\Gamma^h(t))$ such

that

$$\begin{aligned} & \left(\rho^h \vec{U}_t^h \Big|_{\mathcal{D}}, \vec{\xi} \right)_{\Omega^h(t)} + \left(\rho^h ((\vec{U}^h - \vec{W}^h) \cdot \nabla) \vec{U}^h, \vec{\xi} \right)_{\Omega^h(t)} \\ & + 2 \left(\mu^h \underline{\underline{D}}(\vec{U}^h), \underline{\underline{D}}(\vec{\xi}) \right)_{\Omega^h(t)} - \left(P^h, \nabla \cdot \vec{\xi} \right)_{\Omega^h(t)} \\ & - \gamma \left\langle \kappa^h \vec{\nu}^h, \vec{\xi} \right\rangle_{\Gamma^h(t)} = \left(\rho^h \vec{f}_1^h + \vec{f}_2^h, \vec{\xi} \right)_{\Omega^h(t)} \quad \forall \vec{\xi} \in \mathfrak{U}^h(\vec{0}, t), \end{aligned} \quad (6.12a)$$

$$\left(\nabla \cdot \vec{U}^h, \varphi \right)_{\Omega^h(t)} = 0 \quad \forall \varphi \in \tilde{\mathfrak{P}}^h(t), \quad (6.12b)$$

$$\left\langle \vec{\mathcal{V}}^h, \chi \vec{\nu}^h \right\rangle_{\Gamma^h(t)}^h - \left\langle \vec{U}^h, \chi \vec{\nu}^h \right\rangle_{\Gamma^h(t)} = 0 \quad \forall \chi \in W(\Gamma^h(t)), \quad (6.12c)$$

$$\left\langle \kappa^h \vec{\nu}^h, \vec{\eta} \right\rangle_{\Gamma^h(t)}^h + \left\langle \nabla_s \text{id}, \nabla_s \vec{\eta} \right\rangle_{\Gamma^h(t)} = 0 \quad \forall \vec{\eta} \in \underline{V}(\Gamma^h(t)). \quad (6.12d)$$

Here we have defined $\vec{f}_i^h(\cdot, t) := \vec{I}_2^h \vec{f}_i(\cdot, t)$, $i = 1, 2$,

$$\mu^h = \mu_+ \mathcal{X}_{\Omega_+^h(t)} + \mu_- \mathcal{X}_{\Omega_-^h(t)} \in S_0^h(\Omega^h(t)) \quad (6.13)$$

and

$$\rho^h = \rho_+ \mathcal{X}_{\Omega_+^h(t)} + \rho_- \mathcal{X}_{\Omega_-^h(t)} \in S_0^h(\Omega^h(t)), \quad (6.14)$$

where \vec{I}_2^h denotes the standard interpolation operator onto $[S_2^h(\Omega^h(t))]^d$.

The semidiscrete continuous-in-time fitted finite element scheme (6.12a–d) is

a system of ODEs. Indeed, we can define the following matrices and vectors

$$[\vec{M}_\Omega^h(t)]_{ij} := \left((\rho^h \phi_j^{\mathfrak{U}^h} \vec{e}_q, \phi_i^{\mathfrak{U}^h} \vec{e}_r)_{\Omega^h(t)} \right)_{q,r=1}^d, \quad (6.15a)$$

$$[\vec{D}_\Omega^h(t, \vec{U}^h, \vec{\mathcal{W}}^h)]_{ij} := \left((\rho^h ((\vec{U}^h - \vec{\mathcal{W}}^h) \cdot \nabla) \phi_j^{\mathfrak{U}^h} \vec{e}_q, \phi_i^{\mathfrak{U}^h} \vec{e}_r)_{\Omega^h(t)} \right)_{q,r=1}^d, \quad (6.15b)$$

$$[\vec{B}_\Omega^h(t)]_{ij} := 2 \left((\mu^h \underline{\underline{D}}(\phi_j^{\mathfrak{U}^h} \vec{e}_q), \underline{\underline{D}}(\phi_i^{\mathfrak{U}^h} \vec{e}_r))_{\Omega^h(t)} \right)_{q,r=1}^d, \quad (6.15c)$$

$$\vec{c}^h(t, \vec{f}_1^h, \vec{f}_2^h) := (\rho^h \vec{f}_1^h + \vec{f}_2^h, \phi_i^{\mathfrak{U}^h})_{\Omega^h(t)}, \quad (6.15d)$$

$$[\vec{C}_\Omega^h(t)]_{ip} := - \left((\nabla \cdot (\phi_i^{\mathfrak{U}^h} \vec{e}_q), \phi_p^{\mathfrak{P}^h})_{\Omega^h(t)} \right)_{q=1}^d, \quad (6.15e)$$

$$[\vec{N}_{\Gamma,\Omega}^h(t)]_{il} := \langle \phi_i^{\mathfrak{U}^h}, \chi_l^h \vec{\nu}^h \rangle_{\Gamma^h(t)}, \quad (6.15f)$$

$$[\vec{N}_\Gamma^h(t)]_{kl} := \langle \chi_l^h, \chi_k^h \vec{\nu}^h \rangle_{\Gamma^h(t)}^h, \quad (6.15g)$$

$$[\vec{A}_\Gamma^h(t)]_{kl} := \langle \nabla_s \chi_l^h, \nabla_s \chi_k^h \rangle_{\Gamma^h(t)} \text{id}, \quad (6.15h)$$

where $\{\vec{e}_q\}_{q=1}^d$ denotes the standard basis in \mathbb{R}^d , $\{\phi_i^{\mathfrak{U}^h}\}_{i=1}^{K_{\mathfrak{U}^h}}$ is the basis of $\mathfrak{U}^h(\vec{0}, t)$ and $\{\phi_i^{\mathfrak{P}^h}\}_{i=1}^{K_{\mathfrak{P}^h}}$ is the basis of $\mathfrak{P}^h(t)$. Thus (6.12a–d) can be rewritten in algebraic form as

$$\begin{aligned} & \vec{M}_\Omega^h(t) \frac{d}{dt} \vec{U} + \vec{B}_\Omega^h(t) \vec{U} + \vec{D}_\Omega^h(t, \vec{U}^h, \vec{\mathcal{W}}^h) \vec{U} \\ & + \vec{C}_\Omega^h(t) P - \gamma \vec{N}_{\Gamma,\Omega}^h(t) \kappa = \vec{c}^h(t, \vec{f}_1^h, \vec{f}_2^h), \end{aligned} \quad (6.16a)$$

$$[\vec{C}_\Omega^h(t)]^T \vec{U} = 0, \quad (6.16b)$$

$$[\vec{N}_\Gamma^h(t)]^T \frac{d}{dt} \vec{X} - \vec{N}_{\Gamma,\Omega}^h(t) \vec{U} = 0, \quad (6.16c)$$

$$\vec{N}_\Gamma^h(t) \kappa + \vec{A}_\Gamma^h(t) \vec{X} = 0, \quad (6.16d)$$

where \vec{U} , P , κ and \vec{X} are the unknown vectors for the velocity, pressure, interface curvature and interface position, respectively.

6.4 FULLY DISCRETE FINITE ELEMENT APPROXIMATION

We consider the partitioning $0 = t_0 < t_1 < \dots < t_{M-1} < t_M = T$ of $[0, T]$ into possibly variable time steps $\tau_m := t_{m+1} - t_m$, $m = 0, \dots, M - 1$. It is now straightforward to obtain a fully discrete finite element approximation of (6.16a–d), since the only missing part is the temporal discretization. Therefore, applying a semi-implicit Euler scheme to (6.16a–d), we obtain

$$\begin{aligned} & \frac{1}{\tau_m} \vec{M}_\Omega^h(t^{m+1}) \vec{U}^{m+1} + \vec{B}_\Omega^h(t^m) \vec{U}^{m+1} + \vec{D}_\Omega^h(t^m, \vec{U}^{m+1}, \vec{\mathcal{W}}^{m+1}) \vec{U}^{m+1} \\ & + \vec{C}_\Omega^h(t^m) P^{m+1} - \gamma \vec{N}_{\Gamma, \Omega}^h(t^m) \kappa^{m+1} \\ & = \frac{1}{\tau_m} \vec{M}_\Omega^h(t^{m+1}) \vec{U}^m + \vec{c}^h(t^m, \vec{f}_1^{m+1}, \vec{f}_2^{m+1}), \end{aligned} \quad (6.17a)$$

$$[\vec{C}_\Omega^h(t^m)]^T \vec{U}^{m+1} = 0, \quad (6.17b)$$

$$\frac{1}{\tau_m} [\vec{N}_\Gamma^h(t^m)]^T \vec{X}^{m+1} - \vec{N}_{\Gamma, \Omega}^h(t^m) \vec{U}^{m+1} = \frac{1}{\tau_m} [\vec{N}_\Gamma^h(t^m)]^T \vec{X}^m, \quad (6.17c)$$

$$\vec{N}_\Gamma^h(t^m) \kappa^{m+1} + \vec{A}_\Gamma^h(t^m) \vec{X}^{m+1} = 0. \quad (6.17d)$$

We notice that there is a small abuse of notation in (6.17a) for \vec{U}^{m+1} and $\vec{\mathcal{W}}^{m+1}$ in the term $\vec{D}_\Omega^h(t^m, \vec{U}^{m+1}, \vec{\mathcal{W}}^{m+1})$. Indeed only for this term, they denote the discrete fluid velocity and the discrete bulk domain velocity, respectively, and not their associated vectors of degree of freedoms. Moreover, let $\Omega^m = \vec{x}^m(\mathcal{D})$ be an approximation of the domain $\Omega(t_m)$, $m = 0, \dots, M$, where $\vec{x}^m \in [S_1^h(\Omega^m)]^d$ is an approximation to $\vec{x}^h(\cdot, t_m)$, and let h^m be an approximation of $h : \Omega(t) \times [0, T] \rightarrow \mathbb{R}$. Clearly, h^m is defined on the domain Ω^m ; nevertheless it can be transported on any other configuration Ω^s , with $t^s \neq t^m$, using the mapping $\vec{x}^s \circ (\vec{x}^m)^{-1}$. To lighten the notation, whenever we need to integrate h^s on a domain Ω^m we will write simply

$$\int_{\Omega^m} h^s \, d\mathcal{L}^d$$

instead of

$$\int_{\Omega^m} h^s \circ \vec{x}^s \circ (\vec{x}^m)^{-1}.$$

The same notation is used for the inner products.

Following [48], we now rewrite (6.15a–h) into a form that is common in finite element formulations. More precisely, we can substitute (6.15a–h) back into (6.17a–d). Firstly, let

$$\mathfrak{U}^m(\vec{g}) = \{\vec{\phi} : \Omega^m \rightarrow \mathbb{R}^d, \vec{\phi} = \vec{\hat{\phi}} \circ (\vec{x}^m)^{-1}, \vec{\hat{\phi}} \in \mathcal{U}(\vec{g}) \cap [S_2^h(\mathcal{D})]^d\}$$

and

$$\tilde{\mathfrak{P}}^m = \{\eta : \Omega^m \rightarrow \mathbb{R}, \eta = \hat{\eta} \circ (\vec{x}^m)^{-1}, \hat{\eta} \in \tilde{\mathcal{P}} \cap (S_1^h(\mathcal{D}) + S_0^h(\mathcal{D}))\}$$

or, depending on the element chosen,

$$\tilde{\mathfrak{P}}^m = \{\eta : \Omega^m \rightarrow \mathbb{R}, \eta = \hat{\eta} \circ (\vec{x}^m)^{-1}, \hat{\eta} \in \tilde{\mathcal{P}} \cap (S_1^h(\mathcal{D}_-) + S_1^h(\mathcal{D}_+))\},$$

with $\mathcal{D}_- := \mathcal{D} \setminus \overline{\mathcal{D}}_+$. Then, our ALE finite element approximation, which is based on the variational formulation (6.9a–d), is given as follows. Let Ω^0, Γ^0 , and $\vec{U}^0 \in \mathfrak{U}^0(\vec{g})$ be given. For $m = 0, \dots, M-1$, find $(\vec{U}^{m+1}, P^{m+1}, \vec{X}^{m+1}, \kappa^{m+1}, \vec{\mathcal{W}}^{m+1}) \in \mathfrak{U}^{m+1}(\vec{g}) \times \tilde{\mathfrak{P}}^{m+1} \times \underline{V}(\Gamma^m) \times W(\Gamma^m) \times [S_1^h(\Omega^m)]^d$ such that $\vec{\mathcal{W}}^{m+1}|_{\Gamma^m} = \frac{1}{\tau}(\vec{X}^{m+1} - \text{id}|_{\Gamma^m})$ and such that

$$\begin{aligned} & \left(\frac{\rho^m}{\tau_m} \vec{U}^{m+1}, \vec{\xi} \right)_{\Omega^{m+1}} + \left(\rho^m ((\vec{U}^{m+1} - \vec{\mathcal{W}}^{m+1}) \cdot \nabla) \vec{U}^{m+1}, \vec{\xi} \right)_{\Omega^m} \\ & + 2 \left(\mu^m \underline{\underline{D}}(\vec{U}^{m+1}), \underline{\underline{D}}(\vec{\xi}) \right)_{\Omega^m} - \left(P^{m+1}, \nabla \cdot \vec{\xi} \right)_{\Omega^m} - \gamma \left\langle \kappa^{m+1} \vec{\nu}^m, \vec{\xi} \right\rangle_{\Gamma^m} \\ & = \left(\frac{\rho^m}{\tau_m} \vec{U}^m, \vec{\xi} \right)_{\Omega^{m+1}} + \left(\rho^m \vec{f}_1^{m+1} + \vec{f}_2^{m+1}, \vec{\xi} \right)_{\Omega^m} \quad \forall \vec{\xi} \in \mathfrak{U}^m(\vec{0}), \end{aligned} \quad (6.18a)$$

$$(\nabla \cdot \vec{U}^{m+1}, \varphi)_{\Omega^m} = 0 \quad \forall \varphi \in \tilde{\mathfrak{P}}^m, \quad (6.18b)$$

$$\left\langle \frac{\vec{X}^{m+1} - \text{id}}{\tau_m}, \chi \vec{\nu}^m \right\rangle_{\Gamma^m}^h - \left\langle \vec{U}^{m+1}, \chi \vec{\nu}^m \right\rangle_{\Gamma^m} = 0 \quad \forall \chi \in W(\Gamma^m), \quad (6.18c)$$

$$\left\langle \kappa^{m+1} \vec{\nu}^m, \vec{\eta} \right\rangle_{\Gamma^m}^h + \left\langle \nabla_s \vec{X}^{m+1}, \nabla_s \vec{\eta} \right\rangle_{\Gamma^m} = 0 \quad \forall \vec{\eta} \in \underline{V}(\Gamma^m), \quad (6.18d)$$

and set $\Gamma^{m+1} = \vec{X}^{m+1}(\Gamma^m)$, as well as $\Omega^{m+1} = \vec{x}^{m+1}(\mathcal{D})$, where $\vec{x}^{m+1} = \vec{x}^m + \tau \vec{\mathcal{W}}^{m+1}$. Again, we have defined $\vec{f}_i^{m+1}(\cdot) := \vec{I}_2^m \vec{f}_i(\cdot, t_{m+1})$, $i = 1, 2$,

$$\mu^m = \mu_+ \mathcal{X}_{\Omega_+^m} + \mu_- \mathcal{X}_{\Omega_-^m} \in S_0^h(\Omega^m) \quad (6.19)$$

and

$$\rho^m = \rho_+ \mathcal{X}_{\Omega_+^m} + \rho_- \mathcal{X}_{\Omega_-^m} \in S_0^h(\Omega^m). \quad (6.20)$$

It is worth noticing that, at the discrete level, the reference manifold \mathcal{D} is never used. Instead, it is replaced by the actual discrete bulk domain. Therefore, at time step t^{m+1} , the reference manifold is Ω^m . We also want to stress the fact that the ALE finite element approximation (6.18a–d) differs from all other finite element approximations presented in Chapter 5 for the fact that the velocity \vec{U}^{m+1} is only interpolated after a remeshing and not at each time level. Indeed, since the ALE formulation describes the evolution of the solution along trajectories, the velocity \vec{U}^{m+1} is defined on the domain Ω^{m+1} . Instead, in all the schemes presented in Chapter 5, the velocity \vec{U}^{m+1} is always defined on the domain Ω^m and then interpolated on the domain Ω^{m+1} at each time level. Obviously, the velocity \vec{U}^{m+1} still needs to be interpolated when a full bulk remeshing is performed.

6.5 SOLUTION METHOD

The solution technique used to solve the ALE scheme (6.18a–d) is very similar to the one used to solve the implicit standard scheme (5.27a–d). More precisely, using a fixed point iteration, we find a solution for the scheme (6.18a–d) as follows. Let Γ^m and $\vec{U}^m \in \mathfrak{U}^m(\vec{g})$ be given. Set $\vec{U}^{m+1,0} = \vec{U}^m$, $\vec{\psi}^{m+1,0} = \vec{0}$, $\Omega^{m+1,0} = \Omega^m$ and fix $\epsilon_f > 0$. Then, for $s \geq 0$, find $(\vec{U}^{m+1,s+1}, P^{m+1,s+1}, \vec{X}^{m+1,s+1}, \kappa^{m+1,s+1}) \in \mathfrak{U}^m(\vec{g}) \times \tilde{\mathfrak{P}}^m \times \underline{V}(\Gamma^m) \times W(\Gamma^m)$

such that

$$\begin{aligned}
& \left(\frac{\rho^m}{\tau_m} \vec{U}^{m+1,s+1}, \vec{\xi} \right)_{\Omega^{m+1,s}} + \left(\left(\rho^m \left(\vec{U}^{m+1,s} - \frac{\vec{\psi}^{m+1,s}}{\tau_m} \right) \cdot \nabla \right) \vec{U}^{m+1,s+1}, \vec{\xi} \right)_{\Omega^m} \\
& + 2 \left(\mu^m \underline{D}(\vec{U}^{m+1,s+1}), \underline{D}(\vec{\xi}) \right)_{\Omega^m} - \left(P^{m+1,s+1}, \nabla \cdot \vec{\xi} \right)_{\Omega^m} \\
& - \gamma \left\langle \kappa^{m+1,s+1} \vec{\nu}^m, \vec{\xi} \right\rangle_{\Gamma^m} \\
& = \left(\frac{\rho^m}{\tau_m} \vec{U}^m, \vec{\xi} \right)_{\Omega^{m+1,s}} + \left(\rho^m \vec{f}_1^{m+1} + \vec{f}_2^{m+1}, \vec{\xi} \right)_{\Omega^m} \quad \forall \vec{\xi} \in \mathfrak{U}^m(\vec{0}),
\end{aligned} \tag{6.21a}$$

$$\left(\nabla \cdot \vec{U}^{m+1,s+1}, \varphi \right)_{\Omega^m} = 0 \quad \forall \varphi \in \tilde{\mathfrak{P}}^m, \tag{6.21b}$$

$$\left\langle \frac{\vec{X}^{m+1,s+1} - \text{id}}{\tau_m}, \chi \vec{\nu}^m \right\rangle_{\Gamma^m}^h - \left\langle \vec{U}^{m+1,s+1}, \chi \vec{\nu}^m \right\rangle_{\Gamma^m} = 0 \quad \forall \chi \in W(\Gamma^m), \tag{6.21c}$$

$$\left\langle \kappa^{m+1,s+1} \vec{\nu}^m, \vec{\eta} \right\rangle_{\Gamma^m}^h + \left\langle \nabla_s \vec{X}^{m+1,s+1}, \nabla_s \vec{\eta} \right\rangle_{\Gamma^m} = 0 \quad \forall \vec{\eta} \in \underline{V}(\Gamma^m). \tag{6.21d}$$

The iteration is repeated until $\|U^{m+1,s+1} - U^{m+1,s}\|_{L^\infty} \leq \epsilon_f$ and $\|\vec{\psi}^{m+1,s+1} - \vec{\psi}^{m+1,s}\|_{L^\infty} \leq \epsilon_f$. Here the bulk displacement $\vec{\psi}^{m+1,s+1}$ is computed solving the linear elasticity problem (3.46a–b), see §3.12 for more details, and $\Omega^{m+1,s+1}$ is updated accordingly. Finally, set $\Gamma^{m+1} = \vec{X}^{m+1,s+1}(\Gamma^m)$, $\Omega^{m+1,s+1} = \Omega^{m+1}$ and $(\vec{U}^{m+1}, P^{m+1}, \kappa^{m+1}, \vec{\mathcal{W}}^{m+1}) = (\vec{U}^{m+1,s+1}, P^{m+1,s+1}, \kappa^{m+1,s+1}, \frac{1}{\tau} \psi^{m+1,s+1})$. Clearly (6.21a–d), at each time level m , is a fixed point iteration, which consists of solving a coupled linear system of equations for the unknowns $(\vec{U}^{m+1,s+1}, P^{m+1,s+1}, \vec{X}^{m+1,s+1}, \kappa^{m+1,s+1})$ at each step s until the L^∞ -error of the velocity $\|U^{m+1,s+1} - U^{m+1,s}\|_{L^\infty}$ and the L^∞ -error of the bulk displacement $\|\vec{\psi}^{m+1,s+1} - \vec{\psi}^{m+1,s}\|_{L^\infty} \leq \epsilon_f$ are smaller than the required tolerance ϵ_f . The arbitrary domain velocity $\vec{\mathcal{W}}^{m+1}$ is chosen to be the solution of the linear elasticity problem (3.46a–b). Obviously, no mesh smoothing is performed on Ω^{m+1} otherwise all the benefits of the ALE scheme would be lost since a velocity interpolation would be required. Nevertheless, since the mesh smoothing is already embedded in the arbitrary domain velocity, the bulk mesh quality is preserved. In practice, we also require $s > 1$, which means that we do at least two full iterations of the fixed point scheme.

At every step, the linear algebraic system arising from (6.21a–d) is identical to the two-phase Stokes algebraic system (3.34) but with the following terms

$$\begin{aligned}
[\vec{B}_\Omega]_{ij} &:= \left(\frac{\rho^m}{\tau_m} \phi_j^{\mathfrak{U}^m}, \phi_i^{\mathfrak{U}^m} \right)_{\Omega^{m+1,s}} \underline{\underline{\text{id}}} + 2 \left(\left(\mu^m \underline{\underline{D}}(\phi_j^{\mathfrak{U}^m} \vec{e}_q), \underline{\underline{D}}(\phi_i^{\mathfrak{U}^m} \vec{e}_r) \right)_{\Omega^m} \right)_{q,r=1}^d \\
&\quad + \left(\left(\rho^m \left(\vec{U}^{m+1,s} - \frac{\vec{\psi}^{m+1,s}}{\tau_m} \right) \cdot \nabla \right) \phi_j^{\mathfrak{U}^m}, \phi_i^{\mathfrak{U}^m} \right)_{\Omega^m} \underline{\underline{\text{id}}}, \\
\vec{c}_i &:= \left(\frac{\rho^m}{\tau_m} \vec{U}^m \right)_{\Omega^{m+1,s}} + \left(\rho^m \vec{f}_1^{m+1} + \vec{f}_2^{m+1}, \phi_i^{\mathfrak{U}^m} \right)_{\Omega^m}, \\
[\vec{C}_\Omega]_{ip} &:= - \left(\left(\nabla \cdot (\phi_i^{\mathfrak{U}^m} \vec{e}_q), \phi_p^{\mathfrak{P}^m} \right)_{\Omega^m} \right)_{q=1}^d, \quad [\vec{N}_{\Gamma,\Omega}]_{il} := \left\langle \phi_i^{\mathfrak{U}^m}, \chi_l^m \vec{\nu}^m \right\rangle_{\Gamma^m}, \\
\vec{\beta}_i &:= \frac{\left(\phi_i^{\mathfrak{P}^m}, 1 \right)_{\Omega^m}}{(1, 1)_{\Omega^m}} \left\langle \vec{I}_2^m \vec{g}, \vec{n} \right\rangle_{\partial_1 \Omega^m}, \quad [\vec{N}_\Gamma]_{kl} := \left\langle \chi_l^m, \chi_k^m \vec{\nu}^m \right\rangle_{\Gamma^m}^h, \\
[\vec{A}_\Gamma]_{kl} &:= \left\langle \nabla_s \chi_l^m, \nabla_s \chi_k^m \right\rangle_{\Gamma^m} \vec{\text{id}}.
\end{aligned}$$

Then the resulting algebraic system can be solved using the same technique introduced in §3.11.

7

TWO-PHASE NAVIER–STOKES FLOW NUMERICAL RESULTS

In order to test our method, and to allow comparisons with the unfitted finite element approximation in [12], we now present several numerical experiments in 2d.

The chapter is organised as follows: in §7.1 we state two exact solutions to the two-phase Navier–Stokes problem and we verify that they are indeed solutions; in §7.2 we describe the changes needed in the various schemes if the exact solution is not divergence-free, which is indeed the case for one of them; in §7.3 we describe the general settings for the simulations and we define the benchmark quantities; in §7.4 we report on the convergence test; in §7.5 we report on the rising bubble experiments.

7.1 EXACT SOLUTIONS

Let $\Gamma(t) = \{\vec{z} \in \mathbb{R}^d : |\vec{z}| = r(t)\}$ be a sphere of radius $r(t)$ and curvature $\varkappa(t) = -\frac{d-1}{r(t)}$. Moreover let $\alpha, \gamma \in \mathbb{R}_{\geq 0}$ be given. Here, we also allow non

divergence-free problem. Therefore, for the non divergence-free cases, the incompressibility condition (5.1b) is replaced by

$$\nabla \cdot \vec{u} = f_{\text{div}}. \quad (7.1)$$

7.1.1 EXPANDING BUBBLE I

The expanding sphere where

$$r(t) = e^{\alpha t} r(0), \quad (7.2a)$$

together with

$$\vec{u}(\vec{z}, t) = \alpha \vec{z}, \quad p(\vec{z}, t) = -\left[\gamma - 2\alpha \frac{\mu_+ - \mu_-}{d-1} r(t) \right] \varkappa(t) \left[\mathcal{X}_{\Omega_-(t)} - \frac{\mathcal{L}^d(\Omega_-(t))}{\mathcal{L}^d(\Omega)} \right], \quad (7.2b)$$

is an exact solution to the problem (5.1a–i), with (5.1b) replaced by (7.1), on e.g. $\Omega = (-1, 1)^d$ with $\vec{f}(\vec{z}, t) = \rho \alpha^2 \vec{z}$, $f_{\text{div}} = \alpha d$ and $\vec{g} = \alpha \vec{z}$ on $\partial_1 \Omega = \partial \Omega$.

We now verify that (7.2a,b) is indeed an exact solution. Firstly, given that

$$\frac{\partial u_i}{\partial z_j} = \alpha \delta_{ij},$$

the components of the rate-of-deformation tensor are simply

$$[\underline{\underline{D}}(\vec{u})]_{ij} = \frac{1}{2} \left(\frac{\partial u_i}{\partial z_j} + \frac{\partial u_j}{\partial z_i} \right) = \alpha \delta_{ij},$$

and it holds

$$\nabla \cdot \underline{\underline{D}}(\vec{u}) = \vec{0}.$$

Therefore, given that the pressure p is constant in each phase and that \vec{u} does not depend on time, the momentum equation (5.1a) reduces simply to

$$\rho(\vec{u} \cdot \nabla) \vec{u} = \rho \alpha^2 \vec{z}$$

which is indeed the value of forcing term \vec{f} . Also the non divergence-free continuity equation (7.1) is satisfied since we have

$$\nabla \cdot \vec{u} = \sum_{j=1}^d \frac{\partial u_j}{\partial z_j} = \sum_{j=1}^d \alpha = \alpha d,$$

which is indeed equal to f_{div} . Moreover, also the stress balance (5.1f) holds since, substituting (7.2b) in (5.1f), we obtain for the i component

$$\begin{aligned} \left[[2\mu \underline{D}(\vec{u}) \cdot \vec{\nu} - p \vec{\nu}]_i \right]_-^+ &= \left[2\mu \sum_{j=1}^d \frac{\partial u_i}{\partial z_j} \nu_j - p \nu_i \right]_-^+ = \left[2\mu \sum_{j=1}^d \alpha \delta_{ij} \nu_j \right]_-^+ - [p \nu_i]_-^+ \\ &= [2\mu \alpha \nu_i]_-^+ - \left(\gamma - 2\alpha \frac{\mu_+ - \mu_-}{d-1} r \right) \varkappa \nu_i \\ &= 2\alpha(\mu_+ - \mu_-) \nu_i - \gamma \varkappa \nu_i + 2\alpha \frac{\mu_+ - \mu_-}{d-1} r \frac{1-d}{r} \nu_i \\ &= 2\alpha(\mu_+ - \mu_-) \nu_i - \gamma \varkappa \nu_i - 2\alpha(\mu_+ - \mu_-) \nu_i = -\gamma \varkappa \nu_i. \end{aligned}$$

Finally, the dynamic interface condition (5.1g) is satisfied since the fluid velocity on the interface along the normal direction is

$$\vec{u} \cdot \vec{\nu}|_{\Gamma} = \alpha \vec{z} \cdot \frac{\vec{z}}{|\vec{z}|} = \alpha |\vec{z}| = \alpha r,$$

while the interface velocity along the normal direction is

$$\vec{\mathcal{V}} \cdot \vec{\nu} = r' = \alpha r.$$

7.1.2 EXPANDING BUBBLE II

A nontrivial divergence free and radially symmetric solution \vec{u} can be constructed on a domain that does not contain the origin. To this end, consider e.g. $\Omega = (-1, 1)^d \setminus [-\frac{1}{3}, \frac{1}{3}]^d$. Then, the expanding sphere where

$$r(t) = ([r(0)]^d + \alpha t d)^{\frac{1}{d}}, \quad (7.3a)$$

together with

$$\vec{u}(\vec{z}, t) = \alpha \frac{\vec{z}}{|\vec{z}|^d}, \quad p(\vec{z}, t) = -\left(\gamma + 2\alpha \frac{\mu_+ - \mu_-}{r(t)^{d-1}}\right) \varkappa(t) \left[\mathcal{X}_{\Omega_-(t)} - \frac{\mathcal{L}^d(\Omega_-(t))}{\mathcal{L}^d(\Omega)} \right], \quad (7.3b)$$

is an exact solution to the problem (5.1a–i) with $\vec{f}(\vec{z}, t) = \rho(1-d)\alpha^2 \frac{\vec{z}}{|\vec{z}|^{2d}}$ and $\vec{g}(\vec{z}) = \alpha |\vec{z}|^{-d} \vec{z}$ on $\partial_1 \Omega = \partial \Omega$.

We notice that the exact solution (7.3a,b) is identical to the expanding bubble solution of the two-phase Stokes problem presented in §4.1.2. The only change is the forcing term \vec{f} which is now inhomogeneous. Therefore, in order to verify that (7.3a,b) is indeed an exact solution also to the two-phase Navier–Stokes problem, it is sufficient to check that the time derivative plus the convective term in the momentum equation (5.1a) add up to \vec{f} . Firstly, we compute the i component of the convective term as

$$\begin{aligned} [(\vec{u} \cdot \nabla) \vec{u}]_i &= \sum_{j=1}^d \alpha \frac{z_j}{|\vec{z}|^d} \frac{\partial u_i}{\partial z_j} = \sum_{j=1}^d \alpha \frac{z_j}{|\vec{z}|^d} \left(\alpha \frac{\delta_{ij} - dz_i z_j |\vec{z}|^{-2}}{|\vec{z}|^d} \right) \\ &= \frac{\alpha^2}{|\vec{z}|^{2d}} \sum_{j=1}^d (\delta_{ij} z_j - dz_j^2 z_i |\vec{z}|^{-2}) = \frac{\alpha^2}{|\vec{z}|^{2d}} (z_i - dz_i) \\ &= \frac{\alpha^2}{|\vec{z}|^{2d}} (1-d) z_i. \end{aligned}$$

Therefore, given that \vec{u} does not depend on time, we have

$$\rho (\vec{u}_t + (\vec{u} \cdot \nabla) \vec{u}) = \rho (1-d) \alpha^2 \frac{\vec{z}}{|\vec{z}|^{2d}},$$

which is indeed the value of forcing term \vec{f} .

7.2 NON DIVERGENCE-FREE SCHEME MODIFICATIONS

The exact solution presented in §7.1.2 is non divergence-free which means that $\nabla \cdot \vec{u} = f_{\text{div}}$ in $\Omega_{\pm}(t)$. This leads to an additional term in the right-hand side of the continuity equation for the discrete schemes (5.15a–d), (5.24a–d), (5.27a–d) and (6.18a–d). We now derive the correction term only for anti-

symmetric scheme (5.15a–d) since, for the other three schemes, the derivation is analogous.

As for the two-phase Stokes flow, we use the unconstrained pressure space \mathbb{P}^m . Therefore, we rewrite $\varphi \in \mathbb{P}^m$ as

$$\varphi = \varphi - \frac{(\varphi, 1)}{(1, 1)} + \frac{(\varphi, 1)}{(1, 1)}, \quad (7.4)$$

where $\varphi - \frac{(\varphi, 1)}{(1, 1)} \in \tilde{\mathbb{P}}^m$ and $\frac{(\varphi, 1)}{(1, 1)} \in \mathbb{R}$. Substituting (7.4) in (5.15b) we obtain

$$(\nabla \cdot \vec{U}^{m+1}, \varphi) = \left(\nabla \cdot \vec{U}^{m+1}, \varphi - \frac{(\varphi, 1)}{(1, 1)} \right) + \left(\nabla \cdot \vec{U}^{m+1}, 1 \right) \frac{(\varphi, 1)}{(1, 1)}, \quad (7.5)$$

but, given that

$$\left(\nabla \cdot \vec{U}^{m+1}, \varphi - \frac{(\varphi, 1)}{(1, 1)} \right) = \left(f_{\text{div}}, \varphi - \frac{(\varphi, 1)}{(1, 1)} \right), \quad (7.6)$$

and using (3.31), we finally obtain

$$(\nabla \cdot \vec{U}^{m+1}, \varphi) = \left(f_{\text{div}}, \varphi - \frac{(\varphi, 1)}{(1, 1)} \right) + \frac{(\varphi, 1)}{\mathcal{L}^d(\Omega)} \int_{\partial_1 \Omega} (\vec{I}_2^m \vec{g}) \cdot \vec{n} \, d\mathcal{H}^{d-1} \quad \forall \varphi \in \mathbb{P}^m. \quad (7.7)$$

We notice that the first term in the right-hand side of (7.7) is the correction due to the fact that the velocity is non divergence-free, while the second term is the usual correction arising from an inhomogeneous boundary data \vec{g} . We also notice that, if f_{div} is constant, the first term in the right-hand side of (7.7) is zero since f_{div} can be taken out from the integral and what remains is simply the mean of a zero-mean function.

Additionally, only for the antisymmetric case, (5.7) is no longer valid and we need to use (5.6) to derive the antisymmetric weak formulation. Therefore an additional term $\frac{1}{2}(\rho f_{\text{div}} \vec{u}, \vec{\xi})$ appears in the momentum equation (5.11a).

Hence, the weak antisymmetric formulation (5.11a–d) is replaced by

$$\begin{aligned} & \frac{1}{2} \left[\frac{d}{dt} (\rho \vec{u}, \vec{\xi}) + (\rho \vec{u}_t, \vec{\xi}) + (\rho, [(\vec{u} \cdot \nabla) \vec{u}] \cdot \vec{\xi} - [(\vec{u} \cdot \nabla) \vec{\xi}] \cdot \vec{u}) \right] \\ & + 2 \left(\mu \underline{\underline{D}}(\vec{u}), \underline{\underline{D}}(\vec{\xi}) \right) - (p, \nabla \cdot \vec{\xi}) \\ & - \gamma \left\langle \boldsymbol{\varkappa} \vec{\nu}, \vec{\xi} \right\rangle_{\Gamma(t)} = (\vec{f}, \vec{\xi}) + \frac{1}{2} (\rho f_{\text{div}} \vec{u}, \vec{\xi}) \quad \forall \vec{\xi} \in \mathbb{U}(\vec{0}), \end{aligned} \quad (7.8a)$$

$$(\nabla \cdot \vec{u}, \varphi) = (f_{\text{div}}, \varphi) \quad \forall \varphi \in \tilde{\mathbb{P}}, \quad (7.8b)$$

$$\left\langle \vec{\mathcal{V}} - \vec{u}, \chi \vec{\nu} \right\rangle_{\Gamma(t)} = 0 \quad \forall \chi \in H^1(\Gamma(t)), \quad (7.8c)$$

$$\left\langle \boldsymbol{\varkappa} \vec{\nu}, \vec{\eta} \right\rangle_{\Gamma(t)} + \left\langle \nabla_s \text{id}, \nabla_s \vec{\eta} \right\rangle_{\Gamma(t)} = 0 \quad \forall \vec{\eta} \in [H^1(\Gamma(t))]^d. \quad (7.8d)$$

Therefore, the antisymmetric discrete scheme in the non divergence-free case, using the unconstrained pressure space, reads as follow. Let Γ^0 , an approximation to $\Gamma(0)$, and $\vec{U}^0 \in \mathbb{U}^0(\vec{g})$ be given. For $m = 0, \dots, M-1$, find $(\vec{U}^{m+1}, P^{m+1}, \vec{X}^{m+1}, \kappa^{m+1}) \in \mathbb{U}^m(\vec{g}) \times \mathbb{P}^m \times \underline{V}(\Gamma^m) \times W(\Gamma^m)$ such that

$$\begin{aligned} & \left(\frac{\frac{1}{2} (\vec{I}_0^m \rho^{m-1} + \rho^m) \vec{U}^{m+1} - \vec{I}_0^m \rho^{m-1} \vec{I}_2^m \vec{U}^m}{\tau}, \vec{\xi} \right) \\ & + \frac{1}{2} \left((\rho^m \vec{I}_2^m \vec{U}^m \cdot \nabla) \vec{U}^{m+1}, \vec{\xi} \right) - \frac{1}{2} \left((\rho^m \vec{I}_2^m \vec{U}^m \cdot \nabla) \vec{\xi}, \vec{U}^{m+1} \right) \\ & - 2 \left(\mu^m \underline{\underline{D}}(\vec{U}^{m+1}), \underline{\underline{D}}(\vec{\xi}) \right) - (P^{m+1}, \nabla \cdot \vec{\xi}) \\ & - \gamma \left\langle \kappa^{m+1} \vec{\nu}^m, \vec{\xi} \right\rangle_{\Gamma^m} = (\vec{f}^{m+1}, \vec{\xi}) + \frac{1}{2} (\rho^m f_{\text{div}} \vec{U}^m, \vec{\xi}) \quad \forall \vec{\xi} \in \mathbb{U}^m(\vec{0}), \end{aligned} \quad (7.9a)$$

$$\begin{aligned} & \left(\nabla \cdot \vec{U}^{m+1}, \varphi \right) = \left(f_{\text{div}}, \varphi - \frac{(\varphi, 1)}{(1, 1)} \right) \\ & + \frac{(\varphi, 1)}{\mathcal{L}^d(\Omega)} \int_{\partial_1 \Omega} (\vec{I}_2^m \vec{g}) \cdot \vec{n} \, d\mathcal{H}^{d-1} \quad \forall \varphi \in \mathbb{P}^m, \end{aligned} \quad (7.9b)$$

$$\left\langle \frac{\vec{X}^{m+1} - \text{id}}{\tau}, \chi \vec{\nu}^m \right\rangle_{\Gamma^m}^h - \left\langle \vec{U}^{m+1}, \chi \vec{\nu}^m \right\rangle_{\Gamma^m} = 0 \quad \forall \chi \in W(\Gamma^m), \quad (7.9c)$$

$$\left\langle \kappa^{m+1} \vec{\nu}^m, \vec{\eta} \right\rangle_{\Gamma^m}^h + \left\langle \nabla_s \vec{X}^{m+1}, \nabla_s \vec{\eta} \right\rangle_{\Gamma^m} = 0 \quad \forall \vec{\eta} \in \underline{V}(\Gamma^m) \quad (7.9d)$$

and set $\Gamma^{m+1} = \vec{X}^{m+1}(\Gamma^m)$.

7.3 BENCHMARK QUANTITIES

In our numerical simulations, unless otherwise stated, we use the following settings. We employ uniform time steps $\tau_m = \tau$, $m = 0, \dots, M - 1$. The bulk mesh is remeshed only if the angle criterion (3.49) holds with $C_a = 20^\circ$. Moreover, we set the GMRES tolerance to $\text{tol} = 10^{-12}$ and the restart value to 50. We use the Stokes matrix (3.40) or, depending on the pressure space, (3.45) as a preconditioner factorizing it with UMFPACK. Moreover, we use the errors (4.3), (4.4), (4.5), (4.6) and the estimated order of convergence EOC (4.7). See §4.2 for more details.

For later use, we define some benchmark quantities for the continuous solution (\vec{u}, p, Γ) of (5.1a–i). Let

$$z_c(t) = \frac{1}{\mathcal{L}^d(\Omega_-(t))} \int_{\Omega_-(t)} z_d \, d\mathcal{L}^d \quad (7.10)$$

denotes the d -component of the bubble's centre of mass, where z_d is the d -component of the position vector \vec{z} . Let $\$'(t)$ denotes the degree of sphericity of $\Gamma(t)$, which is defined as the ratio between the surface volume of a volume-equivalent hypersphere and $\mathcal{H}^{d-1}(\Gamma(t))$. Let

$$V_c(t) = \frac{1}{\mathcal{L}^d(\Omega_-(t))} \int_{\Omega_-(t)} u_d(t) \, d\mathcal{L}^d \quad (7.11)$$

denotes the bubble's rise velocity, where $u_d(t)$ is the d -component of \vec{u} . Therefore, the discrete counterpart of d -component of the bubble's centre of mass is

$$z_c^m = \frac{1}{\mathcal{L}^d(\Omega_-^m)} \int_{\Omega_-^m} z_d^m \, d\mathcal{L}^d, \quad (7.12)$$

while the degree of sphericity becomes

$$\$'^m = \frac{\pi^{\frac{1}{d}} [2 d \mathcal{L}^d(\Omega_-^m)]^{\frac{d-1}{d}}}{\mathcal{H}^{d-1}(\Gamma^m)} \quad (7.13)$$

J_Γ	J_Ω^0 case I	J_Ω^0 case II	τ	J_Ω^M case I	J_Ω^M case II
32	296	460	$6.4 \cdot 10^{-2}$	310	216
64	1240	1040	$1.6 \cdot 10^{-2}$	1240	444
128	4836	2628	$4 \cdot 10^{-3}$	4836	1384
256	18476	7460	10^{-3}	18476	4484

Table 7.1: Discretization parameters for the expanding bubble problems, adaptive meshes.

and the bubble's rise velocity assumes the following form

$$V_c^m = \frac{1}{\mathcal{L}^d(\Omega_-^m)} \int_{\Omega_-^m} U_d^m \, d\mathcal{L}^d, \quad (7.14)$$

where U_d^m is the d -component of \vec{U}^m evaluated on Ω^m .

7.4 CONVERGENCE TESTS

For the convergence testes, we choose the initial surface $\Gamma(0) = \{\vec{z} \in \mathbb{R}^d : |\vec{z}| = \frac{1}{2}\}$, $\partial_1 \Omega = \partial \Omega$ and adaptive bulk meshes that use a finer resolution close to the interface. We compute the discrete solution over the time interval $[0, 1]$. For the expanding bubble I, see §7.1.1, we fix $\Omega = (-1, 1)^2$ and we choose the parameters $\alpha = 0.15$ and

$$\rho_+ = \rho_- = \mu_+ = \mu_- = \gamma = 1. \quad (7.15)$$

Instead, for the expanding bubble II, see §7.1.2, we fix $\Omega = (-1, 1)^2 \setminus [-\frac{1}{3}, \frac{1}{3}]^2$ and we choose the parameters $\alpha = 0.15$ and

$$\rho_+ = 1000, \quad \rho_- = 100, \quad \mu_+ = 10, \quad \mu_- = 1, \quad \gamma = 1. \quad (7.16)$$

Details on the discretization parameters are given in Table 7.1. Here we explicitly state the final number of bulk elements, J_Ω^M , for the explicit scheme with the P2–P0 element for the two expanding bubble problems.

We report on the errors of the expanding bubble I for the P2–P0, P2–P1^{dgr} and P2–(P1+P0) elements in Tables 7.2, 7.3 and 7.4, respectively. For each element, we compare the explicit, implicit, antisymmetric and ALE

J_Γ	$\ \Gamma^h - \Gamma\ _{L^\infty}$	$\ \vec{U} - I_2^h \vec{u}\ _{L^2}$	EOC	$\ \vec{U} - I_2^h \vec{u}\ _{L^2(H^1)}$	$\ P - p\ _{L^2}$	EOC	CPU[s]
explicit							
32	3.96456e-04	0	-	0	3.05157e-01	-	6
64	1.03429e-04	0	-	0	1.57053e-01	0.96	49
128	2.61302e-05	0	-	0	7.09596e-02	1.15	878
256	6.53463e-06	0	-	0	1.99794e-02	1.79	23993
implicit							
32	3.96456e-04	0	-	0	3.05157e-01	-	7
64	1.03429e-04	0	-	0	1.57053e-01	0.96	78
128	2.61302e-05	0	-	0	7.09596e-02	1.15	1343
256	6.53463e-06	0	-	0	1.99794e-02	1.79	37495
antisymmetric							
32	3.96456e-04	0	-	0	3.05157e-01	-	4
64	1.03429e-04	0	-	0	1.57053e-01	0.96	56
128	2.61302e-05	0	-	0	7.09596e-02	1.15	1186
256	6.53463e-06	0	-	0	1.99794e-02	1.79	24546
ALE							
32	3.96571e-04	6.06205e-06	-	7.02427e-05	3.02004e-01	-	8
64	1.03457e-04	6.05685e-07	3.32	1.50879e-05	1.57053e-01	0.94	128
128	2.61386e-05	1.09841e-07	2.46	4.35730e-06	7.09597e-02	1.15	1734
256	6.53677e-06	1.77615e-08	2.57	1.13170e-06	1.99793e-02	1.79	36462

Table 7.2: ($\rho_+ = \rho_- = \mu_+ = \mu_- = \gamma = 1, \alpha = 0.15$) Expanding bubble problem I on $(-1, 1)^2$ over the time interval $[0, 1]$ for the P2–P0 element, with adaptive meshes and $C_a = 20^\circ$.

scheme derived in Chapter 5 and Chapter 6. Firstly, we observe that the explicit, the implicit and the antisymmetric scheme capture exactly the velocity solution for all the three elements. This is possible because the exact velocity is linear, see (7.2b). We also notice that all the schemes, independently of the element used, capture the pressure and the interface position with the same accuracy. For what concerns the computational time, as expected due to the nature of the schemes, the explicit scheme performs similarly to the antisymmetric scheme while the implicit scheme performs consistently with the ALE scheme.

We report on the errors of the expanding bubble II for the P2–P0, P2–P1^{dg_r} and P2–(P1+P0) elements in Tables 7.5, 7.6 and 7.7, respectively. Again, for each element, we compare the explicit, implicit, antisymmetric

J_Γ	$\ \Gamma^h - \Gamma\ _{L^\infty}$	$\ \vec{U} - I_2^h \vec{u}\ _{L^2}$	EOC	$\ \vec{U} - I_2^h \vec{u}\ _{L^2(H^1)}$	$\ P - p\ _{L^2}$	EOC	CPU[s]
explicit							
32	3.96456e-04	0	-	0	3.05157e-01	-	5
64	1.03429e-04	0	-	0	1.57053e-01	0.96	53
128	2.61302e-05	0	-	0	7.09596e-02	1.15	1162
256	6.53463e-06	0	-	0	1.99794e-02	1.79	26055
implicit							
32	3.96456e-04	0	-	0	3.05157e-01	-	6
64	1.03429e-04	0	-	0	1.57053e-01	0.96	102
128	2.61302e-05	0	-	0	7.09596e-02	1.15	2456
256	6.53463e-06	0	-	0	1.99794e-02	1.79	41406
antisymmetric							
32	3.96456e-04	0	-	0	3.05157e-01	-	6
64	1.03429e-04	0	-	0	1.57053e-01	0.96	66
128	2.61302e-05	0	-	0	7.09596e-02	1.15	1145
256	6.53463e-06	0	-	0	1.99794e-02	1.79	28118
ALE							
32	3.96889e-04	2.59155e-06	-	2.20644e-05	3.00690e-01	-	9
64	1.03462e-04	1.29962e-07	4.32	1.52925e-06	1.57054e-01	0.94	167
128	2.61390e-05	4.27643e-08	1.60	4.19906e-07	7.09597e-02	1.15	2219
256	6.53680e-06	1.09868e-08	1.92	9.79356e-08	1.99793e-02	1.79	41821

Table 7.3: ($\rho_+ = \rho_- = \mu_+ = \mu_- = \gamma = 1, \alpha = 0.15$) Expanding bubble problem I on $(-1, 1)^2$ over the time interval $[0, 1]$ for the P2–P1^{dgr} element, with adaptive meshes and $C_a = 20^\circ$.

J_Γ	$\ \Gamma^h - \Gamma\ _{L^\infty}$	$\ \vec{U} - I_2^h \vec{u}\ _{L^2}$	EOC	$\ \vec{U} - I_2^h \vec{u}\ _{L^2(H^1)}$	$\ P - p\ _{L^2}$	EOC	CPU[s]
explicit							
32	3.96456e-04	0	-	0	3.05157e-01	-	5
64	1.03429e-04	0	-	0	1.57053e-01	0.96	61
128	2.61302e-05	0	-	0	7.09596e-02	1.15	1317
256	6.53463e-06	0	-	0	1.99794e-02	1.79	29194
implicit							
32	3.96456e-04	0	-	0	3.05157e-01	-	6
64	1.03429e-04	0	-	0	1.57053e-01	0.96	134
128	2.61302e-05	0	-	0	7.09596e-02	1.15	2649
256	6.53463e-06	0	-	0	1.99794e-02	1.79	49990
antisymmetric							
32	3.96456e-04	0	-	0	3.05157e-01	-	5
64	1.03429e-04	0	-	0	1.57053e-01	0.96	45
128	2.61302e-05	0	-	0	7.09596e-02	1.15	1567
256	6.53463e-06	0	-	0	1.99794e-02	1.79	30997
ALE							
32	3.96823e-04	1.94467e-06	-	1.74315e-05	3.01900e-01	-	10
64	1.03462e-04	1.27547e-07	3.93	1.33117e-06	1.57054e-01	0.94	160
128	2.61390e-05	4.26296e-08	1.58	3.78211e-07	7.09597e-02	1.15	2420
256	6.53680e-06	1.09827e-08	1.91	9.46271e-08	1.99793e-02	1.79	47181

Table 7.4: ($\rho_+ = \rho_- = \mu_+ = \mu_- = \gamma = 1, \alpha = 0.15$) Expanding bubble problem I on $(-1, 1)^2$ over the time interval $[0, 1]$ for the P2–(P1+P0) element, with adaptive meshes and $C_a = 20^\circ$.

J_Γ	$\ \Gamma^h - \Gamma\ _{L^\infty}$	$\ \vec{U} - I_2^h \vec{u}\ _{L^2}$	EOC	$\ \vec{U} - I_2^h \vec{u}\ _{L^2(H^1)}$	$\ P - p\ _{L^2}$	EOC	CPU[s]
explicit							
32	4.30773e-03	8.20256e-04	-	1.68543e-02	2.15728e-00	-	8
64	1.02563e-03	2.41581e-04	1.76	7.91233e-03	1.09556e-00	0.98	103
128	2.47030e-04	1.63839e-04	0.56	5.68681e-03	5.84940e-01	0.91	2735
256	6.31103e-05	6.41052e-05	1.32	3.79153e-03	2.68975e-01	1.10	112570
implicit							
32	4.30916e-03	8.19133e-04	-	1.68287e-02	2.15708e-00	-	11
64	1.02572e-03	2.41756e-04	1.76	7.91714e-03	1.09555e-00	0.98	115
128	2.47005e-04	1.63964e-04	0.56	5.68939e-03	5.84941e-01	0.91	3051
256	6.31088e-05	6.41051e-05	1.32	3.79145e-03	2.68997e-01	1.10	114150
antisymmetric							
32	-	-	-	-	-	-	-
64	1.00458e-03	2.46961e-04	-	8.41282e-03	2.01659e+01	-	110
128	2.46522e-04	1.93474e-04	0.35	6.65077e-03	2.00687e+01	0.01	3172
256	6.28219e-05	7.41095e-05	1.35	4.27774e-03	2.00294e+01	0	101940
ALE							
32	4.29317e-03	1.44681e-03	-	3.18041e-02	2.97695e-00	-	11
64	1.10556e-03	3.15670e-04	2.20	1.12617e-02	1.61498e-00	0.88	80
128	2.56920e-04	1.50784e-04	1.07	7.75664e-03	8.19860e-01	0.98	971
256	6.25630e-05	7.04122e-05	1.07	3.88244e-03	3.90868e-01	1.04	10828

Table 7.5: ($\rho_+ = 1000, \rho_- = 100, \mu_+ = 10, \mu_- = 1, \gamma = 1, \alpha = 0.15$) Expanding bubble problem II on $(-1, 1)^2 \setminus [-\frac{1}{3}, \frac{1}{3}]^2$ over the time interval $[0, 1]$ for the P2–P0 element, with adaptive meshes and $C_a = 20^\circ$.

and ALE scheme derived in Chapter 5 and Chapter 6. Firstly, we observe that each scheme has almost the same accuracy independently of the element used. Moreover, the velocity and the interface position is captured with similar accuracy by all four schemes. Instead, we notice that the pressure error does not converge with the antisymmetric scheme. Indeed, the antisymmetric scheme has some difficulties handling the viscosity jump. On the other hand, the ALE scheme has a slightly higher pressure error with respect to the explicit and implicit scheme. We also notice that the experiment using the antisymmetric scheme with the P2–P0 element and the coarsest mesh is not present because it fails due to mesh element intersections. For what concerns the computational time, the ALE scheme greatly outperforms the other schemes. Since the bulk domain is not convex, the interpolation rou-

J_Γ	$\ \Gamma^h - \Gamma\ _{L^\infty}$	$\ \vec{U} - I_2^h \vec{u}\ _{L^2}$	EOC	$\ \vec{U} - I_2^h \vec{u}\ _{L^2(H^1)}$	$\ P - p\ _{L^2}$	EOC	CPU[s]
explicit							
32	4.13551e-03	1.13153e-03	-	2.16975e-02	2.27976e-00	-	7
64	1.09044e-03	4.39709e-04	1.36	1.09502e-02	1.19522e-00	0.93	102
128	2.54203e-04	3.27591e-04	0.42	8.97282e-03	5.89086e-01	1.02	2711
256	6.64512e-05	1.29614e-04	1.31	5.24240e-03	2.69734e-01	1.10	84756
implicit							
32	4.14065e-03	1.12412e-03	-	2.15014e-02	2.27964e-00	-	10
64	1.09090e-03	4.39985e-04	1.35	1.09531e-02	1.19512e-00	0.93	114
128	2.54225e-04	3.27943e-04	0.42	8.99056e-03	5.89082e-01	1.02	3006
256	6.64570e-05	1.29619e-04	1.31	5.24247e-03	2.69720e-01	1.10	84746
antisymmetric							
32	7.24917e-02	3.86594e-01	-	1.03225e+01	1.12023e+02	-	8
64	1.06996e-03	4.35177e-04	9.80	1.11906e-02	2.01870e+01	2.47	114
128	2.51928e-04	3.42056e-04	0.35	9.60466e-03	2.00691e+01	0.01	3166
256	6.54386e-05	1.31946e-04	1.34	5.44437e-03	2.00293e+01	0	100520
ALE							
32	4.17956e-03	1.21225e-03	-	2.60063e-02	4.86217e-00	-	11
64	1.11075e-03	4.57492e-04	1.41	1.19033e-02	2.47156e-00	0.98	78
128	2.53693e-04	2.97246e-04	0.62	9.91583e-03	1.24013e-00	0.99	936
256	6.38218e-05	1.25182e-04	1.22	5.18160e-03	6.07846e-01	1.01	12595

Table 7.6: ($\rho_+ = 1000, \rho_- = 100, \mu_+ = 10, \mu_- = 1, \gamma = 1, \alpha = 0.15$) Expanding bubble problem II on $(-1, 1)^2 \setminus [-\frac{1}{3}, \frac{1}{3}]^2$ over the time interval $[0, 1]$ for the P2–P1^{dgr} element, with adaptive meshes and $C_a = 20^\circ$.

J_Γ	$\ \Gamma^h - \Gamma\ _{L^\infty}$	$\ \vec{U} - I_2^h \vec{u}\ _{L^2}$	EOC	$\ \vec{U} - I_2^h \vec{u}\ _{L^2(H^1)}$	$\ P - p\ _{L^2}$	EOC	CPU[s]
explicit							
32	4.13976e-03	1.24661e-03	-	2.59441e-02	2.28403e-00	-	8
64	1.07627e-03	4.80240e-04	1.38	1.35253e-02	1.20439e-00	0.92	102
128	2.55529e-04	3.70025e-04	0.38	1.20309e-02	5.89258e-01	1.03	2810
256	6.66480e-05	1.42910e-04	1.34	6.48222e-03	2.69953e-01	1.10	88056
implicit							
32	3.99899e-03	1.23928e-03	-	2.61424e-02	2.30983e-00	-	11
64	1.07657e-03	4.80445e-04	1.37	1.35256e-02	1.20449e-00	0.94	126
128	2.55562e-04	3.70165e-04	0.38	1.20325e-02	5.89236e-01	1.03	3223
256	6.66478e-05	1.42914e-04	1.34	6.48232e-03	2.69982e-01	1.10	95315
antisymmetric							
32	5.56564e-02	3.33673e-01	-	8.38557e-00	9.98404e+01	-	8
64	1.05282e-03	4.75502e-04	9.45	1.37127e-02	2.01792e+01	2.31	112
128	2.52742e-04	3.82170e-04	0.32	1.24067e-02	2.00690e+01	0.01	3138
256	6.55951e-05	1.45885e-04	1.36	6.67192e-03	2.00294e+01	0	98893
ALE							
32	4.20717e-03	1.33379e-03	-	3.03240e-02	4.92318e-00	-	15
64	1.11280e-03	4.91358e-04	1.44	1.42754e-02	2.47229e-00	0.99	90
128	2.54196e-04	3.30194e-04	0.57	1.31294e-02	1.24058e-00	0.99	991
256	6.37496e-05	1.35898e-04	1.25	6.41819e-03	6.08051e-01	1.01	11970

Table 7.7: ($\rho_+ = 1000, \rho_- = 100, \mu_+ = 10, \mu_- = 1, \gamma = 1, \alpha = 0.15$) Expanding bubble problem II on $(-1, 1)^2 \setminus [-\frac{1}{3}, \frac{1}{3}]^2$ over the time interval $[0, 1]$ for the P2–(P1+P0) element, with adaptive meshes and $C_a = 20^\circ$.

J_Γ	J_Ω^0	J_Ω^M explicit	J_Ω^M implicit	J_Ω^M antisymmetric	J_Ω^M ALE
32	2210	1796	1796	1826	1870
64	8822	7378	7500	7410	7368
128	35092	28358	29210	28018	28982

Table 7.8: Discretization parameters for the rising bubble experiment I, nearly uniform meshes.

tine uses a linear search, instead of an optimized local search involving only neighbours, to locate bulk elements. Therefore, the interpolation routine is very slow and accounts for a substantial share of the total simulation time. But the ALE scheme, which has to interpolate the velocity only when a complete bulk remesh is performed, uses the interpolation routine very rarely, which leads to a significant reduction in the total simulation time. See §5.6 for more details on the velocity interpolation algorithms.

7.5 RISING BUBBLE EXPERIMENTS

We use the same setup described in [42, Figure 2], which is $\Omega = (0, 1) \times (0, 2)$ with $\partial_1\Omega = [0, 1] \times \{0, 2\}$ and $\partial_2\Omega = \{0, 1\} \times (0, 2)$. Moreover, let the initial interface be $\Gamma_0 = \{\vec{z} \in \mathbb{R}^2 : |\vec{z} - (\frac{1}{2}, \frac{1}{2})^T| = \frac{1}{4}\}$. We adopt an uniform time step size $\tau = 10^{-3}$, $T = 3$, $\vec{f} = -0.98 \rho \vec{e}_2$ and $\vec{g} = \vec{0}$.

The physical parameters for the rising bubble experiment I are

$$\rho_+ = 1000, \quad \rho_- = 100, \quad \mu_+ = 10, \quad \mu_- = 1, \quad \gamma = 24.5, \quad (7.17)$$

see the test case 1 in [42, Table I]. We list the discretization parameters in Table 7.8. Here we explicitly state the final number of bulk elements, J_Ω^M , for all the schemes for the P2–P0 element. We report on quantitative results for the rising bubble experiment I for the P2–P0, P2–P1^{dgr} and P2–(P1+P0) elements in Tables 7.9, 7.10 and 7.11, respectively. See §7.3 for the definitions of the various benchmark quantities. For each element, we compare the explicit, implicit, antisymmetric and ALE scheme derived in Chapter 5 and Chapter 6.

	$J_\Gamma = 32$	$J_\Gamma = 64$	$J_\Gamma = 128$
explicit			
$\$_{\min}$	0.8986	0.9002	0.9007
$t_{\$=\$_{\min}}$	2.1560	1.9450	1.9420
$V_{c,\max}$	0.2372	0.2402	0.2404
$t_{V_c=V_{c,\max}}$	1.0190	0.9370	0.9250
$z_c(t=3)$	1.0857	1.0837	1.0816
CPU	13664	24539	211168
implicit			
$\$_{\min}$	0.8986	0.8990	0.9011
$t_{\$=\$_{\min}}$	2.1560	1.9190	1.8400
$V_{c,\max}$	0.2372	0.2402	0.2403
$t_{V_c=V_{c,\max}}$	1.0190	0.9370	0.9240
$z_c(t=3)$	1.0857	1.0862	1.0852
CPU	18142	59221	373182
antisymmetric			
$\$_{\min}$	0.8891	0.8905	0.8897
$t_{\$=\$_{\min}}$	1.8640	1.7330	1.7020
$V_{c,\max}$	0.2298	0.2325	0.2328
$t_{V_c=V_{c,\max}}$	0.9060	0.8900	0.8790
$z_c(t=3)$	1.0630	1.0632	1.0614
CPU	6526	23425	130737
ALE			
$\$_{\min}$	0.9050	0.9022	0.9025
$t_{\$=\$_{\min}}$	1.9370	1.8840	1.9050
$V_{c,\max}$	0.2378	0.2407	0.2406
$t_{V_c=V_{c,\max}}$	0.9430	0.9340	0.9210
$z_c(t=3)$	1.0893	1.0848	1.0820
CPU	11737	52415	265654

Table 7.9: ($\rho_+ = 1000, \rho_- = 100, \mu_+ = 10, \mu_- = 1, \gamma = 24.5$) Rising bubble experiment I on $\Omega = (0, 1) \times (0, 2)$ over the time interval $[0, 3]$ for the P2–P0 element, with nearly uniform meshes and $C_a = 20^\circ$.

	$J_\Gamma = 32$	$J_\Gamma = 64$	$J_\Gamma = 128$
explicit			
$\$_{\min}$	0.8961	0.8985	0.9009
$t_{\$=\$_{\min}}$	1.9090	1.9060	1.8930
$V_{c,\max}$	0.2435	0.2422	0.2411
$t_{V_c=V_{c,\max}}$	0.9390	0.9330	0.9230
$z_c(t=3)$	1.0883	1.0839	1.0820
CPU	5285	29631	150569
implicit			
$\$_{\min}$	0.8961	0.8984	0.9010
$t_{\$=\$_{\min}}$	1.9090	1.8940	1.9020
$V_{c,\max}$	0.2434	0.2422	0.2411
$t_{V_c=V_{c,\max}}$	0.9390	0.9330	0.9230
$z_c(t=3)$	1.0882	1.0832	1.0818
CPU	13469	66270	402979
antisymmetric			
$\$_{\min}$	0.8813	0.8900	0.8903
$t_{\$=\$_{\min}}$	1.7370	1.7170	1.6840
$V_{c,\max}$	0.2356	0.2343	0.2334
$t_{V_c=V_{c,\max}}$	0.8910	0.8840	0.8760
$z_c(t=3)$	1.0653	1.0628	1.0613
CPU	5766	19124	140574
ALE			
$\$_{\min}$	0.9002	0.9012	0.9020
$t_{\$=\$_{\min}}$	1.9170	1.9180	1.8950
$V_{c,\max}$	0.2433	0.2421	0.2411
$t_{V_c=V_{c,\max}}$	0.9370	0.9320	0.9210
$z_c(t=3)$	1.0876	1.0838	1.0821
CPU	12007	59063	311455

Table 7.10: ($\rho_+ = 1000, \rho_- = 100, \mu_+ = 10, \mu_- = 1, \gamma = 24.5$) Rising bubble experiment on $\Omega = (0, 1) \times (0, 2)$ over the time interval $[0, 3]$ for the P2–P1^{dgr} element, with nearly uniform meshes and $C_a = 20^\circ$.

	$J_\Gamma = 32$	$J_\Gamma = 64$	$J_\Gamma = 128$
explicit			
$\$_{\min}$	0.8929	0.8975	0.9001
$t_{\$=\$_{\min}}$	1.9040	1.9040	1.9170
$V_{c,\max}$	0.2439	0.2424	0.2411
$t_{V_c=V_{c,\max}}$	0.9350	0.9300	0.9180
$z_c(t=3)$	1.0829	1.0852	1.0822
CPU	10236	29610	234396
implicit			
$\$_{\min}$	0.8925	0.8973	0.9004
$t_{\$=\$_{\min}}$	2.0410	1.9120	1.9160
$V_{c,\max}$	0.2439	0.2423	0.2410
$t_{V_c=V_{c,\max}}$	0.9340	0.9300	0.9190
$z_c(t=3)$	1.0820	1.0841	1.0819
CPU	17771	72837	403904
antisymmetric			
$\$_{\min}$	0.8788	0.8851	0.8883
$t_{\$=\$_{\min}}$	1.7920	1.7190	1.6790
$V_{c,\max}$	0.2359	0.2344	0.2334
$t_{V_c=V_{c,\max}}$	0.8860	0.8820	0.8750
$z_c(t=3)$	1.0648	1.0622	1.0607
CPU	5887	19703	146538
ALE			
$\$_{\min}$	0.9013	0.9010	0.9030
$t_{\$=\$_{\min}}$	1.9460	1.9050	1.8460
$V_{c,\max}$	0.2435	0.2422	0.2410
$t_{V_c=V_{c,\max}}$	0.9370	0.9330	0.9200
$z_c(t=3)$	1.0877	1.0865	1.0824
CPU	13628	63136	351867

Table 7.11: ($\rho_+ = 1000, \rho_- = 100, \mu_+ = 10, \mu_- = 1, \gamma = 24.5$) Rising bubble experiment I on $\Omega = (0, 1) \times (0, 2)$ over the time interval $[0, 3]$ for the P2–(P1+P0) element, with nearly uniform meshes and $C_a = 20^\circ$.

We observe that the results in Tables 7.9, 7.10 and 7.11 are in very good agreement, except for the antisymmetric scheme, with the corresponding numbers from the finest discretization run of group 3 in [42], which are given by 0.9013, 1.9000, 0.2417, 0.9239 and 1.0817. Here we note that of the three groups in [42], group 3 shows the most accurate and the most consistent results for the test case 1. Their method is based on the ALE approach with a piecewise quadratic velocity space enriched with cubic bubble functions, with a discontinuous piecewise linear pressure space and with a second order, fractional step θ -scheme in time. Similar results are also obtained in [12]. Moreover, we notice that, in all the simulations, the number of remeshing performed during the full time interval is always between 2 and 4. This means that, in each simulation adopting the ALE scheme, the velocity is interpolated, at worst, only 4 times.

In Figure 7.1 we show the evolution of the discrete pressures for a simulation with $J_\Gamma = 128$ interface elements using the P2–P1^{dgr} element and the implicit scheme, while the velocities are visualized in Figure 7.2.

Finally, in Figures 7.3, 7.4, 7.5 and 7.6 are reported, respectively, the evolution of the sphericity $\$$, rising velocity V_c , barycentre z_c and relative inner area $\frac{\mathcal{L}^2(\Omega_-^m)}{\mathcal{L}^2(\Omega_-^0)}$ over time. We notice almost identical results for the explicit, implicit and ALE schemes.

The physical parameters for the rising bubble experiment II are

$$\rho_+ = 1000, \quad \rho_- = 1, \quad \mu_+ = 10, \quad \mu_- = 0.1, \quad \gamma = 1.96, \quad (7.18)$$

see the test case 2 in [42, Table I]. We report on quantitative results for the rising bubble experiment II for the P2–P1^{dgr} and P2–(P1+P0) elements in Table 7.12. See §7.3 for the definitions of the various benchmark quantities. For each element, we compare the explicit, implicit and ALE scheme derived in Chapter 5 and Chapter 6. We use $J_\Gamma = 128$ interface elements with $J_\Omega^0 = 35092$ initial bulk elements. The final number of bulk elements, J_Ω^M , for the explicit scheme for the P2–(P1+P0) element is 10638. We observe that the results in Table 7.12 are in good agreement with the corresponding numbers from the finest discretization run of group 3 in [42], which are given

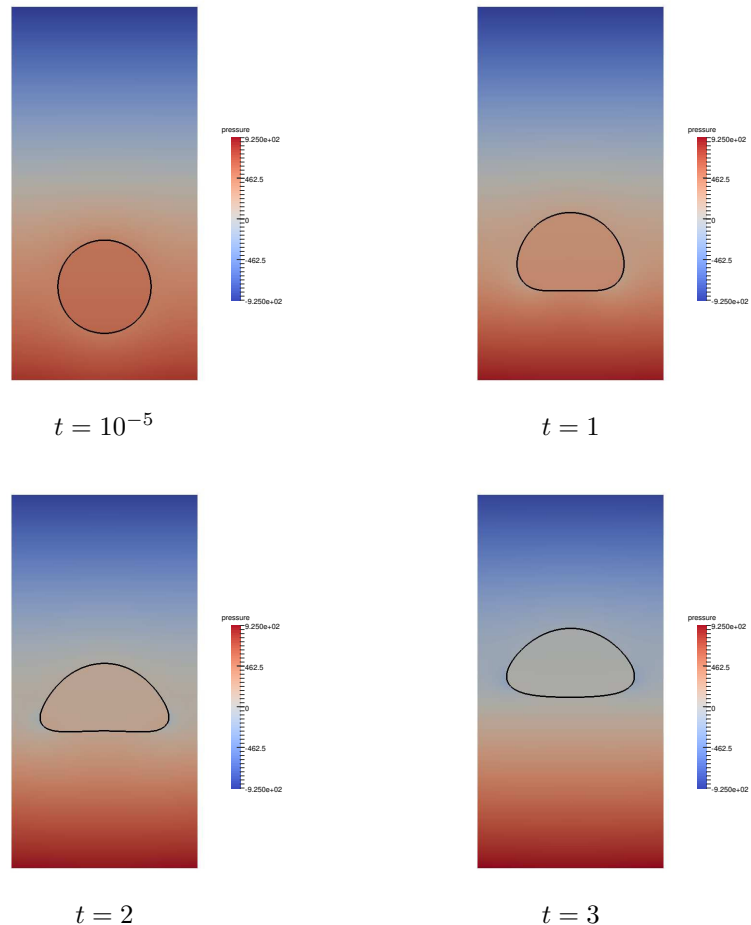


Figure 7.1: ($\rho_+ = 1000, \rho_- = 100, \mu_+ = 10, \mu_- = 1, \gamma = 24.5$) Pressure evolution for the rising bubble experiment I for the P2–P1^{dgr} element and the implicit scheme, nearly uniform mesh with $J_\Gamma = 128$ interface elements and $C_a = 20^\circ$.

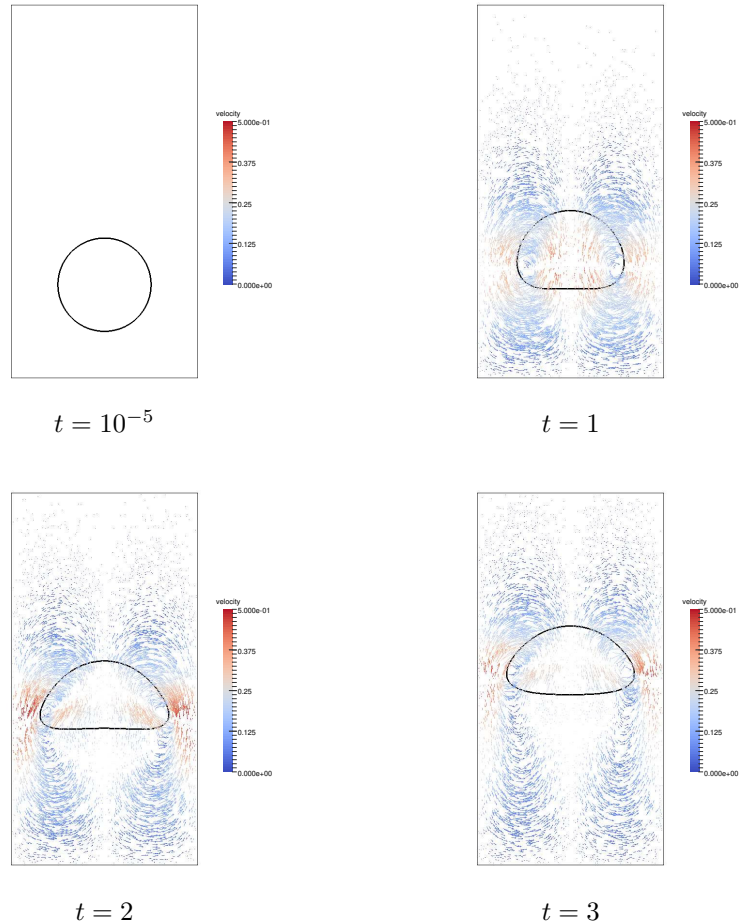


Figure 7.2: Velocity vector field for the simulation in Figure 7.1.

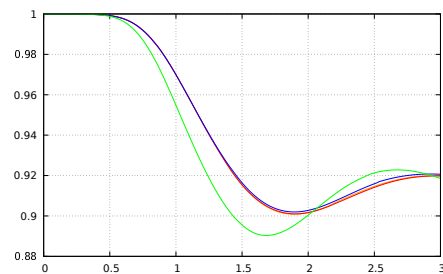


Figure 7.3: A plot of the sphericity ϕ over time for the simulation in Figure 7.1 for the explicit (orange), implicit (red), ALE (blue) and antisymmetric (green) schemes.

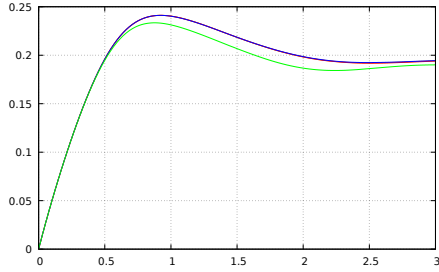


Figure 7.4: A plot of the rising velocity V_c over time for the simulation in Figure 7.1 for the explicit (orange), implicit (red), ALE (blue) and antisymmetric (green) schemes.

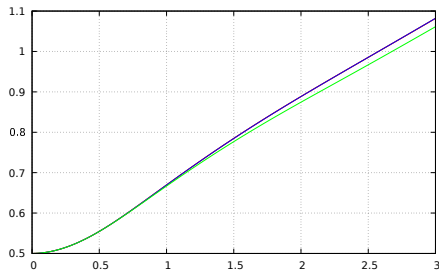


Figure 7.5: A plot of the barycentre z_c over time for the simulation in Figure 7.1 for the explicit (orange), implicit (red), ALE (blue) and antisymmetric (green) schemes.

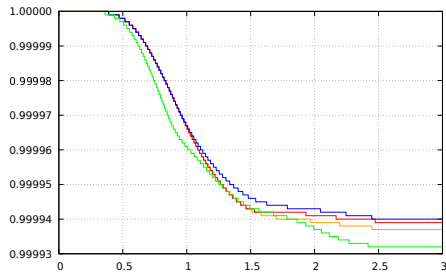


Figure 7.6: A plot of the relative inner area $\frac{\mathcal{L}^2(\Omega_m^-)}{\mathcal{L}^2(\Omega_l^-)}$ over time for the simulation in Figure 7.1 for the explicit (orange), implicit (red), ALE (blue) and antisymmetric (green) schemes.

	P2–P1 ^{dgr}	P2–(P1+P0)
explicit		
$\$_{\min}$	0.5412	0.5435
$t_{\$=\$_{\min}}$	3.0000	3.0000
$V_{c,\max 1}$	0.2501	0.2503
$t_{V_c=V_{c,\max 1}}$	0.7290	0.7290
$V_{c,\max 2}$	0.2402	0.2403
$t_{V_c=V_{c,\max 2}}$	2.1030	2.1070
$z_c(t = 3)$	1.1384	1.1383
CPU	128299	132498
implicit		
$\$_{\min}$	0.5443	0.5473
$t_{\$=\$_{\min}}$	3.0000	3.0000
$V_{c,\max 1}$	0.2501	0.2502
$t_{V_c=V_{c,\max 1}}$	0.7290	0.7290
$V_{c,\max 2}$	0.2402	0.2403
$t_{V_c=V_{c,\max 2}}$	2.1040	2.1540
$z_c(t = 3)$	1.1385	1.1387
CPU	216605	236635
ALE		
$\$_{\min}$	-	0.5266
$t_{\$=\$_{\min}}$	-	3.0000
$V_{c,\max 1}$	-	0.2502
$t_{V_c=V_{c,\max 1}}$	-	0.7300
$V_{c,\max 2}$	-	0.2400
$t_{V_c=V_{c,\max 2}}$	-	2.0670
$z_c(t = 3)$	-	1.1385
CPU	-	236253

Table 7.12: ($\rho_+ = 1000, \rho_- = 1, \mu_+ = 10, \mu_- = 0.1, \gamma = 1.96$) Rising bubble experiment II on $\Omega = (0, 1) \times (0, 2)$ over the time interval $[0, 3]$, with nearly uniform meshes, $J_\Gamma = 128$ and $C_a = 20^\circ$.

by 0.5144, 3.0000, 0.2502, 0.7317, 0.2393, 2.0600 and 1.1376. Here we note that there is little agreement on these results between the three groups in [42], but we believe the numbers of group 3 to be the most reliable ones. Similar results are also obtained in [12]. Some results in Table 7.12 are missing because one simulation had an early termination triggered by a bulk mesh overlap in the last steps.

In Figure 7.7 we show the evolution of the discrete pressures for a simulation with $J_\Gamma = 128$ interface elements using the P2–(P1+P0) element and the explicit scheme, while the velocities are visualized in Figure 7.8.

In Figures 7.9, 7.10, 7.11 and 7.12 are reported, respectively, the evolution of the sphericity $\$$, rising velocity V_c , barycentre z_c and relative inner area $\frac{\mathcal{L}^2(\Omega_-^m)}{\mathcal{L}^2(\Omega_-^0)}$ over time. In Figure 7.12 we observe oscillations in the relative inner area between $t = 2.1$ and $t = 2.3$. In that interval the bubble assumes a more non-convex shape and develops thin filaments which originate these oscillations.

We finally notice that in both experiments, namely the rising bubble I and II, the ALE scheme and the non-ALE schemes are all performing well. Therefore, the downside of having to project the velocity in the non-ALE formulations seems to be less severe than expected. This can be partly explained by the good interface mesh, which never changes even after a full bulk remeshing.

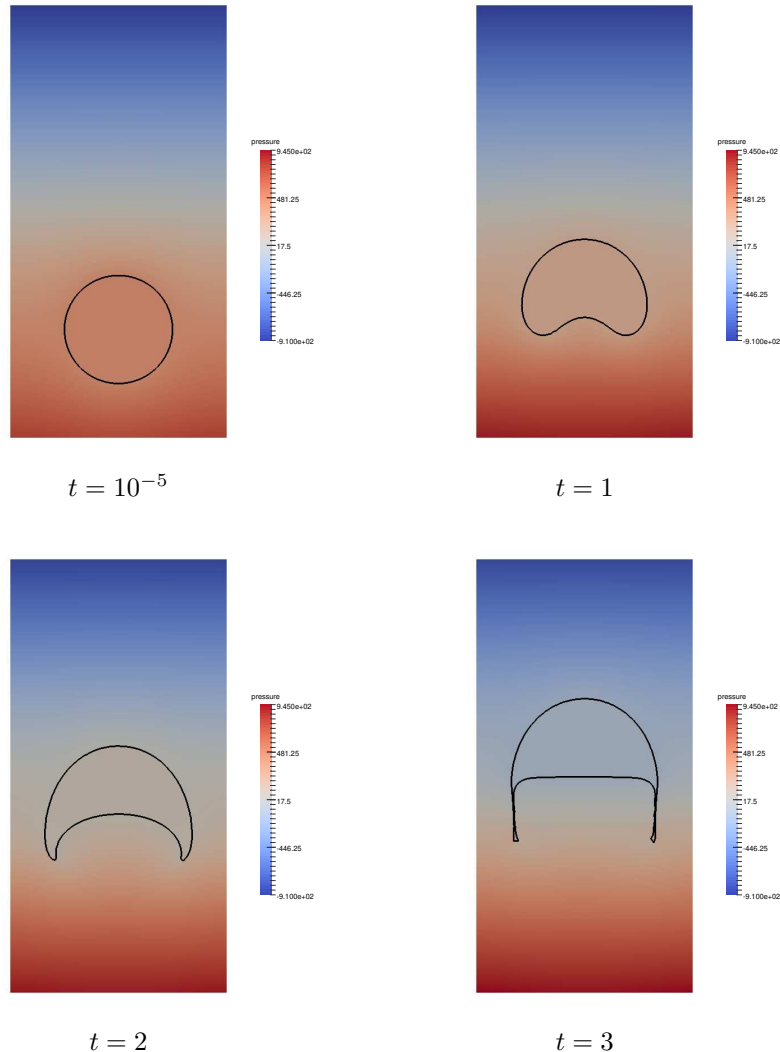


Figure 7.7: ($\rho_+ = 1000, \rho_- = 1, \mu_+ = 10, \mu_- = 0.1, \gamma = 1.96$) Pressure evolution for the rising bubble experiment II for the P2–(P1+P0) element and the explicit scheme, nearly uniform mesh with $J_\Gamma = 128$ interface elements and $C_a = 20^\circ$.

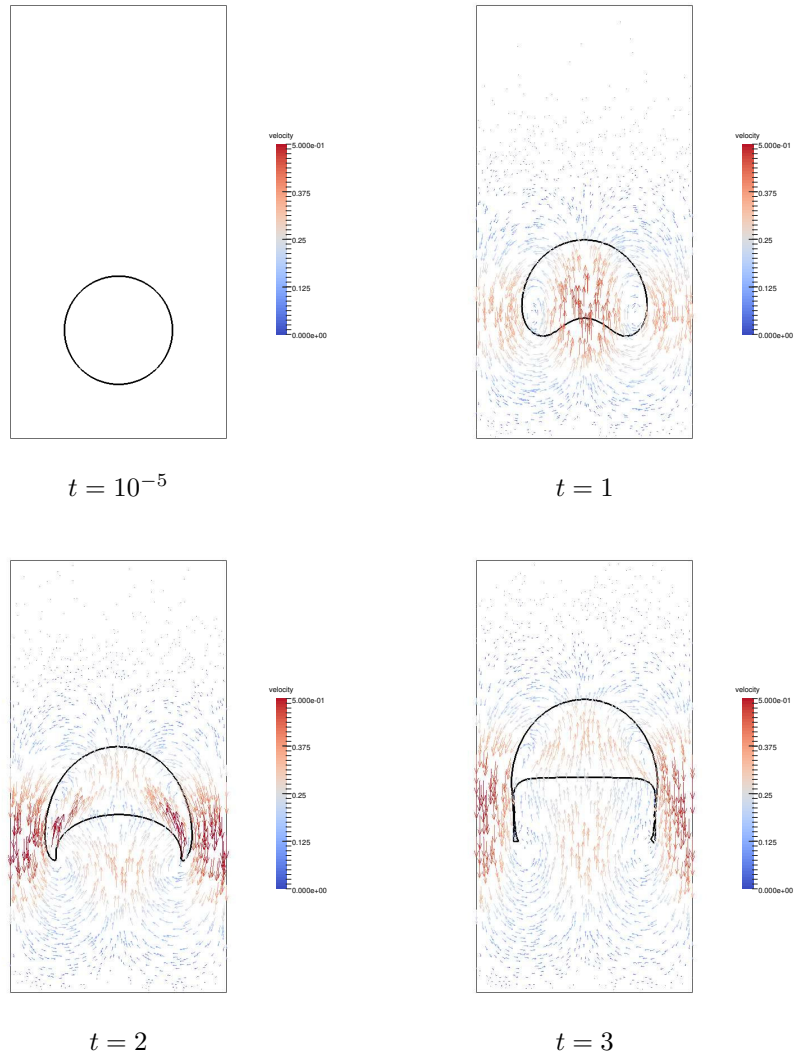


Figure 7.8: Velocity vector field for the simulation in Figure 7.7.

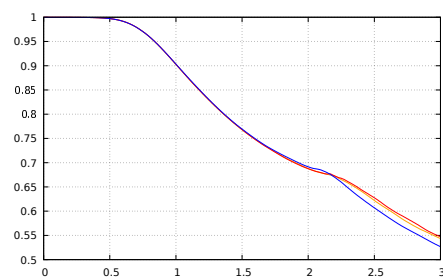


Figure 7.9: A plot of the sphericity δ over time for the simulation in Figure 7.7 for the explicit (orange), implicit (red) and ALE (blue) schemes.

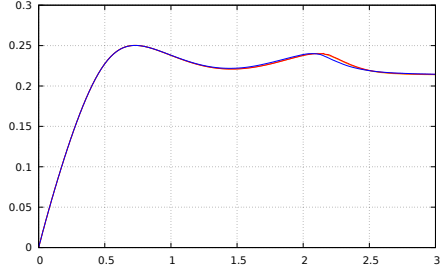


Figure 7.10: A plot of the rising velocity V_c over time for the simulation in Figure 7.7 for the explicit (orange), implicit (red) and ALE (blue) schemes.

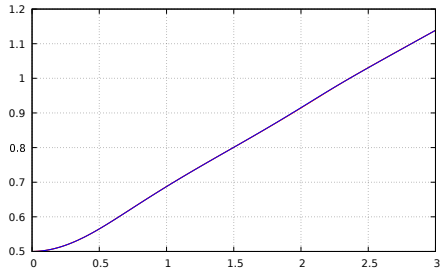


Figure 7.11: A plot of the barycentre z_c over time for the simulation in Figure 7.7 for the explicit (orange), implicit (red) and ALE (blue) schemes.

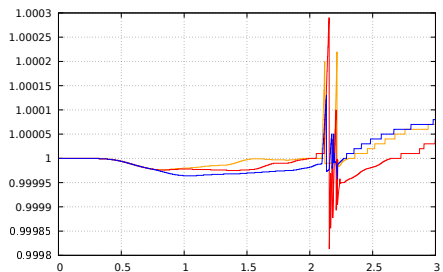


Figure 7.12: A plot of the relative inner area $\frac{\mathcal{L}^2(\Omega_m^-)}{\mathcal{L}^2(\Omega_0^-)}$ over time for the simulation in Figure 7.7 for the explicit (orange), implicit (red) and ALE (blue) schemes.

8

CONCLUSION

In this thesis we have investigated fitted front tracking finite element methods for two-phase incompressible Navier–Stokes flows. In Chapter 1, after introducing the free-boundary fluid flows, we have described the Navier–Stokes equations which model the evolution of a two-phase fluid. In these types of problems, apart from the flow solution in the bulk domain, the interface dividing the phases needs to be determined. Therefore, we have briefly overviewed the different ways to treat the unknown interface and we have detailed the various numerical challenges posed by these types of flows. In Chapter 2 we have introduced the key ideas of the front tracking approach, applying it to the simple problem of purely geometric evolution equations such as mean curvature flow and surface diffusion. Here we have reported on the finite element approximations and we have performed some numerical experiments in order to show the property of the schemes and of the flows. In particular, we have shown that the mesh naturally equidistributes and that the volume is conserved. In Chapter 3 we have proposed a novel finite element approximation for incompressible two-phase Stokes flow. After showing an energy bound and the volume conservation for the weak problem, we have demonstrated that our scheme is unconditionally stable and

we have proved the existence and uniqueness of the discrete approximation. Moreover, we have investigated the equidistribution property and the volume conservation. We have also discussed the mesh generation process together with the smoothing and remeshing procedures used to preserve the mesh quality. In Chapter 4 we have presented several numerical experiments in 2d and 3d to test our method and to allow comparisons with other methods. Using two exact solutions to the two-phase Stokes flow, we have performed various convergence tests. Moreover, we have tested that interface mesh points are naturally equidistributed by our scheme, that our scheme conserves the enclosed volume and that the surface energy monotonically decays. We have also reported on a shear flow experiment. In Chapter 5 we have extended our Stokes scheme to solve the incompressible two-phase Navier–Stokes flow. Here, we have derived a standard finite element approximation and an alternative finite element approximation based on an antisymmetric rewrite. For the antisymmetric discretization, we have proved the existence and uniqueness of a discrete solution and we have demonstrated that this scheme has certain stability properties. We have also examined the techniques used to interpolate the velocity. In Chapter 6 we have presented a different finite element approximation for incompressible two-phase Navier–Stokes flow, which uses the Arbitrary Lagrangian Eulerian method. This technique allows to rewrite the velocity time derivative with respect to a fixed reference manifold. As a consequence, the velocity does not need to be interpolated anymore. Finally, in Chapter 7 we have tested our schemes in several numerical experiments. Using two exact solutions to the two-phase Navier–Stokes flow, we have performed various convergence tests. Then, we have reported on two rising bubble experiments which constitute the standard benchmark for two-phase schemes. Here, we have observed that both the ALE and the standard scheme perform extremely well in terms of accuracy and CPU time. Moreover, in the case of non-convex bulk domains, we have noticed that the standard scheme is much slower than the ALE scheme since an unoptimized velocity interpolation routine has to be used.

There are several lines of research arising from this thesis which should be investigated in order to further improve the accuracy and the performance

of the schemes presented. The main ones can be summarized as follows:

- higher order time discretization schemes;
- solvers and preconditioners for the algebraic linear systems;
- adaptive bulk mesh refinement and coarsening algorithms;
- mesh smoothing techniques;
- higher order spaces for the interface displacement and curvilinear bulk meshes.

REFERENCES

- [1] H. ABELS, H. GARCKE, AND G. GRÜN, *Thermodynamically consistent, frame indifferent diffuse interface models for incompressible two-phase flows with different densities*, Math. Models Methods Appl. Sci., 22 (2012), p. 1150013.
- [2] M. AGNESE AND R. NÜRNBERG, *Fitted finite element discretization of two-phase Stokes flow*, Internat. J. Numer. Methods Fluids, 82 (2016), pp. 709–729.
- [3] D. M. ANDERSON, G. B. MCFADDEN, AND A. A. WHEELER, *Diffuse-interface methods in fluid mechanics*, in Annual review of fluid mechanics, Vol. 30, Annual Reviews, Palo Alto, CA, 1998, pp. 139–165.
- [4] R. ARIS, *Vectors, Tensors and the Basic Equations of Fluid Mechanics*, Dover Publications, New York, 1989.
- [5] E. BÄNSCH, *Finite element discretization of the Navier–Stokes equations with a free capillary surface*, Numer. Math., 88 (2001), pp. 203–235.
- [6] J. W. BARRETT, H. GARCKE, AND R. NÜRNBERG, *On the variational approximation of combined second and fourth order geometric evolution equations*, SIAM J. Sci. Comput., 29 (2007), pp. 1006–1041.
- [7] ——, *A parametric finite element method for fourth order geometric evolution equations*, J. Comput. Phys., 222 (2007), pp. 441–462.
- [8] ——, *On the parametric finite element approximation of evolving hypersurfaces in \mathbb{R}^3* , J. Comput. Phys., 227 (2008), pp. 4281–4307.

- [9] ——, *The approximation of planar curve evolutions by stable fully implicit finite element schemes that equidistribute*, Numer. Methods Partial Differential Equations, 27 (2011), pp. 1–30.
- [10] ——, *Eliminating spurious velocities with a stable approximation of viscous incompressible two-phase Stokes flow*, Comput. Methods Appl. Mech. Engrg., 267 (2013), pp. 511–530.
- [11] ——, *On the stable numerical approximation of two-phase flow with insoluble surfactant*, M2AN Math. Model. Numer. Anal., 49 (2015), pp. 421–458.
- [12] ——, *A stable parametric finite element discretization of two-phase Navier–Stokes flow*, J. Sci. Comp., 63 (2015), pp. 78–117.
- [13] R. BARRETT, M. BERRY, T. F. CHAN, J. DEMMEL, J. M. DONATO, J. DONGARRA, V. EIJKHOUT, R. POZO, C. ROMINE, AND H. VAN DER VORST, *Templates for the Solution of Linear Systems: Building Blocks for Iterative Methods*, Society for Industrial and Applied Mathematics (SIAM), Philadelphia, PA, 1994.
- [14] P. BASTIAN, M. BLATT, A. DEDNER, C. ENGWER, R. KLÖFKORN, R. KORNHUBER, M. OHLBERGER, AND O. SANDER, *A Generic Grid Interface for Parallel and Adaptive Scientific Computing. Part II: Implementation and Tests in DUNE*, Computing, 82 (2008), pp. 121–138.
- [15] P. BASTIAN, M. BLATT, A. DEDNER, C. ENGWER, R. KLÖFKORN, M. OHLBERGER, AND O. SANDER, *A Generic Grid Interface for Parallel and Adaptive Scientific Computing. Part I: Abstract Framework*, Computing, 82 (2008), pp. 103–119.
- [16] D. BOFFI, F. BREZZI, AND M. FORTIN, *Mixed finite element methods and applications*, vol. 44 of Springer Series in Computational Mathematics, Springer, Heidelberg, 2013.
- [17] D. BOFFI, N. CAVALLINI, F. GARDINI, AND L. GASTALDI, *Local mass conservation of Stokes finite elements*, J. Sci. Comput., 52 (2012), pp. 383–400.

- [18] D. BOTHE, M. KÖHNE, AND J. PRÜSS, *On a Class of Energy Preserving Boundary Conditions for Incompressible Newtonian Flows*, SIAM J. Math. Anal., 45 (2013), pp. 3768–3822.
- [19] T. A. DAVIS, *Algorithm 832: UMFPACK V4.3—an unsymmetric-pattern multifrontal method*, ACM Trans. Math. Software, 30 (2004), pp. 196–199.
- [20] ———, *Algorithm 915, SuiteSparseQR: Multifrontal multithreaded rank-revealing sparse QR factorization*, ACM Trans. Math. Software, 38 (2011), pp. 1–22.
- [21] K. DECKELNICK, G. DZIUK, AND C. M. ELLIOTT, *Computation of geometric partial differential equations and mean curvature flow*, Acta Numer., 14 (2005), pp. 139–232.
- [22] A. DEDNER, R. KLÖFKORN, M. NOLTE, AND M. OHLBERGER, *A Generic Interface for Parallel and Adaptive Scientific Computing: Abstraction Principles and the DUNE-FEM Module*, Computing, 90 (2010), pp. 165–196.
- [23] E. DI NEZZA, G. PALATUCCI, AND E. VALDINOCI, *Hitchhiker’s guide to the fractional Sobolev spaces*, Bull. Sci. Math., 136 (2012), pp. 521 – 573.
- [24] J. DONEA, *Arbitrary Lagrangian Eulerian methods*, Comput. Meth. Trans. Anal., 1 (1983).
- [25] G. DZIUK, *An algorithm for evolutionary surfaces*, Numer. Math., 58 (1991), pp. 603–611.
- [26] H. C. ELMAN, D. J. SILVESTER, AND A. J. WATHEN, *Finite elements and fast iterative solvers: with applications in incompressible fluid dynamics*, Numerical Mathematics and Scientific Computation, Oxford University Press, New York, 2005.
- [27] X. FENG, *Fully discrete finite element approximations of the Navier–Stokes–Cahn–Hilliard diffuse interface model for two-phase fluid flows*, SIAM J. Numer. Anal., 44 (2006), pp. 1049–1072.

- [28] L. FORMAGGIA AND F. NOBILE, *Stability analysis of second-order time accurate schemes for ALE–FEM*, Comput. Methods Appl. Mech. Engrg., 193 (2004), pp. 4097–4116.
- [29] S. GANESAN, *Finite element methods on moving meshes for free surface and interface flows*, PhD thesis, University Magdeburg, Magdeburg, Germany, 2006.
- [30] S. GANESAN, G. MATTHIES, AND L. TOBISKA, *On spurious velocities in incompressible flow problems with interfaces*, Comput. Methods Appl. Mech. Engrg., 196 (2007), pp. 1193–1202.
- [31] S. GANESAN AND L. TOBISKA, *An accurate finite element scheme with moving meshes for computing 3D-axisymmetric interface flows*, Internat. J. Numer. Methods Fluids, 57 (2008), pp. 119–138.
- [32] C. GEUZAIN AND J.-F. REMACLE, *Gmsh: A 3-D finite element mesh generator with built-in pre- and post-processing facilities*, Internat. J. Numer. Methods Engrg., 79 (2009), pp. 1309–1331.
- [33] D. GILBARG AND N. S. TRUDINGER, *Elliptic Partial Differential Equations of Second Order*, vol. 224 of Grundlehren der Mathematischen Wissenschaften [Fundamental Principles of Mathematical Sciences], Springer-Verlag, Berlin, second ed., 1983.
- [34] V. GIRAUT, *A combined finite element and Marker and cell method for solving Navier-Stokes equations*, Numer. Math., 26 (1976), pp. 39–59.
- [35] V. GIRAUT AND P.-A. RAVIART, *Finite element methods for Navier–Stokes equations*, vol. 5 of Springer Series in Computational Mathematics, Springer-Verlag, Berlin, 1986. Theory and algorithms.
- [36] S. GROSS AND A. REUSKEN, *An extended pressure finite element space for two-phase incompressible flows with surface tension*, J. Comput. Phys., 224 (2007), pp. 40–58.
- [37] ——, *Numerical methods for two-phase incompressible flows*, vol. 40 of Springer Series in Computational Mathematics, Springer-Verlag, Berlin, 2011.

- [38] G. GRÜN AND F. KLINGBEIL, *Two-phase flow with mass density contrast: Stable schemes for a thermodynamic consistent and frame-indifferent diffuse-interface model*, J. Comput. Phys., 257 (2014), pp. 708–725.
- [39] C. W. HIRT AND B. D. NICHOLS, *Volume of fluid (VOF) method for the dynamics of free boundaries*, J. Comput. Phys., 39 (1981), pp. 201–225.
- [40] P. C. HOHENBERG AND B. I. HALPERIN, *Theory of dynamic critical phenomena*, Rev. Mod. Phys., 49 (1977), pp. 435–479.
- [41] T. HUGHES, W. LIU, AND T. ZIMMERMANN, *Lagrangian-Eulerian finite element formulation for incompressible viscous flows*, Comput. Methods Appl. Mech. Engrg., 29 (1981), pp. 329–349.
- [42] S. HYSING, S. TUREK, D. KUZMIN, N. PAROLINI, E. BURMAN, S. GANESAN, AND L. TOBISKA, *Quantitative benchmark computations of two-dimensional bubble dynamics*, Internat. J. Numer. Methods Fluids, 60 (2009), pp. 1259–1288.
- [43] T. ILMANEN, *Lectures on Mean Curvature Flow and Related Equations*, 1998.
- [44] D. KAY, V. STYLES, AND R. WELFORD, *Finite element approximation of a Cahn–Hilliard–Navier–Stokes system*, Interfaces Free Bound., 10 (2008), pp. 15–43.
- [45] R. J. LEVEQUE AND Z. LI, *Immersed interface methods for Stokes flow with elastic boundaries or surface tension*, SIAM J. Sci. Comput., 18 (1997), pp. 709–735.
- [46] J. LOWENGRUB AND L. TRUSKINOVSKY, *Quasi-incompressible Cahn–Hilliard fluids and topological transitions*, R. Soc. Lond. Proc. Ser. A Math. Phys. Eng. Sci., 454 (1998), pp. 2617–2654.
- [47] K.-A. MARDAL AND R. WINTHER, *An observation on Korn’s inequality for nonconforming finite element methods*, Math. Comp., 75 (2006), pp. 1–6.

- [48] F. NOBILE, *Numerical Approximation Of Fluid-Structure Interaction Problems With Application To Haemodynamics*, PhD thesis, EPFL, Lausanne, 2001.
- [49] F. NOBILE AND L. FORMAGGIA, *A stability analysis for the arbitrary lagrangian: Eulerian formulation with finite elements*, East-West J. Numer. Math., 7 (1999), pp. 105–132.
- [50] R. NÜRNBERG AND A. SACCONI, *An unfitted finite element method for the numerical approximation of void electromigration*, J. Comput. Appl. Math., 270 (2014), pp. 531–544.
- [51] S. OSHER AND R. FEDKIW, *Level Set Methods and Dynamic Implicit Surfaces*, vol. 153 of Applied Mathematical Sciences, Springer-Verlag, New York, 2003.
- [52] C. S. PESKIN, *The immersed boundary method*, Acta Numer., 11 (2002), pp. 479–517.
- [53] S. POPINET, *An accurate adaptive solver for surface-tension-driven interfacial flows*, J. Comput. Phys., 228 (2009), pp. 5838–5866.
- [54] Y. RENARDY AND M. RENARDY, *PROST: a parabolic reconstruction of surface tension for the volume-of-fluid method*, J. Comput. Phys., 183 (2002), pp. 400–421.
- [55] A. SACCONI, *Front-tracking finite element methods for a void electro-stress migration problem*, PhD thesis, Imperial College London, London, 2015.
- [56] A. SCHMIDT AND K. G. SIEBERT, *Design of Adaptive Finite Element Software: The Finite Element Toolbox ALBERTA*, vol. 42 of Lecture Notes in Computational Science and Engineering, Springer-Verlag, Berlin, 2005.
- [57] J. A. SETHIAN, *Level Set Methods and Fast Marching Methods*, Cambridge University Press, Cambridge, 1999.

- [58] M. SUSSMAN, P. SEMEREKA, AND S. OSHER, *A level set approach for computing solutions to incompressible two-phase flow*, J. Comput. Phys., 114 (1994), pp. 146–159.
- [59] P. SVÁČEK, *On numerical approximation of incompressible fluid flow with free surface influenced by surface tension*, EPJ Web Conf., 143 (2017), p. 02122.
- [60] G. TRYGGVASON, B. BUNNER, A. ESMAEELI, D. JURIC, N. ALRAWAHI, W. TAUBER, J. HAN, S. NAS, AND Y.-J. JAN, *A front-tracking method for the computations of multiphase flow*, J. Comput. Phys., 169 (2001), pp. 708–759.
- [61] S. O. UNVERDI AND G. TRYGGVASON, *A front-tracking method for viscous, incompressible multi-fluid flows*, J. Comput. Phys., 100 (1992), pp. 25–37.